

UC San Diego

UC San Diego Electronic Theses and Dissertations

Title

Functionalization of metal-organic frameworks with metalloligands and postsynthetic modification

Permalink

<https://escholarship.org/uc/item/4fk887bn>

Author

Garibay, Sergio J.

Publication Date

2011

Peer reviewed|Thesis/dissertation

UNIVERSITY OF CALIFORNIA, SAN DIEGO

**Functionalization of Metal-Organic Frameworks with Metalloligands and
Postsynthetic Modification**

A Dissertation submitted in partial satisfaction of the requirements for the degree
Doctor of Philosophy

in

Chemistry

by

Sergio J. Garibay

Committee in charge:

Professor Seth M. Cohen, Chair
Professor Arnold Rheingold
Professor Jan Talbot
Professor F. Akif Tezcan
Professor James K. Whitesell

2011

The Dissertation of Sergio J. Garibay is approved, and it is acceptable in quality and form for publication on microfilm and electronically:

Chair

University of California, San Diego

2011

DEDICATION

I dedicate this chapter of my life to my family and friends for their unconditional love and support over the years

TABLE OF CONTENTS

Signature Page	iii
Dedication.....	iv
Table of Contents.....	v
List of Symbols and Abbreviations.....	viii
List of Figures.....	xv
List of Schemes.....	xxiii
List of Tables	xxiv
Acknowledgements	xxv
Vita and Publications	xxviii
Abstract of the Dissertation	xxx
<u>Chapter 1. Metal-Organic Frameworks</u>	1
1.1 Introduction.....	2
1.2 Functionalization of MOFs	7
1.3 Postsynthetic Modification of MOFs.....	9
1.4 Evolution of PSM Reactions.....	14
1.5 Dative Postsynthetic Modification	15
1.6 Postsynthetic Deprotection	17
1.7 References.....	21
<u>Chapter 2. The Use of Metalloligands for the Construction of MOFs</u>	24
2.1 Introduction.....	25
2.2 Results and Discussion	33

2.3	Conclusions	42
2.4	Experimental Methods	43
2.5	Acknowledgements.....	46
2.6	Appendix	47
2.7	References	49
<u>Chapter 3. The Use of Postsynthetic Modification for the Incorporation of Novel Functionality into MOFs.....</u>		52
3.1	Introduction	53
3.2	Results and Discussion	54
3.3	Conclusions	64
3.4	Experimental Methods.....	65
3.5	Acknowledgements.....	70
3.6	References	71
<u>Chapter 4. The Use of Tandem Postsynthetic Modification for the Incorporation of Multifunctionality into MOFs</u>		74
4.1	Introduction	75
4.2	Results and Discussion	77
4.3	Conclusions	92
4.4	Experimental Methods.....	93
4.5	Acknowledgements.....	98
4.6	References	99
<u>Chapter 5. Metal-Organic Framework Organocatalysts Prepared by Postsynthetic.....</u>		102
5.1	Introduction.....	103

5.2 Results and Discussion	106
5.3 Conclusions	126
5.4 Experimental Methods	126
5.5 Acknowledgements.....	130
5.6 References	131
<u>Chapter 6. The Use of Postsynthetic Modification on Chemically Robust MOFs.....</u>	<u>135</u>
6.1 Introduction.....	136
6.2 Results and Discussion	139
6.3 Conclusions	160
6.4 Experimental Methods.....	161
6.5 Acknowledgements.....	170
6.6 References	171

LIST OF SYMBOLS AND ABBREVIATIONS

α	Alpha
Å	Ångström; 10^{-10} m
Å ³	Cubic Ångström
acac	Acetylacetonate
AM	Amide
atm	atmosphere (1 atm = 101.325 kPa)
β	Beta
BET	Brunauer-Emmett-Teller
BDC	Benzenedicarboxylic acid
Bpdc	Biphenyldicarboxylic acid
Bipy	Bipyridine
BTB	4,4',4''-benzene-1,3,5-triyl-tribenzoic acid
Boc	<i>tert</i> -butylcarbamate
°C	Degrees Celsius
ca.	Calculated
CDCl ₃	Deuterated chloroform
CHCl ₃	Chloroform
CD ₂ Cl ₂	Deuterated methylene chloride
CH ₂ Cl ₂	Methylene chloride
CH ₄	Methane
CH ₃ CN	Acetonitrile

CDOD ₃	Deuterated methanol
CF ₃ COOD	Deuterated trifluoro acetic acid
CN	Cyano
CO ₂	Carbon Dioxide
CP	Coordination polymer
4-cpdpm	5-(4'-carboxylphenyl)dipyrromethene
4-cydpm	5-(4'-cyanophenyl)dipyrromethene
δ	Chemical shift; ppm
°	Degree
Δ	Delta, heat
d	Doublet (NMR)
<i>d</i> ⁶ -DMSO	Deuterated DMSO
D ₂ O	Deuterated water
DABCO	1,4-Diazabicyclo[2.2.2]octane
DCI	Deuterated hydrochloric acid
DDQ	2,3-dichloro-5,6-dicyano-1,4-benzoquinone
DEF	Diethylformamide
DMF	Dimethylformamide
DMOF	DABCO-MOF
DMSO	Dimethylsulfoxide
DMT	Dimethyl amino terephthalate
ESI-MS	Electrospray Ionization mass spectrometry

Et ₂ O	Diethyl ether
EtOH	Ethanol
ee	Enantiomeric excess
FT-IR	Fourier transform infrared spectroscopy
γ	Gamma
g	Gram
h	Hour
H ₂	Hydrogen
hex	Hexagonal rod-packing motif
HCl	Hydrochloric acid
HF	Hydrofluoric acid
H ₂ O	Water, hydrate
HKUST	Hong Kong University of Science and Technology
HPLC	High-Performance Liquid Chromatography
H ₂ SO ₄	Sulfuric acid
Hz	Hertz
<i>J</i>	Coupling constant
K	Kelvin
κ	kappa
kgd	Kagomé dual topological network
iSUB	infinite secondary building unit
K ₂ CO ₃	Potassium Carbonate
KOH	Potassium Hydroxide

4-pyrddpm	5-(4'-pyridyl)dipyrromethene
λ Λ	Lambda; wavelength; nm
m	Multiplet
M	Molar; mol L ⁻¹
mg	Milligram
μ L	Microliter
μ m	Micrometers
mL	Milliliter
mm	Millimeter
mmol	Millimole
mmHg	Millimeters mercury
min	minutes
MHz	MegaHertz
MeOH	Methanol
MIL	Material Institut Lavoisier
MOF	Metal-Organic Framework
MS	Mass spectrometry
MTV	Multivariate
MgSO ₄	Magnesium Sulfate
N ₂	Dinitrogen
NaHCO ₃	Sodium Bicarbonate
NaOH	Sodium Hydroxide
NMP	<i>N</i> -methyl-2-pyrrolidone

NMR	Nuclear Magnetic Resonance spectroscopy
opda	<i>ortho</i> -phenylenebis(oxamato)
OTf	Trifluoromethanesulfonate
ox	oxalate
PCP	Porous coordination polymer
pcu	Primitive cubic topology
Ph	Phenyl
PIZA	Porphyritic Illinois zeolite analogue
pK_a	Acid dissociation constant
PSD	Postsynthetic deprotection
PSM	Postsynthetic modification
PXRD	Powder X-ray diffraction
pz	Pyrazine
pyac	3-(4-pyridyl)pentene-2,4-dione
pydca	2,4-pyridinedicarboxylate
<i>rac</i>	racemic
RT	Room temperature
s	Singlet (NMR)
sal	Salicylate
salpy	(<i>R,R'</i>)-(-)-1,2-cyclohexanediamino- <i>N,N'</i> -bis(3- <i>tert</i> -butyl-5-(4-pyridyl)salicylidene)
SBU	Secondary Building Unit

SEM	Scanning electron microscopy
SiO ₂	Silica
STP	Standard conditions for temperature and pressure
θ	Theta
t	Triplet
T_d	Decomposition Temperature
tfz-d	(3,8)-topological network
TCP	tetra(<i>p</i> -cyanophenyl)porphyrin
TCPP	tetra(<i>p</i> -carboxyphenyl)porphyrin
TEA	Triethylamine
TGA	Thermal gravimetric analysis
THF	Tetrahydrofuran
TLC	Thin Layer Chromatography
TOF	Turnover frequency
TON	Turnover number
TPP	tetra(<i>p</i> -pyridyl)porphyrin
UMCM	University of Michigan Crystalline Material
UiO	University of Oslo
UR	Urea
utp	(10,3)-d topological network
UV/VIS	Ultra-Violet/Visible
wt%	Weight percent

XRD

X-ray diffraction

V

Volume

LIST OF FIGURES

Figure 1-1. An early coordination polymer $[\text{Cd}(4,4'\text{-bpy})_2(\text{NO}_3)_2]_n^{2n+}$ utilized for the cyanosilylation of benzaldehyde.....	3
Figure 1-2. Solvothermal synthesis of IRMOF-1.....	5
Figure 1-3. The synthesis of topologically distinct MOFs utilizing 1,4-benzenedicarboxylic with different metal sources. UiO-66 from ZrCl_4 (left), MIL-53 from AlCl_3 (middle), and MIL-101 from $\text{Cr}(\text{NO}_3)_3$ (right) (UiO = University in Oslo, MIL= Material Institut Lavoisier).	6
Figure 1-4. Synthesis of a functionalized MOF through a presynthetic route (top) and introduction of functionality through a postsynthetic modification (PSM) route (bottom).	9
Figure 1-5. Ag^+ 2D coordination polymer with (2,4,6-tris(4-ethynylbenzotrile)phenoxy)ethanol (top) undergoing modification with trifluoroacetic anhydride (bottom).	11
Figure 1-6. Structure of D-POST-1 (top) and schematic representation of N-alkylation through PSM.....	11
Figure 1-7. Cartoon representation of IRMOF-3 being functionalized with acetic anhydride producing amide functionality (top) and ^1H NMR spectra of modified material after digestion with DCl (bottom). The peaks labeled with open black circles correspond to BDC ligands while those marked by open red squares correspond to amide functionalized BDC ligands.....	12
Figure 1-8. Synthesis of D-MOF- NH_2 , IRMOF-3, and UMCM-1- NH_2 and subsequent PSM with anhydrides.	13
Figure 1-9. Cartoon box representation of IRMOF-9 topology and subsequent PSM with 2,4-dinitrophenylhydrazine generating hydrozone functionality (top). Cartoon box representation of IRMOF-16 topology undergoing 'click' PSM to generate triazole functionality.	15
Figure 1-10. Introduction of pyridine groups through dative PSM on HKUST-1.	16
Figure 1-11. Cr-MIL-101- and its solvated and desolvated SBUs (top). Introduction of catalytic proline groups through dative PSM.	17

Figure 1-12. Interpenetrating framework formation with extended ligands (top). Prevention of interpenetration utilizing <i>tert</i> -butyl protecting groups and subsequent PSD generating amine functionalized IRMOF-10.....	19
Figure 2-1. Various metalloligands bearing nitrile (top), pyridyl (middle), oxolate and carboxylate (bottom) metal binding groups.....	26
Figure 2-2. The M(H ₂ salphdc) (M = Cu ²⁺ , Ni ²⁺ , and Co ²⁺) metalloligand and a view of a single non-interpenetrated network of {Zn ₃ (OH) ₂ [M(H ₂ salphdc)] ₂ } _n	27
Figure 2-3. The MnCl(salpy) metalloligand and a view of the 3D pcu network of {Zn ₂ (bpdcc) ₂ MnCl(salpy)} _n . Only the atoms of a single non-interpenetrated framework is shown.....	28
Figure 2-4. The MnCl(salpy) metalloligand and a view of the 3D network of MnSO-MOF.....	29
Figure 2-5. Effects The Zn(5,15-di(<i>p</i> -carboxyphenyl)-10,20-di(mesityl)porphyrinato) metalloligand and a view of one of the interpenetrated networks of PIZA-4.....	31
Figure 2-6. The [Co(4-pyrdpm) ₃] metalloligand and a view of the 3D utp net of {Co(4-pyrdpm) ₃ AgOTf} _n . Only a non-interpenetrated framework's atoms are shown for clarity.....	32
Figure 2-7. A view of the 3D framework of MOF-Co/Zn-5a from the <i>az</i> -plane. Only the framework atoms are shown for clarity (top left). Schematic hexagonal rod-packing motif (top center) and an isolated iSBU (top right). A view of the 3D framework of MOF-Co/Zn-5a along the <i>b</i> -axis (bottom left) and schematic packing motif (bottom right).....	36
Figure 2-8. Schematic representation of MOF-Co/Zn-5a of a (3,8)-connected net tfz-d	37
Figure 2-9. Trinuclear Zn SBU (top) within MOF-Co/Zn-5b (bottom).....	39
Figure 2-10. Chiral HPLC trace or <i>rac</i> -[Co(4-cpdpm) ₃] (top) and resolved Λ-[Co(4-cpdpm) ₃] (bottom).....	40
Figure 2-11. Powder X-ray diffraction patterns of MOF-Co/Zn-5a (left) or MOF-Co/Zn-5b (right) simulated from single X-ray crystallography data (red) experimentally collected pattern (black) and experimentally collected pattern obtained with utilization of Λ-[Co(4-cpdpm) ₃] (blue).....	41

Figure 2-12. TGA traces of MOF-Co/Zn-5a (black) and MOF-Co/Zn-5b (blue). TGA traces of the amorphous product obtained with Λ -[Co(4-cpdpm) ₃] under identical conditions used to prepare MOF-Co/Zn-5a (green) and MOF-Co/Zn-5b (red).....	41
Figure 3-1. Powder X-ray diffraction (PXRD) patterns of anhydride modified IRMOF-3 samples (left). Thermogravimetric analysis (TGA) of modified IRMOF-3 samples (right).....	56
Figure 3-2. ¹ H NMR spectra of digested IRMOF-3 modified with Boc- β -alanine anhydride (left) and Boc-aminovaleric anhydride (right) for 2 days. NH ₂ -BDC resonances are denoted by black circles and RCONH-BDC resonances by red squares.	57
Figure 3-3. ¹ H NMR spectra of digested IRMOF-3 modified with (<i>S</i>)-(+)-2-methyl butyric anhydride for 5 days.	58
Figure 3-4. ¹ H NMR spectra of digested IRMOF-3 modified with maleic (left) and succinic (right) anhydride for 5 days (black) and 1 day (blue).	59
Figure 3-5. ESI-MS(-) of the digested IRMOF-3-AMMal (left) and IRMOF-3-AMSuc (right) showing the mass peaks corresponding to the maleic and succinic acid functionalized BDC ligands.....	59
Figure 3-6. Downfield region of ¹ H NMR spectra of digested IRMOF-3 modified with (<i>S</i>)-(-)-2-acetoxysuccinic anhydride for 5 days (black) and 1 day (blue) with isomeric amide modified products (left). ESI-MS(-) of the digested IRMOF-3-(<i>S</i>)-AMSucAcO (right).	60
Figure 3-7. Downfield Powder X-ray diffraction (PXRD) patterns of IRMOF-3 that were ‘fully modified’ modified samples with cyclic anhydrides.	61
Figure 3-8. ¹ H NMR spectra of digested IRMOF-3 modified with pivalic butyric anhydride for 3 days.....	64
Figure 4-1. ‘Tandem’ step-wise postsynthetic modification of IRMOF-3.....	77
Figure 4-2. ¹ H NMR spectra of multiple modified IRMOF-3 samples, IRMOF-3 samples modified with decanoic anhydride (blue, 51% conversion), propyl isocyanate (green, 60% conversion), allyl isocyanate (purple, 75% conversion), crotonic anhydride (orange, 100% conversion) and unmodified IRMOF-3 (Black) digested in DCI/D ₂ O and <i>d</i> ⁶ -DMSO. Unmodified (NH ₂ -BDC) resonances are denoted by black circles and modified resonances color coded with their corresponding standard spectra.....	80

Figure 4-3. ESI-MS(-) of a digested IRMOF-3-AM9/UR3 single crystal.	81
Figure 4-4. HPLC-MS chromatogram of IRMOF-3-AM9/UR3 (blue), IRMOF-3-AM9/UR3/URAI (red), IRMOF-3-AM9/UR3/URAI/AMCrot- <i>a</i> (black). Part of the chromatogram (13 to 16 minutes) is magnified (7×).	82
Figure 4-5. Powder X-ray diffraction (PXRD) patterns of multiple modified IRMOF-3 samples. Modified IRMOF-3 samples were soaked and exchanged with fresh CHCl ₃ for 3 days.	82
Figure 4-6. Thermogravimetric analysis (TGA) of modified IRMOF-3 samples. All samples were dried under vacuum for 8 h. Modified IRMOF-3 (10-20 mg) was heated at a scan rate of 5 °C min ⁻¹ from 25 to 600 °C.	83
Figure 4-7. ¹ H NMR spectra of multiple modified IRMOF-3 samples, IRMOF-3 samples modified with decanoic anhydride (Blue, 51% conversion), phenyl isocyanate (Olive-green, 53% conversion), allyl isocyanate (Purple, 75% conversion), crotonic anhydride (Orange, 100% conversion) and unmodified IRMOF-3 (Black) digested in DCI/D ₂ O and <i>d</i> ⁶ -DMSO. Unmodified (NH ₂ -BDC) resonances are denoted by black circles and modified resonances color coded with their corresponding standard spectra.	84
Figure 4-8. HPLC-MS chromatogram of IRMOF-3-AM9/URPh (blue), IRMOF-3-AM9/URPh/URAI (red), IRMOF-3-AM9/URPh/URAI/AMCrot- <i>a</i> (black).	85
Figure 4-9. ESI-MS(-) of a digested IRMOF-3-AM9/URPh single crystal.	85
Figure 4-10. ESI-MS(-) of a digested IRMOF-3-AM9/URPh/URAI single crystal.	88
Figure 4-11. ESI-MS(-) of a digested IRMOF-3-AM9/URPh/URAI single crystal.	88
Figure 4-12. ESI-MS(-) of a digested IRMOF-3-AM9/URPh/URAI/AMCrot- <i>a</i> single crystal.	90
Figure 4-13. ESI-MS(-) of a digested IRMOF-3-AM9/URPh/URAI/AMCrot single crystal.	90
Figure 4-14. N ₂ gas adsorption isotherms of IRMOF-3 (black) and IRMOF-3-AM9/UR3/URAI/AMCrot- <i>b</i> (red).	92

Figure 5-1. Cu(bipy)(H ₂ O) ₂ (BF ₄) ₂ (bipy) (top), methanolysis of styrene oxide (bottom left) and representation of the structural rearrangement after introduction of methanol (bottom right).....	104
Figure 5-2. Cu(L-asp)bipy _{0.5} (left) and representation of Cu(L-asp)bipy _{0.5} (HCl) _{0.9} (MeOH) _{0.5} generated after introduction of HCl utilized as a Brønsted acid catalyst for the methanolysis of <i>cis</i> -2,3-epoxybutane (right).....	105
Figure 5-3. ¹ H NMR spectra of modified MIL-53(Al)-NH ₂ samples digested in HF/ <i>d</i> ⁶ -DMSO. Red squares and black circles represent signals of modified and unmodified NH ₂ -BDC, respectively.....	108
Figure 5-4. FT-IR spectra of modified MIL-53(Al)-NH ₂ samples.....	109
Figure 5-5. ESI-MS(-) of digested MIL-53(Al)-AMMal (right) and MIL-53(Al)-AMSuc (left) showing the mass peak associated with their corresponding carboxylate functionalized ligands.....	109
Figure 5-6. ESI-MS(-) of digested MIL-53(Al)-AMCrot (right) and MIL-53(Al)-AM1 (left) showing the mass peak associated with their corresponding amide functionalized ligands.....	110
Figure 5-7. PXRD patterns of MIL-53(Al)-AMMal (purple), MIL-53(Al)-AMSuc (orange), MIL-53(Al)-AMCrot (blue), MIL-53(Al)-AM1 (red), and MIL-53(Al)-NH ₂ (black).....	110
Figure 5-8. Thermogravimetric analysis of MIL-53(Al)-NH ₂ (black), MIL-53(Al)-AMMal (red), MIL-53(Al)-AMMal after catalysis and reactivation (blue), MIL-53(Al)-AMCrot (orange), MIL-53(Al)-AM1 (purple), and MIL-53(Al)-AMSuc (green).....	111
Figure 5-9. ¹ H NMR of catalytic reaction aliquots employing MIL-53(Al)-AMMal (green), MIL-53(Al)-AM1 (blue), MIL-53(Al)-AMCrot (red), and MIL-53(Al)-NH ₂ (black).....	113
Figure 5-10. ¹ H NMR spectra of aliquots removed from solid catalyst MIL-53(Al)-AMMal after 1 day (black), 3 days (red), and 5 days (blue).....	114
Figure 5-11. ¹ H NMR spectra of the methanolysis of <i>cis</i> -2,3-epoxybutane utilizing homogeneous catalyst DMT-AMSuc (black), DMT-AMMal (red), and the supernatant of methanolysis with DMT-AMMal after removal from catalyst (blue).....	115
Figure 5-12. ¹ H NMR spectra of the methanolysis of <i>cis</i> -2,3-epoxybutane utilizing fresh (red) and recycled (black) MIL-53(Al)-AMMal.....	116

Figure 5-13. ^1H NMR spectra of the methanolysis of <i>cis</i> -2,3,-epoxybutane utilizing MIL-53(Al)-AMMal pre-treated with CD_3OD for 7 days (black), 4 days (red), 2 days (blue) and 7 days and subsequently treated with 0.1 M HCl (green).....	117
Figure 5-14. ^1H NMR spectra of the methanolysis of <i>cis</i> -2,3,-epoxybutane utilizing MIL-53(Al)- NH_2 treated with 0.1 M HCl.	118
Figure 5-15. PXRD patterns of MIL-53(Al)- NH_2 (black) and MIL-53(Al)-AMMal (red) and MIL-53(Al)-AMMal treated with 0.1 M HCl.	119
Figure 5-16. ^1H NMR spectra of three consecutive reactions of the methanolysis of <i>cis</i> -2,3,-epoxybutane utilizing MIL-53(Al)-AMMal showing essentially quantitative conversion after the 1 st cycle (black), 2 nd cycle (red), and 3 rd cycle (blue). The MIL was regenerated with HCl between each reaction cycle.....	119
Figure 5-17. ^1H NMR spectra of the methanolysis of <i>cis</i> -2,3,-epoxybutane utilizing MIL-53(Al)-AMMal with 1 (black), 10 (red), and 20 mol% (red) catalyst loadings.....	120
Figure 5-18. ^1H NMR spectra of the methanolysis of cyclopentene oxide utilizing MIL-53(Al)-AMMal (red) and untreated cyclopentene oxide (black).....	123
Figure 5-19. ^1H NMR spectra of the methanolysis of cyclohexene oxide utilizing MIL-53(Al)-AMMal (red) and untreated cyclohexene oxide (black).....	123
Figure 5-20. ^1H NMR spectra of the methanolysis of styrene oxide utilizing MIL-53(Al)-AMMal (blue), DMT-AMMal (red), and untreated styrene oxide (black)....	124
Figure 5-21. ^1H NMR spectra of the methanolysis of <i>trans</i> -stilbene oxide utilizing MIL-53(Al)-AMMal (blue), DMT-AMMal (red) and untreated <i>trans</i> -stilbene oxide (black).....	124
Figure 5-22. ^1H NMR spectra of the methanolysis of 1,2-epoxyhexane oxide utilizing MIL-53(Al)-AMMal (red) and untreated 1,2-epoxyhexane oxide (black).	125
Figure 5-23. ^1H NMR spectra of the methanolysis of propylene oxide utilizing MIL-53(Al)-AMMal (red) and untreated propylene oxide (black).....	125
Figure 6-1. A representation of Cr-MIL-101 (top) and synthesis of Cr-MIL-101- NH_2 through the reduction of Cr-MIL-101- NH_2 and functionalization through PSM (bottom).	137

Figure 6-2. Synthesis and schematic representation of UiO-66 with its Zr_6O_6 cuboctahedron SBU (green) and synthesis of extended analogues UiO-67 and UiO-68 (bottom).....	138
Figure 6-3. Synthesis of UiO-66-Cr(CO) ₃ and UiO-66-Cr(CO) ₂ (N ₂) through PSM.	138
Figure 6-4. PXRD patterns of UiO-66 derivatives.....	140
Figure 6-5. Thermogravimetric analysis of UiO-66 (black), UiO-66-NH ₂ (red), UiO-66-Br (brown), UiO-66-NO ₂ (green), UiO-66-1,4-Naph (purple), UiO-66-AM1 (orange), UiO-66-AM4 (blue), UiO-66-AM7 (cyan), and UiO-66-AMMal (gray)..	141
Figure 6-6. ¹ H NMR Spectra of digested UiO-66 and UiO-66 functionalized samples.	143
Figure 6-7. ¹ H NMR spectra of digested UiO-66 modified samples. Black circles indicate unmodified NH ₂ -BDC and red squares are from modified BDC ligands...	144
Figure 6-8. FT-IR spectra of modified UiO-66-NH ₂ samples.....	147
Figure 6-9. ¹ H NMR spectra of UiO-66-CN produced by thermal and microwave procedures (spectra obtained by digestion with HF in CD ₃ OD). Open black circles indicate Br-BDC and open red squares indicate CN-BDC. A spectrum of unmodified UiO-66-Br is shown for reference...	150
Figure 6-10. ESI-MS(-) of digested UiO-66-CN showing the molecular ion peak associated with the cyano functionalized ligand.....	151
Figure 6-11. Infrared spectrum (ATR-FTIR) of CN-BDC (cyan), Br-BDC (blue), UiO-66-Br (black), and UiO-66-CN (red).....	151
Figure 6-12. PXRD patterns of UiO-66-Br and UiO-66-CN. The UiO-66-CN sample was produced through PSM under microwave irradiation reaction conditions.....	152
Figure 6-13. Scanning electron microscopy images (SEM) of UiO-66-Br (top) and UiO-66-CN (bottom, produced by microwave-assisted PSM, two different magnifications)....	152
Figure 6-14. PXRD patterns of UiO-66 (black), UiO-2,6-Naph (red), UiO-67 (blue), UiO-67-NH ₂ (green), UiO-67(NH ₂) ₂ (purple), UiO-67-(NO ₂) ₂ (orange), UiO-67-NO ₂ (brown), and UiO67-NO ₂ exposed to air (teal).....	156
Figure 6-15. PXRD patterns of UiO-68-NH ₂ (red) and UiO-68-2,5-OH (blue) synthesized with acetic acid compared with that of UiO-67 (black).....	158

Figure 6-16. PXRD pattern of as synthesized UiO-2,6-Naph (blue), UiO-2,6-Naph exposed to air (red) and UiO-2,6-Naph synthesized with acetic acid exposed to air...
.....159

Figure 6-17. ^1H NMR of 2-amino-[1,1'-biphenyl]-4,4'-dicarboxylic acid (blue), UiO-67-NH₂ (red), and UiO-67-AM1 (black), digested in d^6 -DMSO and aqueous HF....160

LIST OF SCHEMES

Scheme 2-1. Synthesis of [Co(4-cpdpm) ₃] metalloligand and an illustration of its organic analogue BTB.	34
Scheme 2-2. Resolution of <i>rac</i> -[Co(4-cpdpm) ₃] generating Δ-[Co(4-cpdpm) ₃] or Λ-[Co(4-cpdpm) ₃] enantiomers.	40
Scheme 3-1. Synthesis of Postsynthetic modification reactions performed with IRMOF-3 using a wide variety of functionalized anhydrides.	54
Scheme 3-2. Postsynthetic modification of IRMOF-3 using a <i>tert</i> -butyl-based asymmetric anhydride and pivalic acid byproduct.	63
Scheme 4-1. Scheme showing the reagents decanoic anhydride (AM9), propyl isocyanate (UR3), phenyl isocyanate (URPh), allyl isocyanate (URAl), and crotonic anhydride (AMCrot) used for multiple PSM reactions with IRMOF-3.	78
Scheme 5-1. Synthesis (top left) and structure (top right) of MIL-53(Al)-NH ₂ . PSM reactions performed on MIL-53-(Al)-NH ₂ relevant to this study (bottom).	107
Scheme 5-2. Methanolysis of <i>cis</i> -2,3-epoxybutane with carboxylate functionalized MIL-53(Al)-AMMal, MIL-53(Al)-AMSuc and control analogues. Letters <i>a-f</i> represent the protons associated with starting material and the ring opening product.	112
Scheme 6-1. Synthesis of isorecticular UiO-66 functionalized analogues UiO-66-NH ₂ , UiO-66-Br, UiO-66-NO ₂ (R=NH ₂ , Br, or NO ₂), and UiO-66-1,4-Naph. The UiO-66 framework is represented as an octahedron.	139
Scheme 6-2. Postsynthetic modification of UiO-66-NH ₂ with various anhydrides.	142
Scheme 6-3. Synthesis of UiO-66-Br (top) and PSM cyanation to UiO-66-CN (bottom). A representation of the UiO-66 framework is shown (top right) with the Zr ₆ O ₆ cuboctahedron SBUs highlighted in green.	149
Scheme 6-4. Synthesis of CN-BDC (3) and the failed direct solvothermal synthesis of UiO-66-CN.	153
Scheme 6-5. UiO-67 and UiO-68 functionalized materials.	155
Scheme 6-6. Synthesis of biphenyl carboxylate ligands.	156

LIST OF TABLES

Table 2-1. Crystallographic Data for MOF-Co/Zn-5a.....	47
Table 2-2. Crystallographic Data for MOF-Co/Zn-5b	48
Table 3-1. Percent conversions of PSM reactions with IRMOF-3 and different anhydrides as determined by ^1H NMR. Values listed are an average (with standard deviations) of at least three independent experiments.	56
Table 3-2. BET surface areas (m^2g^{-1}) of modified IRMOF-3, with different percent conversions of cyclic anhydrides as determined by ^1H NMR. The results of two independent experiments are shown.	61
Table 4-1. Percent Conversion of Multiple Postsynthetic Modification Reaction with IRMOF-3 and Different Anhydrides or Isocyanates As Determined by ^1H NMR ^a	79
Table 4-2. BET surface areas (m^2g^{-1}) of IRMOF-3 modified with multiple reagents. The results of two independent experiments are shown.....	83
Table 5-1. Methanolysis of Epoxides with MIL catalysts. ^a	122
Table 6-1. Conversion of UiO-66-NH ₂ to UiO-66-AM derivatives using different anhydrides.	144
Table 6-2. BET surface areas of UiO-66 functionalized systems (m^2g^{-1}).	146
Table 6-3. BET surface areas of UiO-67 functionalized systems (m^2g^{-1}).	158

ACKNOWLEDGEMENTS

I want to thank my Ph.D. advisor Prof. Seth M. Cohen and my current and former committee members, Prof. F. Akif Tezcan, Prof. James K. Whitesell, Prof. Arnold Rheingold, Prof. William C. Trogler and Prof. Jan Talbot for continued support and advice throughout my Ph.D. career. I am grateful to you for your advice and insightful discussions.

I would like to especially thank my advisor, Prof. Seth M. Cohen to whom I am extremely indebted. Seth, not only did you give me the opportunity to expand my mind but you also gave my life direction and discipline. I have learned a great amount under your guidance. Even though we have had our difficult moments, I will always respect you for pushing me to the limit and for having been a great mentor. It has truly been a pleasure working in your lab and I sincerely thank you for a wonderful graduate experience.

I am grateful to all my lab mates both past and present for truly making my stay at UCSD an enjoyable experience, to Jay, Rick, Joe, Christophe, Min and Kristine for your mentorship and setting the stage for my research; to Jody, Arpita, Jen, Sara, Melissa, Emily, Kim, Marilyn, Corrine, Jamie, Alisa and Jess for being outstanding friends, colleagues and ladies; to Matthieu, Yilong, Vishakha, Chao, David, Kevin, and Phuong for your help and advice during my graduate career.

I would also like to especially thank my amazing friends; Barrett, Amy, Dave, Jamie, Bob, Bill, Mike, Karen, Eric, Jon, Jamros, David, Ilya, Guttman, Morgan, Mela, Vanessa, Monique, Omar, Tim, Jordan, Gene, Ryan, Cosmo, Gaby, Eduardo, Sharon, Gabe, Sulyman, Anthony, Treff, Carrie, Justin, Rey, Lyndsay, Dan, Travis

and Doud. I am thankful and grateful to all of you for being there for me and allowing me to be part of your lives.

Finally, I would like to thank my family for their encouragement and support. My brother Luis for always looking out for me. My parents Rudy and Martha especially, for working hard at providing a great life for their sons and having instilled in me invaluable work and personal ethics. I am forever grateful. I dedicate this chapter of my life to my family with love, because I could not have done it without you.

Text, schemes, and figures in Chapter 2 are in part reprints of the materials published in the following papers: Garibay, S. J., Stork, J. R., Wang, Z., Cohen, S. M. "Enantiopure vs. racemic metalloligands: impact on metal-organic framework structure and synthesis" *Chem. Commun.* **2007**, *49*, 4881-4883; Garibay, S. J., Stork, J. R., Cohen, S. M. "The Use of Metalloligands in Metal-Organic Frameworks" *Prog. Inorg. Chem.* **2009**, *56*, 335-378.

Text, schemes, and figures in Chapter 3 and Chapter 4, are in part reprints of the materials published in the following papers: Garibay, S. J., Wang, Z., Tanabe, K. K., Cohen, S. M. "Postsynthetic Modification: A Versatile Approach Toward Multifunctional Metal-Organic Frameworks" *Inorg. Chem.* **2009**, *48*, 7341-7349.

Text, schemes, and figures in this Chapter 5, are in part reprints of the materials published in the following papers: Garibay, S. J., Wang, Z., Cohen, S. M. "Evaluation of Heterogenous Metal-Organic Framework Organocatalysts Prepared by Postsynthetic Modification" *Inorg. Chem.* **2010**, *49*, 8086-8091.

Text, schemes, and figures in Chapter 6, are in part reprints of the materials

published in the following papers: Garibay, S. J., Cohen, S. M. "Isorecticular synthesis and modification of frameworks with the UiO-66 topology" *Chem. Commun.* **2010**, 46, 7200-7702 and Kim, M., Garibay, S. J., Cohen, S. M. "Microwave-Assisted Cyanation of an Aryl Bromide Directly on a Metal-Organic Framework" *Inorg. Chem.* **2011**, 50, 729-731. The dissertation author was the primary researcher and author for the data presented. The co-authors listed in these publications also participated in the research.

VITA AND PUBLICATIONS

Education

- 2011 Doctor of Philosophy, Chemistry, University of California, San Diego, La Jolla, CA
- 2006 Bachelor of Science, Chemistry, California State University, Bakersfield, CA

Awards and Professional Affiliations

- 2008 NIH/NCI Continuing Umbrella of Research Experiences (CURE) Research Supplement Recipient
- 2008 Division of Inorganic Chemistry American Chemical Society Travel Award
- 2006 NSF Alliance for Graduate Education and the Professoriate (AGEP) Fellowship
- 2006 Dean's Award for Outstanding Undergraduate Paper, California State University, Bakersfield, CA
- 2006 The Outstanding Graduating Senior in Chemistry, California State University, Bakersfield, CA
- 2005-2006 NIH Minority Access to Research Training-Undergraduate Student Training in Academic Research (MARC-USTAR) Fellowship California State University, Bakersfield, CA
- 2006 – Present ACS Member, Division of Inorganic Chemistry

Publications

1. Kim, M.; Garibay, S.J. and Cohen, S.M. "Microwave-Assisted Cyanation of an Aryl Bromide Directly on a Metal-Organic Framework" *Chem. Commun.* **2011**, 50, 729-731.
2. Garibay, S.J. and Cohen, S.M. "Isorecticular Synthesis and Modification of Frameworks with the UiO-66 Topology" *Chem. Commun.* **2010**, 46, 7700-7702.
3. Garibay, S.J.; Wang, Z. and Cohen, S.M. "Evaluation of Heterogeneous Metal-Organic Framework Organocatalyst" *Inorg. Chem.* **2010**, 49, 8086-8091.

4. Garibay, S.J.; Wang, Z.; Tanabe, K.K. and Cohen, S.M. “Postsynthetic Modification: A Versatile Approach Toward Multifunctional Metal-Organic Frameworks” *Inorg. Chem.* **2009**, *56*, 7341-7349.
5. Garibay, S.J.; Stork, J.R. and Cohen, S.M. “The Use of Metalloligands in Metal-Organic Frameworks” *Prog. Inorg. Chem.* **2009**, *56*, 335-378.
6. Garibay, S.J.; Stork, J.R.; Wang, Z. and Cohen, S.M. “Enantiopure Vs. Racemic Metalloligands: Impact on Metal-Organic Framework Structure and Synthesis” *Chem. Commun.* **2007**, 4881-4883.

ABSTRACT OF THE DISSERTATION

Functionalization of Metal-Organic Frameworks with Metalloligands and Postsynthetic Modification

by

Sergio J. Garibay

Doctor of Philosophy in Chemistry

University of California, San Diego, 2011

Professor Seth M. Cohen, Chair

Metal-organic frameworks (MOFs) are a hybrid class of porous materials that are comprised of metal clusters and bridging organic ligands. The modular nature these materials makes them suited for chemical strategies aimed at fine-tuning their structure and function. Significant efforts have been spent on developing MOFs for novel applications through the use of functionalized ligands. However, incorporation of functional groups on the ligands can introduce steric, solubility, and metal-coordinating characteristics that can interfere with MOF formation.

By targeting the organic linking component of the a prefabricated MOF one can utilize various organic reactions to transform it into a new MOF with altered functional groups and thus different physical and chemical properties. The work in this thesis explores the development of functionalized MOFs through both

prefunctionalization and postsynthetic modification (PSM) approaches on a variety of MOFs.

In Chapter 2, the use of chiral tris(dipyrrinato) metalloligands was examined in an attempt to introduce chiral functionality into a set MOFs with distinct topologies realized through the use of a racemic analogue. The results further exemplify the difficulties associated with the functionalized linker strategy and suggest that PSM offers a more viable functionalization route.

In Chapter 3, the versatile nature of the PSM approach is demonstrated with the successful incorporation of chiral, amine protected, and free carboxylic acid groups into an amine functionalized framework through the use of anhydrides.

In Chapter 4, the scope and limitation of a multi-step PSM approach termed tandem PSM is discussed. A set a diverse multifunctional amide and urea MOFs were realized through tandem PSM.

While there have been many studies investigating MOFs as heterogeneous catalysts, most examples utilize unsaturated metal sites. In Chapter 5, the utilization of carboxylic acid functionalized MOFs as a solid state Brønsted acid catalyst for the methanolysis of small epoxides is demonstrated.

The use of PSM and moreover MOFs for commercial applications is limited by the chemical instability of many frameworks. Chapter 6 presents the synthesis of chemically robust frameworks and utilization of these materials in harsh PSM reaction conditions for the conversion of bromide groups to cyano groups.

Chapter 1. Metal-Organic Frameworks

1.1 Introduction

Microporous materials has attracted the interest of chemists, physicists, and material scientists due to their unique chemical and physical properties. Zeolites were one of the first class of porous materials to be synthesized. These microporous three-dimensional (3D) crystalline aluminosilicates have the general formula $M^{n+}_{x/n}[(AlO_2)_x(SiO_2)_y]^{x-} \cdot wH_2O$ (e.g. Na^+ , K^+ , Ca^{2+}).¹ Their structures are composed of corner-sharing $Si(Al)O_4$ tetrahedral units that generate uniformly sized tunnels that encapsulate water and metal ions. These materials have useful applications in gas separation, ion exchange, and catalysis.² These 2D and 3D materials are microporous, and have high chemical and thermal stability. However, these materials have several limiting properties. These materials are restricted to limited types of atoms (Al^{3+} , Si^{4+} , O^{2-}) and contain small pore channels and volumes imposing size constraints and limited accessibility. Additionally, while these materials can be functionalized with organic components through hydrosilylation this can only take place with silanol groups located in the exterior surface of the material.³ These factors limit the ability to design zeolites with specific pores and functionalities.

Research involving the development and characterization of coordination polymers (CPs) began to steadily accelerate in the early 1990s. Some of the earliest CP studies were reported by Hoskins and Robson when they rationally synthesized a 3D framework, $[N(CH_3)_4CuZn(CN)_4]_n$, which was prepared from a tetrahedral $[Zn(CN)_4]^{2-}$ precursor.⁴ In a subsequent study Gable, Hoskins and Robson utilized 4,4'-bipyridine (4,4'-bpy) and a zinc metal precursor for the synthesis a 2D square grid coordination polymer from $[Zn(H_2O)_2(4,4'-bpy)_2]_n^{2n+}$. In 1994, Fujita and coworkers

synthesized an isostructural 2D coordination polymer $[\text{Cd}(4,4'\text{-bpy})_2(\text{NO}_3)_2]_n^{2n+}$ and tested its catalytic properties for the cyanosilylation of aldehydes (Figure 1-1).⁵ This coordination polymer showed size selectivity, as smaller aldehydes that could readily fit into the pores of the material gave higher yields of cyanosilylation compared to more sterically hindered aldehydes. These early coordination polymers studies led to the development of a number of related inorganic porous materials.

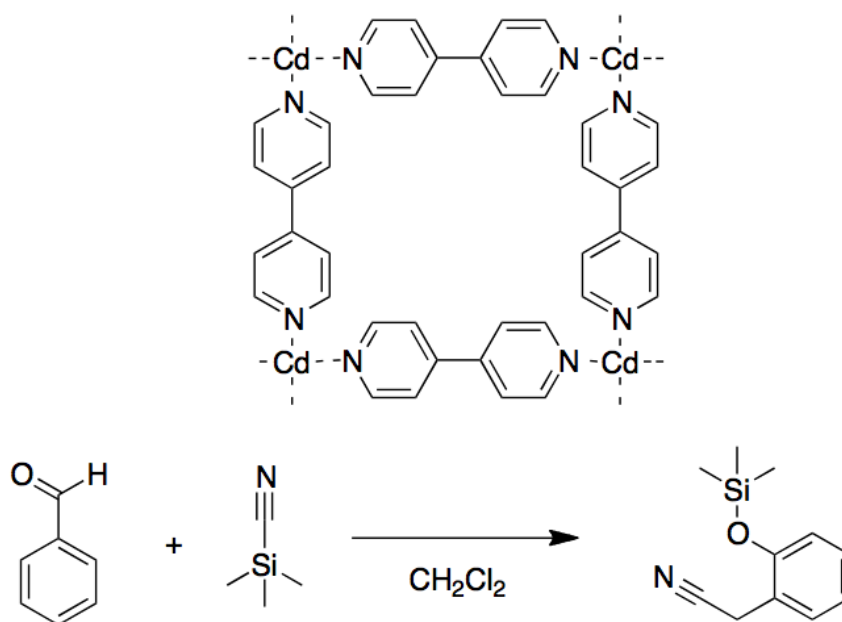


Figure 1-1. An early coordination polymer $[\text{Cd}(4,4'\text{-bpy})_2(\text{NO}_3)_2]_n^{2n+}$ utilized for the cyanosilylation of benzaldehyde.

Metal-organic frameworks (MOFs) which are also referred to as porous coordination polymers (PCPs) are a class of materials that are comprised of metal ions or metal ion clusters and bridging multidentate organic ligands.^{6,7} Indeed, many MOFs have been synthesized using any number of metal ions throughout the periodic

table (e.g., alkali, transition, group 13, lanthanides)⁸ and ligands with varying metal binding groups (e.g., pyridyls, cyanides, carboxylates, and imidazoles).⁹ The construction of MOFs commonly utilizes a molecular building block approach where metal-ligand and metal-cluster copolymerization reactions link the organic ligand and inorganic metal molecular components generating 2D or 3D extended structures.¹⁰ The intrinsic bond geometry of the metal ion and functionality of the organic building block direct the formation of an extended porous framework. Hydrothermal synthesis is the most common synthetic strategy in MOF construction. It entails the use of high-boiling, polar solvents and elevated temperatures to both dissolve the metal or organic components and generate metal-ligand clusters. These metal-ligand clusters, termed secondary building units, (SBUs), possess a well defined geometry that impart rigidity and directionality to the resulting MOF structure.¹¹ The formation of MOF-5, alternatively known as IRMOF-1 (Isorecticular Metal-Organic Framework-1), exemplifies the prototypical solvothermal synthetic route. In the reaction, 1,4-benzenedicarboxylic acid (BDC) and $\text{Zn}(\text{NO}_3)_2 \cdot 4\text{H}_2\text{O}$ are dissolved in diethylformamide (DEF), placed in a sealed container, and heated to 100 °C (Figure 1-2).¹² At this elevated temperature, the BDC and Zn^{2+} ions, combine to generate Zn_4O clusters that are coordinated by six BDC ligands forming an SBU with octahedral geometry. As a consequence, colorless, block-shaped crystals emerge from the reaction mixture forming an extended 3D porous cubic lattice comprised of octahedral SBUs connected by BDC bridging linkers.

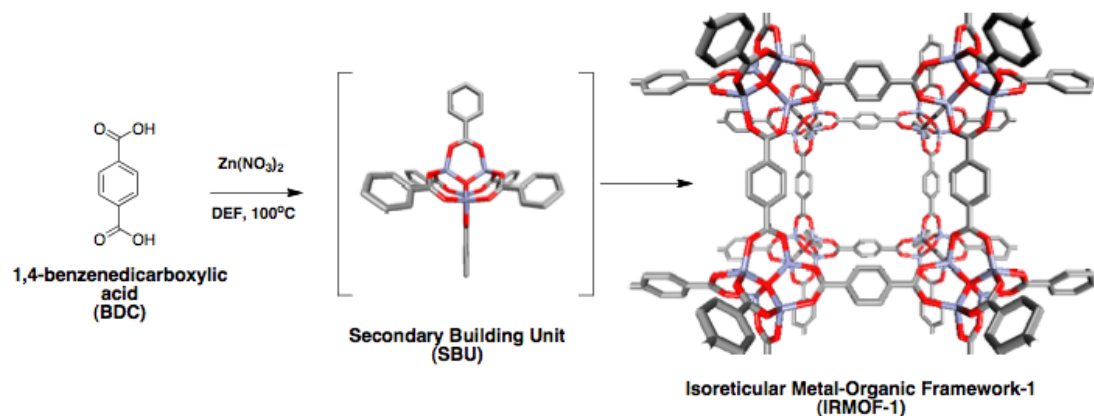


Figure 1-2. Solvothermal synthesis of IRMOF-1.

A multitude of structures and topologies are available through the selection of different metal ions and ligands. (Figure 1-3). For example, the use of BDC with different metal sources produces distinct MOF structures. The combination of BDC with ZrCl_4 heated in 4 mL of dimethylformamide (DMF) at 120°C for 24h produces cubooctahedral SBUs consisting of a six zirconium-oxo core which are connected by twelve BDC ligands which creates a cubic-closed packed 3D named UiO-66 (UiO = University of Oslo).¹³ The combination of BDC with $\text{AlCl}_3 \cdot 9\text{H}_2\text{O}$ at 220°C for 72h in H_2O produces infinite SBUs consisting chains of octahedral Al^{3+} metal centers bridged by hydroxide groups which are interconnected to each other by BDC ligands and produce 3D MOF with 1D diamond shaped channels named MIL-53 (MIL = Material Institute Lavoisier).¹⁴ Lastly, the combination of BDC and $\text{Cr}(\text{NO}_3)_3 \cdot 9\text{H}_2\text{O}$ under distinct solvothermal conditions (220°C for 8h in a dilute HF aqueous solution) produces trimetric chromium-oxo clusters that are bridged together by six BDC ligands which form a 3D MOF with colossal cages named MIL-101.¹⁵

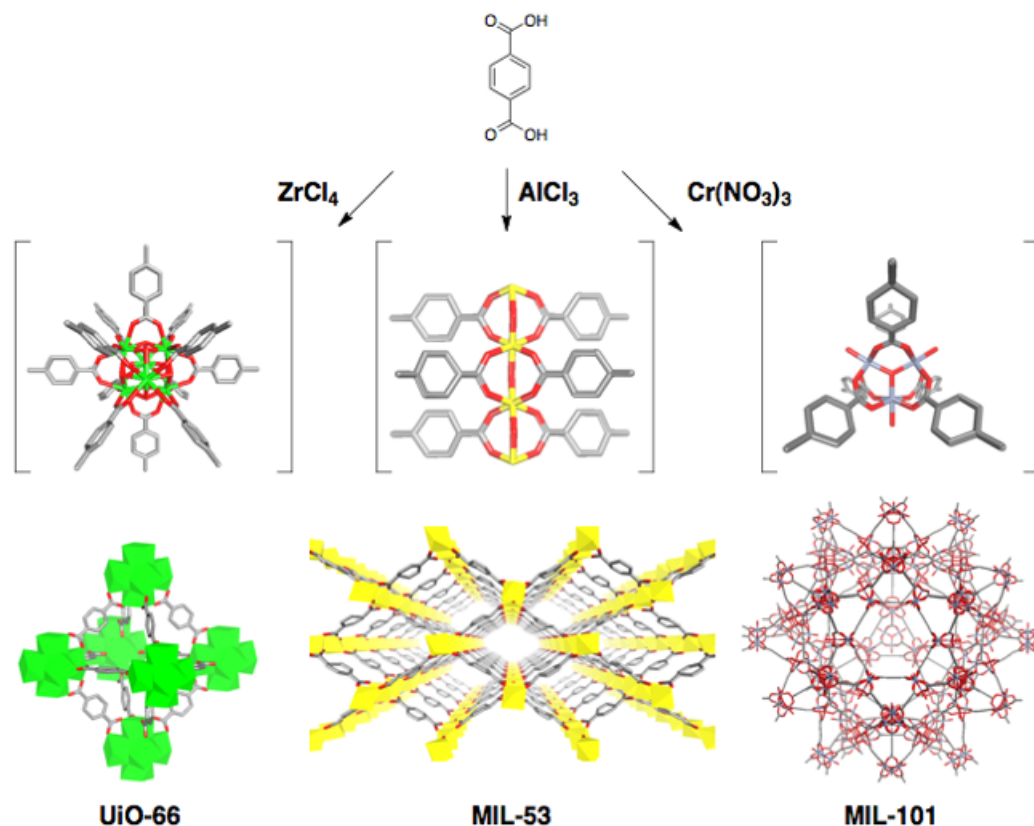


Figure 1-3. The synthesis of topologically distinct MOFs utilizing 1,4-benzenedicarboxylic acid with different metal sources. UiO-66 from ZrCl₄ (left), MIL-53 from AlCl₃ (middle), and MIL-101 from Cr(NO₃)₃ (right) (UiO = University of Oslo, MIL= Material Institut Lavoisier).

The ability to design MOFs with varying pore volumes and surface areas along with their ability to reversibly uptake and release gases has made these materials attractive for applications in gas storage and CO₂ separation. Indeed, there have been extensive efforts toward developing these materials for storage of alternative energy sources such as H₂ and CH₄.¹⁶⁻¹⁸ Several studies suggest MOFs containing SBUs with unsaturated metal centers possess stronger interactions with adsorbed gas molecules.¹⁸⁻

²⁰ In addition, selective adsorption of CO₂ within a mixture of various gasses is

observed with MOFs possessing unsaturated metal centers, small pores, and amine functionalities within the interior of the pores.²¹⁻²³

Beyond gas storage application, MOFs have shown promise in a diverse set of technologies including catalysis and drug delivery. There have been extensive investigations utilizing MOFs containing unsaturated metal centers and/or chiral topologies as enantioselective organocatalysts or Lewis acid catalysts.²⁴ Given their highly porous structures there have been exploratory studies utilizing MOFs for drug encapsulation and controlled-released agents for biomedical applications. Indeed, recent studies have shown the development of iron carboxylate nanoparticle frameworks with higher drug capacities and a more controlled or prolonged release than traditional mesoporous silicas, zeolites and liposome systems.²⁵ The modular nature via the combination of inorganic and organic components of these materials makes them ideally suited for chemical strategies aimed at fine-tuning their structure and function.

1.2 Functionalization of MOFs

Significant efforts have been spent on developing MOFs for novel applications through the use of functionalized organic ligands (i.e introduction of functionality before MOF synthesis) (Figure 1-4). Indeed, Yaghi and coworkers successfully utilized the organic component for installing a variety of chemical moieties (e.g., -NH₂, -Br) into MOFs through a presynthetic approach.¹² Through this route, a series of MOFs with different organic functionalities yet isostructural topologies were constructed. However, the preparation of functionalized MOFs through prefunctionalized ligands has been limited by the traditional solvothermal synthesis of

MOFs. Under solvothermal conditions, ligands containing functionalities that are thermally labile, possess metal-coordinating characteristics (e.g. hydroxyls, carboxylic acids) or have limited solubility will prevent or inhibit MOF formation. The introduction of such groups necessitates alternate reaction conditions that are often non-trivial and time-consuming. Another problem is the development of highly functionalized MOFs with mixed organic components. Recently, multi-functionalized analogues of IRMOFs named Multivariate MOFs (MTV-MOFs) were constructed through the use of multiple BDC analogues generating MOFs with as many as eight different functionalities within a single framework.²⁶ While introduction of multiple functional groups was realized, the introduction of functionalities within the MOF cannot be controlled. Ligands of various functionalities with varying solubilities compete with each other in MOF formation making the overall inclusion unpredictable. For instance, a 1:1 mixture of BDC and 2-amino-1,4-benzenedicarboxylic acid (NH₂-BDC) ligands utilized for MOF construction produced a framework containing a 1:0.57 ratio of the ligands. Alternative methods for the incorporation of functionalities after MOF synthesis have been recently explored and developed .

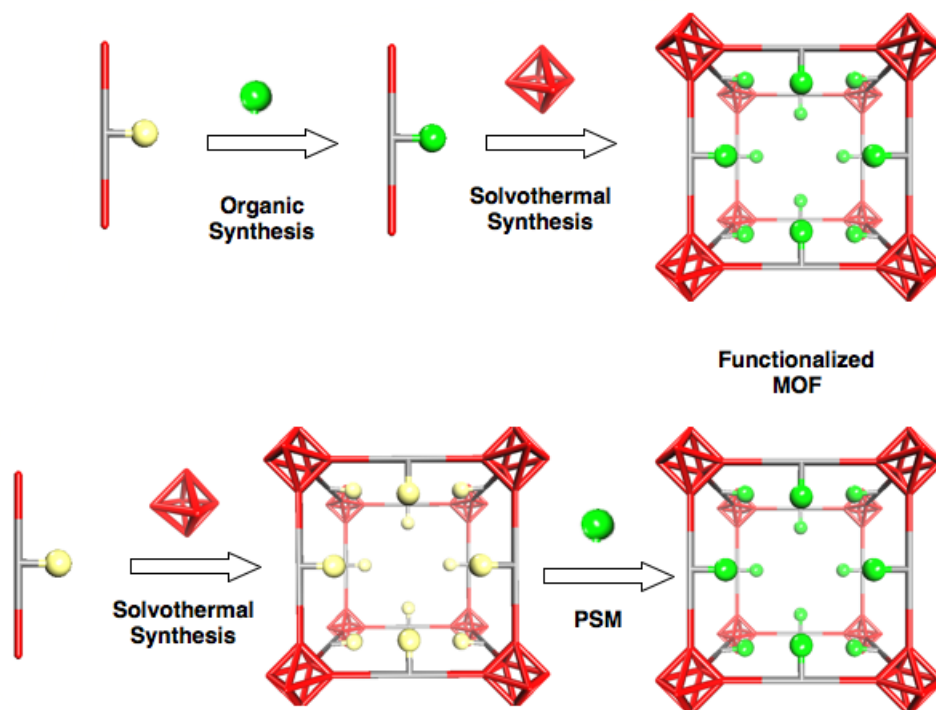


Figure 1-4. Synthesis of a functionalized MOF through a presynthetic route (top) and introduction of functionality through a postsynthetic modification (PSM) route (bottom).

1.3 Postsynthetic Modification of MOFs

In one of his earliest reports describing the cyanate-based coordination polymers synthesis Robson and coworkers suggest, “Relatively unimpeded migration of species throughout the lattice may allow chemical functionalization of the rods subsequent to construction of the framework.”²⁷ However, it was not until almost a decade later where this concept of chemical postsynthetic modification (PSM) was successfully applied to a MOF. In 1999, Lee and coworkers synthesized 2D coordination polymers from $\text{Ag}(\text{OTf})$ (OTf = Trifluoromethanesulfonate) and 2,4,6-tris(4-ethynylbenzotrile)benzene derivatives.²⁸ One of the alcohol functionalized coordination polymers built from (2,4,6-tris(4-ethynylbenzotrile)phenoxy)ethanol,

was investigated for chemical modification. The pendant alcohol group was treated with trifluoroacetic anhydride (Figure 1-5). Conversion of the alcohol into an ester was confirmed by solid-state IR analysis in addition to ^1H NMR analysis upon dissolution of coordination polymer in d^6 -acetone. In 2000, Kim and coworkers synthesized D-POST-1 a 2D MOF comprising of a chiral tartaric pyridine ligand and a trimeric Zn^{2+} SBU (Figure 1-6).²⁹ D-POST-1 was found to contain uncoordinated pyridyl groups within the pores of the framework and the material was subsequently investigated as a catalyst for the transesterification of alcohols. In order to ascertain whether the modest catalytic activity was indeed associated with the unbound pyridyl groups, PSM was conducted and utilized as a negative control. Subsequently, heterogeneous alkylation of the pyridyl groups of D-POST-1 was attempted by submerging the MOF into a solution of iodomethane in DMF. Alkylation was successfully confirmed by ^1H NMR after dissolving or digesting the modified framework with D_2O and CF_3COOD . As expected, the alkylated D-POST-1 was found to have no significant catalytic properties indicating that the free pyridyl groups were the catalytically active sites.

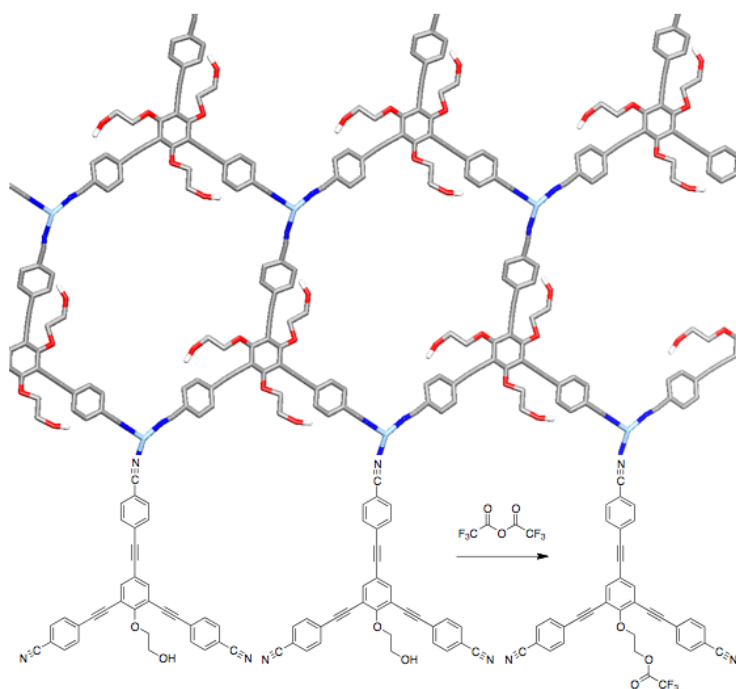


Figure 1-5. Ag^+ 2D coordination polymer with (2,4,6-tris(4-ethynylbenzotrifluoromethylphenoxy)ethanol) (top) undergoing modification with trifluoroacetic anhydride (bottom).

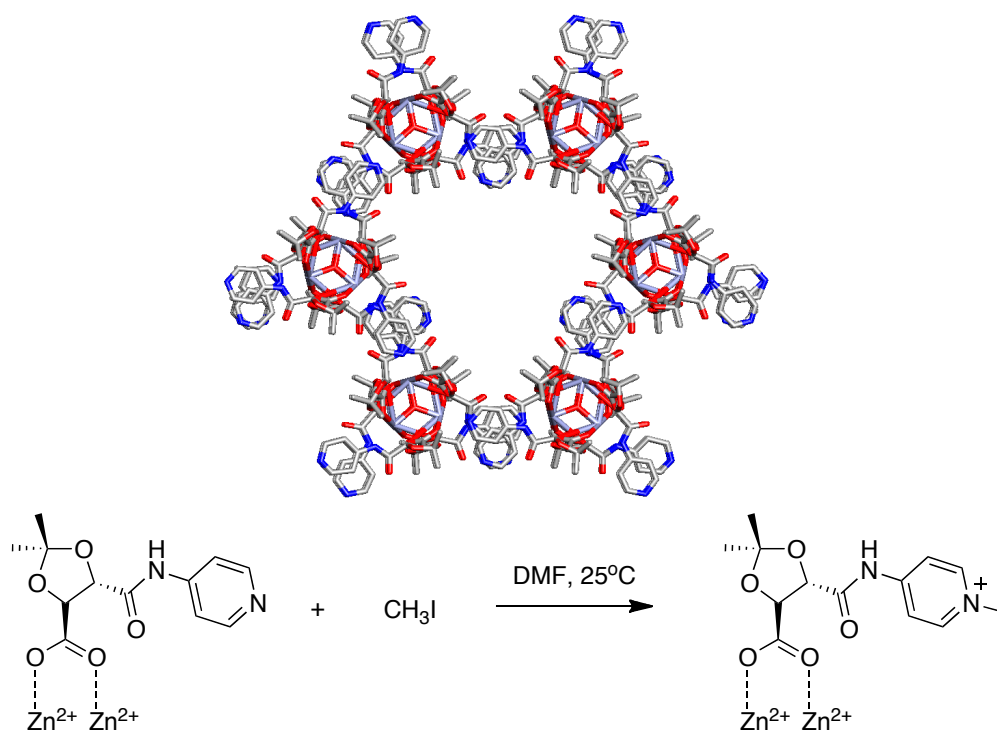


Figure 1-6. Structure of D-POST-1 (top) and schematic representation of N-alkylation through PSM.

In a 2007 seminal study Cohen and coworkers defined the concept of functionalization after MOF formation as postsynthetic modification. Utilizing a solution of acetic anhydride Wang and Cohen successfully acylated the pendant or uncoordinated amino group of 2-amino-1,4-benzenedicarboxylic acid ($\text{NH}_2\text{-BDC}$) within IRMOF-3, producing an amide functionalized framework designated as IRMOF-3-AM1 (AM = amide).³⁰ The newly introduced amide functionalities could not be characterized by single X-ray crystallography due to the positional disorder of the amino groups within the framework. Subsequently, modified samples were digested with diluted acid (35% DCI/ D_2O in $d^6\text{-DMSO}$) and the amide functionality was confirmed by ^1H NMR and mass spectrometry (Figure 1-7).

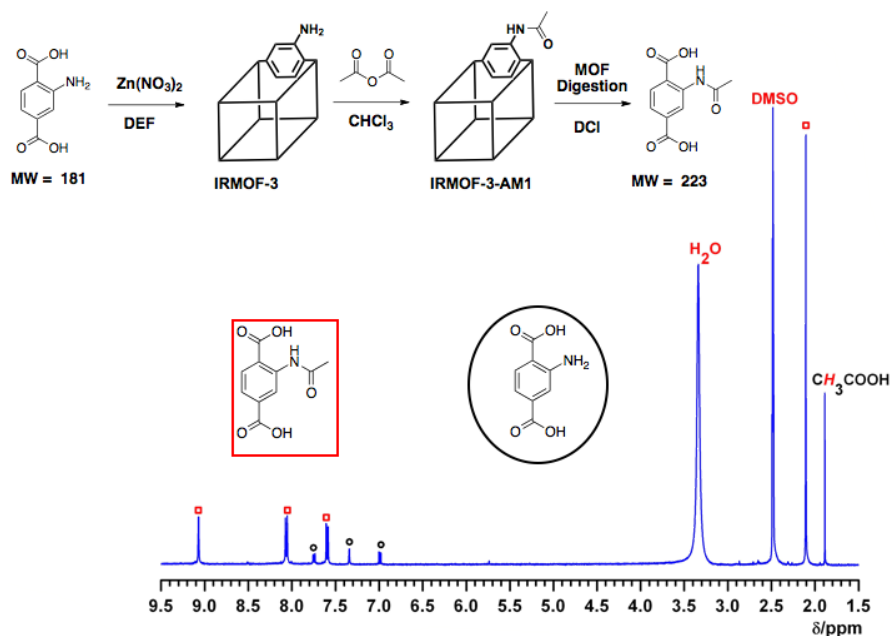


Figure 1-7. Cartoon representation of IRMOF-3 being functionalized with acetic anhydride producing amide functionality (top) and ^1H NMR spectra of modified material after digestion with DCI (bottom). The peaks labeled with open black circles correspond to BDC ligands while those marked by open red squares correspond to amide functionalized BDC ligands.

In a later study, Wang, Tanabe and Cohen investigated PSM on a variety of amino functionalized frameworks possessing distinct topologies and pores synthesized through a prefunctionalization approach (Figure 1-8).³¹ Through a systematic study utilizing aliphatic anhydrides of various chain lengths, it was concluded that both the size of the reagent and the pores of the MOFs affects the degree of PSM. Attempts to modify D-MOF-NH₂ or IRMOF-3 (MOFs with pore widths of 6 and 12 Å respectively) with relatively large anhydrides led to limited modification while moderate conversion was observed with the mesoporous (32 Å pore width) UMCM-1-NH₂ (UMCM = University of Michigan Crystalline Material) under identical reaction conditions. These early studies indicate that PSM is a general and efficient method for the introduction of functionality.

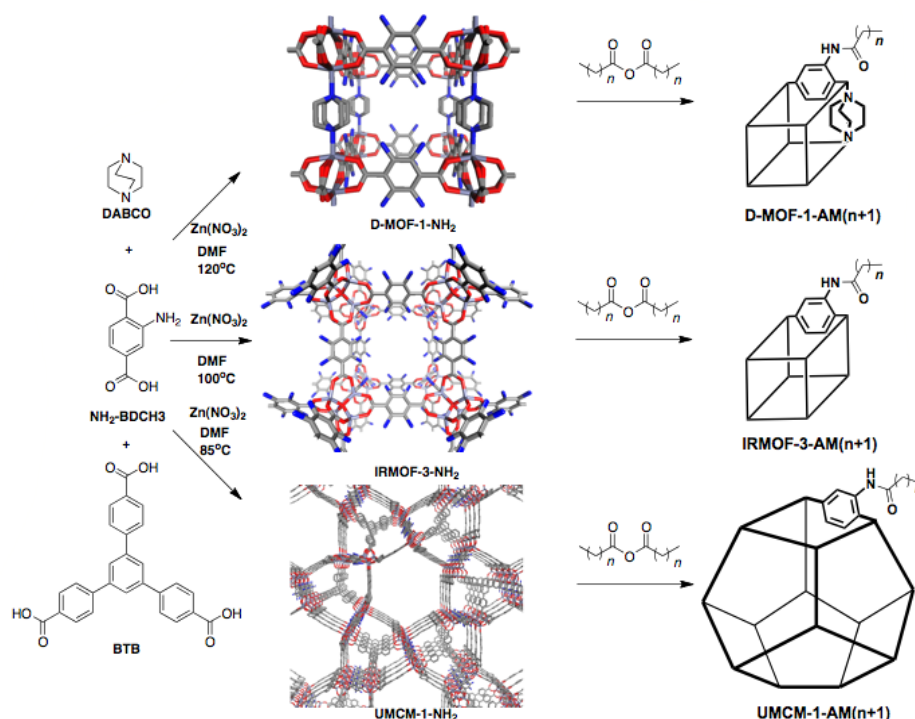


Figure 1-8. Synthesis of D-MOF-NH₂, IRMOF-3, and UMCM-1-NH₂ and subsequent PSM with anhydrides.

1.4 Evolution of PSM Reactions

The use of PSM for incorporating novel functionalities into MOFs has drastically skyrocketed since the aforementioned exploratory PSM studies. There has been an increase in the use of alternative handles (non-structure-defining functionality that can be transformed postsynthetically) and subsequently new reaction pathways for the introduction of novel functionalities. Burrows and coworkers utilized $\text{Zn}(\text{NO}_3)_2 \cdot 6\text{H}_2\text{O}$ and 2-formyl-biphenyl-4,4'-dicarboxylic acid to generate an interpenetrated IRMOF-9 analog that contained aldehyde functionality (Figure 1-9).³² Treatment with a solution of 2,4-dinitrophenylhydrazine in DMF at room temperature resulted in covalent PSM with hydrazone functionality. 'Click' chemistry is an important and popular chemical approach for the efficient conjugation of molecules ranging from proteins to polymers. Recently, Sada and coworkers utilized an azide functionalized ligand to construct a framework with IRMOF topology.³³ Subsequent treatment of this MOF with alkynes and CuBr resulted in triazole functionalized MOFs (Figure 1-9).

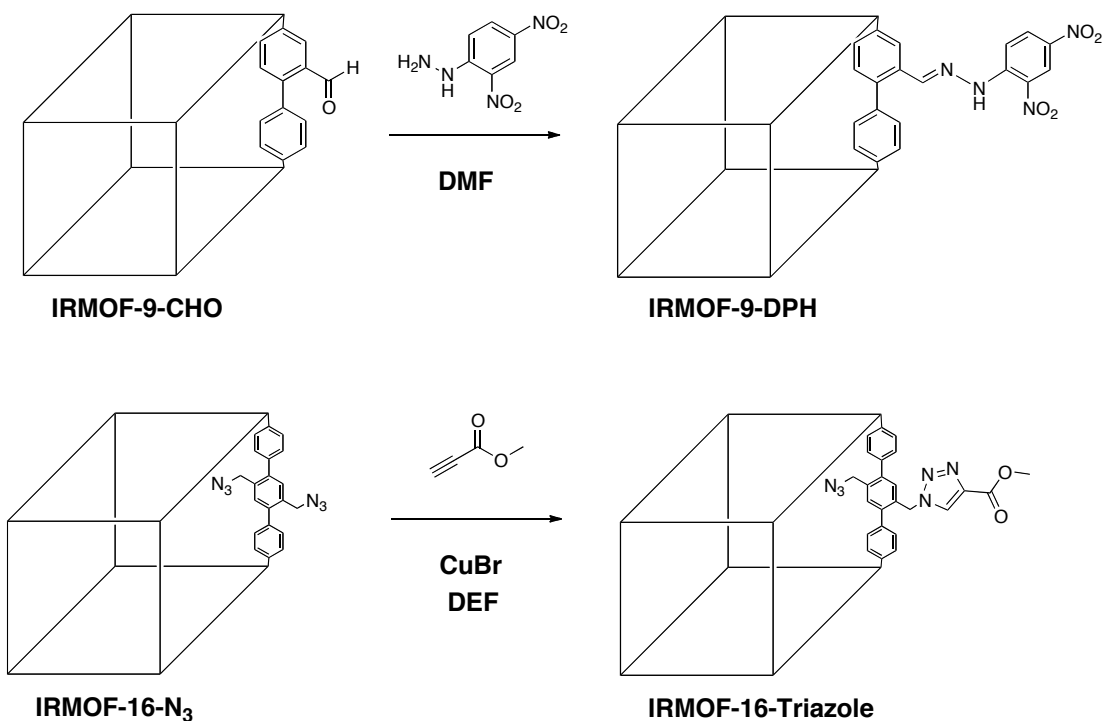


Figure 1-9. Cartoon box representation of IRMOF-9 topology and subsequent PSM with 2,4-dinitrophenylhydrazine generating hydrozone functionality (top). Cartoon box representation of IRMOF-16 topology undergoing ‘click’ PSM to generate triazole functionality.

1.5 Dative Postsynthetic Modification

While covalent modification was one of the first methods utilized for introduction of functionality, new postsynthetic methods have also been developed. Dative PSM involves the use of a reagent that forms a dative (i.e. metal-ligand) bond with a component of the MOF in a postsynthetic manner. One of the first examples utilized the Cu²⁺ metal centers in the paddlewheel SBU of HKUST-1 (HKUST = Hong Kong University of Science and Technology).³⁴ The authors were able to remove the coordinated axial water molecules from the SBU by heating the MOF to 110 °C. Subsequent treatment with pyridine produced a material that contained pyridine molecules bound to the SBU (Figure 1-10).

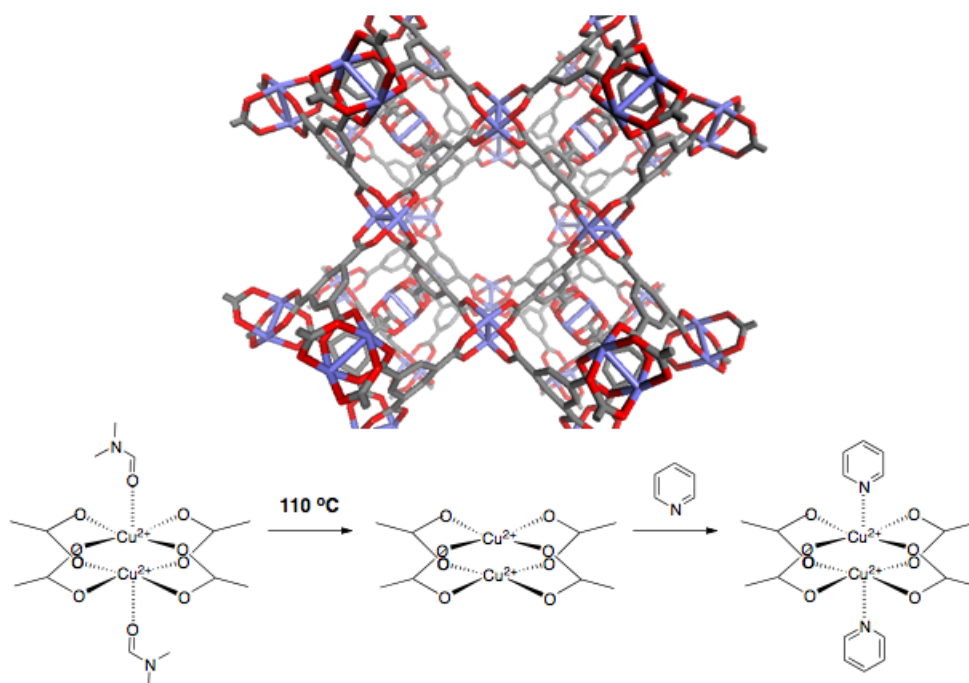


Figure 1-10. Introduction of pyridine groups through dative PSM on HKUST-1.

Recently, dative PSM has been used to introduce catalytic functionality into a MOF. Kim and coworkers were able to modify the vacant coordination sites of Cr-MIL-101 with (*S*)-*N*-(pyridin-4-yl)-pyrrolidine-2-carboxamide (Figure 1-11).³⁵ The modified MOF designated CMIL-2 contained free pendant proline groups that were bound to the SBU via the pyridyl group of the ligand. The catalytic properties of the MOF was examined and found to be a catalyst for the asymmetric aldol reaction among aromatic aldehydes and ketones generating great yields (60-90%) with modest ee (enantiomeric excess) values (55-80%). However, the catalytic properties of CMIL-2 were found to diminish after repeated catalytic cycles presumably to leaching of the ligand from the SBU.

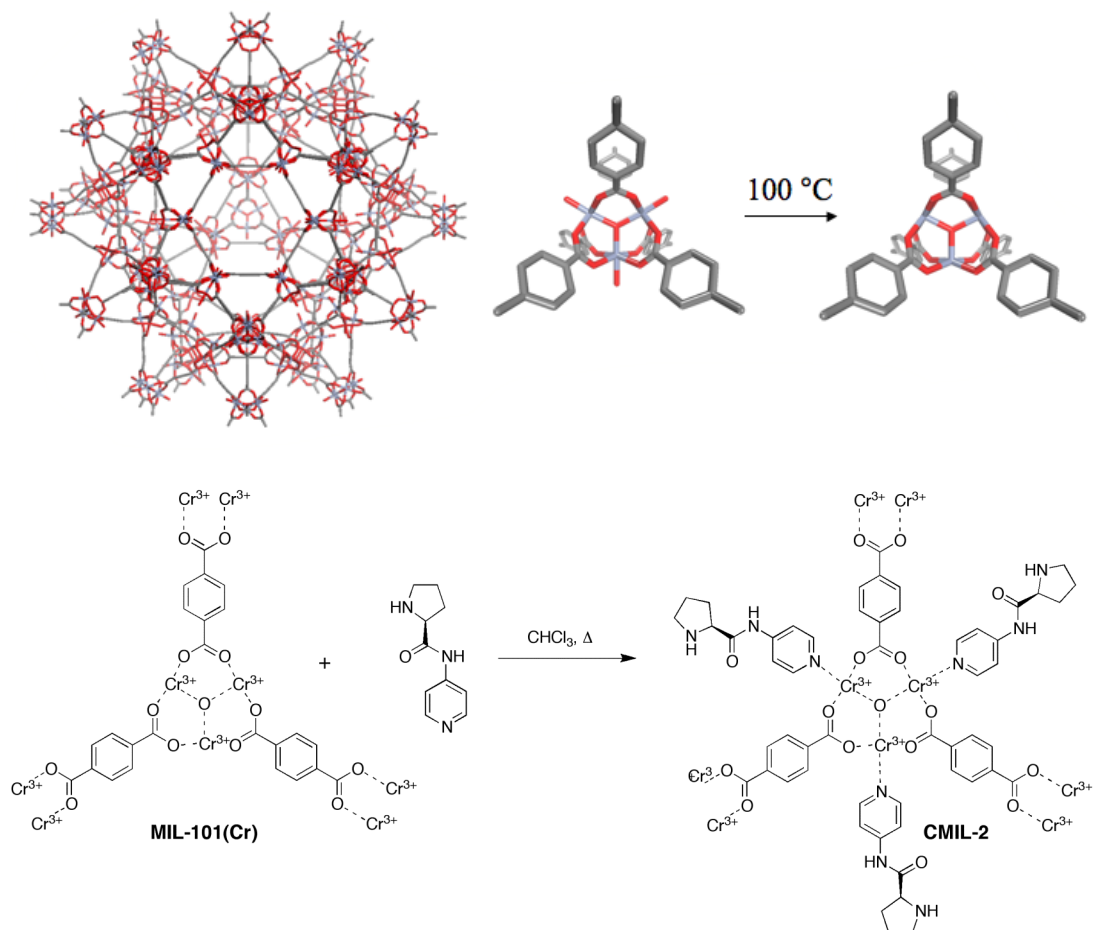


Figure 1-11. Cr-MIL-101 and its solvated and desolvated SBUs (top). Introduction of catalytic proline groups through dative PSM.

1.6 Postsynthetic Deprotection

Postsynthetic deprotection (PSD) is a newly emerging postsynthetic functionalization method that combines elements from prefunctionalization and PSM methods. A protected functional group is introduced onto an organic linker and incorporated into a MOF under standard solvothermal conditions, the protecting group is then removed in a postsynthetic fashion to reveal the desired functionality.

The use of extended linkers for the construction of larger isostructural MOFs often results in the formation of two interpenetrated frameworks (Figure-1-12).¹²

Telfer and coworkers recently demonstrated the use of PSD as a means of preventing the formation of framework interpenetration.³⁵ An amine biphenyl linker (2-aminobiphenyl-4,4'-dicarboxylate) was functionalized with a bulky *tert*-butylcarbamate (Boc) protecting group and utilized for construction of IRMOF-10. The bulky *tert*-butyl group of the ligands prevented interpenetration. The Boc groups were then removed by thermolysis at 150 °C (generating carbon dioxide and butylene) to produce an amine functionalized IRMOF-10 (Figure 1-12). This result is of great importance as attempts to produce IRMOF-10 directly from 2-aminobiphenyl-4,4'-dicarboxylate were not successful. In a subsequent report Telfer and coworkers utilized a proline Boc protected biphenyl linker for the construction of a non-interpenetrated IRMOF (IRMOF-Pro-Boc).³⁶ Treatment with microwave irradiation removed the Boc group and generated a MOF with free proline groups. However, thermolysis caused racimization of the proline groups which reduced IRMOF-Pro ability to facilitate the aldol reaction producing modest yields and ee values compared to Kim and coworkers earlier study.

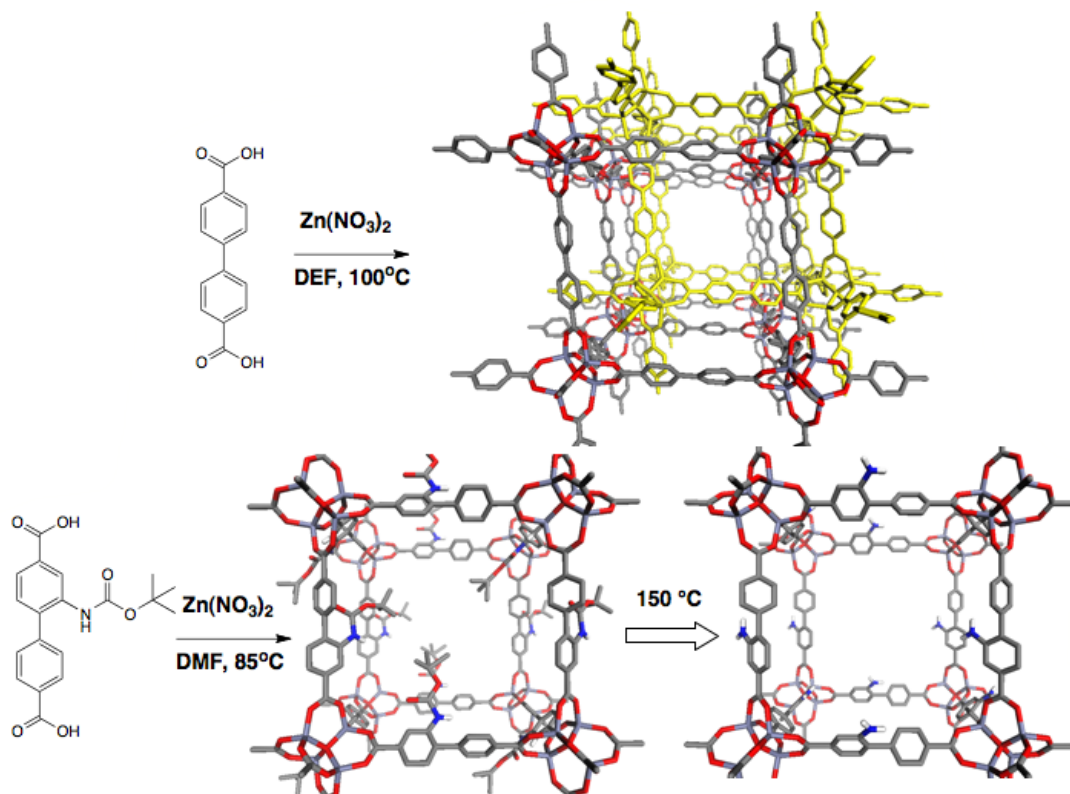


Figure 1-12. Interpenetrating framework formation with extended ligands (top). Prevention of interpenetration utilizing *tert*-butyl protecting groups and subsequent PSD generating amine functionalized IRMOF-10.

The work in this thesis explores the development of functionalized MOFs through presynthetic and covalent PSM approaches on a variety of MOFs. Due to the modular nature of these materials incorporation of functionality into isostructural frameworks may be achieved through the use of functionalized linkers. Attempts to introduce chiral functionality through the use of tris(dipyrrinato) coordination complexes will be discussed in Chapter 2. The versatile nature of PSM provides an opportunity to develop MOFs with a variety of novel functionalities through diverse reagents and organic reactions. The incorporation of novel functional groups such as free carboxylic acids through the use of covalent PSM will be addressed in Chapter 3.

The scope and limitation of a multi-step PSM approach termed tandem PSM, which allows incorporation of multiple groups, will be discussed in Chapter 4. While there have been many studies investigating MOFs as heterogeneous catalysts, most examples utilize the SBU metal centers as the catalytic sites. Chapter 5 focuses on utilization of covalent PSM in the development of organocatalytic MOFs. The use of PSM on MOFs allows access to novel functionalities that may be applicable to promising diverse applications. However, utilization of PSM and the use of MOFs for commercial applications are limited by the chemical instability of many MOF frameworks. Chapter 6 will present the synthesis of chemically robust frameworks and utilization of these materials for harsh PSM conditions.

1.7 References

- (1) Cheetham, A. K.; Ferey, G.; Loiseau, T. *Angew. Chem. Int. Ed.* **1999**, *38*, 3268-3292.
- (2) Corma, A.; Garcia, H. *Catal. Today* **1997**, *38*, 257-308.
- (3) Lee, D. H.; Choi, M.; Yu, B. W.; Ryoo, R. *Chem. Commun.* **2009**, 74-76.
- (4) Hoskins, B. F.; Robson, R. *J. Am. Chem. Soc.* **1990**, *112*, 1546-1554.
- (5) Fujita, M.; Kwon, Y. J.; Washizu, S.; Ogura, K. *J. Am. Chem. Soc.* **1994**, *116*, 1151-1152.
- (6) Kitagawa, S.; Kitaura, R.; Noro, S. *Angew. Chem. Int. Ed.* **2004**, *43*, 2334-2375.
- (7) Ferey, G. *Chem. Soc. Rev.* **2008**, *37*, 191-214.
- (8) Tranchemontagne, D. J.; Mendoza-Cortes, J. L.; O'Keeffe, M.; Yaghi, O. M. *Chem. Soc. Rev.* **2009**, *38*, 1257-1283.
- (9) Yaghi, O. M.; O'Keeffe, M.; Ockwig, N. W.; Chae, H. K.; Eddaoudi, M.; Kim, J. *Nature* **2003**, *423*, 705-714.
- (10) Eddaoudi, M.; Moler, D. B.; Li, H.; Chen, B.; Reineke, T. M.; O'Keeffe, M.; Yaghi, O. M. *Acc. Chem. Res.* **2001**, *34*, 319-330.
- (11) Rosi, N. L.; Eddaoudi, M.; Kim, J.; O'Keeffe, M.; Yaghi, O. M. *Angew. Chem. Int. Ed.* **2002**, *41*, 284-287.
- (12) Eddaoudi, M.; Kim, J.; Rosi, N.; Vodak, D.; Wachter, J.; O'Keeffe, M.; Yaghi, O. M. *Science* **2002**, *295*, 469-472.
- (13) Cavka, J. H.; Jakobsen, S.; Olsbye, U.; Guillou, N.; Lamberti, C.; Bordiga, S.; Lillerud, K. P. *J. Am. Chem. Soc.* **2008**, *130*, 13850-13851.

- (14) Loiseau, T.; Serre, C.; Huguenard, C.; Fink, G.; Taulelle, F.; Henry, M.; Bataille, T.; Ferey, G. *Chem. Eur. J.* **2004**, *10*, 1373-1382.
- (15) Ferey, G.; Mellot-Draznieks, C.; Serre, C.; Millange, F.; Dutour, J.; Surble, S.; Margiolaki, I. *Science* **2005**, *309*, 2040-2042.
- (16) Murray, L. J.; Dinca, M.; Long, J. R. *Chem. Soc. Rev.* **2009**, *38*, 1294-314.
- (17) Furukawa, H.; Ko, N.; Go, Y. B.; Aratani, N.; Choi, S. B.; Choi, E.; Yazaydin, A. O.; Snurr, R. Q.; O'Keeffe, M.; Kim, J.; Yaghi, O. M. *Science* **2010**, *329*, 424-428.
- (18) Wu, H.; Zhou, W.; Yildirim, T. *J. Am. Chem. Soc.* **2009**, *131*, 4995-5000.
- (19) Britt, D.; Tranchemontagne, D.; Yaghi, O. M. *Proc. Natl. Acad. Sci. U. S. A.* **2008**, *105*, 11623-11627.
- (20) Rowsell, J. L. C.; Yaghi, O. M. *Angew. Chem. Int. Ed.* **2005**, *44*, 4670-4679.
- (21) Britt, D.; Furukawa, H.; Wang, B.; Glover, T. G.; Yaghi, O. M. *Proc. Natl. Acad. Sci. U S A* **2009**, *106*, 20637-20640.
- (22) An, J.; Geib, S. J.; Rosi, N. L. *J. Am. Chem. Soc.* **2010**, *132*, 38-39.
- (23) Li, J. R.; Kuppler, R. J.; Zhou, H. C. *Chem. Soc. Rev.* **2009**, *38*, 1477-1504.
- (24) Lee, J.; Farha, O. K.; Roberts, J.; Scheidt, K. A.; Nguyen, S. T.; Hupp, J. T. *Chem. Soc. Rev.* **2009**, *38*, 1450-1459.
- (25) McKinlay, A. C.; Morris, R. E.; Horcajada, P.; Ferey, G.; Gref, R.; Couvreur, P.; Serre, C. *Angew. Chem. Int. Ed.* **2010**, *49*, 6260-6266.
- (26) Deng, H.; Doonan, C. J.; Furukawa, H.; Ferreira, R. B.; Towne, J.; Knobler, C. B.; Wang, B.; Yaghi, O. M. *Science* **2010**, *327*, 846-850.
- (27) Hoskins, B. F.; Robson, R. *J. Am. Chem. Soc.* **1990**, *112*, 1546-1554.

- (28) Kiang, Y.-H.; Gardner, G. B.; Lee, S.; Xu, Z.; Lobkovsky, E. B. *J. Am. Chem. Soc.* **1999**, *121*, 8204-8215.
- (29) Seo, J. S.; Whang, D.; Lee, H.; Jun, S. I.; Oh, J.; Jeon, Y. J.; Kim, K. *Nature* **2000**, *404*, 982-986.
- (30) Wang, Z.; Cohen, S. M. *J. Am. Chem. Soc.* **2007**, *129*, 12368-12369.
- (31) Wang, Z.; Tanabe, K. K.; Cohen, S. M. *Inorg. Chem.* **2009**, *48*, 296-306.
- (32) Burrows, A. D.; Frost, C. G.; Mahon, M. F.; Richardson, C. *Angew. Chem. Int. Ed.* **2008**, *47*, 8482-8486.
- (33) Goto, Y.; Sato, H.; Shinkai, S.; Sada, K. *J. Am. Chem. Soc.* **2008**, *130*, 14354-14355.
- (34) Chui, S. S.; Lo, S. M.; Charmant, J. P.; Orpen, A. G.; Williams, I. D. *Science* **1999**, *283*, 1148-1150.
- (35) Banerjee, M.; Das, S.; Yoon, M.; Choi, H. J.; Hyun, M. H.; Park, S. M.; Seo, G.; Kim, K. *J. Am. Chem. Soc.* **2009**, *131*, 7524-7525.
- (36) Lun, D. J.; Waterhouse, G. I.; Telfer, S. G. *J. Am. Chem. Soc.* **2011**, *133*, 5806-5809.

Chapter 2. The Use of Metalloligands for the Construction of MOF

2.1 Introduction

Among the approaches to the design and synthesis of MOFs, the use of ‘metalloligands’ has gained some popularity as described in recent reviews.^{1,2} This strategy employs a coordination complex (metalloligand) with pendant donor groups available for binding a second metal ion resulting in the construction of porous materials with specific structures and properties (Figure 2-1). The choice of metal complex allows for control over stoichiometry and geometry of the resulting structure. Through this approach materials with unsaturated metal centers may also be obtained. Open metal centers can be utilized both as scaffolds in the construction of MOFs and as sites for guest binding or catalysis within the framework. In this chapter, the utilization of carboxylate metalloligands as building blocks for the synthesis of MOFs will be described.

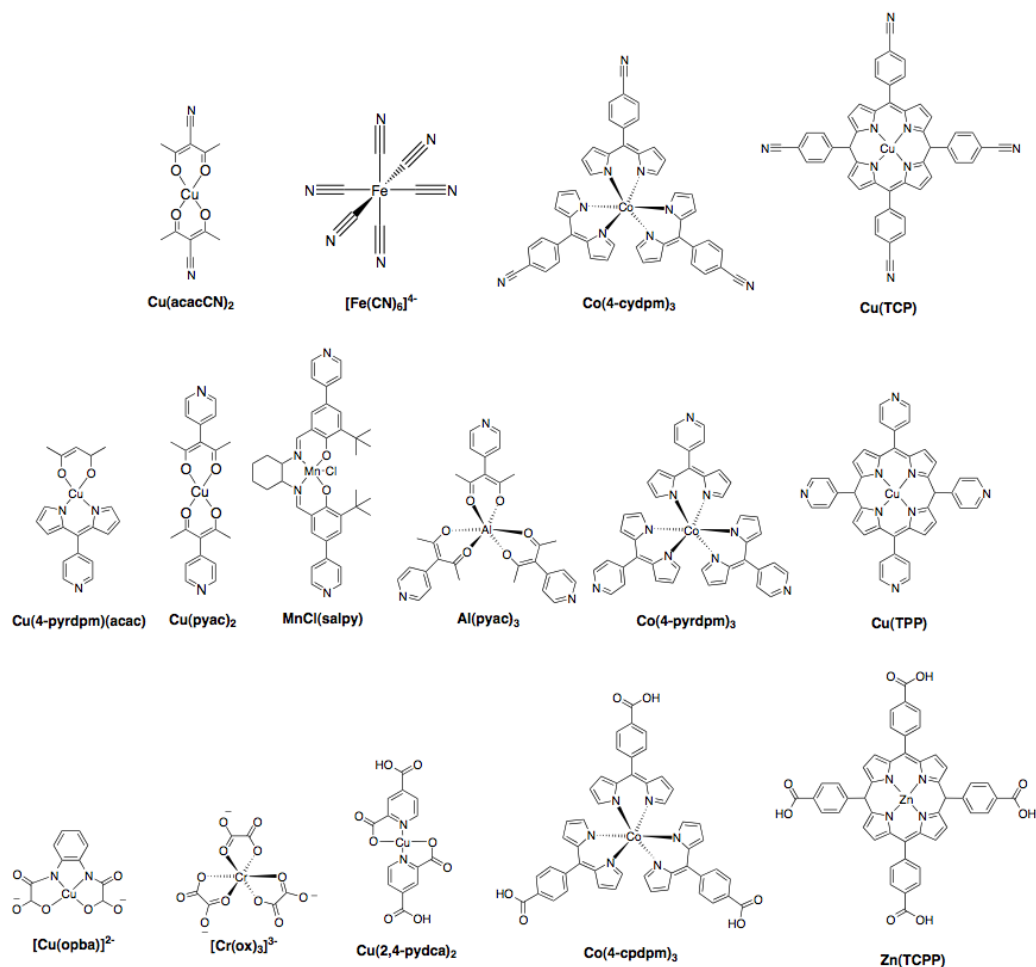


Figure 2-1. Various metalloligands bearing nitrile (top), pyridyl (middle), oxolate and carboxylate (bottom) metal binding groups.

Metal complexes prepared from derivatives of salen ligands have enjoyed wide utility as constituents of coordination polymers and MOFs.²⁻¹⁰ If the central metal of the complex is not used in building the superstructure it can then be coordinatively unsaturated and accessible to guest moieties. This combination of properties may lead to useful functions such as catalysis. Kitagawa and coworkers prepared isomorphous

interpenetrated MOFs, $\{\text{Zn}_3(\text{OH})_2[\text{M}(\text{H}_2\text{salphdc})]_2\}_n$ (where $\text{M} = \text{Cu}^{2+}$, Ni^{2+} , and Co^{2+} ; $\text{H}_2\text{salphdc}$ = dianion of *N,N'*-phenylenebis(salicylideneimine)dicarboxylic acid) with a **pcu** topology.^{2,8} The infinite clusters are connected by $\text{M}(\text{salphdc})$ metalloligands in a rectangular array to afford roughly square 1D channels that comprise about 53% of the structure (Figure 2-2). The channels are lined with the coordinatively unsaturated metal centers of the metalloligands, which might lend themselves to catalytic activity.

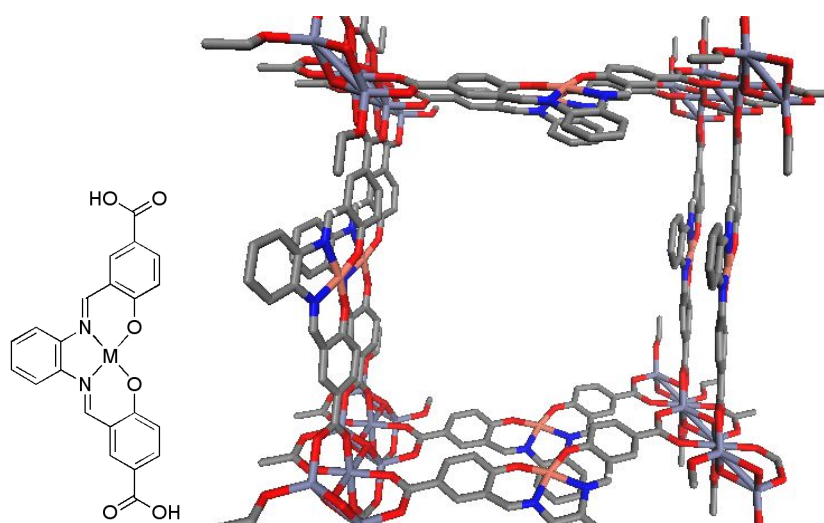


Figure 2-2. The $\text{M}(\text{H}_2\text{salphdc})$ ($\text{M} = \text{Cu}^{2+}$, Ni^{2+} , and Co^{2+}) metalloligand and a view of a single non-interpenetrated network of $\{\text{Zn}_3(\text{OH})_2[\text{M}(\text{H}_2\text{salphdc})]_2\}_n$.

Hupp and coworkers prepared a salen-derived MOF

$\{\text{Zn}_2(\text{bpdc})_2\text{MnCl}(\text{salpy})\}_n$, via solvothermal synthesis from a mixture of biphenyldicarboxylic acid (H_2bpdc) and the chiral metalloligand (*R,R'*)-(-)-1,2-cyclohexanediamino-*N,N'*-bis(3-*tert*-butyl-5-(4-pyridyl)salicylidene)MnCl ($\text{MnCl}(\text{salpy})$), with $\text{Zn}(\text{NO}_3)_2 \cdot 6\text{H}_2\text{O}$ in DMF.⁵ The resulting MOF had the distinction of incorporating both bpdc carboxylate based linkers and pyridyl linkers

from Mn(salpy) on the $\text{Zn}_2(\text{CO}_2)_4$ paddlewheel SBU. 2D sheets were formed through the bpdc linkers which were further cross-linked by Mn(salpy) metalloligands via coordination of the pyridyl nitrogens to the apical positions of the Zn^{2+} ions of the SBU, affording a 3D framework (Figure 2-3). $\{\text{Zn}_2(\text{bpdc})_2\text{MnCl}(\text{salpy})\}_n$ was evaluated for activity as an asymmetric catalyst in the epoxidation of 2,2-dimethyl-2*H*-chromene by 2-(*tert*-butylsulfonyl)iodosylbenzene. The MOF was found to catalyze the reaction with both higher turnover number (TON) and higher turnover frequency (TOF) when compared with the free Mn(salpy) complex. However, the enantiomeric excess (ee) when using the MOF was slightly worse at 82% compared to 88% ee for the free Mn(salpy) complex.

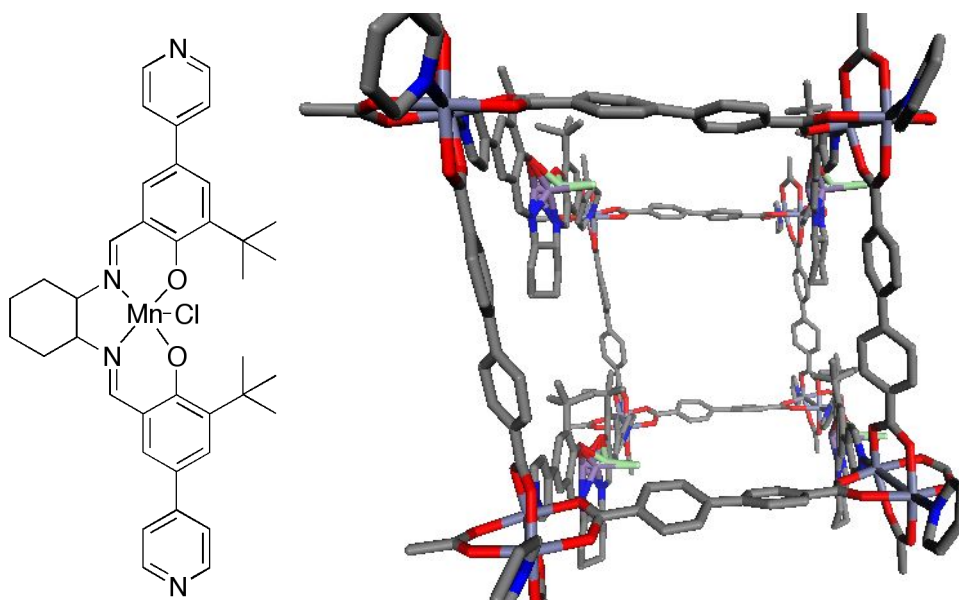


Figure 2-3. The MnCl(salpy) metalloligand and a view of the 3D **pcu** network of $\{\text{Zn}_2(\text{bpdc})_2\text{MnCl}(\text{salpy})\}_n$. Only the atoms of a single non-interpenetrated framework is shown.

Recently, Hupp and coworkers prepared a 3D noncatenated mixed-ligand, zinc paddlewheel MOF designated MnSO-MOF with the MnCl(salpy) metalloligand, a tetracarboxylic acid (tetrakis(4-carboxyphenyl)benzene and $\text{Zn}(\text{NO}_3)_2 \cdot 6\text{H}_2\text{O}$ in DMF (Figure 2-4).¹¹ Through the careful use of an aqueous H_2O_2 methanol solution the Mn^{3+} centers could be partially demetalated. In a subsequent study, fully demetalated MnSO-MOF (dSO-MOF) was utilized in the preparation of unsaturated M^{2+} metal functionalized derivatives MSO-MOFs ($\text{M} = \text{Cr}, \text{Co}, \text{Mn}, \text{Ni}, \text{Cu}, \text{and Zn}$).¹² Notably, these new analogues could not be directly synthesized readily because of competitive self-association with M^{2+} metallosalens.

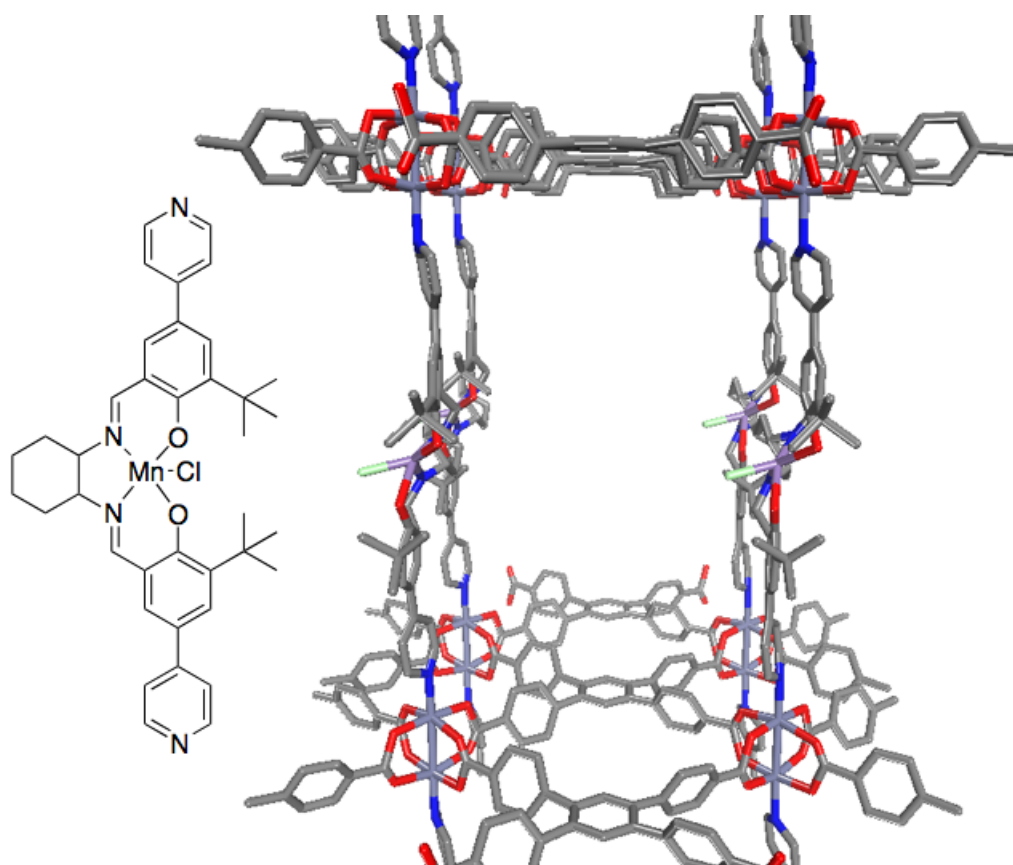


Figure 2-4. The MnCl(salpy) metalloligand and a view of the 3D network of MnSO-MOF.

Among the many investigations using metalloligands a number of studies have focused on porphyrins for supramolecular assemblies. Several reviews are available that discuss the synthesis and properties of porphyrin functionalized CPs and MOFs.^{2,13-16} Porphyrins comprise a natural ligand family for such studies because they can be readily modified to include substituted aryl groups in the meso positions. With appropriate design, these moieties can then serve as ligands to a second metal center. One of the most well studied families of porphyrins for use as metalloligands is comprised of metallated *meso*-tetra(*p*-carboxyphenyl)porphyrins (TCPPs). As with other supramolecular structures, the structures of these TCPP MOFs are dictated by the geometries of their nodes. Typically, TCPP MOFs have two types of nodes: the 4-connected, approximately square planar porphyrins, and the SBUs, which can have various geometries but generally consist of metal carboxylate clusters. Because of their carboxylate moieties, TCPP MOFs can have SBUs that are quite similar to those found in other carboxylate-based MOFs. Suslick and coworkers utilized a metalloporphyrin with two *trans*-carboxylate moieties in the formation of a MOF designated PIZA-4 (PIZA = porphyrinic Illinois zeolite analogue) with both Zn₄O carboxylate cluster SBUs and topologies reminiscent of those seen in the IRMOF series (Figure 2-5).¹⁷ The crystalline product was a robust, interpenetrated framework built around Zn₄O(CO₂)₆ SBUs with linear *trans*-carboxylate porphyrin linkers. The connectivity was essentially identical to the IRMOF series of frameworks.¹⁸

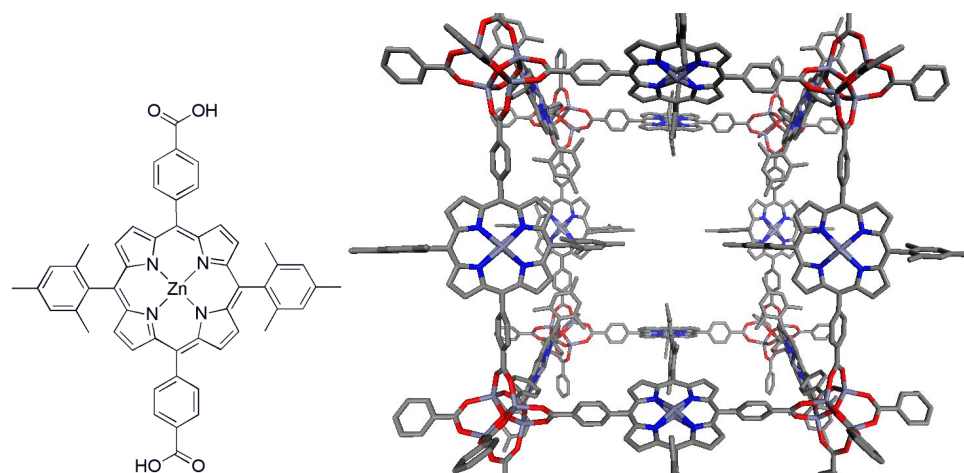


Figure 2-5. The Zn(5,15-di(*p*-carboxyphenyl)-10,20-di(mesityl)porphyrinato) metalloligand and a view of one of the interpenetrated networks of PIZA-4.

As porphyrin-related precursors, dipyrromethenes (dipyrins) are π -conjugated bidentate, monoanionic ligands that readily form bis- and tris-dipyrinato metal complexes with a variety of transition metal ions. An excellent recent review of these ligands has recently been published.¹⁹ Indeed, dipyrin ligands with donor atoms in the meso position have been used in the construction of 1D, 2D, and 3D structures. Homoleptic tris-dipyrinato metalloligands have been utilized for the construction of numerous MOFs. The 4-pyrdpm (4-pyrdpm = 5-(4'-pyridyl)dipyrromethene) ligand was combined with both Fe^{3+} and Co^{3+} producing complexes with distorted octahedral coordination environments.²⁰ These complexes have pseudo three-fold D_3 symmetry and offer a secondary ligating site for preparation of MOFs. Halper and Cohen showed that combining either $\text{Fe}(4\text{-pyrdpm})_3$ or $\text{Co}(4\text{-pyrdpm})_3$ with various Ag^+ salts produced crystals (via slow evaporation) of a new class of heterometallic MOFs.²⁰ The first structures isolated were of 2-fold interpenetrated **utp** networks²¹ where each Ag^+ ion binds to three pyridyl groups of three separate dipyrin metalloligands (Figure

2-6). These MOFs are achiral, containing alternating Δ and Λ metal centers at each tris-dipyrinato chelate. However, a chiral heterometallic MOF was realized with a nitrile bearing dipyrin metalloligand $\text{Co}(4\text{-cydpm})_3$ (4-cydpm = 5-(4'-cyanophenyl)dipyrromethene).²² Although the synthesis of the MOF began with a racemic mixture of $\text{Co}(4\text{-cydpm})_3$, spontaneous resolution occurred during growth and produced an eight interpenetrated framework possessing solely Λ metal centers. Further elaboration of these studies showed that group 13 metal ions, such as Ga^{3+} and In^{3+} salts, could also be used to construct metalloligands and subsequent heterometallic MOFs.²³ These MOFs may be of interest as molecular sensors, as it has been found that some Ga^{3+} and In^{3+} dipyrin complexes display strong luminescence.²⁴ However, these heterometallic MOFs were found to be unstable upon removal from solvent due to the relatively weak dative bonds between the pyridyl groups of the metalloligand and Ag^+ ions.

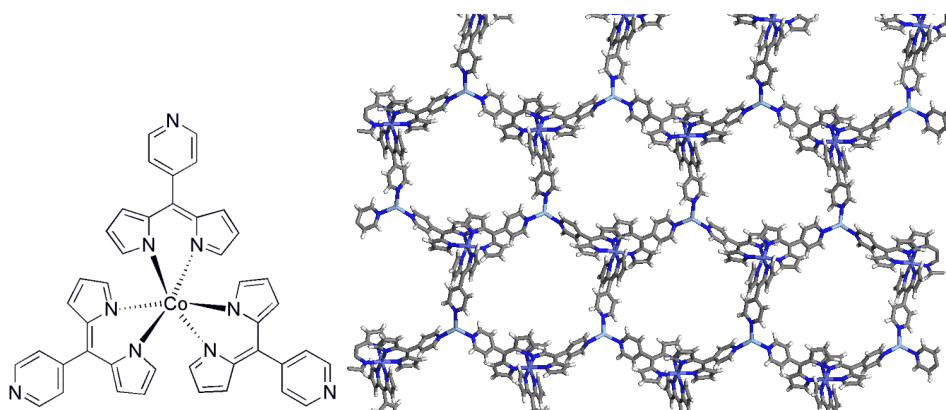


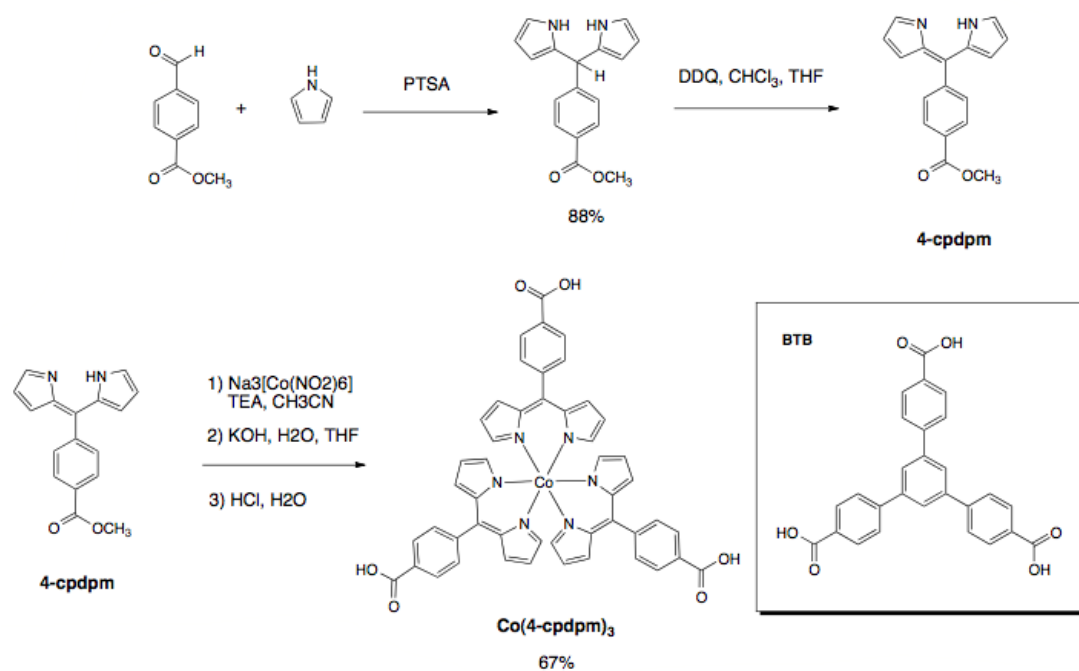
Figure 2-6. The $[\text{Co}(4\text{-pyrdpm})_3]$ metalloligand and a view of the 3D **utp** net of $\{\text{Co}(4\text{-pyrdpm})_3\text{AgOTf}\}_n$. Only a non-interpenetrated framework's atoms are shown for clarity.

One of the most successful approaches to preparing MOFs with high thermal stability and chemical robustness is the combination of a polycarboxylate ligand with divalent and trivalent metal ions such as Cu^{2+} , Zn^{2+} , In^{3+} , and others under solvothermal synthesis conditions.^{25,26} We sought to develop dipyrinato metalloligands that could mimic the MOF structures obtained by these polycarboxylate ligands. Due to their range of interesting topologies and high porosity, structures based on 3-fold symmetric tricarboxylates were specifically targeted.^{27,28} Of particular interest was MOF-177, which is comprised of 1,3,5-benzenetribenzoate (BTB, Scheme 2-1) and Zn_4O SBUs. MOF-177 has enormous pores capable of absorbing guest molecules as large as Nile Red and C_{60} .²⁷ To this end the metalloligand $[\text{Co}(4\text{-cpdpm})_3]$ (4-cpdpm = 5-(4'-carboxylphenyl)dipyrromethene) has been synthesized, characterized, and resolved into its Δ and Λ enantiomers in an attempt to make chiral analogues of structures such as MOF-177.

2.2 Results and Discussion

The carboxylate tris(dipyrinato) cobalt complex $[\text{Co}(4\text{-cpdpm})_3]$ was previously reported by Dolphin and co-workers²⁹ and utilized by Telfer et al. as tectons for the construction of hydrogen-bonded networks.³⁰ 5-(4'-carboxymethylphenyl) dipyrromethane was synthesized through a condensation reaction between freshly distilled pyrrole and catalytic amounts of *p*-toluene sulfonic acid. The dipyrromethane was then oxidized with 2,3-dichloro-5,6-dicyano-1,4-benzoquinone (DDQ) in CHCl_3 , deprotonated with TEA, and then metallated in situ with $\text{Na}_3\text{Co}(\text{NO}_2)_6$ in CH_3CN . The $[\text{Co}(4\text{-cpdpm})_3]$ complex was then hydrolyzed

with a solution of 4% $\text{KOH}_{(\text{aq})}$ in THF followed by acidification with concentrated HCl to yield the acid functionalized metalloligand $[\text{Co}(4\text{-cpdpm})_3]$ (Scheme 2-1). ^1H NMR spectroscopic data of the $[\text{Co}(4\text{-cpdpm})_3]$ complex was consistent with literature results.^{29,30}



Scheme 2-1. Synthesis of $[\text{Co}(4\text{-cpdpm})_3]$ metalloligand and an illustration of its organic analogue BTB.

After screening a number of solvothermal conditions with $\text{Zn}(\text{NO}_3)_2 \cdot 4\text{H}_2\text{O}$ dichroic red-green crystals were obtained with a mixed solution of water, ethanol and DEF. The crystals were examined by single crystal X-ray diffraction and found to be a 3D MOF containing infinite secondary building units (iSBUs) designated MOF-Co/Zn-5a (Figure 2-5). The asymmetric unit consists of a single $[\text{Co}(4\text{-cpdpm})_3]$ complex, a portion of an infinite, zigzag chain of zinc-hydroxy clusters, a guest DEF

solvent molecule, and electron density assigned to partially occupied severely disordered solvent. The $[\text{Co}(4\text{-cpdpm})_3]$ complex has an octahedral geometry similar to other dipyrinato complexes reported in the literature,^{22,29,30} however, the complex is slightly distorted such that the disposition of the peripheral carboxylate ligands is of considerably lower symmetry than idealized D_3 symmetry would predict. The iSBU is an extended cluster that can be considered as an alternating arrangement of two types of corner-sharing $\text{Zn}_3(\text{CO}_2)_3\text{OH}$ triangles (Figure 2-7). The first type of triangles (type I triangles) are close to equilateral and contain μ^3 -hydroxy groups with Zn-Zn separations of 3.332, 3.380, and 3.547 Å. The second ‘type II’ triangles are more nearly isosceles with one long Zn-Zn separation of 5.250 Å and two shorter distances of 3.497 and 3.741 Å. The type II triangles incorporate μ -hydroxy groups that are statistically distributed between two edges of the triangles. The two types of triangular units share an edge motif that involves one edge that is bridged by two carboxylate moieties from $[\text{Co}(4\text{-cpdpm})_3]$, one edge comprised of a single bridging carboxylate moiety, and one open edge that is not bridged by a carboxylate group.

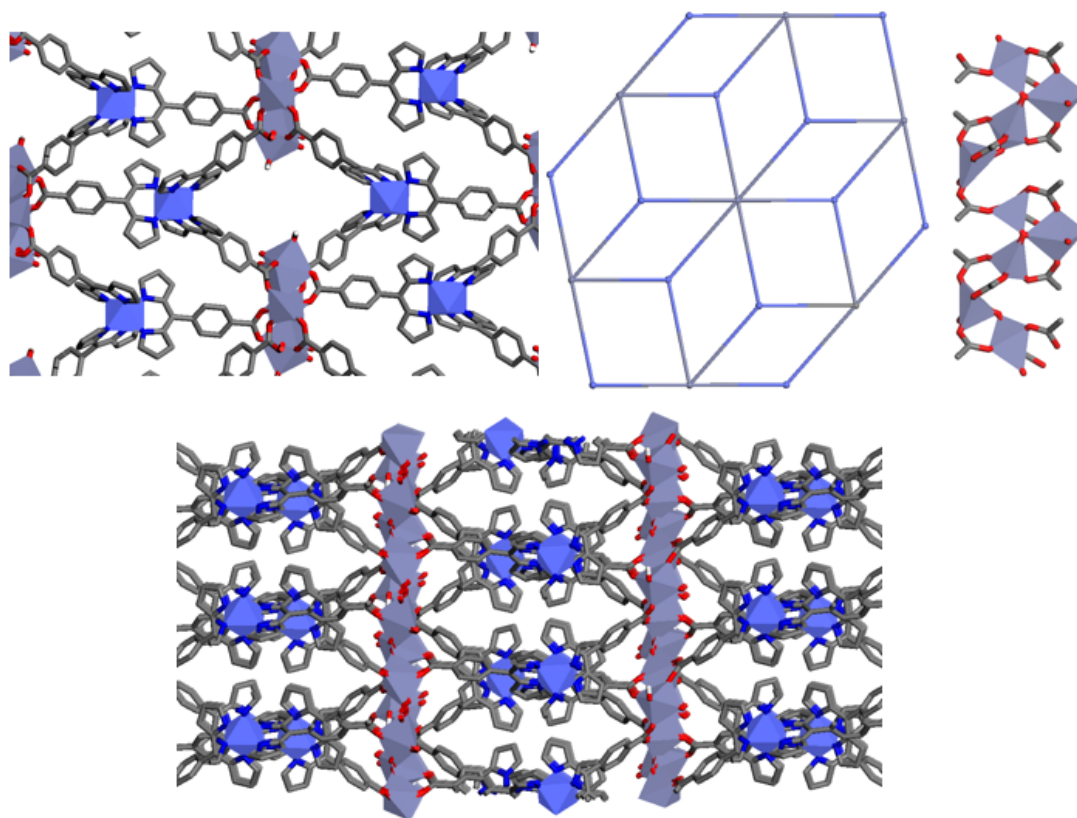


Figure 2-7. A view of the 3D framework of MOF-Co/Zn-5a from the *az*-plane. Only the framework atoms are shown for clarity (top left). Schematic hexagonal rod-packing motif (top center) and an isolated iSBU (top right). A view of the 3D framework of MOF-Co/Zn-5a along the *b*-axis (bottom left)).

Each of the $[\text{Co}(4\text{-cpdpm})_3]$ metalloligands bridges three distinct iSBUs so that the chains are arranged in a somewhat distorted hexagonal network (Figure 2-7). The rod-shaped chains present in MOF-Co/Zn-5a extend along the crystallographic *b*-axis, and MOF-Co/Zn-5a thus represents an example of a family of MOFs that are derived from iSBUs.^{8,26,31} Because of the complicated connectivity of iSBU based MOFs, as opposed to the simple node-and-spacer type MOFs, different topological perspectives are necessary in order to facilitate their structural illustration. Yaghi, O’Keeffe et al. have recently enumerated 14 different ways in which rod-shaped iSBUs can be

arranged in three-dimensional structures.²⁶ In this context, MOF-Co/Zn-5a exemplifies, if only iSBUs are considered, the prototypical hexagonal rod-packing motif (**hex**) (Figure 2-7). However, if the $[\text{Co}(4\text{-cpdpm})_3]$ metalloligands are also considered and treated as trigonal nodes, a new structural type, which is associated with the (3,8)-connected net **tfz-d** can be formulated (Figure 2-8). It should be noted that most existing iSBU-based MOFs are constructed from ditopic ligands and structures incorporating higher connectivity ligand systems remain largely unexplored.²⁶

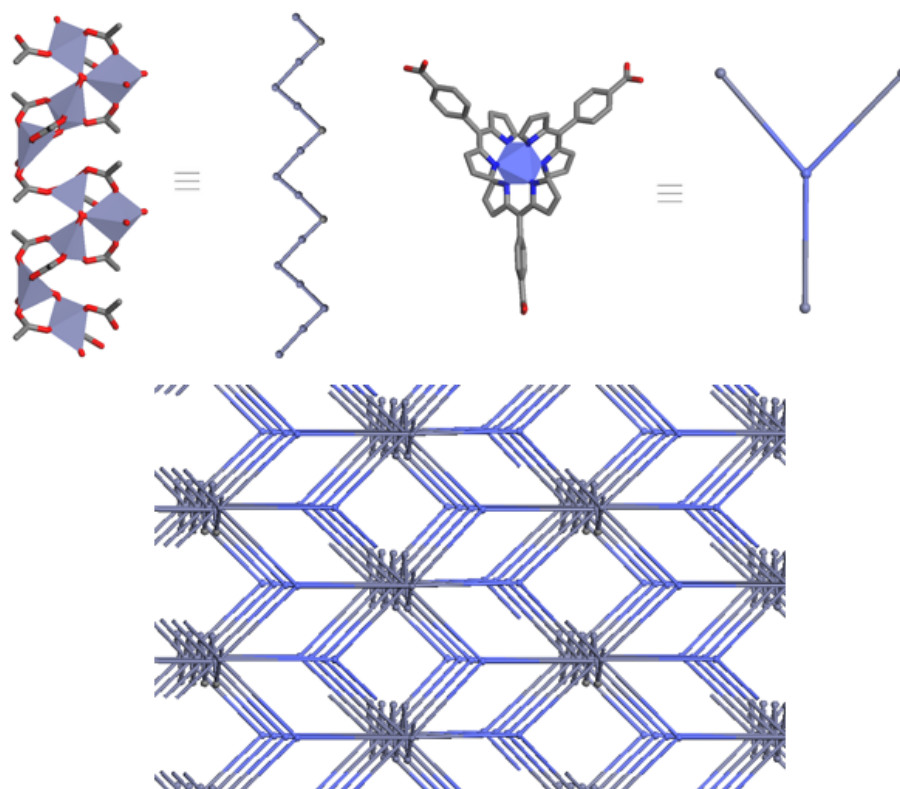


Figure 2-8. Schematic representation of MOF-Co/Zn-5a of a (3,8)-connected net **tfz-d**.

Upon obtaining MOF-Co/Zn-5a, additional reaction conditions were explored in

a continuing effort to obtain more novel MOF structures. Removal of water from the mixed solvent system and lowering the concentration of $\text{Zn}(\text{NO}_3)_2 \cdot 4\text{H}_2\text{O}$ resulted in red block-like crystals of a new compound, MOF-Co/ Zn-5b. The structure of MOF-Co/Zn-5b was determined by single-crystal X-ray diffraction, which revealed a 2D lattice (Figure 2-9). The asymmetric unit consists of one molecule of $[\text{Co}(4\text{-cpdpm})_3]$, two disordered DEF molecules, and 1.5 Zn^{2+} ions, with one located at an inversion center. A trinuclear Zn^{2+} SBU was found, which is composed of a central zinc atom that is octahedrally coordinated by six carboxyl groups. This central, 6-coordinate Zn^{2+} ion is flanked by two tetrahedral Zn^{2+} ions that are each connected to the central zinc atom by three bridging carboxylate groups (Figure 2-9). Disordered DEF molecules bind the apical sites of the flanking 4-coordinate Zn^{2+} ions. Each SBU is connected by six carboxylate groups each from a distinct $[\text{Co}(4\text{-cpdpm})_3]$ metalloligand. This creates a hexagonal, pinwheel-like geometry and an overall S_6 symmetry at the SBU. The topology underlying MOF-Co/Zn-5b is related to the hexagonal **kgd** (Kagomé dual) net, which is a 2D (3,6)-connected lattice containing 4-membered rings. This topology is exceedingly rare among observed MOF structures. It should be noted that, structurally, MOF-Co/Zn-5b and MOF-Co/Zn-5a are closely related to each other in that a schematic representation of the 2-D MOF resembles the individual layers of the 3-D MOF when viewed along the b-axis. The resemblance of the MOFs is due to the similar connectivity found in the SBUs of these MOFs.

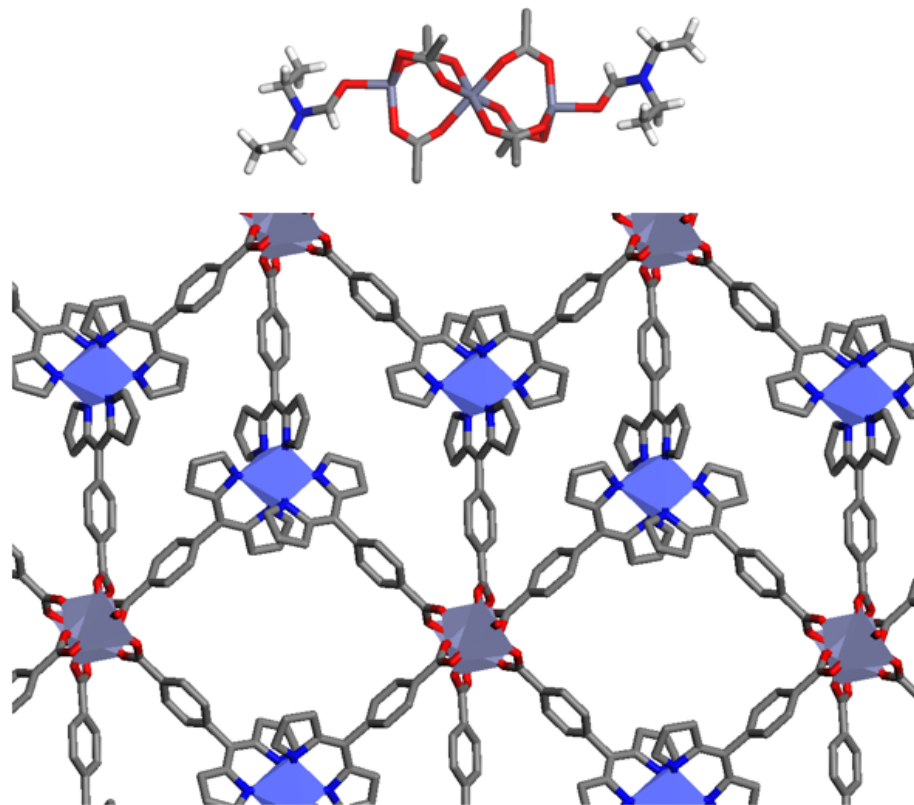
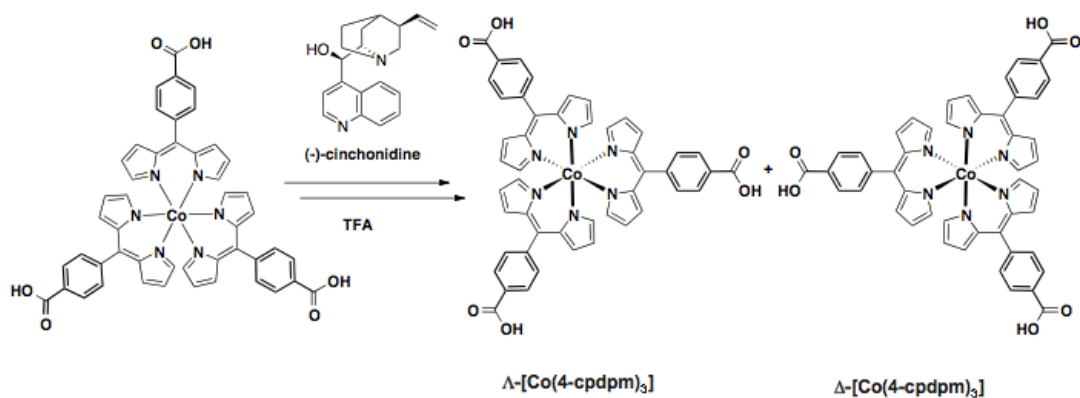


Figure 2-9. Trinuclear Zn SBU (top) within MOF-Co/Zn-5b (bottom).

With both a 2D and 3D MOF in hand, we sought to generate homochiral structures by exploiting the chirality of the octahedral, tris(chelate) metal center of the $[\text{Co}(4\text{-cpdpm})_3]$ metalloligand. Resolution of *rac*- $[\text{Co}(4\text{-cpdpm})_3]$ was performed with (2)-cinchonidine using a published procedure (Scheme 2-2).³⁰ Enantiopurity of the resolved metalloligand was confirmed by chiral HPLC (Figure 2-10).



Scheme 2-2. Resolution of rac -[Co(4-cpdpm)₃] generating Δ -[Co(4-cpdpm)₃] or Λ -[Co(4-cpdpm)₃] enantiomers.

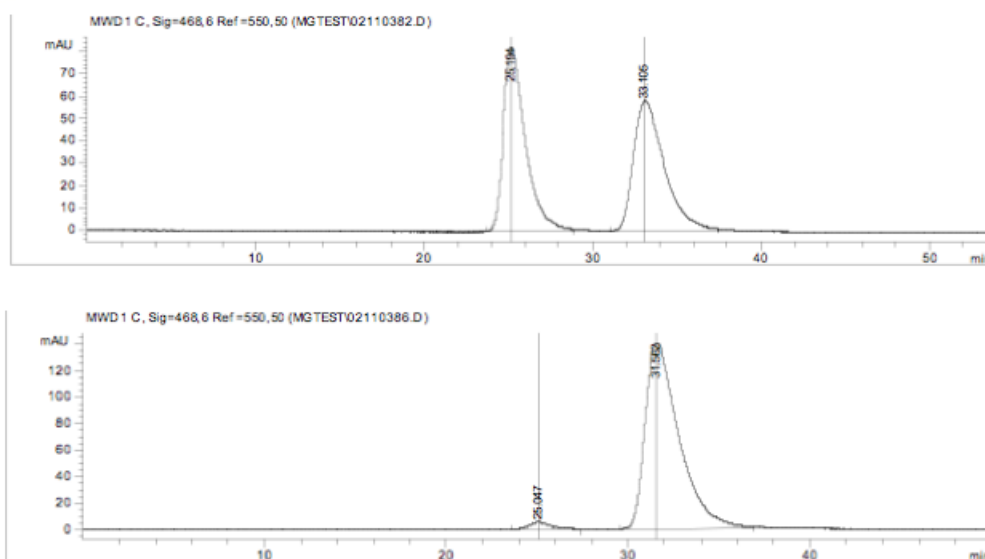


Figure 2-10. Chiral HPLC trace of rac -[Co(4-cpdpm)₃] (top) and resolved Δ -[Co(4-cpdpm)₃] (bottom).

Subjecting enantiopure Δ -[Co(4-cpdpm)₃] or Λ -[Co(4-cpdpm)₃] to identical reaction conditions as those used for MOF-Co/Zn-5a or MOF-Co/Zn-5b produced amorphous, red precipitates. Examination of these solids by X-ray powder diffraction (PXRD) showed that they lacked long-range order (Figure 2-11). Further validation

that these powders were not the desired MOFs was obtained by thermal gravimetric analysis (TGA). While both MOF-Co/Zn-5a and MOF-Co/Zn-5b are stable up to 400 °C, the amorphous solids obtained from Λ -[Co(4-cpdpm)₃] showed significant weight losses at temperatures as low as 100 °C (Figure 2-12).

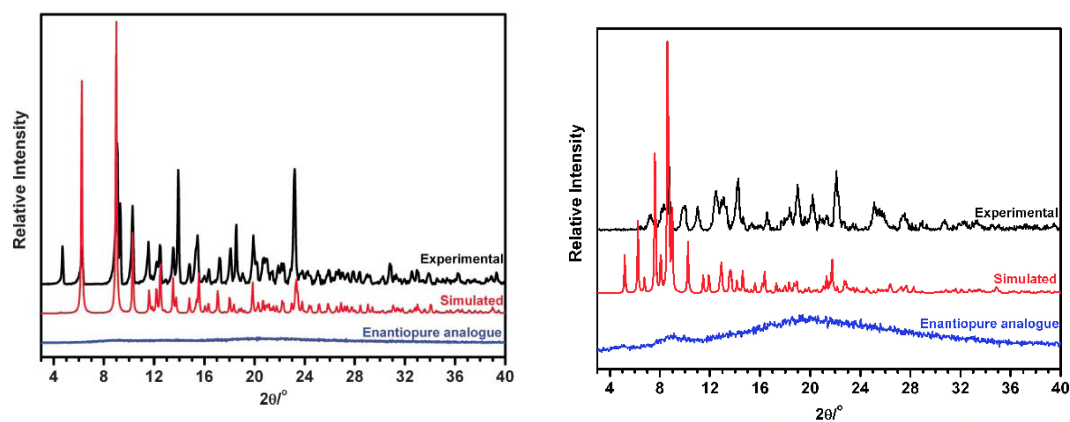


Figure 2-11. Powder X-ray diffraction patterns of MOF-Co/Zn-5a (left) or MOF-Co/Zn-5b (right) simulated from single X-ray crystallography data (red) experimentally collected pattern (black) and experimentally collected pattern obtained with utilization of Λ -[Co(4-cpdpm)₃] (blue).

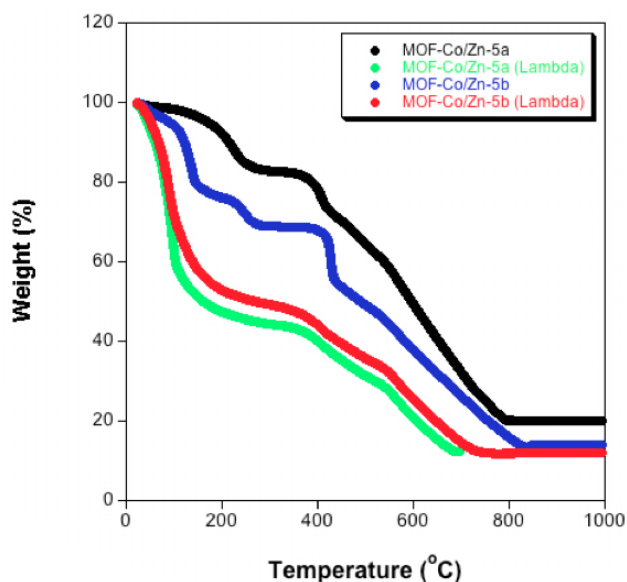


Figure 2-12. TGA traces of MOF-Co/Zn-5a (black) and MOF-Co/Zn-5b (blue). TGA traces of the amorphous product obtained with Λ -[Co(4-cpdpm)₃] under identical conditions used to prepare MOF-Co/Zn-5a (green) and MOF-Co/Zn-5b (red).

The inability of constructing homochiral analogues of Co/Zn-5a or MOF-Co/Zn-5b with Δ -[Co(4-cpdpm)₃] is important in the context of using metalloligands in the preparation of chiral MOFs and the capacity of such systems to produce predictable structure types. When examining the structures of MOF-Co/Zn-5a or MOF-Co/Zn-5b, there is no obvious topological incompatibility with the use of a homochiral metalloligand. Indeed similar cyano metalloligands [Co(4-cydpm)₃] (4-cydpm = 5-(4'-cyanophenyl)dipyrromethene) were found to form homochiral MOFs after spontaneous resolution of *rac*-[Co(4-cydpm)₃] during framework formation.²² However, other factors such as differences in solubility of the enantiopure versus racemic metalloligand may prevent the direct substitution of one for the other under identical solvothermal reaction conditions. This suggests that alternate reaction conditions are required to generate homochiral analogues of MOF-Co/Zn-5a or MOF-Co/Zn-5b. However, the development of these solvothermal reaction conditions is non-trivial as slight alterations in concentration or temperature may produce MOFs with different topologies.

2.3 Conclusions

In summary, two new MOFs based on the metalloligand *rac*-[Co(4-cpdpm)₃] have been prepared and characterized. Both MOFs contain unusual structural motifs, one involving an iSBU and the other a trinuclear SBU. When preparing these MOFs, we find that the products are obtained only when the racemate is used. Under identical reaction conditions enantiopure metalloligands lead only to amorphous solids. These findings are significant within the context of designing and synthesizing new MOFs and their homochiral analogues.

2.4 Experimental Methods

General. All starting materials were obtained from commercial suppliers and used without further purification. Elemental analysis was performed at NuMega Resonance Labs, San Diego, California. Powder X-ray diffraction (PXRD) data were collected on a Rigaku Miniflex II diffractometer at 30kV, 15mA for Cu K α ($\lambda = 1.5418 \text{ \AA}$), with a scan speed of $5 \text{ }^\circ\text{C min}^{-1}$ and a step size of 0.005° in $3\text{-}40 \text{ }^\circ 2\theta$ at room temperature. The experimental backgrounds were corrected using Jade 5.0. The simulated PXRD patterns were calculated from single-crystal diffraction data using Mercury 1.5. Thermogravimetric analysis (TGA) was performed at a scan speed of $5 \text{ }^\circ\text{C min}^{-1}$ under nitrogen gas on a TA Instrument Q600 SDT.

5-(4-Methyloxycarbonylphenyl)-4,6-dipyrromethane. Freshly distilled pyrrole (20 mL, 0.29 mol) and methyl-4-formylbenzoate (4.98 g, 30 mmol) were dissolved in 200 mL of toluene. The solution was purged with N₂ for 20 min by using a gas dispersion tube. *p*-Toluene sulfonic acid (50 mg, 0.26 mmol) was added to the reaction mixture and heated to reflux for 2 h under N₂. After the solution was evaporated to dryness through rotary evaporation. The solid was suspended in ~20 mL of chloroform and filtered and dried under vacuum. Yield: 5.38 g (19.1 mmol, 63% yield). ¹H NMR (CDCl₃, 400 MHz, 25 °C); δ 3.87 (s, 3H), 5.50 (m, 1H), 5.85 (s, 2H), 6.13 (m, 2H), 6.69 (br s, 2H), 7.25 (d, $J = 8.1\text{Hz}$, 2H), 7.94 (d, $J = 8.1\text{Hz}$, 2H).

[Co(4-cpdpm)₃]. 2,3-Dicyano-5,6-dichloro-parabenzoquinone (1.93 g, 8.5 mmol) was dissolved in 30 mL of THF and added drop-wise to a solution of 5-(4'-methoxycarbonylphenyl)-4,6-dipyrromethane (1.98 g, 7.1 mmol) in CHCl₃ (200 mL) cooled under an ice bath. The solution was subsequently stirred under nitrogen gas for

2 h. The chloroform was removed on a rotary evaporator producing a brown solid, which was used in the next step of the reaction. $\text{Na}_3\text{Co}(\text{NO}_2)_6$ (0.95 g, 2.4 mmol) was dissolved in a 3:7 acetonitrile: H_2O mixture and added to a solution of the crude dipyrromethene dissolved in acetonitrile (200 mL). An excess of triethylamine (10 mL) was added and the solution was refluxed at 80 °C under nitrogen gas overnight (~14 h). The solution was evaporated and dissolved with dichloromethane and a few drops of methanol. The product was chromatographed on SiO_2 using dichloromethane as an eluant. The isolated complex was dried in a vacuum oven overnight. Yield: 1.15 g (1.3 mmol, 55%). The complex (1.15 g, 1.3 mmol) was hydrolyzed in a 1:1 THF : 4% KOH solution (75 mL). The solution was refluxed at 80 °C under nitrogen gas for 6 h. The solution was allowed to cool to room temperature and the product was precipitated using 6N HCl (~15 mL). The red solid was filtered onto a glass frit and washed several times with cold water. The product was dried in a vacuum oven overnight. Yield: 1.06 g (1.25 mmol, 97%). ^1H NMR (d^6 -DMSO, 400 MHz, 25 °C); δ 6.33 (s, 1H), 6.45 (m, 1H), 6.63 (m, 1H), 7.52 (d, $J = 9$ Hz), 8.06 (d, $J = 9$ Hz).

Resolution of $[\text{Co}(4\text{-cpdpm})_3]$. Racemic $[\text{Co}(4\text{-cpdpm})_3]$ (805 mg, 0.95 mmol) was dissolved in hot THF (~70 °C, 20 mL) and a solution of (-)-cinchonidine in hot THF (20 mL). The dark-orange solution was allowed to cool and stood covered overnight. An orange precipitate was filtered and chromatographed on SiO_2 with an ethyl acetate/trifluoroacetic acid (99.7/0.3) solution. The solution was evaporated and dried overnight in a vacuum oven resulting in Λ - $[\text{Co}(4\text{-cpdpm})_3]$, (443 mg, 0.52 mmol, 55% of starting racemic compound) with an ee of less than 70%. Another subsequent round of resolution of the enriched Λ - $[\text{Co}(4\text{-cpdpm})_3]$ was performed with

(-)-cinchonidine (221 mg 0.75 mmol) was performed. The orange precipitate obtained was filtered and washed with hot THF, CH₂Cl₂, and acetone. This precipitate was again purified by chromatography resulting in (286 mg, 0.33 mmol, 64%) of Λ -[Co(4-cpdpm)₃] with an ee of 97% as determined by chiral HPLC (ChiralPak 1A, 150×4.6mm, hexane/THF/TFA, 85/15/0.05, flow rate 3 mL/min) $t = 33$ min.³⁰

Synthesis of MOF-Co/Zn-5a. Racemic [Co(4-cpdpm)₃] (2.1 mg, 2.48×10⁻⁶ mol) and Zn(NO₃)₂•4H₂O (6.5 mg, 2.47×10⁻⁵ mol) were dissolved in DEF/EtOH/H₂O (1/0.25/0.25 mL) in a 4 mL screw top vial. The mixture was heated to 90 °C at a rate of 2.0 °C min⁻¹ for 23 h and cooled to room temperature at 0.2 °C min⁻¹. The resulting red-green, plate-like crystals were filtered, washed with DEF, and briefly dried in air.

Synthesis of MOF-Co/Zn-5b. Racemic [Co(4-cpdpm)₃] (2.1 mg, 2.48×10⁻⁶ mol) and Zn(NO₃)₂•4H₂O (1.29 mg, 4.93×10⁻⁶ mol) were dissolved in DEF/EtOH (1/0.49 mL) in a 4 mL screw top vial. The mixture was heated to 90 °C at a rate of 2.0 °C min⁻¹ for 23 h and cooled to room temperature at 0.2 °C min⁻¹. The resulting red, block-like crystals were filtered, washed with DEF, and briefly dried in air.

2.5 Acknowledgements

Text, schemes, and figures in this chapter, in part, are reprints of the materials published in the following papers: Garibay, S. J., Stork, J. R., Wang, Z., Cohen, S. M. "Enantiopure vs. racemic metalloligands: impact on metal-organic framework structure and synthesis" *Chem. Commun.* **2007**, *49*, 4881-4883; Garibay, S. J., Stork, J. R., Cohen, S. M. "The Use of Metalloligands in Metal-Organic Frameworks" *Prog. Inorg. Chem.* **2009**, *56*, 335-378. The dissertation author was the primary researcher and author for the data presented. The co-authors listed in these publications also participated in the research.

2.6 Appendix

Table 2-1. Crystallographic Data for MOF-Co/Zn-5a.

Compound	MOF-Co/Zn-5a
Empirical formula	$C_{53}H_{41.5}CoN_7O_{9.5}Zn_2$
Formula weight	1118.10
Temperature	100(2) K
Wavelength	0.71073 Å
Crystal system	Monoclinic
Space group	$P2_1/n$
Unit cell dimensions	a = 15.229(4) Å $\alpha = 90^\circ$ b = 8.796(2) Å $\beta = 89.977(5)^\circ$ c = 38.650(11) Å $\gamma = 90^\circ$
Volume	5177(2) Å ³
Z	4
Density (calculated)	1.434 Mg/m ³
Absorption coefficient	1.299 mm ⁻¹
F(000)	2286
Crystal size	0.27 x 0.23 x 0.04 mm ³
Theta range for data collection	1.34 to 26.37°
Index ranges	-19 =h =19, -10 =k =10, -48 =l =48
Reflections collected	43650
Independent reflections	10531 [R(int) = 0.0841]
Completeness to theta = 25.00°	99.8 %
Max. and min. transmission	0.96078 and 0.74449
Data / restraints / parameters	10531 / 0 / 690
Goodness-of-fit on F ²	1.042
Final R indices [I>2σ(I)]	R1 = 0.0787, wR2 = 0.2051
R indices (all data)	R1 = 0.1109, wR2 = 0.2285
Largest diff. peak and hole	1.369 and -0.634 e.Å ⁻³

Table 2-2. Crystallographic Data for MOF-Co/Zn-5b

Compound	MOF-Co/Zn-5b
Empirical formula	C _{55.5} H ₄₆ Co N _{7.5} O _{7.5} Zn _{1.5}
Formula weight	1094.98
Temperature	100(2) K
Wavelength	0.71073 Å
Crystal system	Triclinic
Space group	<i>P</i> -1
Unit cell dimensions	a = 13.626(3) Å α = 81.062(4)° b = 14.766(3) Å β = 81.660(4)° c = 17.357(4) Å γ = 75.534(4)°
Volume	3319.8(12) Å ³
Z	2
Density (calculated)	1.095 Mg/m ³
Absorption coefficient	0.835 mm ⁻¹
F(000)	1127
Crystal size	0.15 x 0.15 x 0.05 mm ³
Theta range for data collection	1.19 to 26.37°.
Index ranges	-16 =h =17, -18 =k =18, -21 =l =21
Reflections collected	36922
Independent reflections	13380 [R(int) = 0.0800]
Completeness to theta = 25.00°	98.9 %
Max. and min. transmission	0.9594 and 0.8850
Refinement method	Full-matrix least-squares on F ²
Data / restraints / parameters	13380 / 0 / 736
Goodness-of-fit on F ²	0.906
Final R indices [I>2σ(I)]	R1 = 0.0605, wR2 = 0.1507
R indices (all data)	R1 = 0.0905, wR2 = 0.1642
Largest diff. peak and hole	0.811 and -0.413 e.Å ⁻³

2.7 References

- (1) Garibay, S. J.; Stork, J. R.; Cohen, S. M. *Prog. Inorg. Chem.* **2009**, *56*, 335-378.
- (2) Kitagawa, S.; Noro, S.-i.; Nakamura, T. *Chem. Commun.* **2006**, 701-707.
- (3) Byrd, H.; Buff, R. S.; Butler, J. M.; Gray, G. M. *J. Chem. Cryst.* **2003**, *33*, 515-519.
- (4) Chiang, W.; Ho, D. M.; Van Engen, D.; Thompson, M. E. *Inorg. Chem.* **1993**, *32*, 2886-2893.
- (5) Cho, S. H.; Ma, B.; Nguyen, S. T.; Hupp, J. T.; Albrecht-Schmitt, T. E. *Chem. Commun.* **2006**, 2563-2565.
- (6) Jeon, Y. M.; Heo, J.; Mirkin, C. A. *J. Am. Chem. Soc.* **2007**, *129*, 7480-7481.
- (7) Zhou, H.; Strates, K. C.; Muñoz, M. A.; Little, K. J.; Pajerowski, D. M.; Meisiel, M. W.; Talham, D. R.; Lachgar, A. *Chem. Mater.* **2007**, *19*, 2238-2246.
- (8) Kitaura, R.; Onoyama, G.; Sakamoto, H.; Matsuda, R.; Noro, S.; Kitagawa, S. *Angew. Chem. Int. Ed.* **2004**, *43*, 2684-2687.
- (9) Song, F.; Wang, C.; Falkowski, J. M.; Ma, L.; Lin, W. *J. Am. Chem. Soc.* **2010**, *132*, 15390-15398.
- (10) Falkowski, J. M.; Wang, C.; Liu, S.; Lin, W. *Angew. Chem. Int. Ed.* **2011**, *50*, 8674-8678.
- (11) Shultz, A. M.; Farha, O. K.; Adhikari, D.; Sarjeant, A. A.; Hupp, J. T.; Nguyen, S. T. *Inorg. Chem.* **2011**, *50*, 3174-3176.
- (12) Shultz, A. M.; Sarjeant, A. A.; Farha, O. K.; Hupp, J. T.; Nguyen, S. T. *J. Am. Chem. Soc.* **2011**, *133*, 13252-13255.

- (13) Suslick, K. S.; Bhyrappa, P.; Chou, J. H.; Kosal, M. E.; Nakagaki, S.; Smithenry, D. W.; Wilson, S. R. *Acc. Chem. Res.* **2005**, *38*, 283-291.
- (14) Goldberg, I. *Chem. Commun.* **2005**, 1243-1254.
- (15) Kosal, M. E.; Chou, J. H.; Wilson, S. R.; Suslick, K. S. *Nat. Mater.* **2002**, *1*, 118-121.
- (16) Kempe, R. *Z. Anorg. Allg. Chem.* **2005**, *631*, 1038-1040.
- (17) Smithenry, D. W.; Wilson, S. R.; Suslick, K. S. *Inorg. Chem.* **2003**, *42*, 7719-7721.
- (18) Eddaoudi, M.; Kim, J.; Rosi, N.; Vodak, D.; Wachter, J.; O'Keeffe, M.; Yaghi, O. M. *Science* **2002**, *295*, 469-472.
- (19) Wood, T. E.; Thompson, A. *Chem. Rev.* **2007**, *107*, 1831-1861.
- (20) Halper, S. R.; Cohen, S. M. *Inorg. Chem.* **2005**, *44*, 486-488.
- (21) Ockwig, N. W.; Delgado-Friedrichs, O.; O'Keeffe, M.; Yaghi, O. M. *Acc. Chem. Res.* **2005**, *38*, 176-182.
- (22) Murphy, D. L.; Malachowski, M. R.; Campana, C. F.; Cohen, S. M. *Chem. Commun.* **2005**, 5506-5508.
- (23) Stork, J. R.; Thoi, V. S.; Cohen, S. M. *Inorg. Chem.* **2007**, *46*, 11213-11223.
- (24) Thoi, V. S.; Stork, J. R.; Magde, D.; Cohen, S. M. *Inorg. Chem.* **2006**, *45*, 10688-10697.
- (25) Eddaoudi, M.; Moler, D. B.; Li, H.; Chen, B.; Reineke, T. M.; O'Keeffe, M.; Yaghi, O. M. *Acc. Chem. Res.* **2001**, *34*, 319-330.
- (26) Rosi, N. L.; Kim, J.; Eddaoudi, M.; Chen, B.; O'Keeffe, M.; Yaghi, O. M. *J. Am. Chem. Soc.* **2005**, *127*, 1504-1518.

- (27) Chae, H. K.; Siberio-Perez, D. Y.; Kim, J.; Go, Y.; Eddaoudi, M.; Matzger, A. J.; O'Keeffe, M.; Yaghi, O. M. *Nature* **2004**, *427*, 523-527.
- (28) Ke, Y.; Collins, D. J.; Sun, D.; Zhou, H. C. *Inorg. Chem.* **2006**, *45*, 1897-1899.
- (29) Brückner, C.; Zhang, Y.; Rettig, S. J.; Dolphin, R. *Inorg. Chim. Acta* **1997**, *263*, 279-286.
- (30) Telfer, S. G.; Wuest, J. D. *Chem. Commun.* **2007**, 3166-3168.
- (31) Barthelet, K.; Marrot, J.; Riou, D.; Ferey, G. *Angew. Chem. Int. Ed.* **2002**, *41*, 281-284.

Chapter 3. The Use of Postsynthetic Modification for the Incorporation Novel Functionality into MOFs

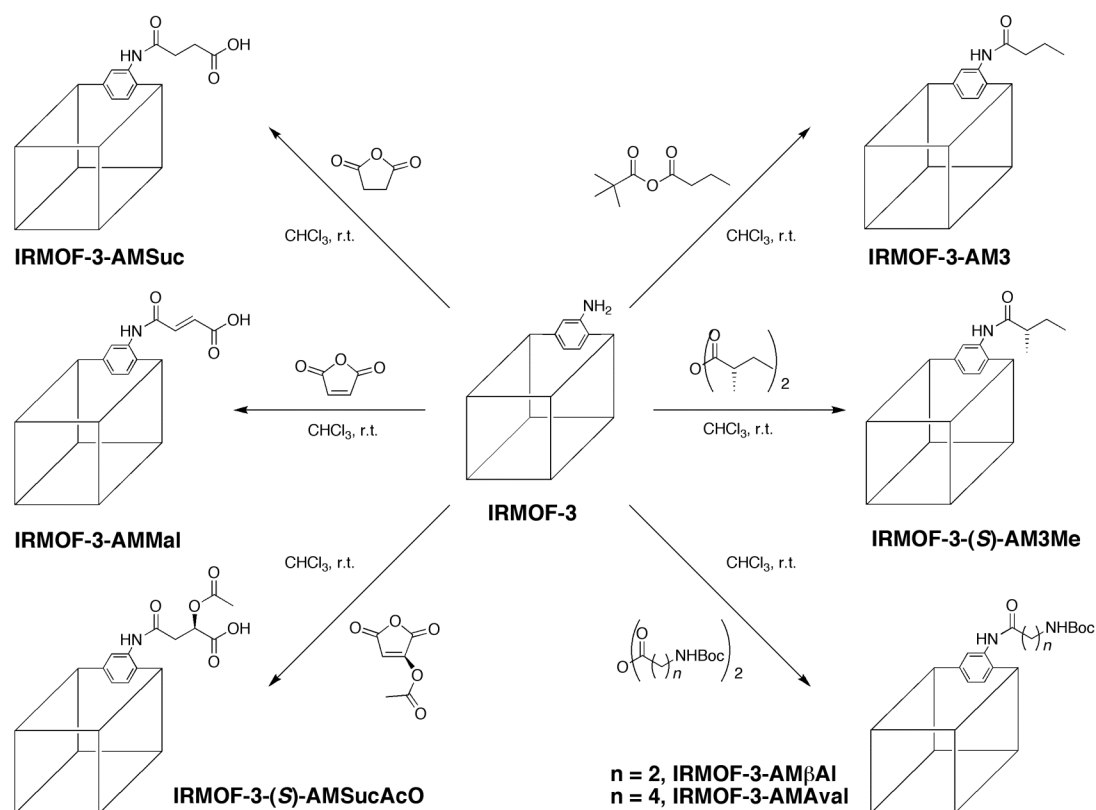
3.1 Introduction

The two methods for introducing functionality into MOFs, prefunctionalization,^{1,2} which is the direct use of a functionalized ligand during MOF synthesis and postsynthetic modification (PSM)³⁻⁵ which introduces functionality through chemical alterations on a pre-formed MOF were discussed in Chapter 1. Chapter 2 exemplified the difficulties associated with introducing functionality through a prefunctionalization approach. As discussed earlier, the incorporation of functional groups on the linking ligands can introduce steric, solubility, and metal-coordinating characteristics that can interfere with MOF formation. Our group⁶⁻¹⁰ and others¹¹⁻²⁰ have recently demonstrated the practical use of PSM to produce functionalized systems by targeting the organic linking group of pre-fabricated MOF crystals. More specifically, our efforts have focused on the heterogeneous acylation with linear anhydrides of the pendant amino group of 2-amino-1,4-benzenedicarboxylate (NH₂-BDC) inside a variety of MOFs.¹⁰ In previous studies IRMOF-3 was shown to undergo modification with linear alkyl chain anhydrides^{6,8} and isocyanates⁹ to produce amide- and urea-functionalized materials. The versatile nature of PSM provides an opportunity to develop MOFs with a variety of novel functionalities through diverse reagents and organic reactions. In this chapter, new postsynthetic approaches that allow for the incorporation of novel functional entities into the MOF structure will be described. Among the new findings described here are: 1) introduction of amine derivatives by use of *N*-Boc (Boc= *tert*-butyloxycarbonyl) aminoanhydrides; 2) generation of free carboxylic groups using cyclic anhydrides; 3)

generation of chiral MOFs by modification with chiral anhydrides; 4) selective transformation of a MOF with *tert*-butyl-containing asymmetric anhydrides.

3.2 Results and Discussion

Seven diverse anhydrides were examined for their ability to modify IRMOF-3 and generate new functionalized MOF systems. The anhydrides studied included two Boc-protected aminoanhydrides (β -alanine anhydride and aminovaleric anhydride), a chiral alkyl anhydride ((*S*)-2-methylbutyric anhydride), three cyclic anhydrides (maleic anhydride, succinic anhydride, and (*S*)-(-)-2-acetoxysuccinic anhydride), and an asymmetric anhydride (butyric pivalic anhydride) (Scheme 3-1).



Scheme 3-1. Postsynthetic modification reactions performed with IRMOF-3 using a wide variety of functionalized anhydrides.

The modifications were performed under various reaction conditions, given the diverse properties of the reagents (e.g., solubility in CHCl_3 , reactivity, etc.), in order to achieve high conversions and maintain good crystal quality with each reagent. Percent conversion were determined by using peak integration from ^1H NMR of digested samples. By comparing the relative areas of the singlet aromatic resonance (corresponding to the C3-position) of the modified and unmodified dicarboxylate ligands the conversion was obtained (Table 3-1). The bulk crystallinity of each modified IRMOF-3 was evaluated by powder X-ray diffraction (PXRD); modified IRMOF-3 samples have been shown to display powder patterns essentially identical to unmodified IRMOF-3 (Figure 3-1). Additionally, the thermal stability of modified samples were evaluated by thermogravimetric analysis (TGA), which are generally comparable to that of IRMOF-3 ($T_d \sim 430^\circ\text{C}$) (Figure 3-1).

Table 3-1. Percent conversions of PSM reactions with IRMOF-3 and different anhydrides as determined by ^1H NMR. Values listed are an average (with standard deviations) of at least three independent experiments.

IRMOF-3-	Reagent	Reaction Conditions	% Conversion
AM β Ala	Boc- β -alanine anhydride	2 equiv anhydride, 2 mL CHCl_3 , 2 d	7 \pm 1
AMAval	Boc-aminovaleric anhydride	2 equiv anhydride, 4 mL CHCl_3 , 2 d	14 \pm 8
(<i>S</i>)-AM3Me	(<i>S</i>)-(+)-2-methylbutyric anhydride	2 equiv anhydride, 2 mL CHCl_3 , 5 d	99 \pm 1
AMMal	Maleic anhydride	0.5 equiv anhydride, 2 mL CHCl_3 , 1 d	49 \pm 1
AMSuc	Succinic anhydride	0.5 equiv anhydride, 2 mL CHCl_3 , 1 d	49 \pm 1
(<i>S</i>)-AMSucAcO	(<i>S</i>)-(-)-2-acetoxysuccinic anhydride	0.5 equiv anhydride, 2 mL CHCl_3 , 1 d	41 \pm 3
AM3	Butyric pivalic anhydride	2 equiv anhydride, 8 mL CHCl_3 , 3 d	74 \pm 2

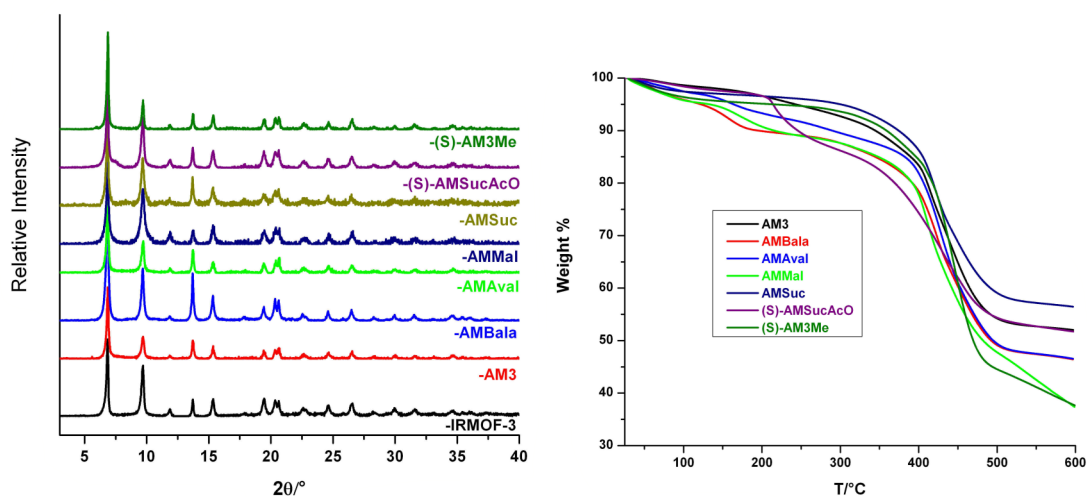


Figure 3-1. Powder X-ray diffraction (PXRD) patterns of anhydride modified IRMOF-3 samples (left). Thermogravimetric analysis (TGA) of modified IRMOF-3 samples (right).

Conversion was found to be dependent on the nature of the reagent applied. Boc-protected aliphatic aminoanhydrides, β -alanine anhydride, and aminovaleric anhydride, were found to show poor reactivity (<15%) with IRMOF-3 (Table 3-1, Figure 3-2). The low conversion is attributed to the bulky Boc protecting groups. Under similar conditions, linear alkyl anhydrides with analogous chain lengths were found to undergo greater than 50% conversion.⁸ On account of their metal-coordinating characteristics it is difficult to introduce alkylamine functionalities into the pores of MOFs with amine based ligands through solvothermal synthesis. Because of their affinity for CO₂ the incorporation of pendant alkylamine functionalities into MOFs offers the opportunity for their utilization as selective capture materials.^{21,22} The production of IRMOF-3-AM β Ala and IRMOF-3AMAVAl would allow access to unprecedented covalently attached aliphatic amine functionality. In a related study, Boc protected amines were utilized by Telfer et al. as a protection strategy to obtain amine and proline functionalities within MOFs.^{23,24}

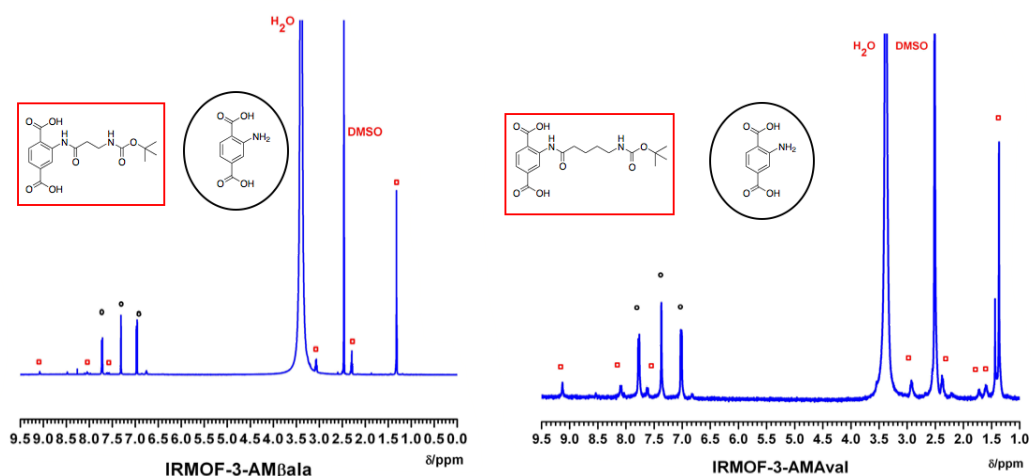


Figure 3-2. ¹H NMR spectra of digested IRMOF-3 modified with Boc- β -alanine anhydride (left) and Boc-aminovaleric anhydride (right) for 2 days. NH₂-BDC resonances are denoted by black circles and RCONH-BDC resonances by red squares.

In contrast to the Boc-protected aminoanhydrides, (*S*)-2-methylbutyric anhydride displayed nearly quantitative conversion to give IRMOF-3-(*S*)-AM3Me, similar to small linear alkyl anhydrides that have been previously studied (Figure 3-3).^{6,8} While there have been several reports utilizing chiral ligands in the construction of chiral MOFs,²⁵ this latter finding deserves particular note, as it is the first time an achiral MOF has been converted into a chiral MOF material via a PSM approach.

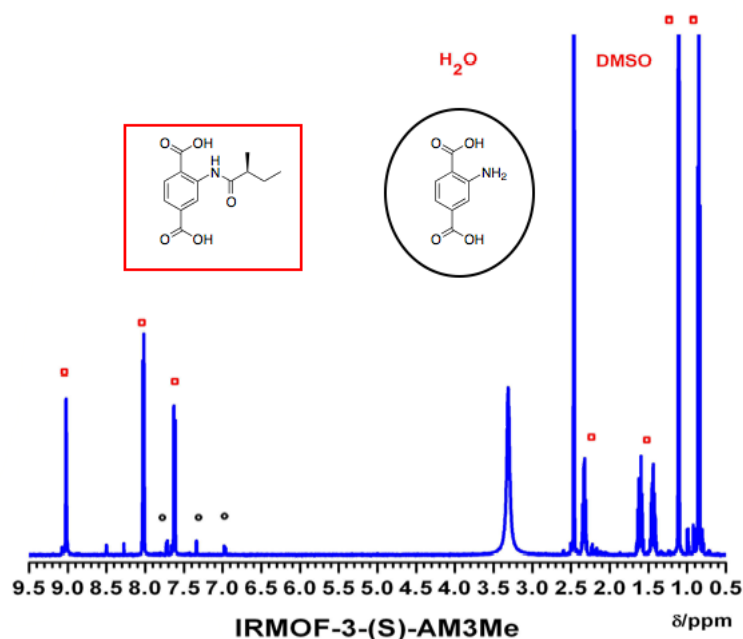


Figure 3-3. ¹H NMR spectra of digested IRMOF-3 modified with (*S*)-(+)-2-methylbutyric anhydride for 5 days.

The cyclic anhydrides, maleic anhydride, succinic anhydride, and (*S*)-(-)-2-acetoxysuccinic anhydride were found to quantitatively react with IRMOF-3 (using 0.5 equiv gave ~50% conversion). ¹H NMR and ESI-MS analysis indicated that upon modification these anhydrides formed open chain products (as opposed to cyclic imides) generating pendant carboxylic acid groups (Figure 3-4, Figure 3-5). This is consistent with PSM studies using maleic and succinic anhydride reported by Fujita et

al. that were structurally verified by single-crystal X-ray diffraction.²⁶ ^1H NMR indicates that IRMOF-3 modified with (*S*)-(-)-2-acetoxysuccinic anhydride produces two distinct isomeric modified groups with 41% and 6% conversion, respectively (Figure 3-6). The asymmetry of acetoxysuccinic anhydride can allow ring opening in two directions. Based on literature reports, the most likely product possesses an amide with an acetoxy group adjacent to the carboxylic acid (see Figure 3-6).²⁷

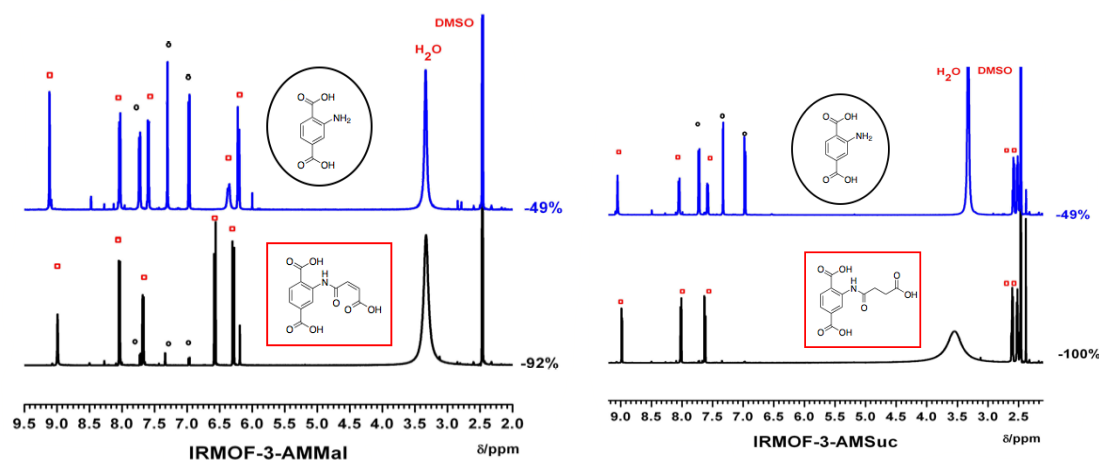


Figure 3-4. ^1H NMR spectra of digested IRMOF-3 modified with maleic (left) and succinic (right) anhydride for 5 days (black) and 1 day (blue).

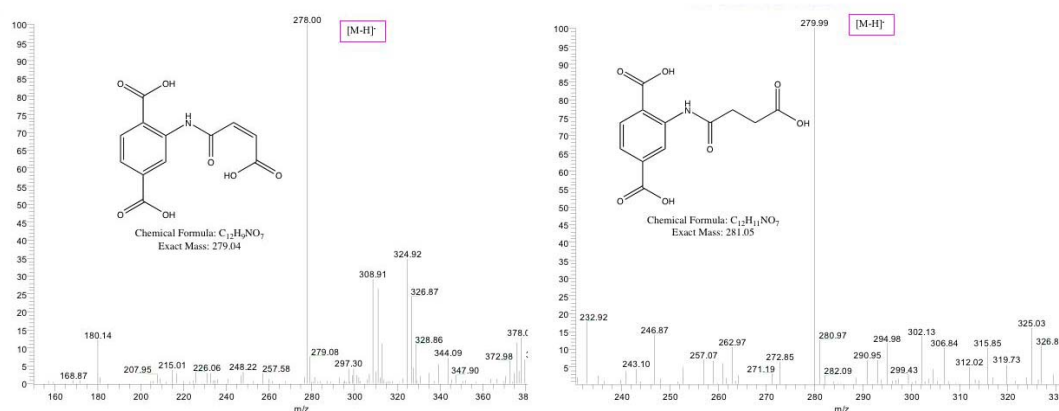


Figure 3-5. ESI-MS(-) of the digested IRMOF-3-AMMal (left) and IRMOF-3-AMSuc (right) showing the mass peaks corresponding to the maleic and succinic acid functionalized BDC ligands.

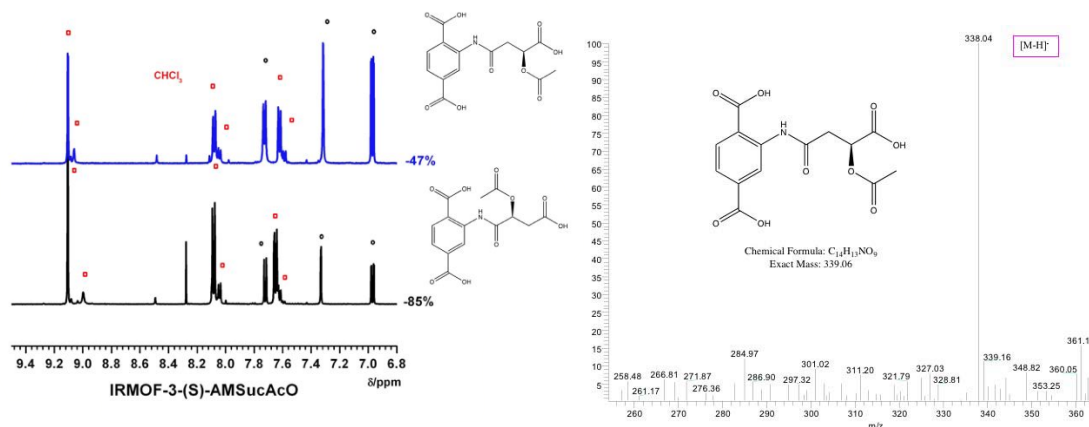


Figure 3-6. Downfield region of ^1H NMR spectra of digested IRMOF-3 modified with (*S*)-(-)-2-acetoxysuccinic anhydride for 5 days (black) and 1 day (blue) with isomeric amide modified products (left). ESI-MS(-) of the digested IRMOF-3-(*S*)-AMSucAcO (right).

While IRMOF-3 could be $>85\%$ converted under optimized reaction conditions (2 equiv of anhydride, 5 days, $25\text{ }^\circ\text{C}$), these highly-modified samples showed loss of crystal quality (Figure 3-7). This was confirmed by Brunauer-Emmett-Teller (BET) surface area measurements, performed with N_2 , which gave extremely low surface areas (e.g. $29\text{ m}^2\text{g}^{-1}$ for IRMOF-3-AMMal at 92% conversion, Table 3-2). Given that these modified MOFs contain large numbers of free carboxylate groups, it is proposed that the acidic nature and coordinating ability of these carboxylate groups disrupt the material resulting in a phase change and collapse.

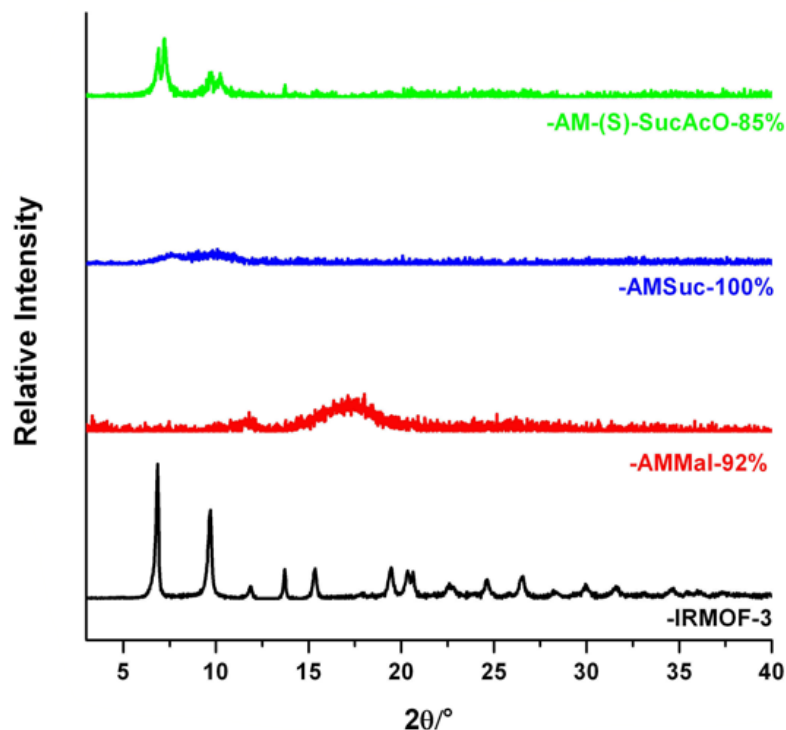


Figure 3-7. Powder X-ray diffraction (PXRD) patterns of IRMOF-3 that were ‘fully modified’ modified samples with cyclic anhydrides.

Table 3-2. BET surface areas (m^2g^{-1}) of modified IRMOF-3, with different percent conversions of cyclic anhydrides as determined by ^1H NMR. The results of two independent experiments are shown.

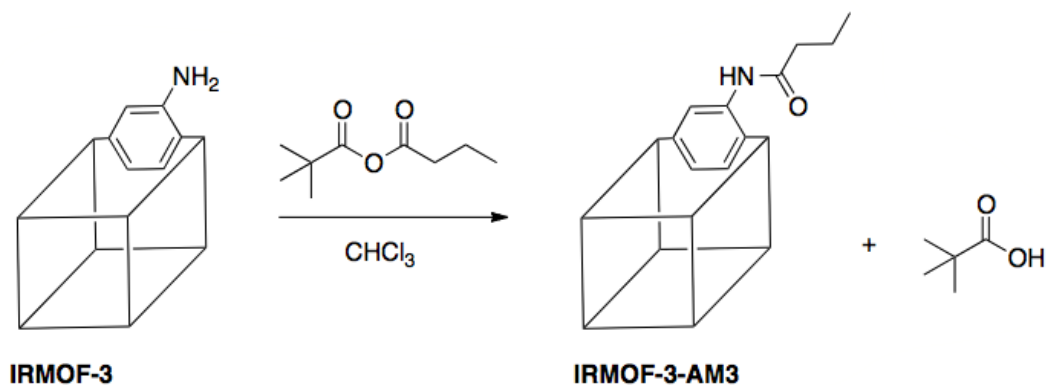
IRMOF	AMMal	AMMal	AMSuc	AMSuc	(S)-AMSucAcO
-3-	(92%)	(49%)	(99%)	(49%)	(47%)
Trial 1	29	2025	1.10	1558	1217
Trial 2	3	1785	3.20	1212	1021

In an effort to circumvent the aforementioned degradation of IRMOF-3, the framework was reacted with half equivalents (0.1mmol) of cyclic anhydrides. ^1H NMR indicates that IRMOF-3 treated with cyclic anhydrides produced materials with ~50 % carboxylate functionalites. These moderately functionalized MOFs were found

to be structurally stable and possessed porosity as indicated by PXRD and BET measurements (Figure 3-1, Table 3-2). In view of the difficulty associated with incorporating free carboxylic acids into MOFs through conventional solvothermal synthesis, the facile preparation of IRMOF-3 -AMMal, -AMSuc and -(*S*)-AMSucAcO highlights the significance of the PSM approach. Indeed, in a subsequent study, Yaghi et al. utilized analogous ring-opening reactions with heterocycles to generate sulfonate groups within IRMOF-3.²⁸ Furthermore, IRMOF-3-(*S*)-AMSucAcO represents the introduction of both a chiral substituent and an acidic group in a single PSM event.

The development of asymmetric anhydrides for selective covalent modification was explored with butyric pivalic anhydride. Our studies have shown that utilization of anhydrides for PSM can be restricted by the production of strongly acidic byproducts which results in degradation of the IRMOF lattice. For example, acylation of IRMOF-3 with trifluoroacetic anhydride produces trifluoroacetic acid, which destroys the framework by catalyzing hydrolysis of the secondary building unit.²⁹ We reasoned that such functional groups could be delivered to IRMOF-3 in the form of an asymmetric anhydride, where reaction of IRMOF-3 with an asymmetric anhydride would strongly favor delivery of one substituent over another. The lack of reactivity of *tert*-butyl anhydride and *tert*-butyl isocyanate with IRMOF-3 in previous studies,^{9,10} ascribed to the sterics of the *tert*-butyl group, offered an opportunity to exploit steric effects to selectively incorporate functional groups through asymmetric anhydrides. As a proof of concept, treatment of IRMOF-3 with the asymmetric anhydride produced the previously described IRMOF-3-AM3 (Scheme 3-2). The ¹H NMR spectra of the modified sample indicates a conversion of ~74% which is lower than

that of IRMOF-3 treated with butyric anhydride (~99%) under identical reaction conditions (Figure 3-8).⁸ The reduced conversion likely correlates with the introduction of the bulky *tert*-butyl group. Nonetheless, a reasonable conversion to the modified product is obtained and shows that the mixed anhydride can be used to deliver groups to the MOF structure without degradation of its framework (Figure 3-1). The utilization of *tert*-butyl-based asymmetric anhydrides would provide a synthetic route towards selective modification of novel groups and circumvents degradation by generating the benign pivalic acid byproduct.



Scheme 3-2. Postsynthetic modification of IRMOF-3 using a *tert*-butyl-based asymmetric anhydride and pivalic acid byproduct.

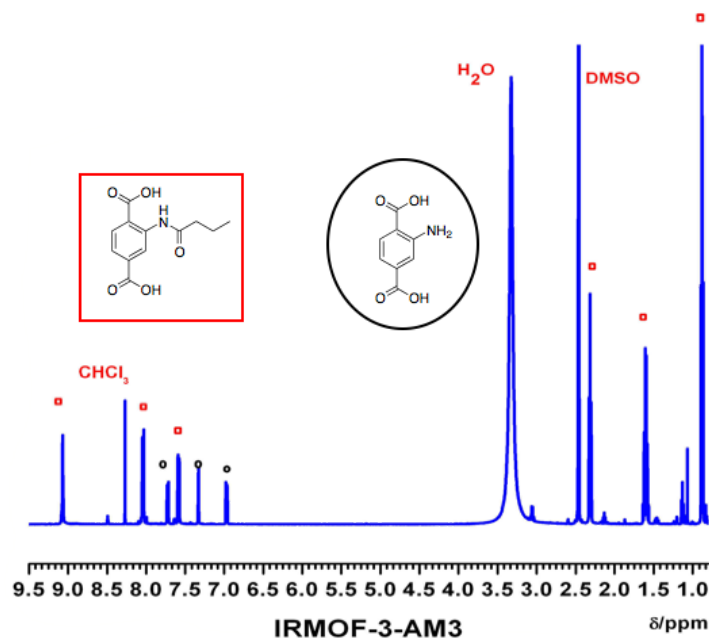


Figure 3-8. ^1H NMR spectra of digested IRMOF-3 modified with pivalic butyric anhydride for 3 days.

3.3 Conclusions

In summary, the findings presented in this chapter demonstrate that postsynthetic modification is a versatile method for the functionalization of MOFs. IRMOF-3 has been postsynthetically modified with alkyl and cyclic anhydrides. A *tert*-butyl based asymmetric anhydride was shown to selectively deliver a ‘payload’ moiety to IRMOF-3. This could potentially be utilized to deliver novel chemical groups that generate damaging byproducts. Other anhydrides successfully transformed IRMOF-3 into a diverse set of new IRMOFs functionalized with protected aliphatic amines, carboxylate, and chiral groups, which can be explored for applications in CO_2 sequestration, enantioselective separation and catalysis.

3.4 Experimental Methods

General. Starting materials and solvents were purchased and used without further purification from commercial suppliers (Sigma-Aldrich, Alfa Aesar, EMD, TCI, Cambridge Isotope Laboratories, Inc., and others). IRMOF-3 was synthesized and activated as described previously.^{10,30} Boc- β -alanine anhydride was synthesized as described previously.³¹

Butyric pivalic anhydride. Butyric acid (0.92 mL, 10 mmol) was added to a solution of THF (20 mL) containing triethylamine (1.39 mL, 10 mmol) and placed in an ice bath. Trimethylacetyl chloride (1.23 mL, 10 mmol) was added to the mixture and stirred for 30 min at 0 °C. The reaction was allowed to reach room temperature and stirred for an additional 30 min. The white triethylamine chloride salt was filtered and the solvent was removed under vacuum producing an oil. Yield = 85%. ¹H NMR (500 MHz, CDCl₃): δ 2.4 (t, 2 H), 1.7 (q, 2H), 1.2 (s, 9H), 0.9 (t, 3H). ESI-MS m/z 189.98 [M+NH₄]⁺, 195.01 [M+Na]⁺.

Boc-aminovaleric acid. 5-Aminovaleric acid (1.31 g, 11.2 mmol) was dissolved in 2:1 Dioxane:H₂O (30 mL). 10 mL of a 1.0 M NaOH solution was added and the mixture was placed in an ice bath. Di-*tert*-butyl dicarbonate (2.61 g, 12.3 mmol) was added to the mixture at 0 °C. The solution was allowed to reach room temperature and stirred ~18 h. The solvent was removed under rotary vacuum and redissolved with 10 mL of EtOAc. 10 mL of a 5% citric acid solution was added and the organic layer was collected and then washed with brine. The organic layer was dried over MgSO₄, filtered, and dried under vacuum producing a colorless oil. Approximately 20 mL of pentane was added, precipitating a white solid. The mixture

was filtered producing a white solid. Yield = 27%. $^1\text{H NMR}$ (500 MHz, CDCl_3): δ 4.6 (s, br, 1H), 3.1 (d, 2H), 2.3 (t, 2H), 1.6 (q, 2H), 1.5 (q, 2H), 1.4 (s, 9H). ESI-MS m/z 216.0 $[\text{M-H}]^-$.

Boc-aminovaleric anhydride. Boc-aminovaleric acid (0.65 g, 3 mmol) was dissolved with 3 mL of anhydrous CH_2Cl_2 and placed in an ice bath. A solution of DCC (0.3 g, 1.4 mmol) in 2 mL of anhydrous CH_2Cl_2 was added. The mixture was stirred for 15 min at 0 °C. The solution was allowed to warm to room temperature and stirred for 2 h. The mixture was filtered and dried under vacuum. The colorless oil was dissolved in EtOAc to precipitate any remaining DCC and filtered. The solvent was removed by rotary evaporation producing an oil. Yield = 49%. $^1\text{H NMR}$ (500 MHz, CDCl_3): δ 4.6 (s, br, 1H), 3.1 (d, 2H), 2.5 (t, 2H), 1.67 (q, 2H) 1.54 (q, 2H), 1.4 (s, 9H). ESI-MS m/z 416.91 $[\text{M+H}]^+$.

IRMOF-3-AM β Ala. Approximately 60 mg of IRMOF-3 (ca. 0.20 mmol equiv of $-\text{NH}_2$) was placed in a vial with 2 equiv (0.4 mmol) of Boc protected β -alanine anhydride dissolved in 2 mL of CHCl_3 . After allowing the sample to stand for 2 days, the solution was decanted and the crystals were washed with 3 \times 6 mL of CHCl_3 then soaked in 10 mL of pure CHCl_3 (i.e. without anhydride) for three days, with fresh CHCl_3 added every 24 h. After three days of soaking the crystals were stored in the last CHCl_3 solution until analyzed.

IRMOF-3-AM α Val. Approximately 60 mg of IRMOF-3 (ca. 0.20 mmol equiv of $-\text{NH}_2$) was placed in a vial with 2 equiv (0.4 mmol) of Boc-aminovaleric anhydride dissolved in 4 mL of CHCl_3 . After allowing the sample to stand for 2 days, the solution was decanted and the crystals were washed with 3 \times 6 mL of CHCl_3 then

soaked in 10 mL of pure CHCl_3 for three days, with fresh CHCl_3 added every 24 h. After three days of soaking the crystals were stored in the last CHCl_3 solution until analyzed.

IRMOF-3-(S)-AM3Me. Approximately 60 mg of IRMOF-3 (ca. 0.20 mmol equiv of $-\text{NH}_2$) was placed in a vial with 2 equiv (0.4 mmol) of (S)-(+)-2-methylbutyric anhydride dissolved in 2 mL of CHCl_3 . After allowing the sample to stand for 5 days, the solution was decanted and the crystals were washed with 3×6 mL of CHCl_3 then soaked in 10 mL of pure CHCl_3 for three days, with fresh CHCl_3 added every 24 h. After three days of soaking the crystals were stored in the last CHCl_3 solution until analyzed.

IRMOF-3-AMMal, IRMOF-3-AMSuc, IRMOF-3-(S)-AMSucAcO.

Approximately 60 mg of IRMOF-3 (ca. 0.20 mmol equiv of $-\text{NH}_2$) was placed in a vial with 0.5 equiv (0.1 mmol) of the cyclic anhydrides (maleic, succinic, and (S)-(-)-2-acetoxysuccinic anhydride, respectively) dissolved in 5 mL of CHCl_3 . After allowing the sample to stand for 1 day, the solution was decanted and the crystals were washed with 3×6 mL of CHCl_3 then soaked in 10 mL of pure CHCl_3 for three days, with fresh CHCl_3 added every 24 h. After three days of soaking the crystals were stored in the last CHCl_3 solution until analyzed.

IRMOF-3-AM3. Approximately 60 mg of IRMOF-3 (ca. 0.20 mmol equiv of $-\text{NH}_2$) was placed in a vial with 2 equiv (0.4 mmol) of butyric pivalic anhydride dissolved in 8 mL of CHCl_3 . After allowing the sample to stand for 3 d, the solution was decanted and the crystals were washed with 3×6 mL of CHCl_3 then soaked in 10

mL of pure CHCl_3 for three days, with fresh CHCl_3 added every 24 h. After three days of soaking the crystals were stored in the last CHCl_3 solution until analyzed.

Digestion and Analysis by ^1H NMR. ^1H NMR spectra were recorded on a JEOL ECA spectrometer (500 MHz). Approximately 5 mg of modified IRMOF-3 samples was dried under vacuum at room temperature or at 90 °C overnight and digested with sonication in 500 mL of d^6 -DMSO and 100 mL of dilute DCl (23 mL of 35% DCl in D_2O diluted with 1.0 mL of d^6 -DMSO).

Digestion and Analysis by ESI-MS. Electrospray ionization mass spectrometry (ESI-MS) was performed using a ThermoFinnigan LCQ-DECA mass spectrometer and the data was analyzed using the Xcalibur software suite. Crystals of modified IRMOF-3 (~0.1-1 mg) were digested in 1 mL of MeOH (or H_2O) with sonication.

Thermal Gravimetric Analysis. Samples were analyzed under a stream of dinitrogen using a TA Instrument Q600 SDT running from room temperature to 600 °C with a scan rate of 5 °C min^{-1} . Approximately 10-20 mg of modified IRMOF-3 samples were used for TGA measurements.

PXRD Analysis. PXRD data were collected at ambient temperature on a Bruker Advance D8 diffractometer at 40 kV, 40 mA for $K\alpha$ ($\lambda = 1.5418 \text{ \AA}$) with a scan speed of 0.3° min^{-1} , a step size of 0.02° in 2θ and a 2θ range of 3-40°. Approximately 15 mg of modified IRMOF-3 samples (typically soaked in CHCl_3) were air dried before PXRD analysis. The experimental backgrounds were corrected using the Jade 5.0 software package.

BET Surface Area Analysis. BET surface area (m^2g^{-1}) measurements were collected at 77 K by dinitrogen on an ASAP 2020 using volumetric technique. Approximately 40-60 mg of modified IRMOF-3 samples were evacuated on a vacuum line for 5-18 h. The sample was then transferred to a preweighed sample tube and degassed at 105 °C for approximately 24 h or until the outgas rate was <5 mmHg. The sample tube was re-weighed to obtain a consistent mass for the degassed modified IRMOF-3.

3.5 Acknowledgements

Text, schemes, and figures in this chapter, in part, are reprints of the materials published in the following papers: Garibay, S. J., Wang, Z., Tanabe, K. K., Cohen, S. M. "Postsynthetic Modification: A Versatile Approach Toward Multifunctional Metal-Organic Frameworks" *Inorg. Chem.* **2009**, *48*, 7341-7349. The dissertation author was the primary researcher and author for the data presented. The co-authors listed in these publications also participated in the research.

3.6 References

- (1) Deng, H.; Doonan, C. J.; Furukawa, H.; Ferreira, R. B.; Towne, J.; Knobler, C. B.; Wang, B.; Yaghi, O. M. *Science*, **2010**, *327*, 846-850.
- (2) Eddaoudi, M.; Kim, J.; Rosi, N.; Vodak, D.; Wachter, J.; O'Keeffe, M.; Yaghi, O. M. *Science* **2002**, *295*, 469-472.
- (3) Wang, Z.; Cohen, S. M. *Chem. Soc. Rev.* **2009**, *38*, 1315-1329.
- (4) Tanabe, K. K.; Cohen, S. M. *Chem. Soc. Rev.* **2011**, *40*, 498-519.
- (5) Cohen, S. M. *Chem. Sci.* **2010**, 32-36.
- (6) Wang, Z.; Cohen, S. M. *J. Am. Chem. Soc.* **2007**, *129*, 12368-12369.
- (7) Wang, Z.; Cohen, S. M. *Angew. Chem. Int. Ed.* **2008**, *47*, 4699-4702.
- (8) Tanabe, K. K.; Wang, Z.; Cohen, S. M. *J. Am. Chem. Soc.* **2008**, *130*, 8508-8517.
- (9) Dugan, E.; Wang, Z.; Okamura, M.; Medina, A.; Cohen, S. M. *Chem. Commun.* **2008**, 3366-3368.
- (10) Wang, Z.; Tanabe, K. K.; Cohen, S. M. *Inorg. Chem.* **2009**, *48*, 296-306.
- (11) Haneda, T.; Kawano, M.; Kawamichi, T.; Fujita, M. *J. Am. Chem. Soc.* **2008**, *130*, 1578-1579.
- (12) Kaye, S. S.; Long, J. R. *J. Am. Chem. Soc.* **2008**, *130*, 806-807.
- (13) Ingleson, M. J.; Barrio, J. P.; Bacsá, J.; Dickinson, C.; Park, H.; Rosseinsky, M. J. *Chem. Commun.* **2008**, 1287-1289.

- (14) Costa, J. S.; Gamez, P.; Black, C. A.; Roubeau, O.; Teat, S. J.; Reedijk, J. *Eur. J. Inorg. Chem.* **2008**, 1551-1554.
- (15) Ingleson, M. J.; Barrio, J. P.; Guilbaud, J. B.; Khimyak, Y. Z.; Rosseinsky, M. *J. Chem. Commun.* **2008**, 2680-2682.
- (16) Horike, S.; Dinca, M.; Tamaki, K.; Long, J. R. *J. Am. Chem. Soc.* **2008**, *130*, 5854-5855.
- (17) Hwang, Y. K.; Hong, D. Y.; Chang, J. S.; Jhung, S. H.; Seo, Y. K.; Kim, J.; Vimont, A.; Daturi, M.; Serre, C.; Ferey, G. *Angew. Chem. Int. Ed.* **2008**, *47*, 4144-4148.
- (18) Morris, W.; Doonan, C. J.; Furukawa, H.; Banerjee, R.; Yaghi, O. M. *J. Am. Chem. Soc.* **2008**, *130*, 12626-12627.
- (19) Ahnfeldt, T.; Gunzelmann, D.; Loiseau, T.; Hirsemann, D.; Senker, J.; Ferey, G.; Stock, N. *Inorg. Chem.* **2009**, *48*, 3057-3064.
- (20) Gadzikwa, T.; Lu, G.; Stern, C. L.; Wilson, S. R.; Hupp, J. T.; Nguyen, S. T. *Chem. Commun.* **2008**, 5493-5495.
- (21) Demessence, A.; D'Alessandro, D. M.; Foo, M. L.; Long, J. R. *J. Am. Chem. Soc.* **2009**, *131*, 8784-8786.
- (22) D'Alessandro, D. M.; Smit, B.; Long, J. R. *Angew. Chem. Int. Ed.* **2010**, *49*, 6058-6082.
- (23) Deshpande, R. K.; Minnaar, J. L.; Telfer, S. G. *Angew. Chem. Int. Ed.* **2010**, *49*, 4598-4602.
- (24) Lun, D. J.; Waterhouse, G. I.; Telfer, S. G. *J. Am. Chem. Soc.* **2011**, *133*, 5806-5809.
- (25) Lin, W. B. *J. Solid State Chem.* **2005**, *178*, 2486-2490.

- (26) Kawamichi, T.; Kodama, T.; Kawano, M.; Fujita, M. *Angew. Chem. Int. Ed.* **2008**, *47*, 8030-8032.
- (27) Faucaud, A. *Bull. Soc. Chim. France* **1963**, 873.
- (28) Britt, D.; Lee, C.; Uribe-Romo, F. J.; Furukawa, H.; Yaghi, O. M. *Inorg. Chem.* **2010**, *49*, 6387-6389.
- (29) Kaye, S. S.; Dailly, A.; Yaghi, O. M.; Long, J. R. *J. Am. Chem. Soc.* **2007**, *129*, 14176-14177.
- (30) Rowsell, J. L. C.; Yaghi, O. M. *J. Am. Chem. Soc.* **2006**, *128*, 1304-1315.
- (31) Li, B.; Martin, A. L.; Gillies, E. R. *Chem. Commun.* **2007**, 5217-5219.

Chapter 4. The Use of Tandem Postsynthetic Modification for the Incorporation of Multifunctionality into MOFs

4.1 Introduction

The modular nature of MOFs via their inorganic and organic components makes them ideally suited for strategies aimed at fine-tuning their chemical properties. The combination of different functionalities (i.e. geometrical constraints, hydrophobicity, catalytic metal centers) should allow MOFs to facilitate complex cascade reactions that are often found in enzymes.^{1,2} One way of introducing multiple functionalities into the pores of a MOF is through the use of different functionalized linkers during synthesis. Indeed, there has been an increase use of this mixed-component strategy.³⁻¹⁷

Recently, multi-functionalized analogues of IRMOFs named Multivariate MOFs (MTV-MOFs) were constructed through the use of multiple BDC analogues generating MOFs with as many as eight different functionalites within a single framework.⁸ Incorporation into the MOF structure should proceed in an equivalent manner assuming that the different linkers have similar length, donor groups and solubilities. However, each functionalized linker possess distinct solubility, steric, and metal-coordinating characteristics. The linkers additionally compete with each other during MOF formation making the overall inclusion of certain functionalities unpredictable. Indeed, while introduction of multiple functional groups was realized in the MTV-MOFs, precise control over the relative abundance of different functional groups within the MOF cannot be controlled. For instance, a 1:1 mixture of BDC and 2-amino-1,4-benzenedicarboxylic acid (NH₂-BDC) ligands utilized for MOF construction produced a framework containing a 1:0.57 ratio of the ligands.

An alternative strategy for the incorporation of multifunctionality is the epitaxial growth or layering of a MOF on a different MOF.¹⁸⁻²⁵ Under some circumstances, a heterogeneous material with two distinct MOF ‘shells’ containing different functionalized linkers may be obtained. Recently, Matzger and coworkers utilized pre-nascent IRMOF-1 or IRMOF-3 crystals seeds and carefully exchanged their respective mother liquors.¹⁹ The resulting MOFs had ‘core-shell’ structures where cores of either MOF were surrounded by different functionalized MOFs. The formation of core-shell MOFs requires the structures of two individual ‘parent’ MOFs to be closely related. Meaning that multiple incorporation of functionalities is restricted to certain frameworks through this method.

Most of the early studies on MOF PSM showed the introduction of only a single chemical modification into the MOF lattice. Only a handful demonstrated that more than one chemical reagent could be used to covalently modify a single MOF structure.^{26,27} The degree of modification by a reagent with a given MOF can be modulated by the concentration of the reagent(s), reaction temperature, and reaction time.²⁸ Given the ability to control the degree of modification in a MOF it is possible to incorporate multiple functionalities into a single framework through partial, step-wise modification referred to as termed ‘tandem postsynthetic modification’. In a previous study, tandem PSM of IRMOF-3 with two different anhydrides was reported.²⁶ IRMOF-3 was modified with alkyl and olefin containing acetic and crotonic anhydride reagents (Figure 4-1). In an effort to expand upon the range of functionality within a MOF, a series of tandem postsynthetic modifications was attempted with various anhydrides and isocyanates on a single MOF lattice. In this

chapter, the modification of the IRMOF-3 lattice with multiple reagents to produce several different amide and urea functionalized frameworks materials is described.

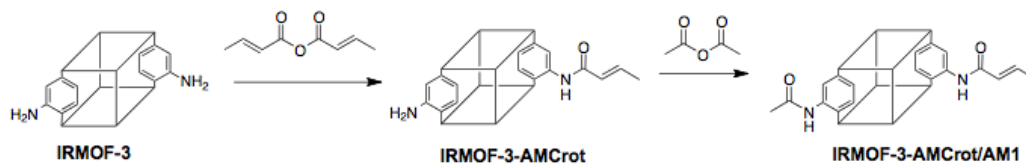
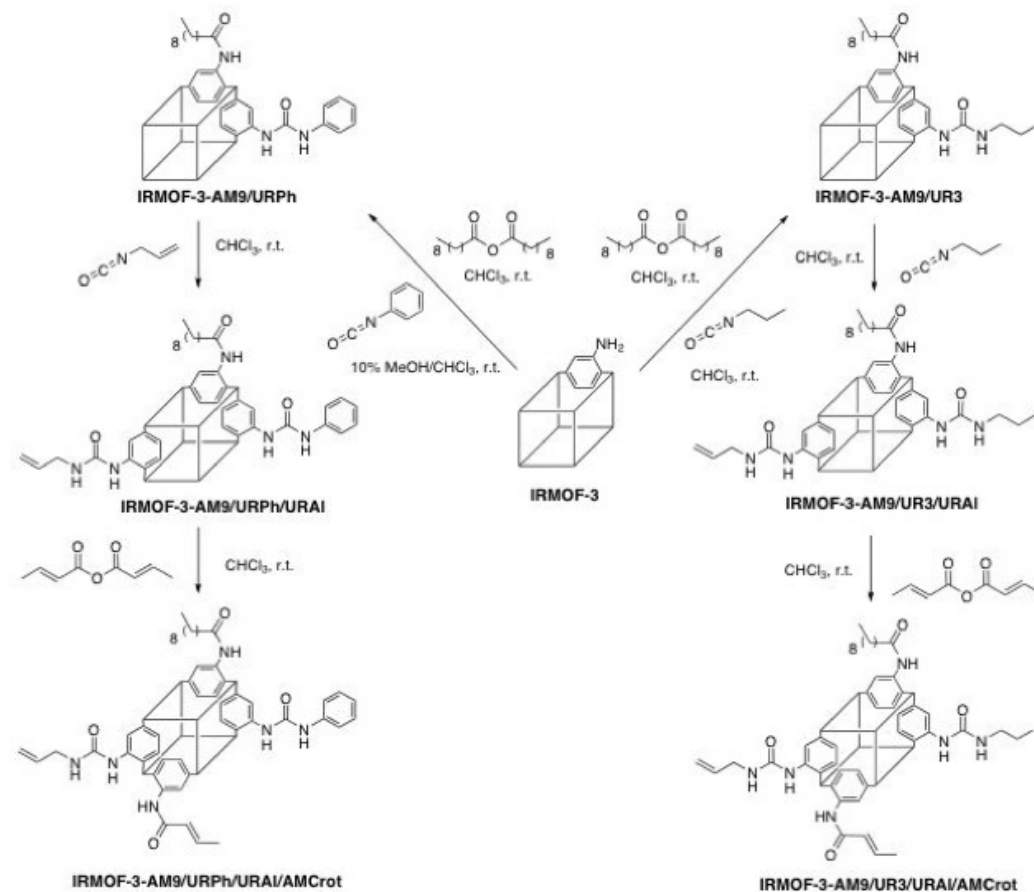


Figure 4-1. ‘Tandem’ step-wise postsynthetic modification of IRMOF-3.

4.2 Results and Discussion

Five diverse reagents were examined for their ability to modify IRMOF-3 and generate new multifunctionalized MOF systems (Scheme 4-1). The reagents utilized included two anhydrides (decanoic anhydride and crotonic anhydride), and three isocyanates (propyl, phenyl, and allyl isocyanates). Conversion was determined by using ^1H NMR spectroscopy upon digestion of the modified MOFs in dilute acid. The conversion was obtained by comparing the relative areas of the singlet aromatic resonance (corresponding to the C3-position) or the doublet resonances associated with the phenyl (C5 or C6 position) protons of the modified to that of the aromatic resonances of the unmodified dicarboxylate ligands (Table 4-1).



Scheme 4-1. Scheme showing the reagents decanoic anhydride (AM9), propyl isocyanate (UR3), phenyl isocyanate (URPh), allyl isocyanate (URAI), and crotonic anhydride (AMCrot) used for multiple PSM reactions with IRMOF-3.

Table 4-1. Percent Conversion of Multiple Postsynthetic Modification Reaction with IRMOF-3 and Different Anhydrides or Isocyanates As Determined by ^1H NMR^a

IRMOF-3-	Reagents ^b	% Conversion ^a			
		AM9	UR3 or URPh	URAI	AMCrot
AM9/UR3	(1) DA	21 ± 1	21 ± 3		
	(2) PI				
AM9/UR3/URAI	(1) DA	21 ± 4	22 ± 1	23 ± 1	
	(2) PI				
	(3) AI				
AM9/UR3/URAI/AMCrot- <i>a</i>	(1) DA	24 ± 4	18 ± 6	21 ± 3	17 ± 1
	(2) PI				
	(3) AI				
	(4) CA				
AM9/UR3/URAI/AMCrot- <i>b</i> ^c	(1) DA	23 ± 1	8 ± 2	13 ± 2	17 ± 1
	(2) PI				
	(3) AI				
	(4) CA				
AM9/URPh	(1) DA	24 ± 2	32 ± 2		
	(2) PhI				
AM9/URPh/URAI	(1) DA	26 ± 5	28 ± 2	20 ± 3	
	(2) PhI				
	(3) AI				
AM9/URPh/URAI/AMCrot	(1) DA	20 ± 1	30 ± 1	20 ± 1	8 ± 1
	(2) PhI				
	(3) AI				
	(4) CA				

^a Values listed are an average (with standard deviations) of at least three independent experiments. ^b AI = allyl isocyanate; CA = crotonic anhydride; DA = decanoic anhydride; PI = propyl isocyanate; PhI = phenyl isocyanate. ^c Propyl and allyl isocyanate reaction times were reduced to 3 h each.

In an effort to determine whether two distinct types of functionalities could be introduced into a MOF, IRMOF-3 was treated sequentially with two equivalents of the relatively large decanoic anhydride and then with eight equivalents of the small propyl isocyanate. The ^1H NMR spectra of the modified MOF designated IRMOF-3-AM9/UR3, shows two singlet resonances associated with the phenyl (C-3 position)

protons of the corresponding amide (AM9) and urea (UR3) dicarboxylate products (Figure 4-1). The spectrum also contains two sets of doublet resonances associated with the phenyl (C-5 and C-6 positions) protons of both the amide- and urea-modified products, clearly demonstrating modification by both reagents. IRMOF-3-AM9/UR3 was found to contain ~21% of both the amide and urea modified products while 58% remains unmodified (i.e. NH₂-BDC).

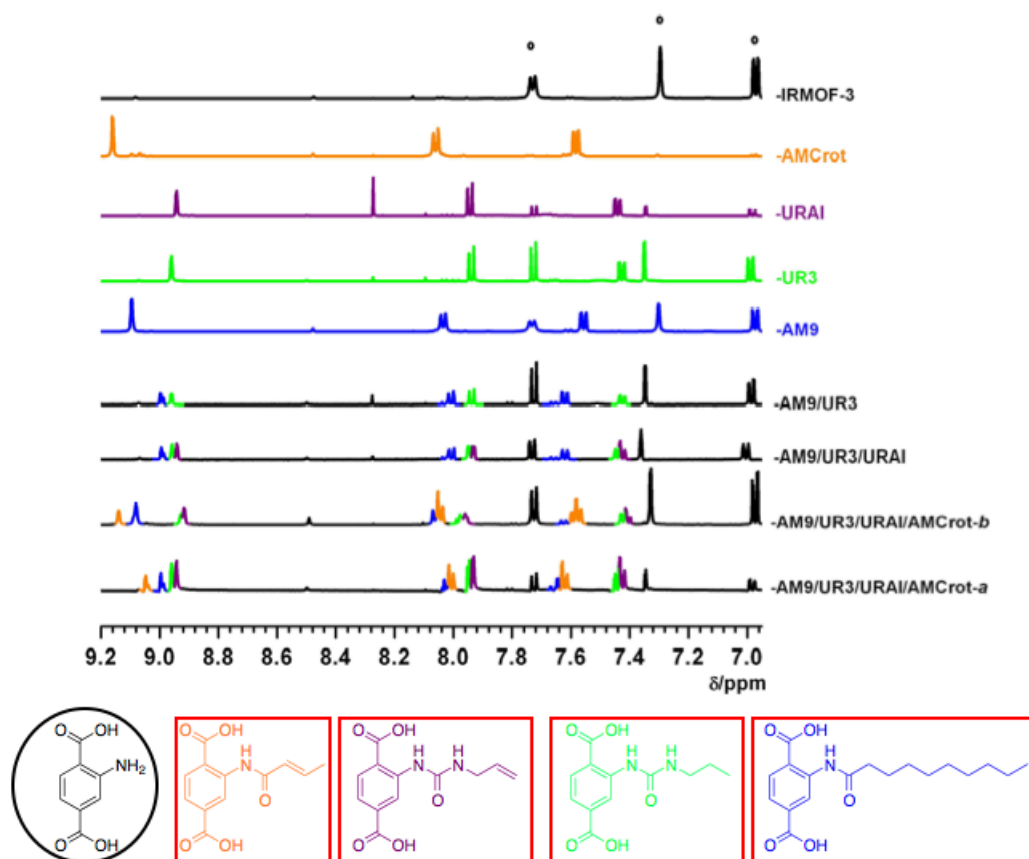


Figure 4-2. ¹H NMR spectra of multiple modified IRMOF-3 samples, IRMOF-3 samples modified with decanoic anhydride (blue, 51% conversion), propyl isocyanate (green, 60% conversion), allyl isocyanate (purple, 75% conversion), crotonic anhydride (orange, 100% conversion) and unmodified IRMOF-3 (Black) digested in DCI/D₂O and *d*⁶-DMSO. Unmodified (NH₂-BDC) resonances are denoted by black circles and modified resonances color coded with their corresponding standard spectra.

The presence of both modified products were also confirmed by ESI-MS analysis from a single, digested crystal (Figure 4-3). Additionally, high-performance liquid chromatography mass spectrometry (HPLC-MS) was performed on the modified sample to verify the presence of the three different dicarboxylate components. The HPLC-MS trace (as measured using UV absorbance at 254 nm) indicates the presence of three distinct species that correspond to the unmodified NH_2 -BDC, the amide modified product (AM9), and the urea modified product (UR3) (Figure 4-4). The crystallinity and porosity of the framework were maintained after multiple modification as evidenced by PXRD (Figure 4-5) and BET gas adsorption measurements (Table 4-2). While the material does not show complete thermal degradation until ~ 430 °C, IRMOF-3-AM9/UR3 does display a measurable weight loss (measured 14 wt%, calc. $\sim 16.4\%$) at ~ 250 °C which has also been observed in other urea modified MOFs (Figure 4-6).²⁹

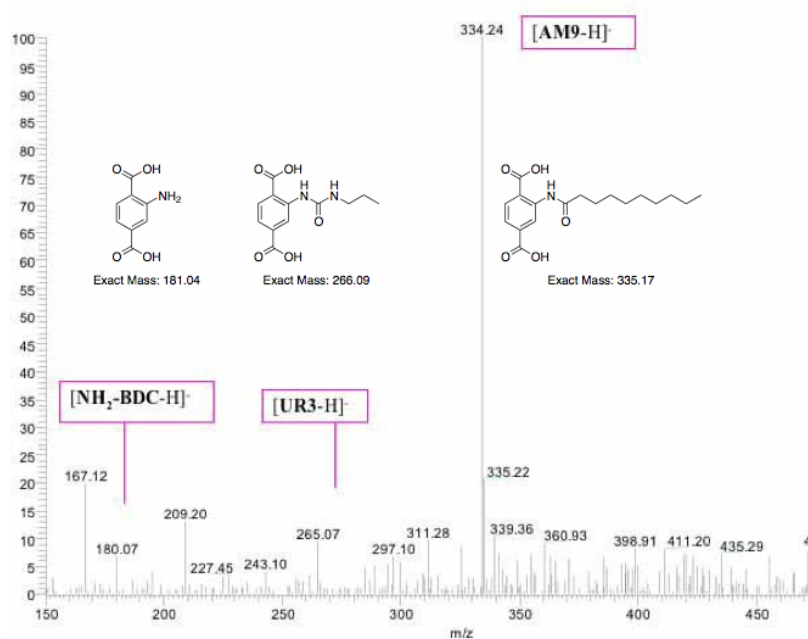


Figure 4-3. ESI-MS(-) of a digested IRMOF-3-AM9/UR3 single crystal.

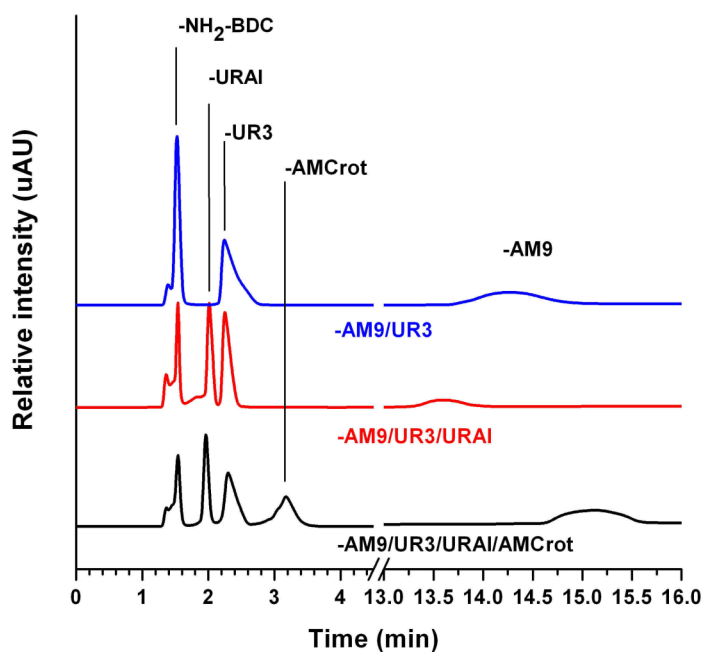


Figure 4-4. HPLC-MS chromatogram of IRMOF-3-AM9/UR3 (blue), IRMOF-3-AM9/UR3/URAI (red), IRMOF-3-AM9/UR3/URAI/AMCrot-*a* (black). Part of the chromatogram (13 to 16 minutes) is magnified (7 \times).

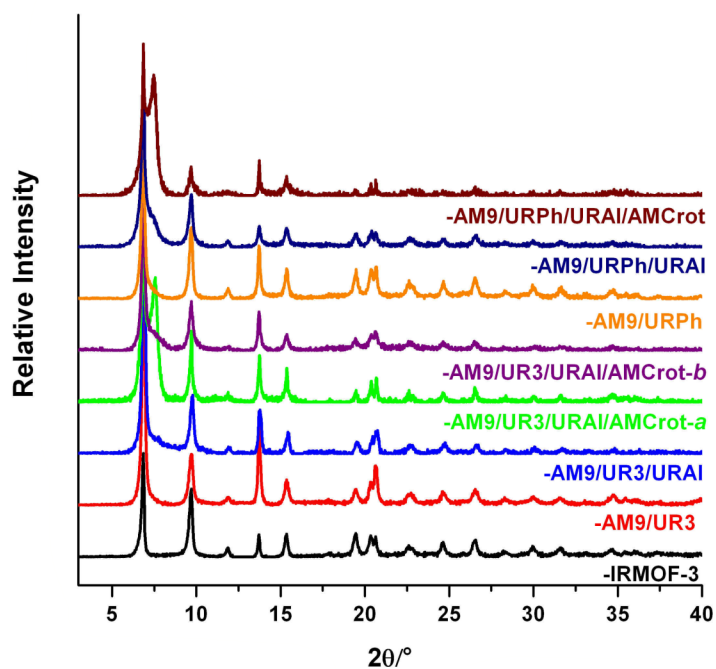


Figure 4-5. Powder X-ray diffraction (PXRD) patterns of multiple modified IRMOF-3 samples. Modified IRMOF-3 samples were soaked and exchanged with fresh CHCl_3 for 3 days.

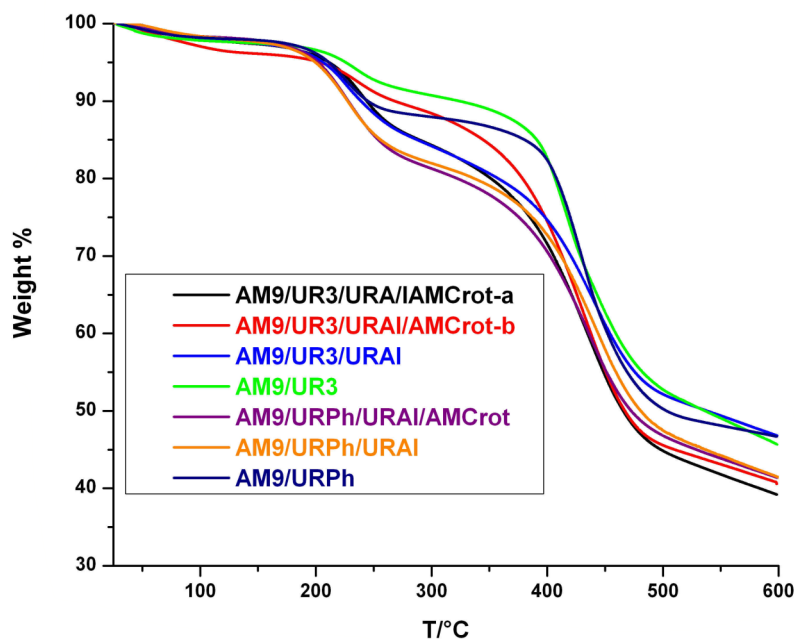


Figure 4-6. Thermogravimetric analysis (TGA) of modified IRMOF-3 samples. All samples were dried under vacuum for 8 h. Modified IRMOF-3 (10-20 mg) was heated at a scan rate of $5\text{ }^{\circ}\text{C min}^{-1}$ from 25 to 600 $^{\circ}\text{C}$.

Table 4-2. BET surface areas (m^2g^{-1}) of IRMOF-3 modified with multiple reagents. The results of two independent experiments are shown.

IRMOF-3-	AM9/ UR3	AM9/ URPh	AM9/UR3/ URAI/AMCrot- <i>a</i>	AM9/UR3/ URAI/AMCrot- <i>b</i>	AM9/URPh/ URAI/AMCrot
Trial 1	1267	1671	427	1330	540
Trial 2	916	1441	482	1286	475

To examine how the size of different reagents affects subsequent modification processes in a single MOF lattice, IRMOF-3 was treated with decanoic anhydride and the bulky reagent phenyl isocyanate. As shown by ^1H NMR the designated material IRMOF-3-AM9/URPh contained 24% of the alkyl amide and 32% of the phenyl urea ligands (Figure 4-7). HPLC-MS was performed on the modified sample to verify the presence of the three different dicarboxylate components. The HPLC-MS chromatogram indicates the presence of three distinct species that correspond to the

unmodified $\text{NH}_2\text{-BDC}$, the amide modified product (AM9), and the urea modified product (URPh) (Figure 4-8). The mass spectrometry of a single digested crystal of IRMOF-3-AM9/URPh confirm the introduction of both amide (AM9) and urea (URPh) functionalities (Figure 4-9). The material showed similar crystallinity (Figure 4-5), thermal stability (Figure 4-6), and microporosity (Table 4-2), to that found for IRMOF-3-AM9/UR3. The preparation of IRMOF-3-AM9/UR3 and IRMOF-3-AM9/URPh unequivocally demonstrated for the first time, that IRMOF-3 could be modified with both anhydride and isocyanate reagents, generating materials with at least three, distinct functional groups within the pores (amine, amide, and urea).

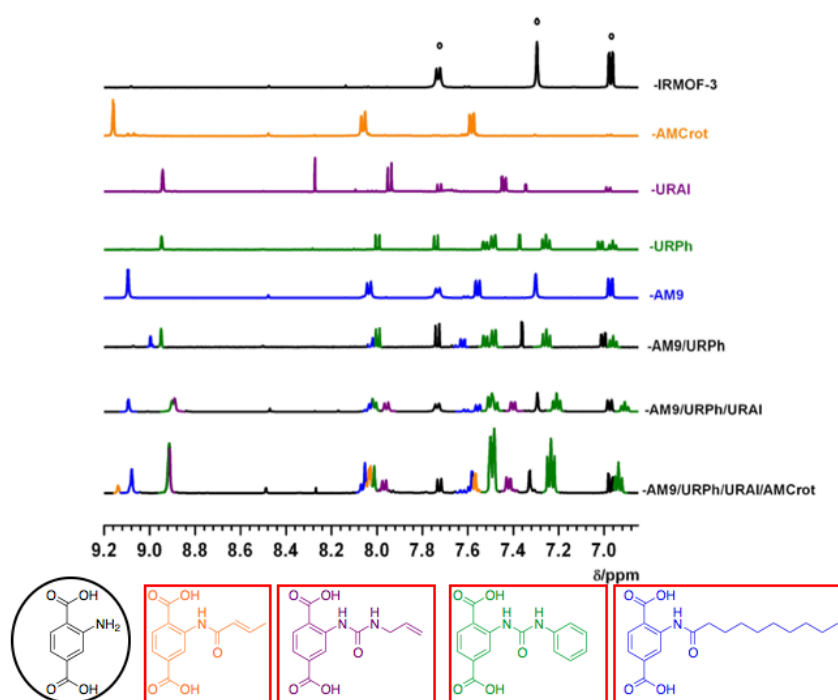


Figure 4-7. ^1H NMR spectra of multiple modified IRMOF-3 samples, IRMOF-3 samples modified with decanoic anhydride (Blue, 51% conversion), phenyl isocyanate (Olive-green, 53% conversion), allyl isocyanate (Purple, 75% conversion), crotonic anhydride (Orange, 100% conversion) and unmodified IRMOF-3 (Black) digested in $\text{DCI}/\text{D}_2\text{O}$ and $d^6\text{-DMSO}$. Unmodified ($\text{NH}_2\text{-BDC}$) resonances are denoted by black circles and modified resonances color coded with their corresponding standard spectra.

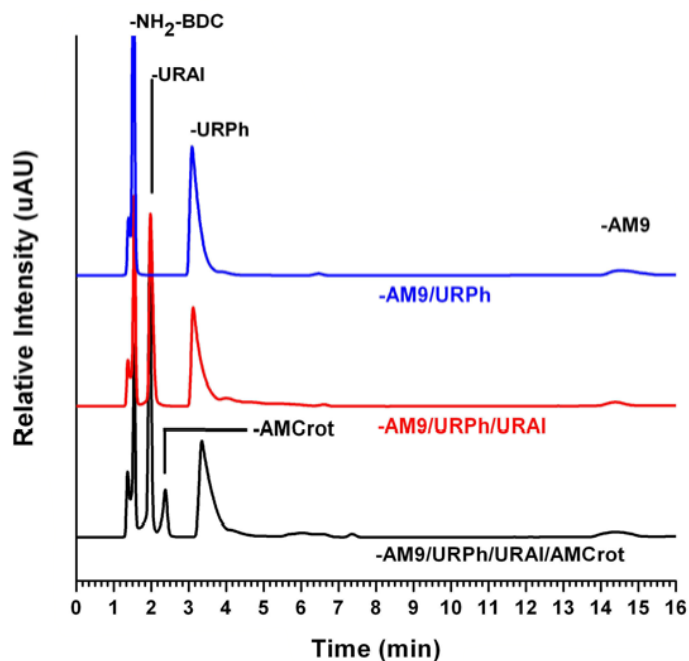


Figure 4-8. HPLC-MS chromatogram of IRMOF-3-AM9/URPh (blue), IRMOF-3-AM9/URPh/URAI (red), IRMOF-3-AM9/URPh/URAI/AMCrot-*a* (black).

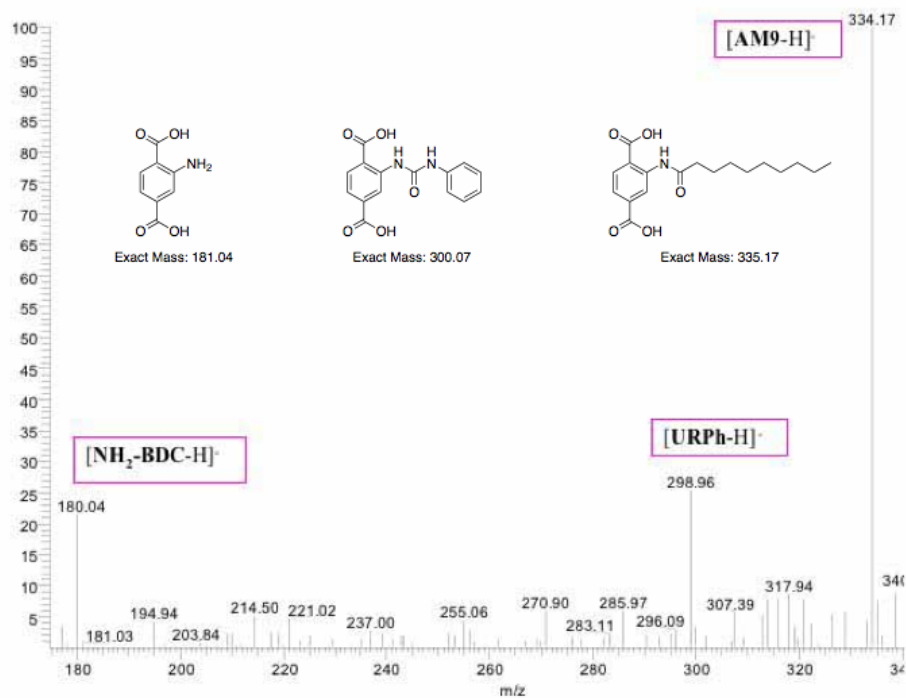


Figure 4-9. ESI-MS(-) of a digested IRMOF-3-AM9/URPh single crystal.

Having demonstrated that IRMOF-3 could be modified with both anhydride and isocyanate reagents, the extent to which tandem PSM could be performed with additional reagents was explored on IRMOF-3-AM9/UR3 and IRMOF-3-AM9/URPh. The MOFs were further treated with allyl isocyanate followed by crotonic anhydride. IRMOF-3-AM9/UR3 was subsequently treated with eight equivalents of allyl isocyanate. The relatively bulky phenyl urea and alkyl amide groups in IRMOF-3-AM9/URPh was found not to inhibit the reactivity of allyl isocyanate in the modification process. The ^1H NMR spectra of digested IRMOF-3-AM9/UR3/URAl contains resonances at 7.4 and 7.9 ppm that show overlap among doublet peaks associated with the phenyl (C5, C6 position) protons of modified urea (UR3, URAl) ligands (Figure 4-2). Nonetheless, modification by all three reagents can be established with three distinct singlet resonances associated with the phenyl (C-3 position) protons of the two urea (UR3, URAl) and amide (AM9) ligands. IRMOF-3-AM9/UR3/URAl was found to contain 21% of the amide and 22% and 23% of the urea (UR3 and URAl, respectively) functionalities leaving 34% unmodified amine groups. Interestingly, unlike IRMOF-3-AM9/UR3/URAl, the ^1H NMR spectrum of digested IRMOF-3-AM9/URPh/URAl contains overlap among the singlet phenyl protons associated with the two urea (URPh, URAl) products (8.9 ppm) (Figure 4-7). However, the doublet resonances associated with one of the phenyl (C5 or C6 position) protons of their respective urea products (URPh \sim 7.5 ppm and UR3 \sim 7.4 ppm) are clearly distinguishable allowing for the determination of conversion. ^1H NMR indicates that IRMOF-3-AM9/URPh/URAl contains 48% of urea species (28%

and 20% for URPh and URAI, respectively), 26% of the amide product (AM9), and 26% unmodified NH₂-BDC.

The additional urea functionality is also evidenced by TGA as IRMOF-3-AM9/UR3/URAI demonstrates an increased weight loss (20 wt%) at ~250 °C relative to that of IRMOF-3-AM9/UR3 (14 wt%) (Figure 4-6). HPLC-MS and single-crystal ESI-MS confirm the presence of four individual species corresponding to the amine (NH₂-BDC), amide (AM9), and urea (UR3, URAI) functional groups (Figure 4-4, Figure 4-10). Both multiple modified materials display PXRD peaks consistent with the IRMOF-3 starting material (Figure 4-5). HPLC-MS (Figure 4-8) and ESI-MS (Figure 4-11) of digested IRMOF-AM9/URPh/URAI further confirm the presence of four species in the two systems consistent with unmodified NH₂-BDC, the amide product (AM9), and the two ureas (URPh, URAI). The development of IRMOF-AM9/UR3/URAI and IRMOF-AM9/URPh/URAI further suggests that multiple reagents can be utilized in tandem postsynthetic modification to generate multifunctional materials, without MOF degradation.

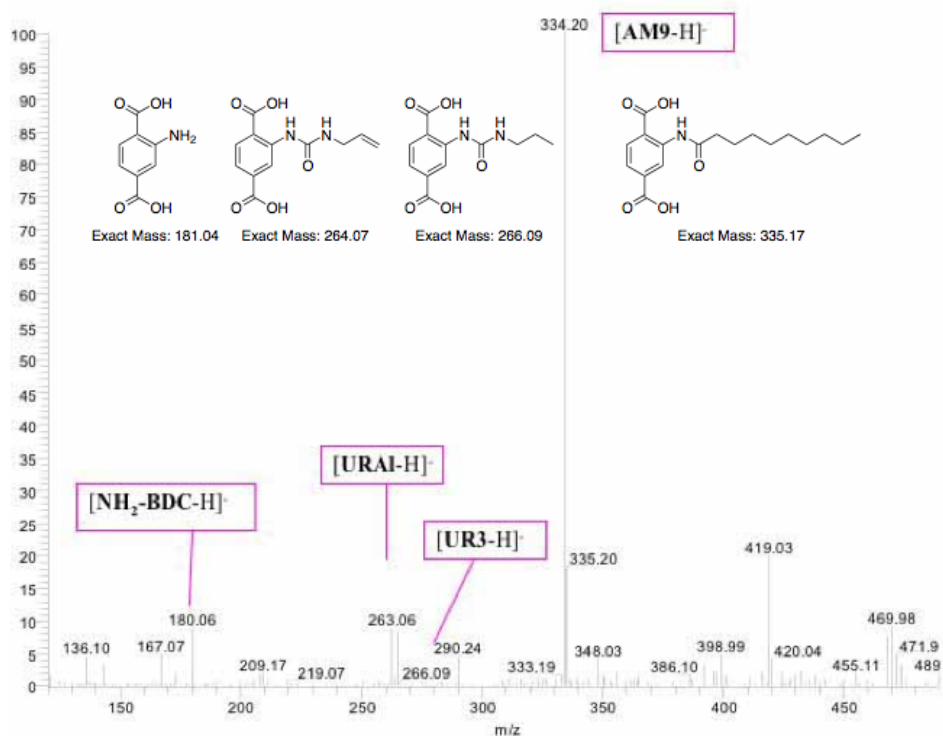


Figure 4-10. ESI-MS(-) of a digested IRMOF-3-AM9/URPh/URAl single crystal.

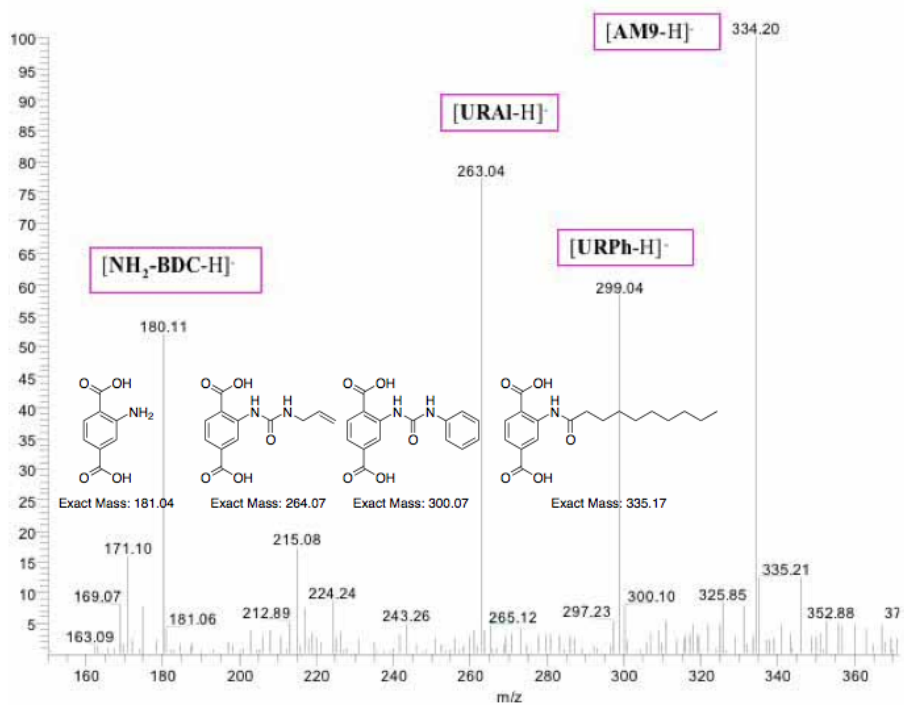


Figure 4-11. ESI-MS(-) of a digested IRMOF-3-AM9/URPh/URAl single crystal.

Due to its relatively small size and high reactivity,²⁶ crotonic anhydride was utilized for a final, additional modification on IRMOF-3-AM9/UR3/URAI and IRMOF-3-AM9/URPh/URAI. The modified functional groups of the preceding systems significantly affected the subsequent modification with crotonic anhydride. IRMOF-3-AM9/UR3/URAI/AMCrot-*a* was found to contain 24% and 17% of the amide products (AM9 and AMCrot, respectively) in addition to 18% and 21% of the urea products (UR3 and URAI, respectively) leaving ~20% unmodified (NH₂-BDC). IRMOF-3-AM9/URPh/URAI/AMCrot consists of 20% and 8% of amide (AM9 and AMCrot, respectively) products along with 30% and 20% of urea (URPh and URAI, respectively) products. The low conversion of the crotonic amide product (AMCrot) relative to that of the IRMOF-3-AM9/UR3/URAI/AMCrot-*a* system reflects the reduced ability for crotonic anhydride to diffuse and react with available amine groups, likely due to the larger phenyl urea groups already present in the material. The presence of five distinct species correlating to unmodified NH₂-BDC, the amide products (AM9, AMCrot), and urea products (UR3 or URPh and URAI) were confirmed by HPLC-MS (Figure 4-4, Figure 4-8) and ESI-MS (Figure 4-12, 4-13).

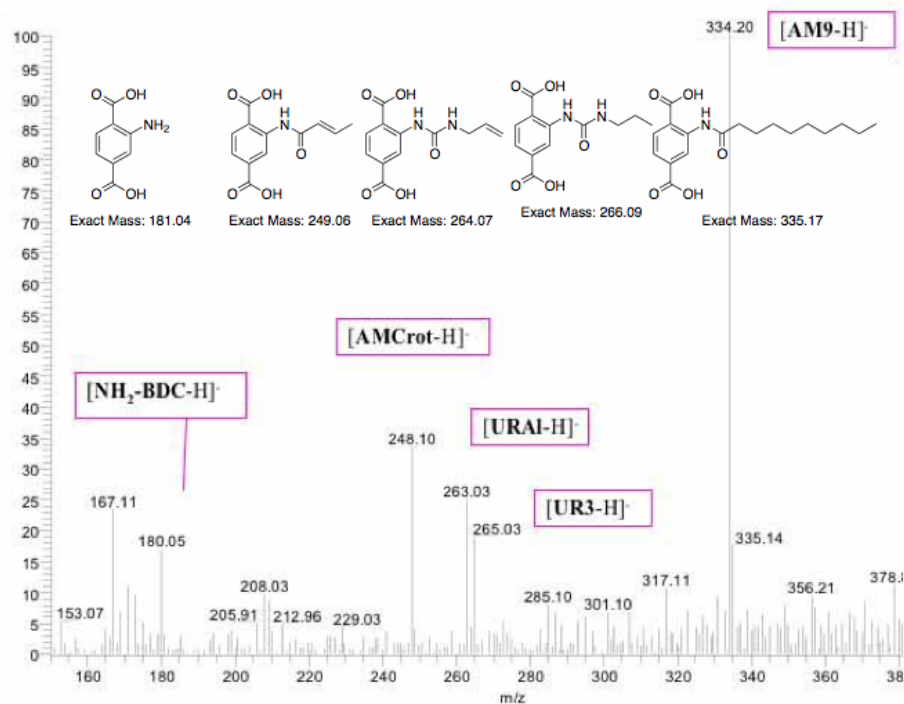


Figure 4-12. ESI-MS(-) of a digested IRMOF-3-AM9/URPh/URAI/AMCrot-*a* single crystal.

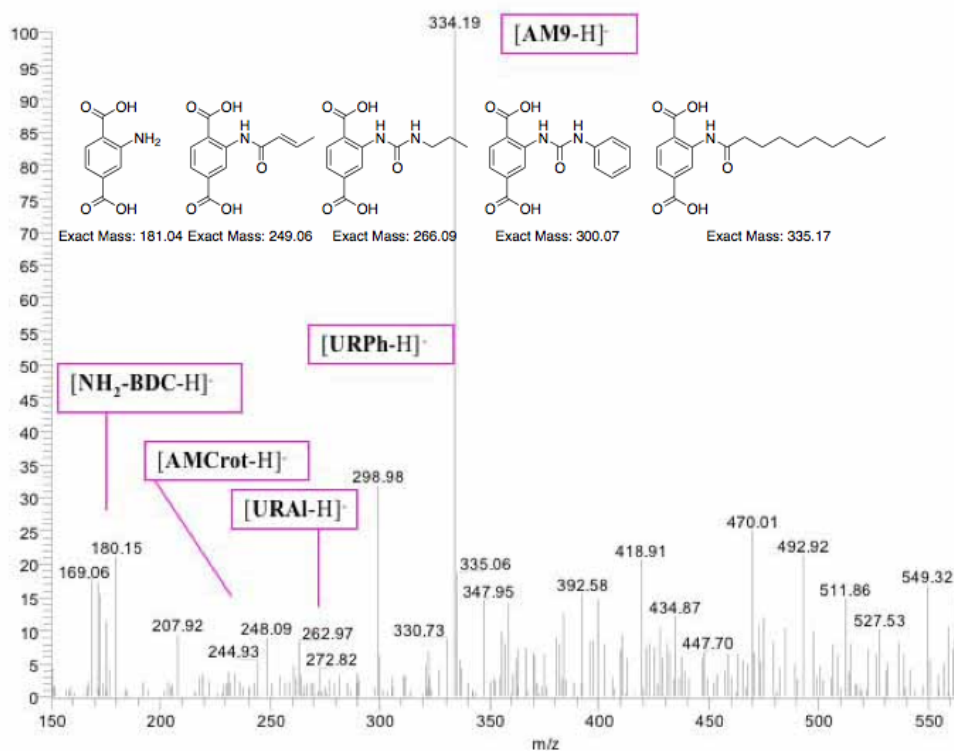


Figure 4-13. ESI-MS(-) of a digested IRMOF-3-AM9/URPh/URAI/AMCrot single crystal.

Both systems showed a near identical weight loss at ~ 250 °C as their precursors and similar overall thermal stability to IRMOF-3 (Figure 4-6). However, PXRD clearly indicates some degradation of the framework in both systems on account of the additional modification reactions, with the emergence of a shoulder at $2\theta = 7.4^\circ$ (Figure 4-5). Degradation may have arisen from the prolonged exposure to ambient moisture from the air or solvents during the sequential reactions and the additional time employed in the preparation of the multiple modified materials.

Given the facile ability to control the heterogeneous nature of postsynthetic modification some experiments were performed to modulate the relative abundance of the functional groups in a highly-modified MOF. Multiple tandem modification reactions were attempted with the aforementioned anhydrides (decanoic, crotonic) and isocyanates (propyl, allyl) using shorter reaction times to produce a MOF designated IRMOF-3-AM9/UR3/URAI/AMCrot-*b*. Based on ^1H NMR, the aforementioned MOF was found to contain 23% and 13% of amide (AM9 and AMCrot, respectively) products along with 8% and 13% of urea (UR3 and URAI, respectively) products leaving $\sim 53\%$ of the framework unmodified (Figure 4-2). The reduced reaction time circumvents structural degradation as the multiple modified sample displays PXRD peaks consistent with IRMOF-3 (Figure 4-5). Microporosity is maintained as nitrogen uptake ($350\text{-}400\text{ cm}^3\text{g}^{-1}$) and BET gas adsorption measurements showed reasonable surface areas ($\sim 1330\text{ m}^2\text{g}^{-1}$) (Figure 4-14, Table 4-2). The development of IRMOF-3-AM9/UR3/URAI/AMCrot-*b* confirms that modification of multiple reagents can be tuned with varying reaction conditions. More importantly, it demonstrates the facile synthesis of multifunctional materials through a tandem PSM approach. Given the

facile control over reaction time, reagent concentration, and other reaction parameters, tandem postsynthetic modification offers a viable route to functionalized MOFs with unprecedented chemical complexity.

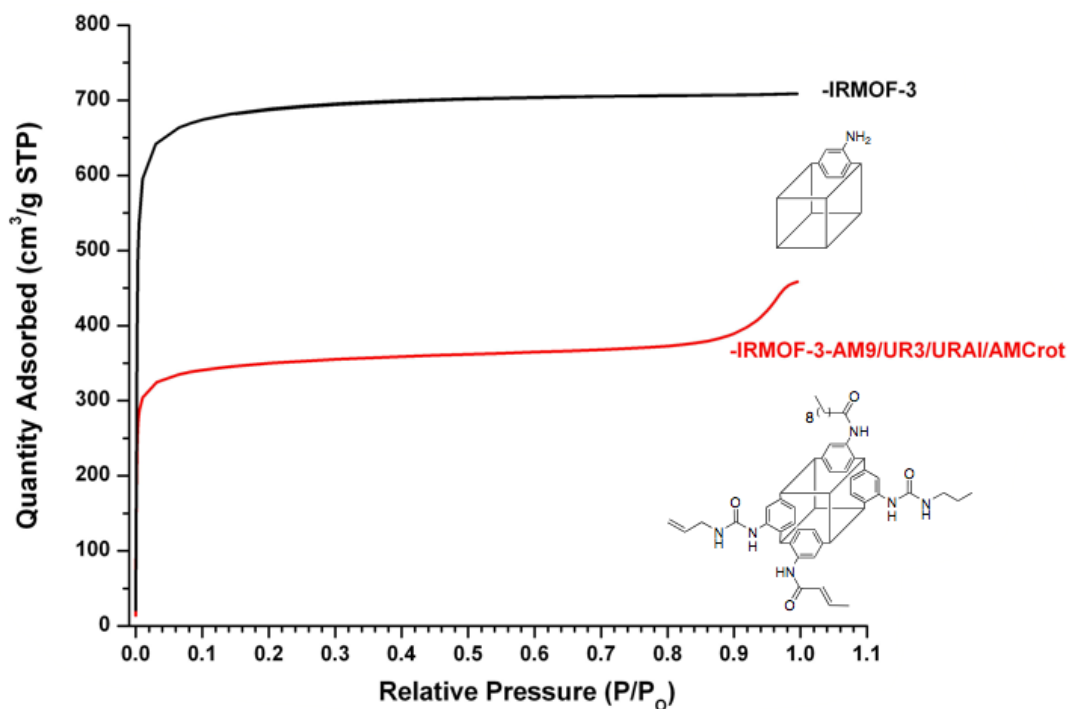


Figure 4-14. N₂ gas adsorption isotherms of IRMOF-3 (black) and IRMOF-3-AM9/UR3/URAI/AMCrot-*b* (red).

4.3 Conclusions

In summary, the findings presented in this chapter again demonstrate that PSM is a versatile method for the functionalization of MOFs. For the first time incorporation of two distinct types of functionalites (urea and amide) was realized in a MOF through the use of sequential or ‘tandem’ modification. Continued modification on two sets of multifunctional MOFs containing distinct aliphatic and aromatic substituents with identical reagents produced multifunctional MOFs with as many as five different substituents. Modification on multifunctionalized MOFs was

found to be affected by the size of the previously incorporated substituents. With bulkier moieties inhibiting the diffusion of new reagents into the pores of the framework and subsequently altering modification. The relative abundance of different functionalities could be modulated by altering PSM reaction conditions. The findings presented in this chapter clearly illustrate that PSM represents a powerful means to access new MOF compounds with unprecedented chemical complexity, which may serve as the basis of multifunctional bio-mimetic materials.

4.4 Experimental Methods

General. Starting materials and solvents were purchased and used without further purification from commercial suppliers (Sigma-Aldrich, Alfa Aesar, EMD, TCI, Cambridge Isotope Laboratories, Inc., and others). IRMOF-3 was synthesized and activated as described previously.^{28,30}

IRMOF-3-AM9/URPh. Approximately 60 mg of IRMOF-3 (ca. 0.20 mmol equiv of -NH₂) was placed in a vial with 2 equiv (0.4 mmol) of decanoic anhydride dissolved in 8 mL of CHCl₃. After allowing the sample to stand for 1 day, the solution was decanted and the crystals were washed with 3×6 mL of CHCl₃. The crystals were then treated with 8 equiv (1.6 mmol) of phenyl isocyanate dissolved in 2 mL of a 10% MeOH/CHCl₃ solution. After allowing the samples to stand for 1 day, the solution was decanted and the crystals were washed with 3×6 mL of CHCl₃. Samples not undergoing subsequent modification were then soaked in 10 mL of pure CHCl₃ for three days, with fresh CHCl₃ added every 24 h.

IRMOF-3-AM9/URPh/URAI. Allyl isocyanate (1.6 mmol) was added to approximately 60 mg of IRMOF-3-AM9/URPh in 2 mL of CHCl_3 . After allowing the sample to stand for 1 day, the solution was decanted and the crystals were washed with 3×6 mL of CHCl_3 . Samples not undergoing subsequent modification were then soaked in 10 mL of pure CHCl_3 for three days, with fresh CHCl_3 added every 24 h.

IRMOF-3-AM9/URPh/URAI/AMCrot. Crotonic anhydride (0.4 mmol) was added to approximately 60 mg of IRMOF-3-AM9/URPh/URAI in 4 mL of CHCl_3 . After allowing the sample to stand for 3 days, the crystals were washed with 3×6 mL of CHCl_3 then soaked in 10 mL of pure CHCl_3 for three days, with fresh CHCl_3 added every 24 h.

IRMOF-3-AM9/UR3. Approximately 60 mg of IRMOF-3 (ca. 0.20 mmol equiv of $-\text{NH}_2$) was placed in a vial with 2 equiv (0.4 mmol) of decanoic anhydride dissolved in 8 mL of CHCl_3 . After allowing the samples to stand for 1 day, the solution was decanted and the crystals were washed with 3×6 mL of CHCl_3 . The crystals were then treated with 8 equiv (1.6 mmol) of propyl isocyanate dissolved in 2 mL of CHCl_3 solution. After allowing the samples to stand for 1 day, the solution was decanted and the crystals were washed with 3×6 mL of CHCl_3 . Samples not undergoing subsequent modification were then soaked in 10 mL of pure CHCl_3 for three days, with fresh CHCl_3 added every 24 h.

IRMOF-3-AM9/UR3/URAI. Allyl isocyanate (1.6 mmol) was added to approximately 60 mg of IRMOF-3-AM9/UR3 in 2 mL of CHCl_3 . After allowing the sample to stand for 1 day, the solution was decanted and the crystals were washed

with 3×6 mL of CHCl₃. Samples not undergoing subsequent modification were then soaked in 10 mL of pure CHCl₃ for three days, with fresh CHCl₃ added every 24 h.

IRMOF-3-AM9/UR3/URAI/AMCrot-a. Crotonic anhydride (0.4 mmol) was added to ~60 mg of IRMOF-3-AM9/UR3/URAI in 4 mL of CHCl₃. After allowing the sample to stand for 3 days, the crystals were washed with 3×6 mL of CHCl₃ then soaked in 10 mL of pure CHCl₃ for three days, with fresh CHCl₃ added every 24 h.

IRMOF-3-AM9/UR3/URAI/AMCrot-b. Approximately 60 mg of IRMOF-3 (ca. 0.20 mmol equiv of -NH₂) was placed in a vial with 2 equiv (0.4 mmol) of decanoic anhydride dissolved in 8 mL of CHCl₃. After allowing the samples to stand for 1 day, the solution was decanted and the crystals were washed with 3×6 mL of CHCl₃. The crystals were then treated with 8 equiv (1.6 mmol) of propyl isocyanate dissolved in 2 mL of CHCl₃ solution. After allowing the samples to stand for 3 h, the solution was decanted and the crystals were washed with 3×6 mL of CHCl₃. The crystals were then treated with 8 equiv (1.6 mmol) of allyl isocyanate dissolved in 2 mL of CHCl₃. After allowing the samples to stand for 3 h, the solution was decanted and the crystals were washed with 3×6 mL of CHCl₃. Subsequently, the samples were treated with 2 equiv (0.4 mmol) of crotonic anhydride dissolved in 4 mL of CHCl₃. After 1 day, the crystals were washed with 3×6 mL of CHCl₃ then soaked in 10 mL of pure CHCl₃ for three days, with fresh CHCl₃ added every 24 h.

Digestion and Analysis by ¹H NMR. ¹H NMR spectra were recorded on a JEOL ECA spectrometer (500 MHz). Approximately 5 mg of modified IRMOF-3 samples was dried under vacuum at room temperature or at 90 °C overnight and

digested with sonication in 500 μL of d^6 -DMSO and 100 μL of dilute DCl (23 μL of 35% DCl in D_2O diluted with 1.0 mL of d^6 -DMSO).

Digestion and Analysis by ESI-MS. Electrospray ionization mass spectrometry (ESI-MS) was performed using a ThermoFinnigan LCQ-DECA mass spectrometer and the data was analyzed using the Xcalibur software suite. Crystals of modified IRMOF-3 (~0.1-1 mg) were digested in 1 mL of MeOH (or H_2O) with sonication.

Digestion and Analysis by HPLC-MS. High-performance liquid chromatography mass spectrometry (HPLC-MS) was performed using a ThermoFinnigan LCQ-deca mass spectrometer with electrospray ionization source (ESI) and was operated under negative ion mode. The data was analyzed using the Xcalibur software suite. Crystals of modified IRMOF-3 (~5 mg) were digested in 1.5 mL of 10% MeOH/ H_2O with sonication and filtered. 10 μL of this solution was injected into an Agilent Eclipse XBD-C18 column (5 μm , 4.6 x 150 mm). The solvent system consisted of MeOH in H_2O (5% at 0 min rising to 90% at 20 min then 5% after 26 min) with a with a flow rate of 1.0 mL/min. The chromatogram was monitored at $\lambda = 254$ nm over 30 min.

Thermal Gravimetric Analysis. Samples were analyzed under a stream of dinitrogen using a TA Instrument Q600 SDT running from room temperature to 600 $^\circ\text{C}$ with a scan rate of 5 $^\circ\text{C min}^{-1}$. Approximately 10-20 mg of modified IRMOF-3 samples were used for TGA measurements.

PXRD Analysis. PXRD data were collected at ambient temperature on a Bruker Advance D8 diffractometer at 40 kV, 40 mA for $K\alpha$ ($\lambda = 1.5418 \text{ \AA}$) with a

scan speed of $0.3^{\circ} \text{ min}^{-1}$, a step size of 0.02° in 2θ , and a 2θ range of $3\text{-}40^{\circ}$.

Approximately 15 mg of modified IRMOF-3 samples (typically soaked in CHCl_3) were air dried before PXRD analysis. The experimental backgrounds were corrected using the Jade 5.0 software package.

BET Surface Area Analysis. BET surface area (m^2g^{-1}) measurements were collected at 77 K by dinitrogen on an ASAP 2020 using volumetric technique. Approximately 40-60 mg of modified IRMOF-3 samples were evacuated on a vacuum line for 5-18 h. The sample was then transferred to a preweighed sample tube and degassed at 105°C for approximately 24 h or until the outgas rate was $<5 \mu\text{mHg}$. The sample tube was re-weighed to obtain a consistent mass for the degassed modified IRMOF-3.

4.5 Acknowledgements

Text, schemes, and figures in this chapter, in part, are reprints of the materials published in the following paper: Garibay, S. J., Wang, Z., Tanabe, K. K., Cohen, S. M. "Postsynthetic Modification: A Versatile Approach Toward Multifunctional Metal-Organic Frameworks" *Inorg. Chem.* **2009**, *48*, 7341-7349. The dissertation author was the primary researcher and author for the data presented. The co-authors listed in these publications also participated in the research.

4.6 References

- (1) Farrusseng, D.; Aguado, S.; Pinel, C. *Angew. Chem. Int. Ed.* **2009**, *48*, 7502-7513.
- (2) Lillerud, K. P.; Olsbye, U.; Tilset, M. *Top. Catal.* **2010**, *53*, 859-868.
- (3) Chun, H.; Dybtsev, D. N.; Kim, H.; Kim, K. *Chem. Eur. J.* **2005**, *11*, 3521-3529.
- (4) Burrows, A. D. *CrystEngComm* **2011**, *13*, 3623-3642.
- (5) Kleist, W.; Jutz, F.; Maciejewski, M.; Baiker, A. *Eur. J. Inorg. Chem.* **2009**, 3552-3561.
- (6) Burrows, A. D.; Frost, C. G.; Mahon, M. F.; Richardson, C. *Angew. Chem. Int. Ed.* **2008**, *47*, 8482-8486.
- (7) Burrows, A. D.; Fisher, L. C.; Richardson, C.; Rigby, S. P. *Chem. Commun.* **2011**, *47*, 3380-3382.
- (8) Deng, H.; Doonan, C. J.; Furukawa, H.; Ferreira, R. B.; Towne, J.; Knobler, C. B.; Wang, B.; Yaghi, O. M. *Science* **2010**, *327*, 846-850.
- (9) Kim, M.; Cahill, J. F.; Prather, K. A.; Cohen, S. M. *Chem. Commun.* **2011**, *47*, 7629-7631.
- (10) Wang, C.; Xie, Z.; Dekrafft, K. E.; Lin, W. *J. Am. Chem. Soc.* **2011**, *133*, 13445-13454.
- (11) Hirai, K.; Furukawa, S.; Kondo, M.; Uehara, H.; Sakata, O.; Kitagawa, S. *Angew. Chem. Int. Ed.* **2011**, 8057-8061.
- (12) Taylor-Pashow, K. M.; Della Rocca, J.; Xie, Z.; Tran, S.; Lin, W. *J. Am. Chem. Soc.* **2009**, *131*, 14261-14263.

- (13) Shultz, A. M.; Farha, O. K.; Hupp, J. T.; Nguyen, S. T. *J. Am. Chem. Soc.* **2009**, *131*, 4204-4205.
- (14) Farha, O. K.; Shultz, A. M.; Sarjeant, A. A.; Nguyen, S. T.; Hupp, J. T. *J. Am. Chem. Soc.* **2011**, *133*, 5652-5655.
- (15) Cho, S. H.; Ma, B.; Nguyen, S. T.; Hupp, J. T.; Albrecht-Schmitt, T. E. *Chem. Commun.* **2006**, 2563-2565.
- (16) Bae, Y. S.; Mulfort, K. L.; Frost, H.; Ryan, P.; Punnathanam, S.; Broadbelt, L. J.; Hupp, J. T.; Snurr, R. Q. *Langmuir* **2008**, *24*, 8592-8598.
- (17) Gadzikwa, T.; Zeng, B. S.; Hupp, J. T.; Nguyen, T. S. *Chem. Commun.* **2008**, 3672-3674.
- (18) Furukawa, S.; Hirai, K.; Nakagawa, K.; Takashima, Y.; Matsuda, R.; Tsuruoka, T.; Kondo, M.; Haruki, R.; Tanaka, D.; Sakamoto, H.; Shimomura, S.; Sakata, O.; Kitagawa, S. *Angew. Chem. Int. Ed.* **2009**, *48*, 1766-1770.
- (19) Koh, K.; Wong-Foy, A. G.; Matzger, A. J. *Chem. Commun.* **2009**, 6162-6164.
- (20) Yoo, Y.; Jeong, H.-K. *Cryst. Growth Des.* **2010**, *10*, 1283-1288.
- (21) Furukawa, S.; Hirai, K.; Takashima, Y.; Nakagawa, K.; Kondo, M.; Tsuruoka, T.; Sakata, O.; Kitagawa, S. *Chem. Commun.* **2009**, 5097-5099.
- (22) Zacher, D.; Schmid, R.; Woll, C.; Fischer, R. A. *Angew. Chem. Int. Ed.* **2011**, *50*, 176-199.
- (23) Qian, K.; Fang, G.; Wang, S. *Chem. Commun.* **2011**, *47*, 10118-10120.
- (24) Park, T.-H.; Koh, K.; Wong-Foy, A. G.; Matzger, A. J. *Cryst. Growth Des.* **2011**, *11*, 2059-2063.
- (25) Burnett, B. J.; Barron, P. M.; Hu, C.; Choe, W. *J. Am. Chem. Soc.* **2011**, *133*, 9984-9987.

- (26) Wang, Z.; Cohen, S. M. *Angew. Chem. Int. Ed.* **2008**, *47*, 4699-4702.
- (27) Gadzikwa, T.; Lu, G.; Stern, C. L.; Wilson, S. R.; Hupp, J. T.; Nguyen, S. T. *Chem. Commun.* **2008**, 5493-5495.
- (28) Wang, Z.; Tanabe, K. K.; Cohen, S. M. *Inorg. Chem.* **2009**, *48*, 296-306.
- (29) Dugan, E.; Wang, Z.; Okamura, M.; Medina, A.; Cohen, S. M. *Chem. Commun.* **2008**, 3366-3368.
- (30) Rowsell, J. L. C.; Yaghi, O. M. *J. Am. Chem. Soc.* **2006**, *128*, 1304-1315.

Chapter 5. Metal-Organic Framework Organocatalysts Prepared by Postsynthetic Modification

5.1 Introduction

The ability to design MOFs with varying pore volumes and surface areas^{1,2} through their organic and inorganic components has made these materials attractive for applications in gas storage.³⁻⁹ Moreover, MOFs have shown promise in a diverse set of technologies including separation,^{10,11} drug delivery,¹²⁻¹⁴ and catalysis.¹⁵ Throughout the last several years, several groups have shown that MOFs can act as heterogeneous catalysts in a variety of reactions such as alkene oxidation,^{16,17} aldol condensations,^{18,19} hydrogenation,²⁰⁻²² and epoxide ring opening reactions.²³ Compared to homogeneous reactions, the use of heterogeneous catalysts simplifies the reaction work-up by requiring only filtration to separate the catalyst from the product for reuse.

While there have been many studies investigating MOFs as heterogeneous catalysts, most examples utilize the SBU metal centers as the catalytic sites. Recently, Baiker and coworkers utilized a 4,4'-bipyridine-Cu²⁺ based MOF Cu(bipy)(H₂O)₂(BF₄)₂(bipy) for the methanolysis of epoxides demonstrating high activity and selectivity.²⁴ However, further investigation of this system revealed that the excellent catalytic properties were due to a structural rearrangement of the MOF and subsequent release of copper clusters upon exposure to methanol (Figure 5-1).²⁵

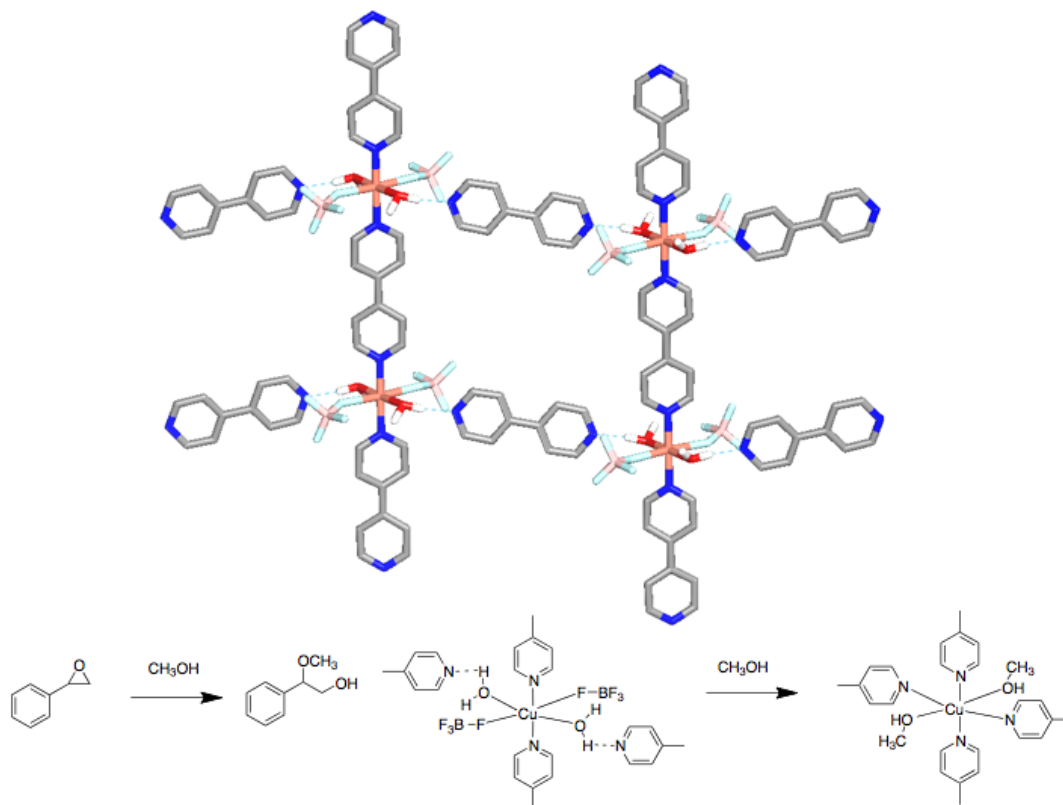


Figure 5-1. Cu(bipy)(H₂O)₂(BF₄)₂(bipy) (top), methanolysis of styrene oxide (bottom left) and representation of the structural rearrangement after introduction of methanol (bottom right).

Rosseinsky and coworkers cleverly developed catalytically active chiral aspartate MOFs.²⁶ With the careful addition of HCl the MOFs could be protonated at a carboxylate group bound to the Cu²⁺ or Ni²⁺ metal centers, thereby introducing Brønsted acid sites (Figure 5-2). While the Brønsted acid functionalized materials showed modest activity and enantioselectivity in the methanolysis of small epoxides, the recyclability and robustness of these catalytic materials was not described.

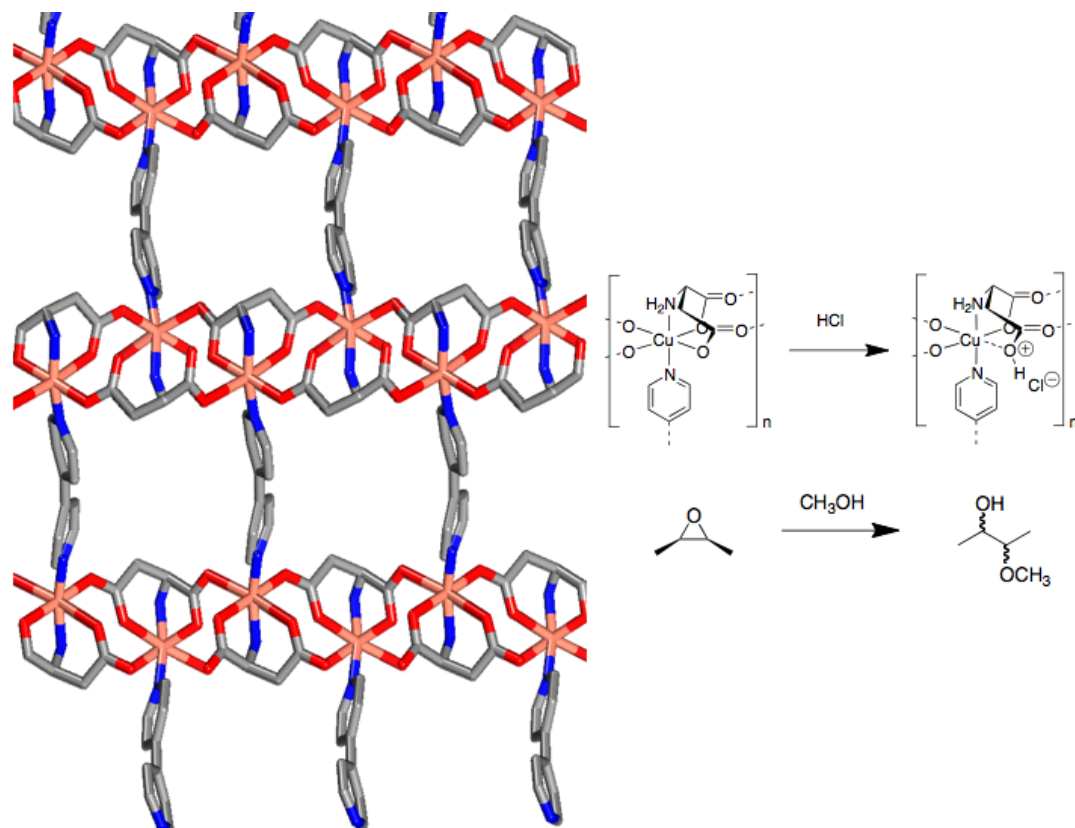


Figure 5-2. Cu(L-asp)bipy_{0.5} (left) and representation of Cu(L-asp)bipy_{0.5}(HCl)_{0.9}(MeOH)_{0.5} generated after introduction of HCl utilized as a Brønsted acid catalyst for the methanolysis of *cis*-2,3-epoxybutane (right).

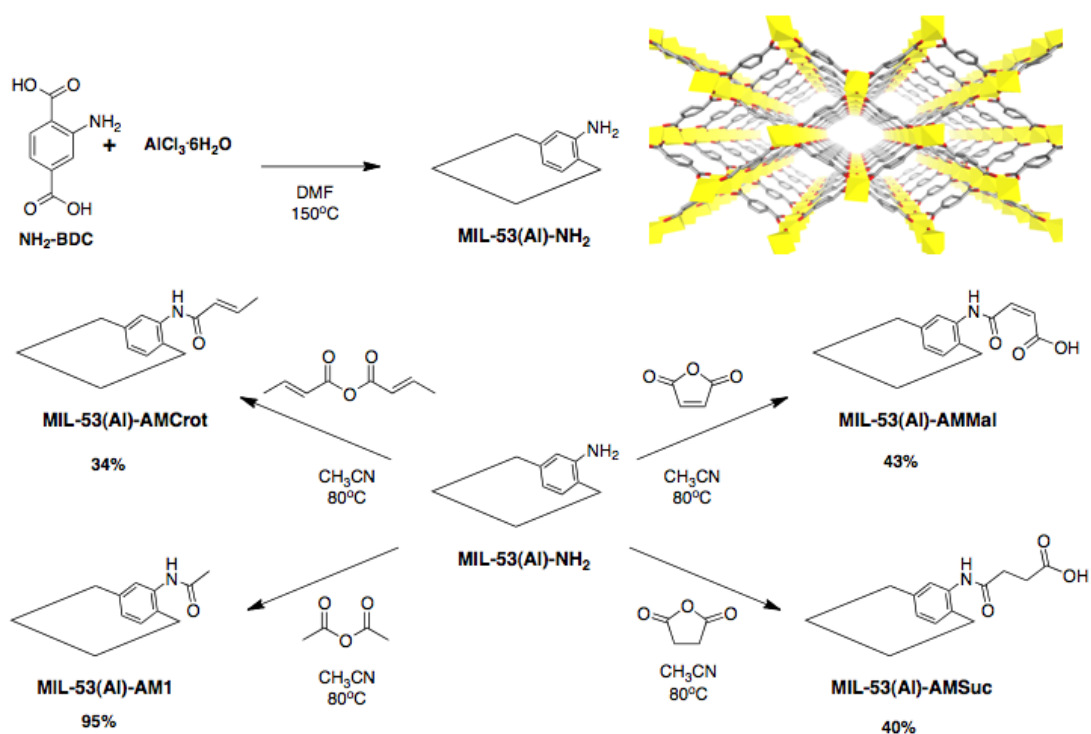
A recent study utilized coordinative postsynthetic modification with pyridyl L-proline onto the open metal coordination sites of MIL-101 (MIL = Material Institut Lavoisier) (Figure 1-11).¹⁹ Through this approach MIL-101 was transformed into a catalytically active homochiral material that was competent for asymmetric aldol reactions between aldehydes and ketones. While the material displayed high catalytic activities and enantioselectivity, its catalytic properties diminished over time on account of leaching of the pyridyl groups after repeated use.

Our group and others have recently demonstrated the practical use of postsynthetic modification (PSM) to produce functionalized systems by targeting the

organic linking group or secondary building unit of pre-fabricated MOFs.²⁷ Covalent PSM of these systems provides an opportunity to develop MOFs with stable and reusable organocatalytic functionality. In this chapter, we demonstrate the utilization of carboxylic acid functionalized MOFs as a solid state Brønsted acid catalyst for the ring opening of small epoxides by methanol. The findings described here demonstrate that these modified MOFs act as a heterogeneous catalysts that be reused after regeneration without loss of activity.

5.2 Results and Discussion

In order to develop a heterogeneous MOF catalyst, a chemically robust framework was selected for compatibility with the protic solvents used during epoxide ring opening reaction conditions. The MIL-53(Al) framework is chemically stable to many protic solvents and acidic environments, unlike Zn^{2+} -carboxylate MOFs (IRMOF-3 derivatives),²⁸ which degrade under the reaction conditions that will be described below. Recently MIL-53(Al)-NH₂, a MIL-53(Al) analogue incorporating NH₂-BDC, was synthesized and could be postsynthetically modified with formic acid to produce formamide functionality.²⁹ With this literature report available, PSM of MIL-53(Al)-NH₂ was attempted with a variety of anhydrides (Scheme 5-1).



Scheme 5-1. Synthesis (top left) and structure (top right) of MIL-53(Al)-NH₂. PSM reactions performed on MIL-53-(Al)-NH₂ relevant to this study (bottom).

The use of maleic and succinic anhydride generated carboxylic acid functionalized MIL-53(Al)-AMMal and MIL-53(Al)-AMSuc with modest conversions of ~43% and ~40%, respectively. Percent conversion was determined by using peak integration from ¹H NMR of digested samples. The conversion was obtained by comparing the relative areas of the singlet aromatic resonance (corresponding to the C3-position) of the modified and unmodified dicarboxylate ligands (Figure 5-3).

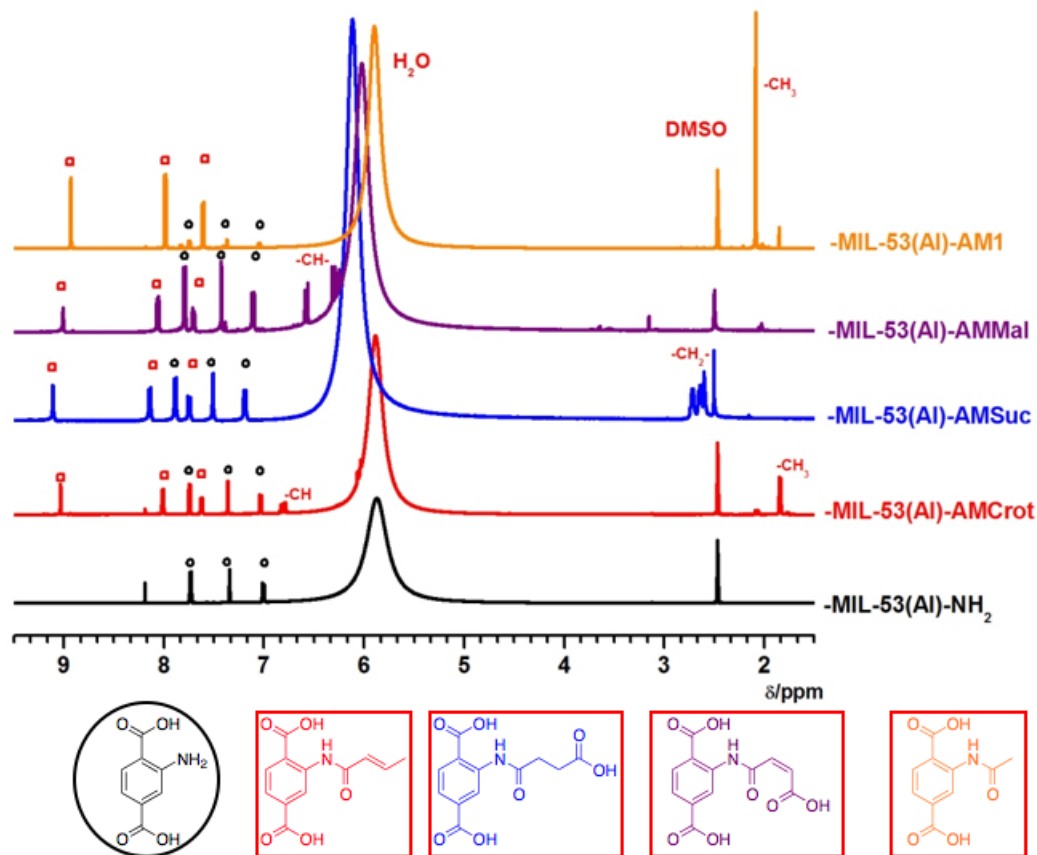


Figure 5-3. ^1H NMR spectra of modified MIL-53(Al)- NH_2 samples digested in $\text{HF}/d^6\text{-DMSO}$. Red squares and black circles represent signals of modified and unmodified $\text{NH}_2\text{-BDC}$, respectively.

Fourier transform infrared spectroscopy (FT-IR) on MIL-53(Al)-AMMal and MIL-53-(Al)-AMSuc showed new stretches around 1720 cm^{-1} characteristic of carbonyl group. In addition, the N-H bands at 3500 to 3387 cm^{-1} , associated with the amine of the $\text{NH}_2\text{-BDC}$ ligand, were notably diminished (Figure 5-4). In addition, electrospray ionization mass spectroscopy (ESI-MS) of modified materials (digested in an $\text{HF}/\text{CH}_3\text{CN}$ solution) confirmed PSM on the $\text{NH}_2\text{-BDC}$ ligands (Figure 5-5 and Figure 5-6). The structural and thermal properties of the modified MILs were found to closely resemble that of MIL-53(Al)- NH_2 as evidenced by power X-ray diffraction

(PXRD) (Figure 5-7) and thermogravimetric analysis (TGA) (Figure 5-8). Taken together, the data show that the modified MIL-53(Al)-NH₂ materials were functionalized as expected, while remaining robust, crystalline solids.

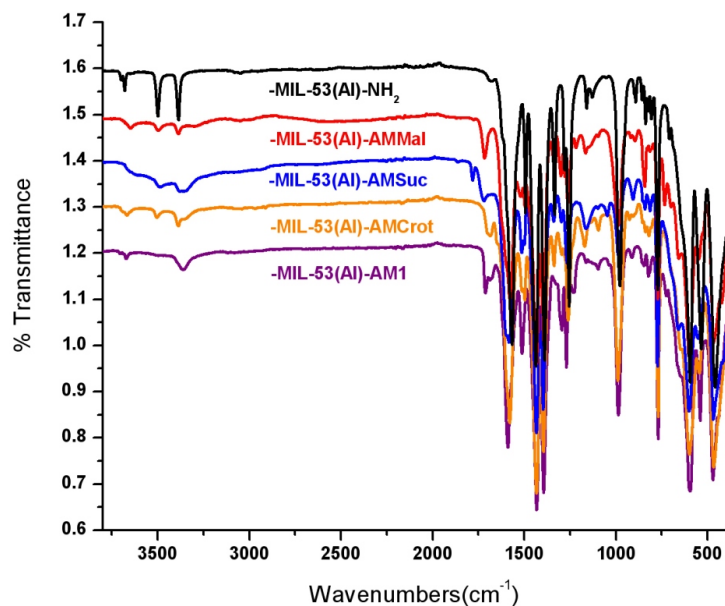


Figure 5-4. FT-IR spectra of modified MIL-53(Al)-NH₂ samples.

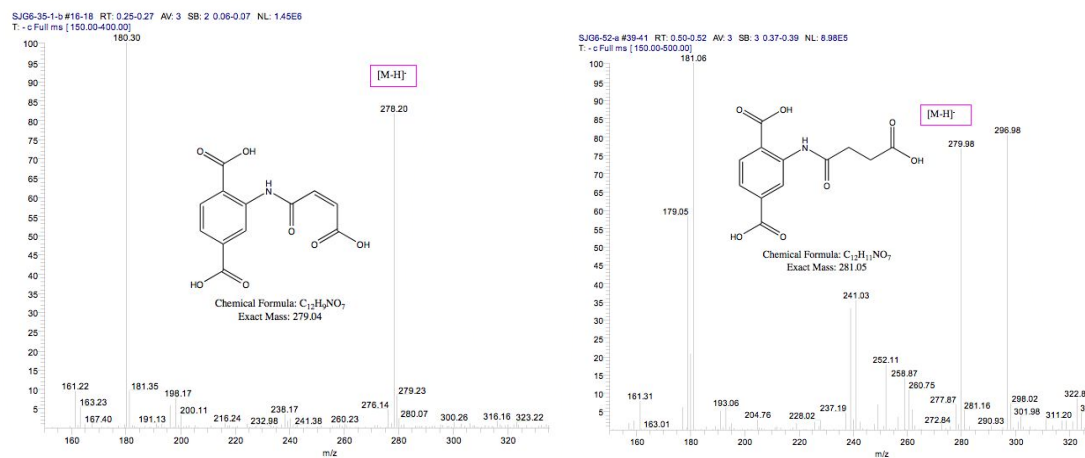


Figure 5-5. ESI-MS(-) of digested MIL-53(Al)-AMMal (right) and MIL-53(Al)-AMSuc (left) showing the mass peak associated with their corresponding carboxylate functionalized ligands.

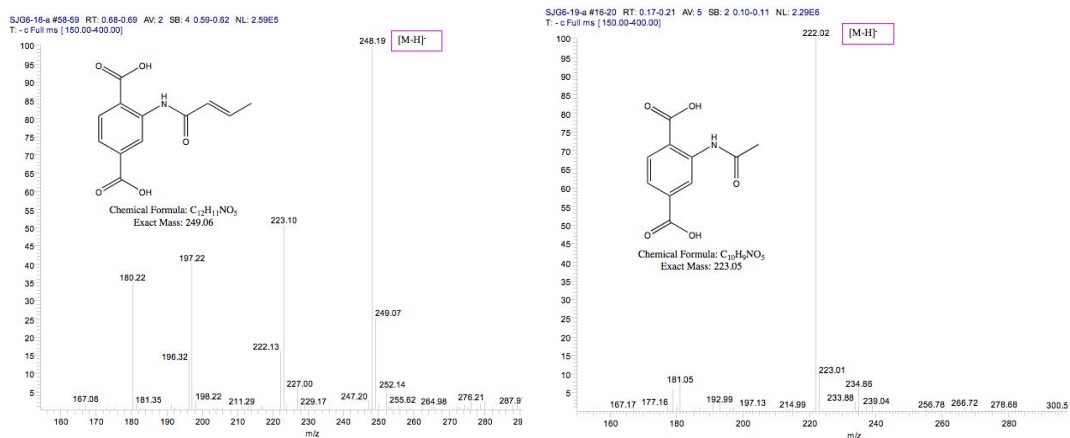


Figure 5-6. ESI-MS(-) of digested MIL-53(Al)-AMCrot (right) and MIL-53(Al)-AM1 (left) showing the mass peak associated with their corresponding amide functionalized ligands.

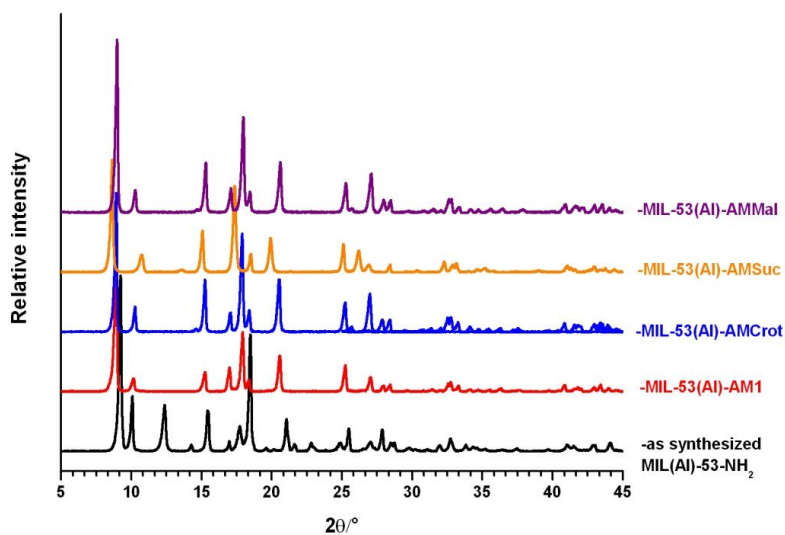


Figure 5-7. PXRD patterns of MIL-53(Al)-AMMal (purple), MIL-53(Al)-AMSuc (orange), MIL-53(Al)-AMCrot (blue), MIL-53(Al)-AM1 (red), and MIL-53(Al)-NH₂ (black).

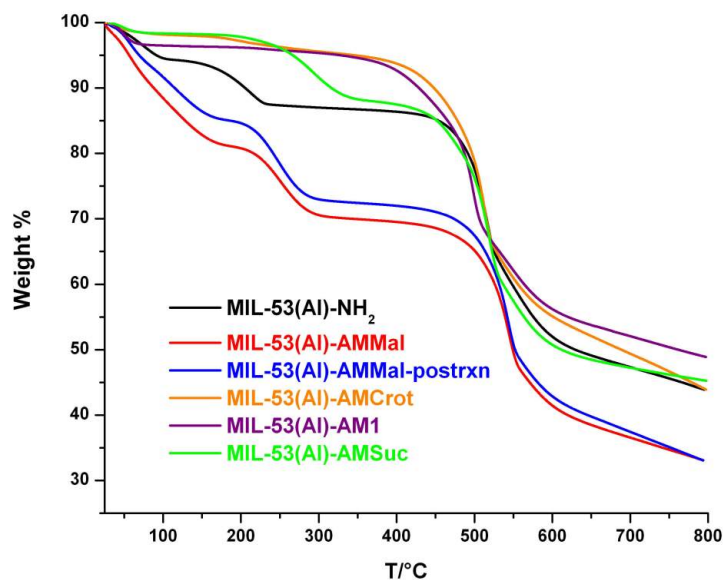
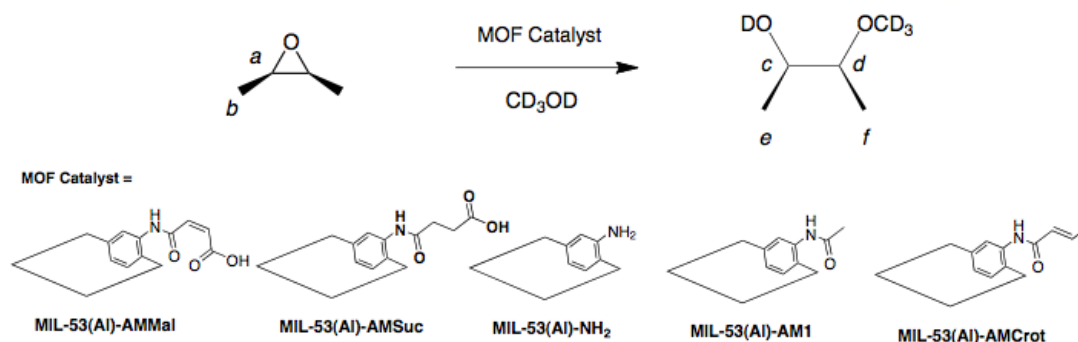


Figure 5-8. Thermogravimetric analysis of MIL-53(Al)-NH₂ (black), MIL-53(Al)-AMMal (red), MIL-53(Al)-AMMal after catalysis and reactivation (blue), MIL-53(Al)-AMCrot (orange), MIL-53(Al)-AM1 (purple), and MIL-53(Al)-AMSuc (green).

Having demonstrated that MIL-53(Al)-NH₂ could be modified with these cyclic anhydrides without degradation of the framework, the ability of these solid-state Brønsted acid materials to perform as catalysts in the methanolysis of *cis*-2,3-epoxybutane was explored. In order to confirm the origin of catalysis (i.e. Brønsted acid catalysis), control experiments with the structural surrogates MIL-53(Al)-NH₂, MIL-53(Al)-AM1, and MIL-53(Al)-AMCrot were performed in parallel (Scheme 5-2).



Scheme 5-2. Methanolysis of *cis*-2,3-epoxybutane with carboxylate functionalized MIL-53(Al)-AMMal, MIL-53(Al)-AMSuc and control analogues. Letters *a-f* represent the protons associated with starting material and the ring opening product.

The MOF solids (~0.08 mmol of carboxylate group) were pre-dried for ~5 h and were then added to a CD₃OD solution containing epoxide (0.40 mmol). After two days under ambient conditions, ¹H NMR revealed that the epoxide essentially underwent complete (>95%) conversion with MIL-53(Al)-AMMal, but there was no conversion with MIL-53(Al)-AMSuc or any of the control materials (Figure 5-9). These results strongly suggested that the carboxylate groups in MIL-53(Al)-AMMal were essential to catalyze the methanolysis of *cis*-2,3-epoxybutane.

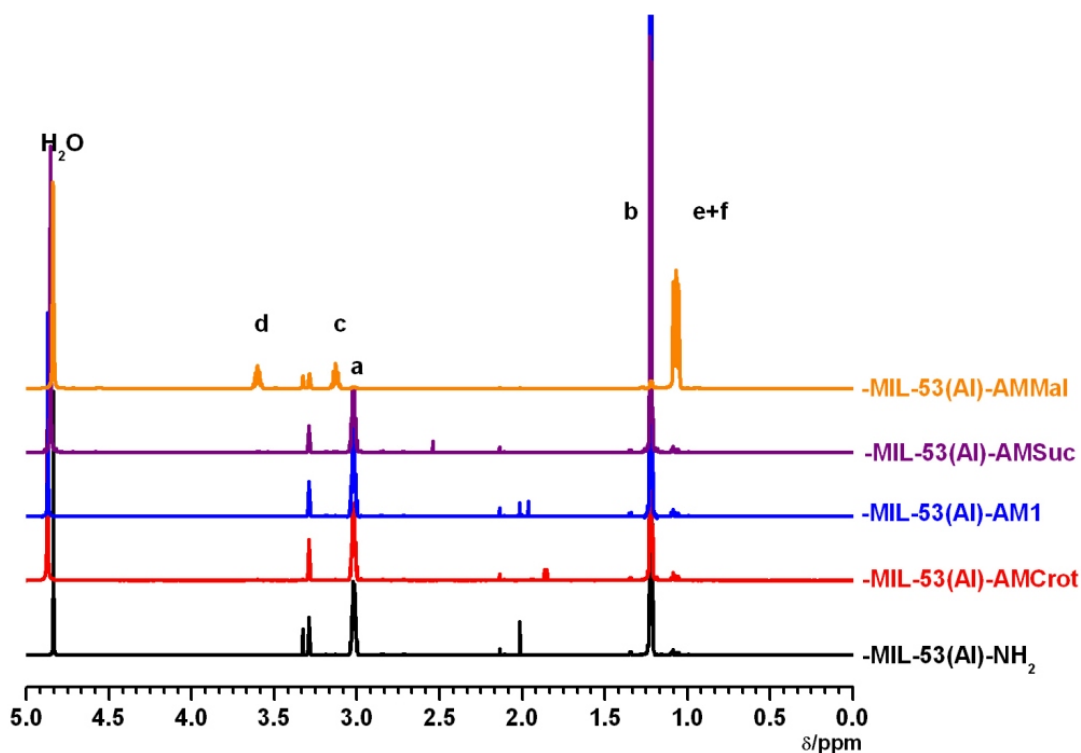


Figure 5-9. ^1H NMR of catalytic reaction aliquots employing MIL-53(Al)-AMMal (green), MIL-53(Al)-AM1 (blue), MIL-53(Al)-AMCrot (red), and MIL-53(Al)- NH_2 (black).

To confirm that MIL-53(Al)-AMMal was acting in a heterogeneous manner, aliquots of the reaction mixture were taken after undergoing partial conversion and monitored by ^1H NMR over the course of several days for up to one week. The methanolysis of *cis*-2,3-epoxybutane is indeed a heterogeneous reaction, as the signals associated with product formation did not change after removal of the MIL catalysis (Figure 5-10).

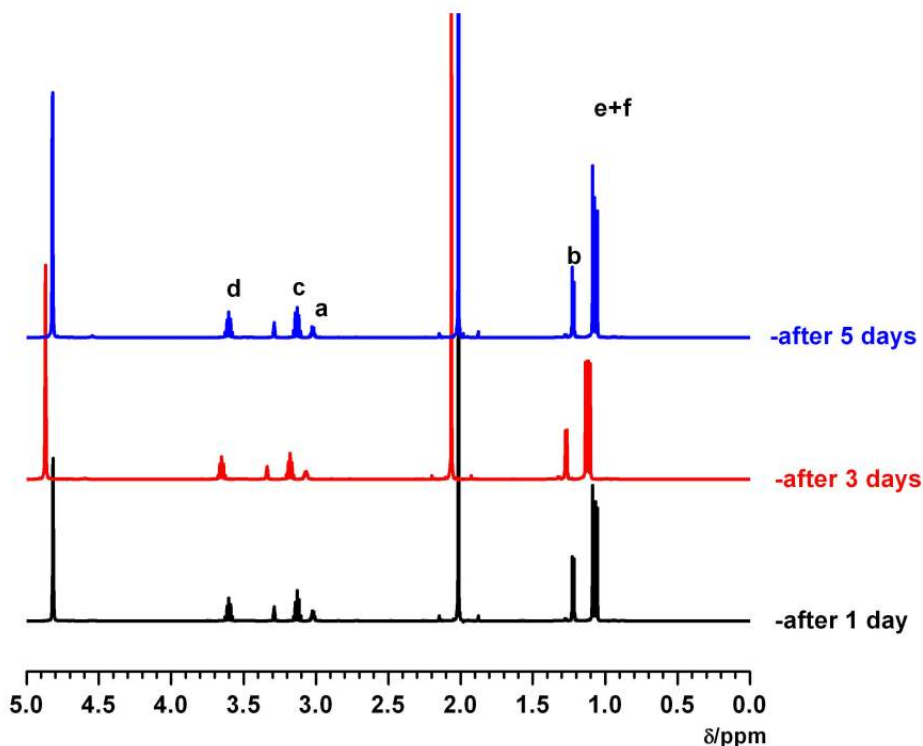


Figure 5-10. ^1H NMR spectra of aliquots removed from solid catalyst MIL-53(Al)-AMMal after 1 day (black), 3 days (red), and 5 days (blue).

The observation that MIL-53(Al)-AMSuc did not show good catalytic activity when compared with MIL-53(Al)-AMMal was particularly intriguing. While MIL-53(Al)-AMSuc contains approximately the same number of free carboxylate groups, it does not show catalytic activity above that observed with the control materials studied (Figure 5-9). The disparity in catalytic activity likely originates from the difference in the acidity of the carboxylic acids. Unlike the succinic acid functionality, the maleic acid contains a conjugated C=C double bond, which can resonance stabilize the conjugate base resulting in higher acidity. As a rough approximation, propionic acid has a pK_a of 4.87, while its conjugated analogue, acrylic acid, has a pK_a of 4.25, more than a half a log unit lower. Consistent with the MOF findings, homogenous experiments for the methanolysis of *cis*-2,3,-epoxybutane using maleic and succinic

modified dimethyl amino terephthalate ligands (DMT-AMMal, and DMT-AMSuc) gave similar results (Figure 5-11), with the DMT-AMMal ligand promoting the reaction much more effectively than DMT-AMSuc (21% compared to 2%, respectively).

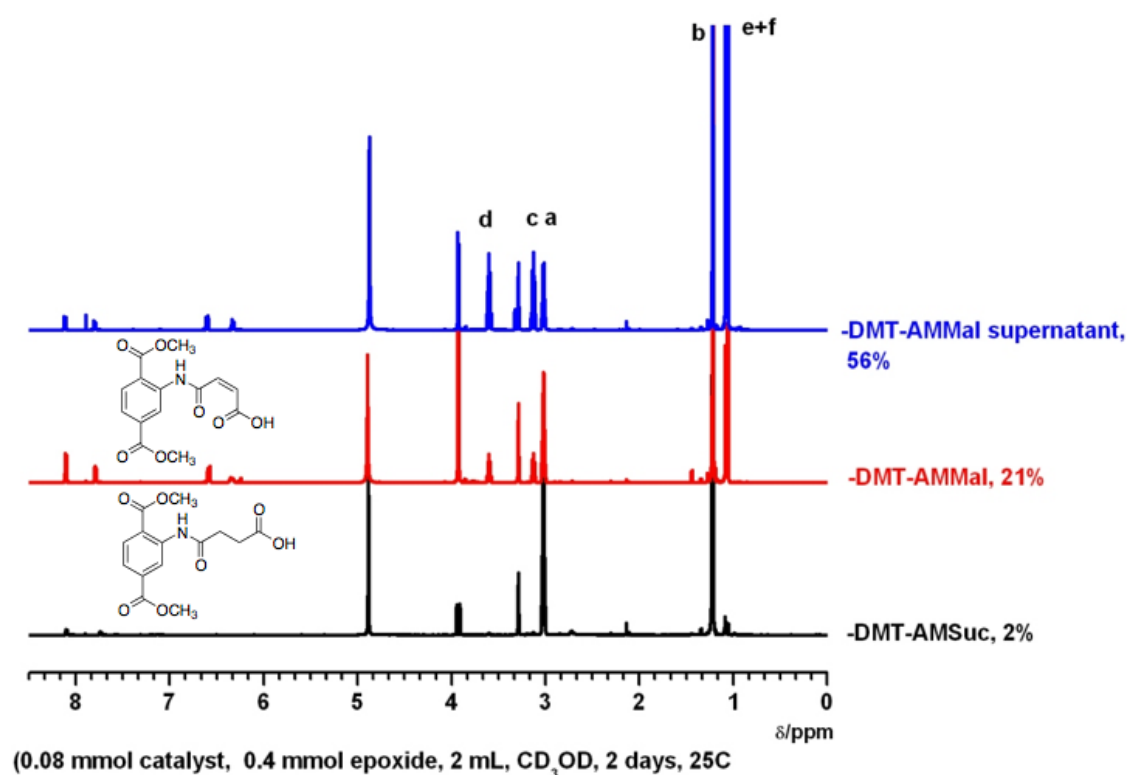


Figure 5-11. ^1H NMR spectra of the methanolysis of *cis*-2,3-epoxybutane utilizing homogeneous catalyst DMT-AMSuc (black), DMT-AMMal (red), and the supernatant of methanolysis with DMT-AMMal after removal from catalyst (blue).

To establish the recyclability of MIL-53(Al)-AMMal, the reaction mixtures were removed and the catalyst extensively washed with CD_3OD . The solid catalyst was then placed in a second catalytic reaction employing the same reaction conditions. Unfortunately, the recycled catalyst showed a significant reduction in activity (10 % compared to 95%) (Figure 5-12). Given that the MOF is exposed to a large excess of

methanol during catalysis, it was suspected that esterification of the carboxylic acid moieties could be responsible for the reduction in activity of subsequent catalytic reactions. Indeed, prolonged exposure of MIL-53(Al)-AMMal to methanol prior to the first catalytic cycle significantly hampered its ability to perform the methanolysis of *cis*-2,3,-epoxybutane. For example, freshly synthesized MIL-53-AMMal samples were treated with CD₃OD (2 mL) and allowed to stand at ambient conditions for 2, 4, and 7 days. These pre-treated samples were utilized as catalysts in the methanolysis of *cis*-2,3,-epoxybutane, but ¹H NMR revealed a decrease in product formation as a consequence of prolonged exposure to CD₃OD (Figure 5-13). Based on ¹H NMR integration, conversion from these pretreated MIL-53-AMMal samples for 2, 4, and 7 days were 43, 33, and 2%, respectively. These findings support the hypothesis that esterification of the carboxylate moieties is responsible for the reduced catalytic properties of MIL-53-AMMal after the first round of catalysis.

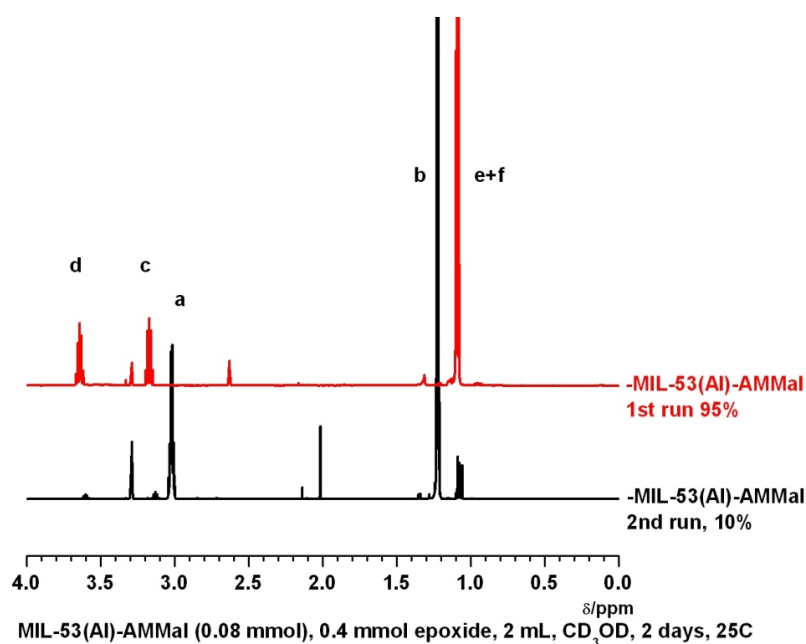


Figure 5-12. ¹H NMR spectra of the methanolysis of *cis*-2,3-epoxybutane utilizing fresh (red) and recycled (black) MIL-53(Al)-AMMal.

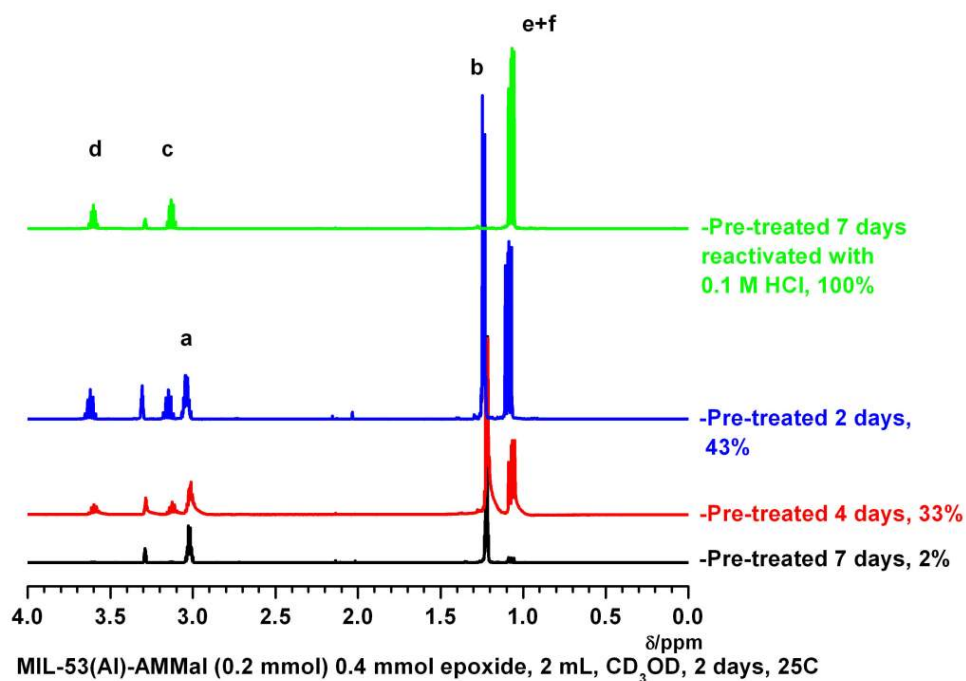


Figure 5-13. ^1H NMR spectra of the methanolysis of *cis*-2,3-epoxybutane utilizing MIL-53(Al)-AMMal pre-treated with CD_3OD for 7 days (black), 4 days (red), 2 days (blue) and 7 days and subsequently treated with 0.1 M HCl (green).

We reasoned that if the carboxylate groups of MIL-53(Al)-AMMal were undergoing esterification then hydrolysis should re-establish the activity of the solid state Brønsted acid catalyst. To test this hypothesis, inactive MIL-53(Al)-AMMal that had been through one catalytic cycle was soaked 0.1 M HCl (13 mL) overnight, followed by washing with H_2O (3×6 mL) and drying at 100°C . Treatment with HCl successfully restored the catalytic activity of MIL-53(Al)-AMMal (Figure 5-14). Due to the robust nature of the MIL-53(Al) system, treatment with HCl does not degrade the structural integrity of MIL-53(Al)- NH_2 or MIL-53(Al)-AMMal as evidenced by PXRD (Figure 5-15). The catalytic properties of inactive MIL-53(Al)-AMMal (turnover $<2\%$), pretreated with CD_3OD for a week, showed complete restoration of

activity upon treatment with HCl. We confirmed that the renewed catalytic activity is not the result of residual HCl, as a control reaction involving MIL-53(Al)-NH₂, MIL-53(Al)-AM1, and MIL-53(Al)-AMSuc treated identically with HCl led to insignificant catalytic activity (<2%, Figure 5-14). These findings suggest that the observed reduction in reactivity of MIL-53(Al)-AMMal is likely due to ester formation, which can be reversed upon hydrolysis with acid. With acidic treatment, MIL-53(Al)-AMMal provides a robust and recyclable solid-state catalyst. MIL-53(Al)-AMMal can successfully undergo three catalytic cycles or more with consistent activity (Figure 5-16).

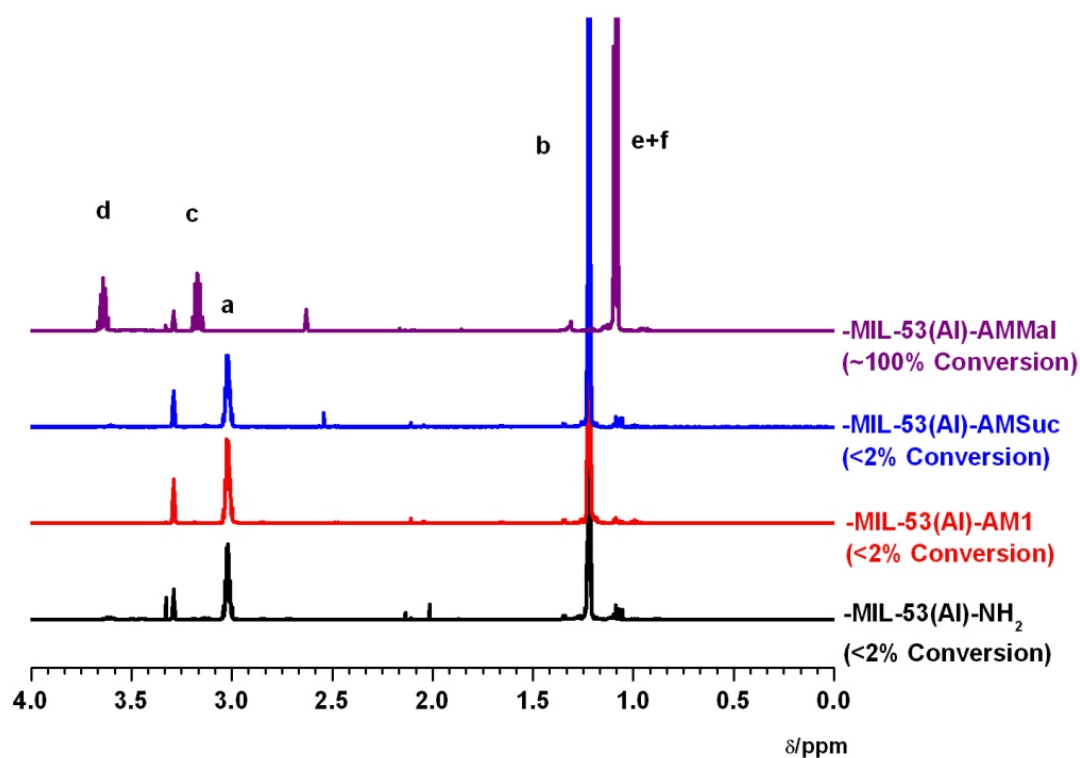


Figure 5-14. ¹H NMR spectra of the methanolysis of *cis*-2,3-epoxybutane utilizing MIL-53(Al)-NH₂ treated with 0.1 M HCl.

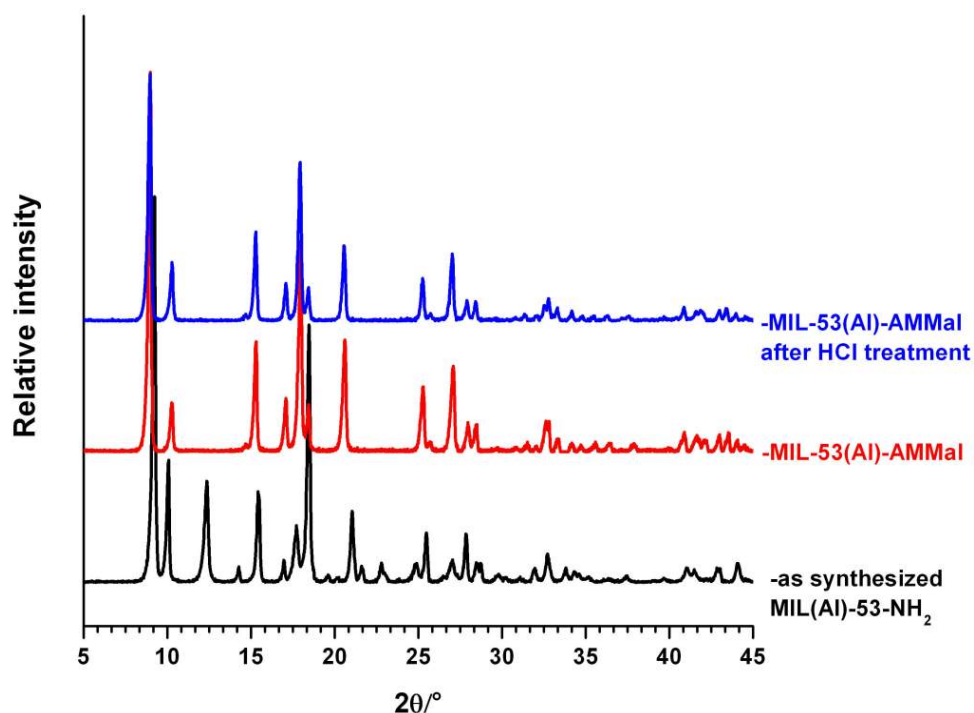


Figure 5-15. PXRD patterns of MIL-53(Al)-NH₂ (black) and MIL-53(Al)-AMMal (red) and MIL-53(Al)-AMMal treated with 0.1 M HCl.

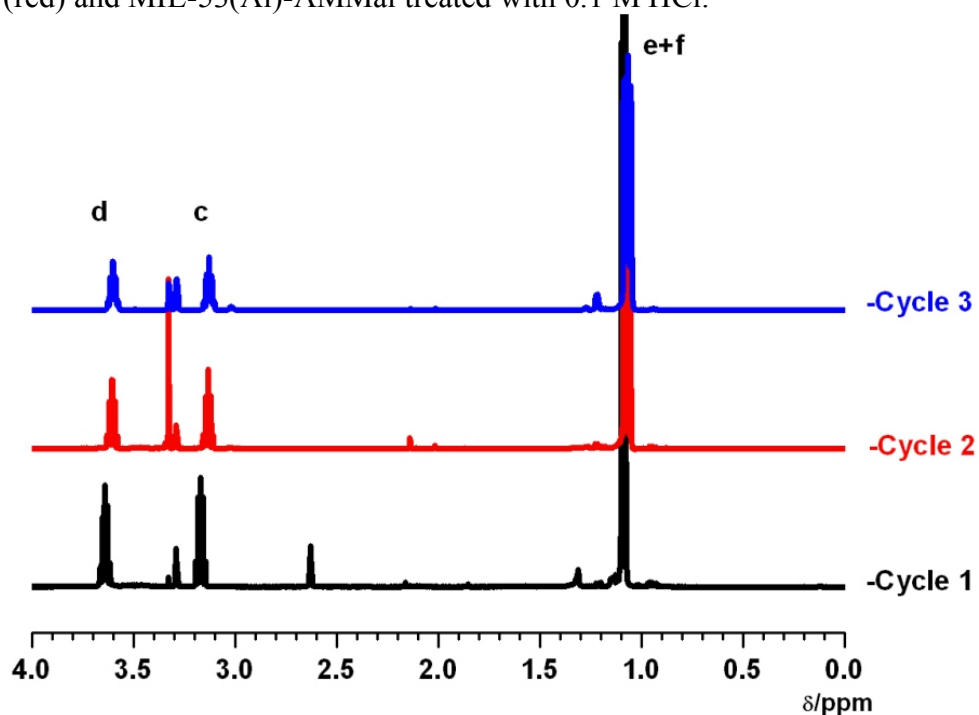


Figure 5-16. ¹H NMR spectra of three consecutive reactions of the methanolysis of *cis*-2,3-epoxybutane utilizing MIL-53(Al)-AMMal showing essentially quantitative conversion after the 1st cycle (black), 2nd cycle (red), and 3rd cycle (blue). The MIL was regenerated with HCl between each reaction cycle.

Attempts were made to determine the minimum catalyst loading for these reactions. MIL-53(Al)-AMMal samples containing 0.08 mmol of the catalytic group (maleic acid functionality) were introduced to solutions containing 8, 0.8, and 0.4 mmol of *cis*-2,3-epoxybutane, which corresponds to 1, 10, and 20% catalyst loadings. ^1H NMR of these reaction mixtures after two days under ambient conditions showed that the methanolysis reactions with 1, 10, and 20 % catalyst loading led to ~10%, 90%, and ~95% conversion, respectively (Figure 5-17). Therefore, under the present reaction conditions, at least 10% loading was required to obtain high conversions within two days.

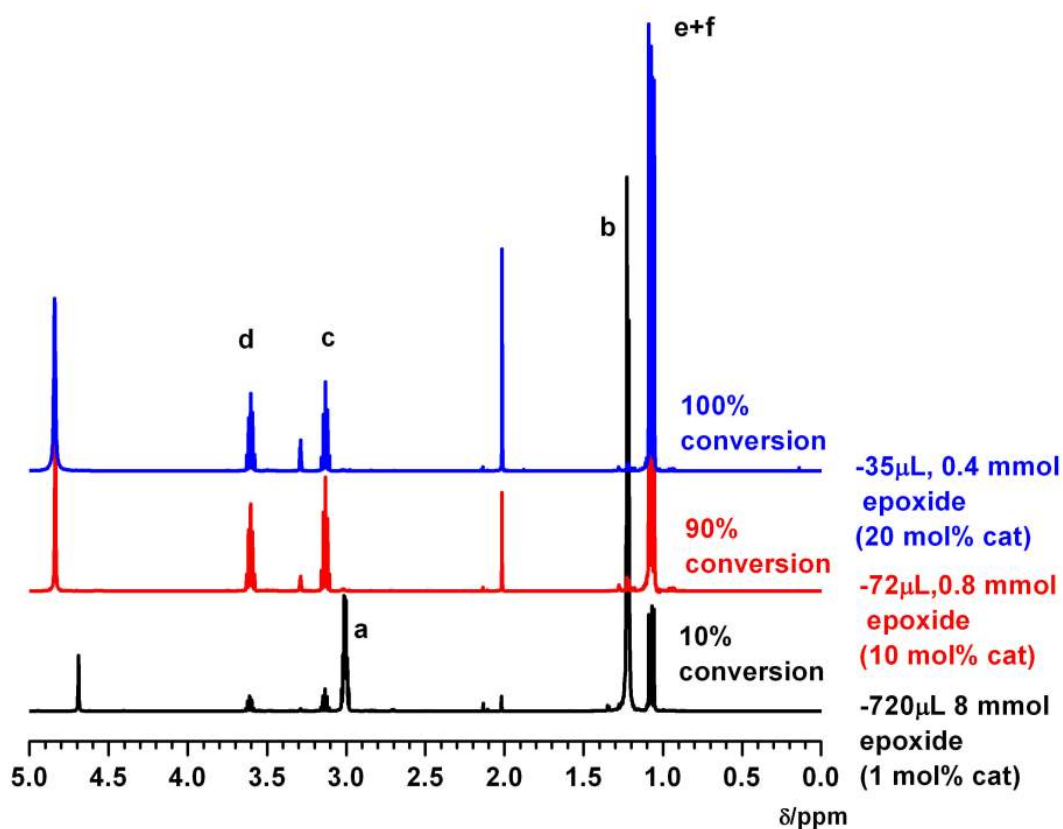

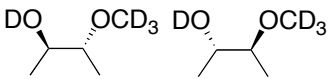

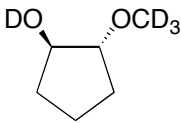
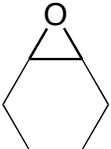
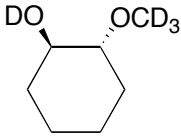
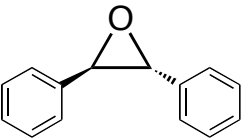
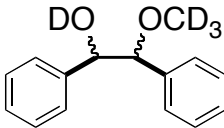
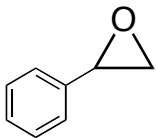
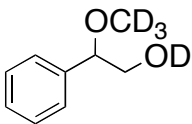
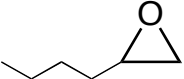
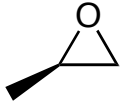
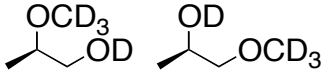


Figure 5-17. ^1H NMR spectra of the methanolysis of *cis*-2,3-epoxybutane utilizing MIL-53(Al)-AMMal with 1 (black), 10 (red), and 20 mol% (red) catalyst loadings.

Given the modest success in facilitating the methanolysis of *cis*-2,3,-epoxybutane, the catalytic scope of MIL-53(Al)-AMMal in the transformation of different epoxides was investigated. Under identical conditions, MIL-53(Al)-AMMal initiates the methanolysis of several epoxides (Table 5-1). MIL-53(Al)-AMMal promotes the methanolysis of cyclopentene oxide, cyclohexene oxide, styrene oxide, and *trans*-stilbene oxide, while the asymmetric 1,2-epoxyhexane is not activated by the catalyst (Figures 5-18 to 5-23). It is unclear why the latter substrate is not efficiently turned over by the MIL-53(Al)-AMMal catalyst. Size exclusion from the MIL pores does not explain this result as the sterically more crowded cyclohexene oxide, styrene oxide, and *trans*-stilbene oxide are converted with MIL-53(Al)-AMMal as a catalyst. The only apparent feature of 1,2-epoxyhexane is its asymmetric structure, although it is unclear why this feature would inhibit catalytic turnover, as it does not appear to inhibit the reaction with styrene oxide. Nonetheless, consistent with this finding, (*R*)-(+)-propylene oxide was a significantly poorer substrate for MIL-53(Al)-AMMal than *cis*-2,3,-epoxybutane, giving a yield of only 59% (Figure 5-23).

Table 5-1. Methanolysis of Epoxides with MIL catalysts.^a

Reagent	Product	Catalyst MIL-53(Al)-	Conversion [%] ^b
<i>cis</i> -2,3-epoxybutane		AMMal	95 ± 2
		AMSuc	<2
		AMCrot	<2
		AM1	<2
		NH ₂	<2
Cyclopentene oxide		AMMal	44 ± 4
			
Cyclohexene oxide		AMMal	100 ± 2
			
<i>trans</i> -stilbene oxide		AMMal	37 ± 4
			
Styrene oxide		AMMal	100 ± 2
			
1,2-epoxyhexane	No reaction	AMMal	No reaction
			
(<i>R</i>)-(+)-propylene oxide		AMMal	59 ± 4
			

^aMIL catalysts (*ca.* 0.08 mmol) were added to a CD₃OD solution containing the epoxide substrate (*ca.* 0.40 mmol) and was allowed to stand for 2 days at RT. ^bThe conversions are based on at least three independent trials.

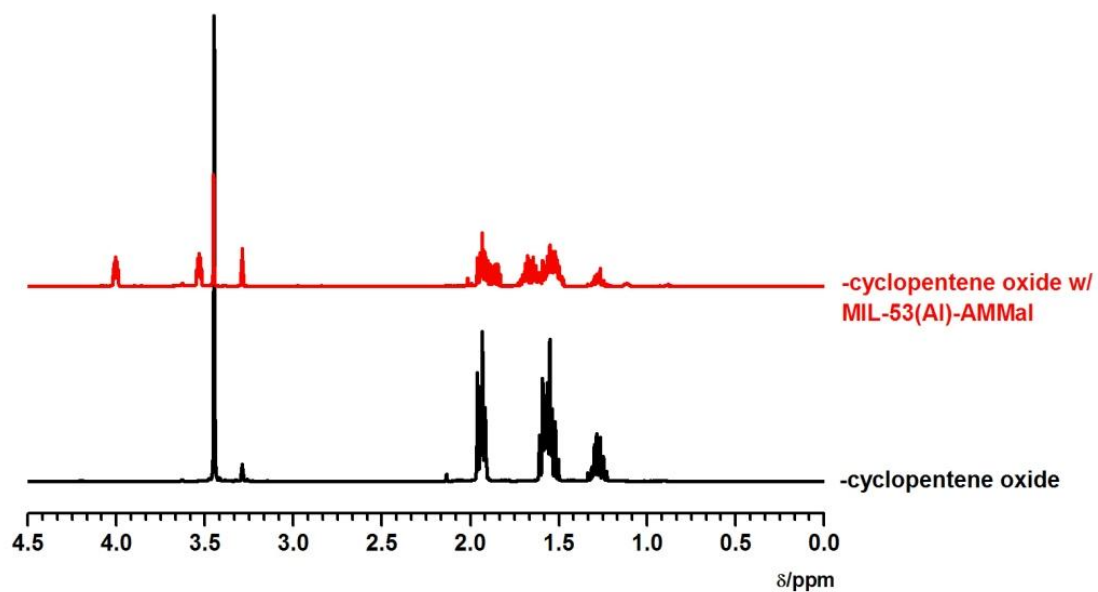


Figure 5-18. ¹H NMR spectra of the methanolysis of cyclopentene oxide utilizing MIL-53(Al)-AMMal (red) and untreated cyclopentene oxide (black).

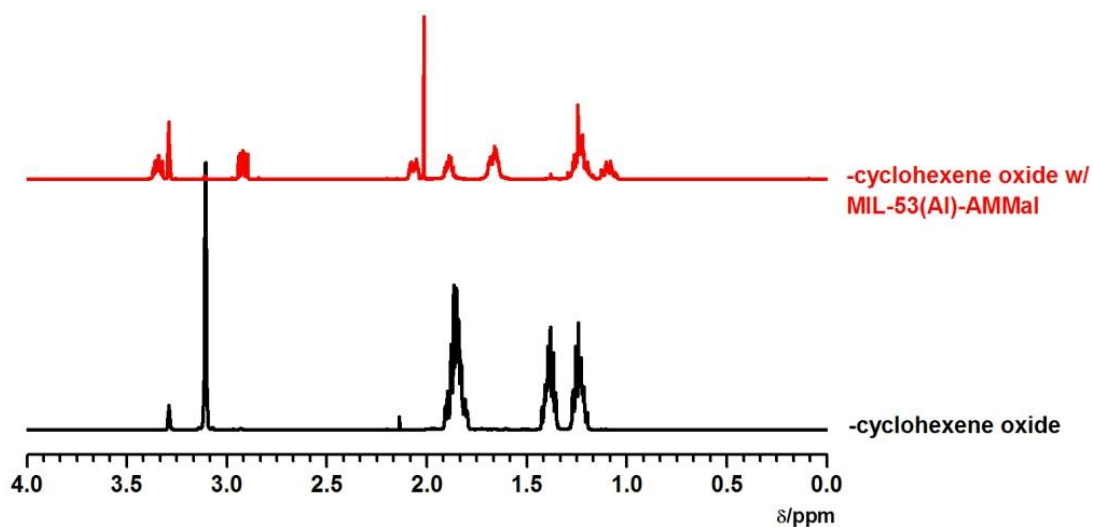


Figure 5-19. ¹H NMR spectra of the methanolysis of cyclohexene oxide utilizing MIL-53(Al)-AMMal (red) and untreated cyclohexene oxide (black).

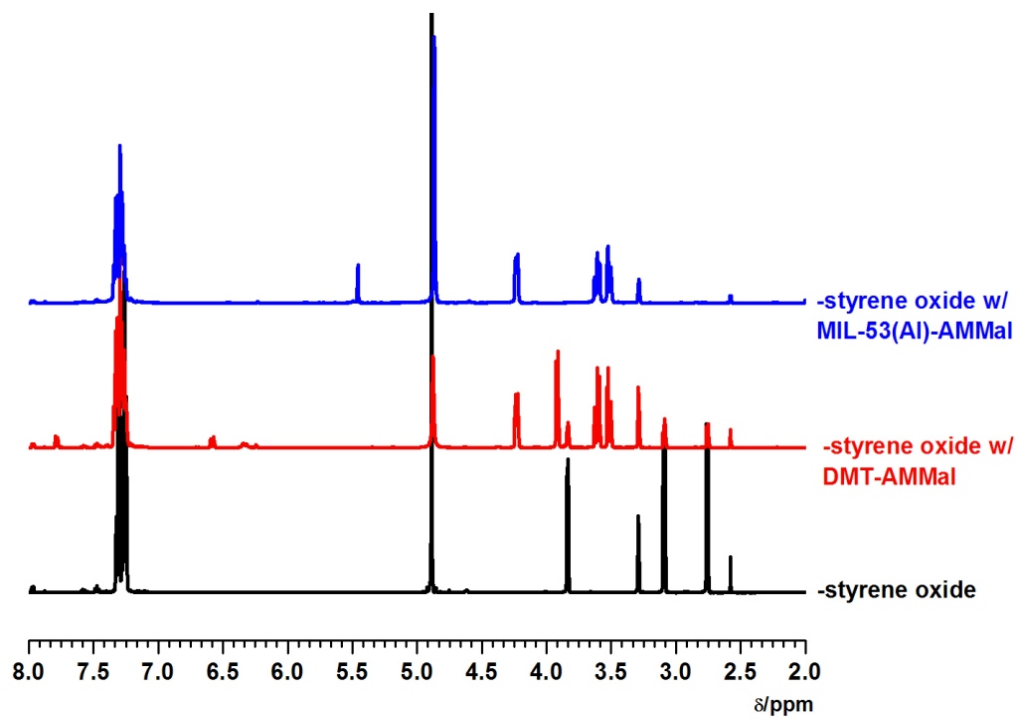


Figure 5-20. ^1H NMR spectra of the methanolysis of styrene oxide utilizing MIL-53(Al)-AMMal (blue), DMT-AMMal (red), and untreated styrene oxide (black).

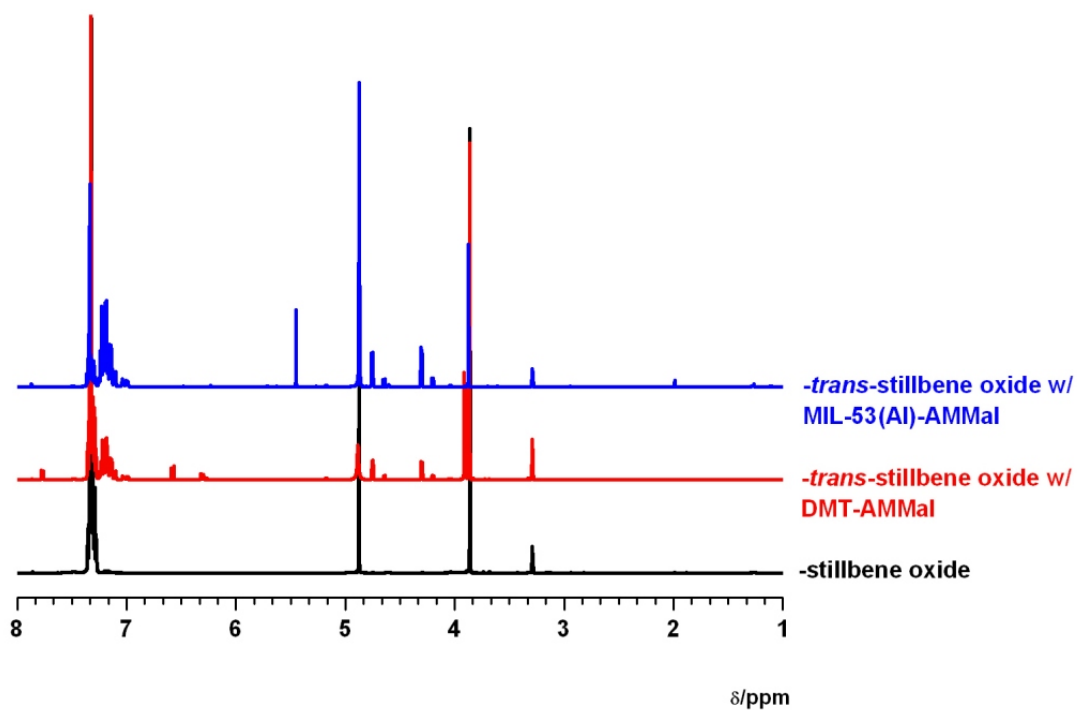


Figure 5-21. ^1H NMR spectra of the methanolysis of *trans*-stilbene oxide utilizing MIL-53(Al)-AMMal (blue), DMT-AMMal (red) and untreated *trans*-stilbene oxide (black).

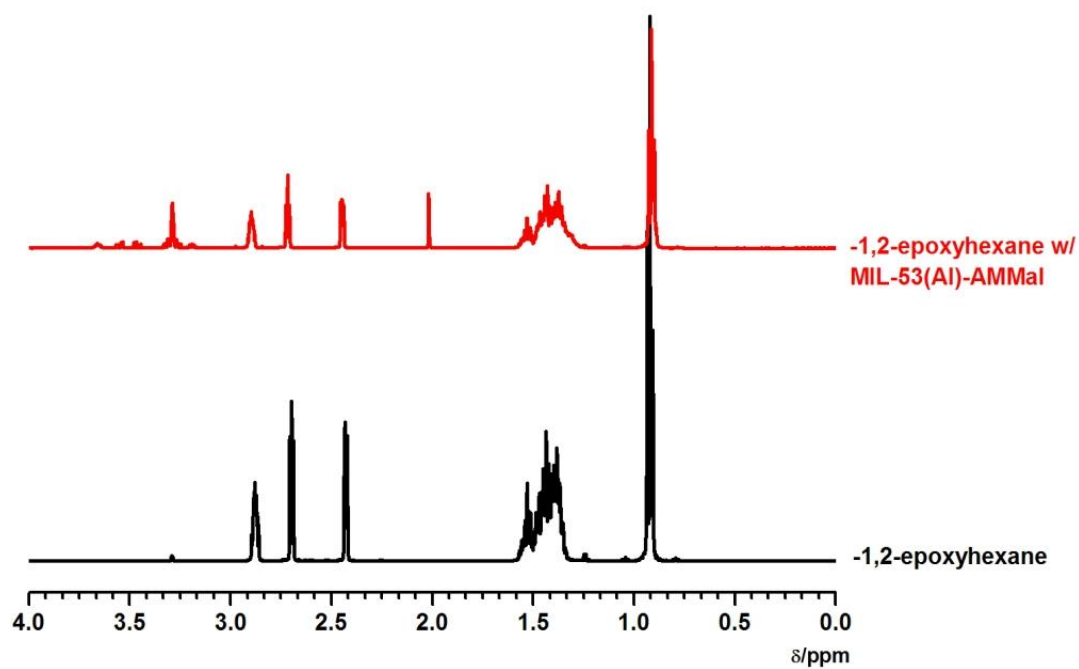


Figure 5-22. ^1H NMR spectra of the methanolysis of 1,2-epoxyhexane oxide utilizing MIL-53(Al)-AMMal (red) and untreated 1,2-epoxyhexane oxide (black).

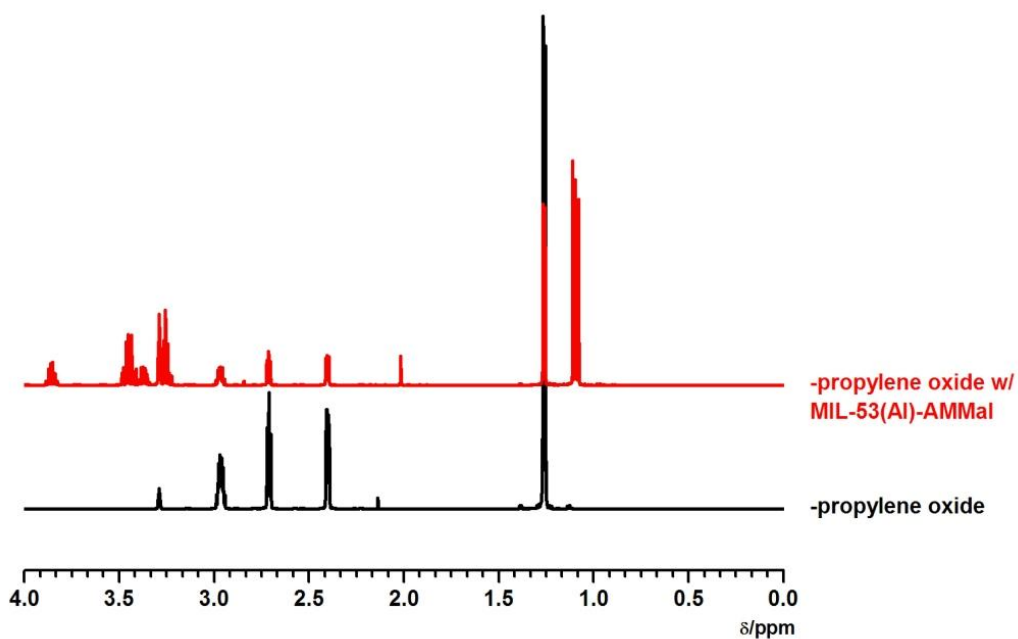


Figure 5-23. ^1H NMR spectra of the methanolysis of propylene oxide utilizing MIL-53(Al)-AMMal (red) and untreated propylene oxide (black).

5.3 Conclusions

In summary, the findings presented in this study demonstrate that PSM is a viable method for incorporating an acidic, organocatalytic group into a MOF. MIL-53(Al)-NH₂ was treated with maleic anhydride producing a carboxylate acid functionalized material. The carboxylate groups residing in the framework were utilized as Brønsted acid catalytic sites for the methanolysis of epoxides. While MIL-53(Al)-AMMal facilitated the ring opening of several epoxides, another carboxylate functionalized MIL possessing a weaker acidic group, MIL-53(Al)-AMSuc, did not facilitate catalysis. The methanolysis reaction was found to be genuinely heterogeneous, but required regeneration with exogenous acid for recovery as a reusable catalyst.

5.4 Experimental Methods

General. Starting materials and solvents were purchased and used without further purification from commercial suppliers (Sigma-Aldrich, Alfa Aesar, EMD, TCI, Cambridge Isotope Laboratories, Inc., and others). MIL-53(Al)-NH₂²⁹ and MIL-53(Al)-AM1³⁰ were synthesized and activated as described previously.

DMT-AMMal. Maleic anhydride (17.4 g, 177 mmol) was added to a solution of dimethyl amino terephthalate (1.06 g, 5.1 mmol) in ~125 mL of CHCl₃. The solution was stirred for 24 h at room temperature. The solvent was removed by rotary evaporation. The brown solid was washed with ~100 mL of ethyl acetate, filtered, and washed with ~100 mL of CHCl₃. The product was dried at ~85 °C. Yield = 27%. ¹H

NMR (500 MHz, d^6 -DMSO): δ 10.75 (s, 1 H), 8.7 (s, 1H), 7.96-7.6 (d, 2H), 6.5-6.34 (d, 2H), 3.8 (s, 6H). ESI-MS m/z 306.07 [M-H]⁻.

DMT-AMSuc. Succinic anhydride (17.9 g, 177 mmol) was added to a solution of dimethyl amino terephthalate (1.06 g, 5.1 mmol) in ~125 mL of CHCl₃. The solution was stirred for 24 h at room temperature. The solvent was removed by rotary evaporation. The brown solid was washed with ~100 mL of ethyl acetate filtered and washed with ~100 mL of CHCl₃. The product was dried at ~85 °C. Yield = 67%. ¹H NMR (500 MHz, d^6 -DMSO): δ 12.19 (s, 1H), 10.54 (s, 1 H), 8.7 (s, 1H), 7.96-7.6 (d, 2H), 3.8 (s, 6H), 2.6-2.5 (d, 4H). ESI-MS m/z 308.00 [M-H]⁻.

MIL-53(Al)-AMMal. In a typical reaction, residual DMF was removed from microcrystalline MIL-53(Al)-NH₂ (~60 mg) by heating at 150 °C for 5 h. The activated MIL-53(Al)-NH₂ (~50 mg 0.2 mmol-NH₂) was treated with a 5 mL solution of CH₃CN containing the anhydride (12 mmol) and heated at 80 °C for 24 h. After the reaction was complete the sample was rinsed with CH₃CN (3×6 mL), centrifuged, and dried at 80 °C for up to 2 h resulting in 43±4% (-AMMal), 39±4% (-AMSuc), and 34±4% (-AMCrot) conversion.

¹H NMR Digestion and Analysis. Approximately 10 mg of microcrystalline MIL was digested by sonication in one of two digestion cocktails: a) 400 μ L D₂O and 200 μ L of NaOH 40 wt. % of D₂O; or b) 570 μ L of d^6 -DMSO and 30 μ L of HF. After complete dissolution of the crystals, the solution was used to collect a ¹H NMR spectrum. ¹H NMR spectra were recorded on a JEOL ECA spectrometer (500 MHz).

ESI-MS Analysis. Electrospray ionization mass spectrometry (ESI-MS) was performed using a ThermoFinnigan LCQ-DECA mass spectrometer and the data were

analyzed using the Xcalibur software suite in negative ion mode. MIL samples were digested by sonicating the materials in a mixture of 10 μL of HF and 1.0 mL of CH_3CN .

Thermal Gravimetric Analysis. Approximately 10-20 mg of modified MIL samples were dried at 150 $^\circ\text{C}$ for 5 h and used for TGA measurements. Samples were analyzed under a stream of dinitrogen using a TA Instrument Q600 SDT running from room temperature to 800 $^\circ\text{C}$ with a scan rate of 5 $^\circ\text{C min}^{-1}$.

PXRD Analysis. PXRD data were collected at ambient temperature on a Bruker Advance D8 diffractometer at 40 kV, 40 mA for $K\alpha$ ($\lambda = 1.5418 \text{ \AA}$) with a scan speed of 3 $^\circ \text{min}^{-1}$, a step size of 0.02 $^\circ$ in 2θ and a 2θ range of 5-45 $^\circ$. Approximately 15 mg of microcrystalline MIL samples were dried at 150 $^\circ\text{C}$ for at least 2 h before PXRD analysis. The experimental backgrounds were corrected using the Jade 5.0 software package.

FT-IR Analysis. Approximately 5-10 mg of modified MIL was dried at 150 $^\circ\text{C}$ for at least 2 h before FT-IR analysis. FT-IR spectra were collected using a Bruker ALPHA-P FT-IR spectrometer with a diamond ATR.

Catalysis Experiments. In a typical reaction, the MIL microcrystalline solids (*ca.* 0.20 mmol equiv of BDC ligand and) were pre-dried for ~ 5 h and added to a CD_3OD solution (2 mL) containing the epoxide substrate (0.40 mmol). The reaction was allowed to stand for 2 d at 25 $^\circ\text{C}$. At the end of the reaction, *ca.* 0.8 mL aliquot was taken from the mixture and used for ^1H NMR measurements.

Catalyst Recycling. After the completion of a reaction with epoxide, the CD_3OD solution was decanted and the MIL solids were washed with CHCl_3 (3 \times 6 mL,

isolated by centrifugation between washes) before soaking in 10 mL of pure CHCl_3 for three days, with fresh CHCl_3 added every 24 h. After three days of soaking the solids were stored in the last CHCl_3 solution until needed.

Catalyst Regeneration. The CHCl_3 storage solution was decanted away from the inactive MOF catalysts (see Catalyst Recycling above), and the solids were dried at 55 °C for up to 2 h. To the dried MOFs, ~13 mL of a 0.1 M HCl aqueous solution was added and allowed to stand for ~18 h. The solids was centrifuged and washed with H_2O (3×6 mL) and dried at 100 °C for at least 2 h.

5.5 Acknowledgements

Text, schemes, and figures in this chapter, in part, are reprints of the materials published in the following papers: Garibay, S. J., Wang, Z., Cohen, S. M. "Evaluation of Heterogeneous Metal-Organic Framework Organocatalysts Prepared by Postsynthetic Modification" *Inorg. Chem.* **2010**, *49*, 8086-8091. The dissertation author was the primary researcher and author for the data presented. The co-authors listed in these publications also participated in the research.

5.6 References

- (1) Eddaoudi, M.; Moler, D. B.; Li, H.; Chen, B.; Reineke, T. M.; O'Keeffe, M.; Yaghi, O. M. *Acc. Chem. Res.* **2001**, *34*, 319-330.
- (2) Ockwig, N. W.; Delgado-Friedrichs, O.; O'Keeffe, M.; Yaghi, O. M. *Acc. Chem. Res.* **2005**, *38*, 176-182.
- (3) Furukawa, H.; Yaghi, O. M. *J. Am. Chem. Soc.* **2009**, *131*, 8875-8883.
- (4) Rowsell, J. L. C.; Yaghi, O. M. *Angew. Chem. Int. Ed.* **2005**, *44*, 4670-4679.
- (5) Llewellyn, P. L.; Bourrelly, S.; Serre, C.; Vimont, A.; Daturi, M.; Hamon, L.; De Weireld, G.; Chang, J. S.; Hong, D. Y.; Kyu Hwang, Y.; Hwa Jung, S.; Ferey, G. *Langmuir* **2008**, *24*, 7245-7250.
- (6) Latroche, M.; Surble, S.; Serre, C.; Mellot-Draznieks, C.; Llewellyn, P. L.; Lee, J. H.; Chang, J. S.; Jhung, S. H.; Ferey, G. *Angew. Chem. Int. Ed.* **2006**, *45*, 8227-8231.
- (7) Dinca, M.; Dailly, A.; Liu, Y.; Brown, C. M.; Neumann, D. A.; Long, J. R. *J. Am. Chem. Soc.* **2006**, *128*, 16876-16883.
- (8) Ma, S.; Zhou, H. C. *Chem. Commun.* **2010**, *46*, 44-53.
- (9) Britt, D.; Tranchemontagne, D.; Yaghi, O. M. *Proc. Natl. Acad. Sci. U. S. A.* **2008**, *105*, 11623-11627.
- (10) Ahmad, R.; Wong-Foy, A. G.; Matzger, A. J. *Langmuir* **2009**, *25*, 11977-11979.
- (11) Nuzhdin, A. L.; Dybtsev, D. N.; Bryliakov, K. P.; Talsi, E. P.; Fedin, V. P. *J. Am. Chem. Soc.* **2007**, *129*, 12958-12959.
- (12) Horcajada, P.; Serre, C.; Maurin, G.; Ramsahye, N. A.; Balas, F.; Vallet-Regi, M.; Sebban, M.; Taulelle, F.; Ferey, G. *J. Am. Chem. Soc.* **2008**, *130*, 6774-6780.

- (13) Horcajada, P.; Serre, C.; Vallet-Regi, M.; Sebban, M.; Taulelle, F.; Ferey, G. *Angew. Chem. Int. Ed.* **2006**, *45*, 5974-5978.
- (14) Taylor-Pashow, K. M.; Della Rocca, J.; Xie, Z.; Tran, S.; Lin, W. *J. Am. Chem. Soc.* **2009**, *131*, 14261-14263.
- (15) Lee, J.; Farha, O. K.; Roberts, J.; Scheidt, K. A.; Nguyen, S. T.; Hupp, J. T. *Chem. Soc. Rev.* **2009**, *38*, 1450-1459.
- (16) Tonigold, M.; Lu, Y.; Bredenkotter, B.; Rieger, B.; Bahnmueller, S.; Hitzbleck, J.; Langstein, G.; Volkmer, D. *Angew. Chem. Int. Ed.* **2009**, *48*, 7546-7550.
- (17) Maksimchuk, N. V.; Kovalenko, K. A.; Arzumanov, S. S.; Chesalov, Y. A.; Melgunov, M. S.; Stepanov, A. G.; Fedin, V. P.; Kholdeeva, O. A. *Inorg. Chem.* **2010**, *49*, 2920-2930.
- (18) Dhakshinamoorthy, A.; Alvaro, M.; Garcia, M. *Adv. Synth. Catal.* **2010**, *352*, 711-717.
- (19) Banerjee, M.; Das, S.; Yoon, M.; Choi, H. J.; Hyun, M. H.; Park, S. M.; Seo, G.; Kim, K. *J. Am. Chem. Soc.* **2009**, *131*, 7524-7525.
- (20) Hu, A.; Ngo, H. L.; Lin, W. *J. Am. Chem. Soc.* **2003**, *125*, 11490-11491.
- (21) Xamena, F. X. L. I.; Abad, A.; Corma, A.; Garcia, H. *J. Catal.* **2007**, *250*, 294-298.
- (22) Prats, A. E. P.; de la Pena-O'Shea, V. A.; Iglesias, M.; Snejko, N.; Monge, A.; Gutierrez-Puebla, E. *Chemcatchem* **2010**, *2*, 147-149.
- (23) Tanaka, K.; Oda, S.; Shiro, M. *Chem. Commun.* **2008**, 820-822.
- (24) Jiang, D.; Mallat, T.; Krumeich, F.; Baiker, A. *J. Catal.* **2008**, *257*, 390-395.
- (25) Jiang, D.; Urakawa, A.; Yulikov, M.; Mallat, T.; Jeschke, G.; Baiker, A. *Chem. Eur. J.* **2009**, *15*, 12255-12262.

- (26) Ingleson, M. J.; Barrio, J. P.; Bacsá, J.; Dickinson, C.; Park, H.; Rosseinsky, M. J. *Chem. Commun.* **2008**, 1287-1289.
- (27) Wang, Z.; Cohen, S. M. *Chem. Soc. Rev.* **2009**, 38, 1315-1329.
- (28) Garibay, S. J.; Wang, Z.; Tanabe, K. K.; Cohen, S. M. *Inorg. Chem.* **2009**, 48, 7341-7349.
- (29) Ahnfeldt, T.; Gunzelmann, D.; Loiseau, T.; Hirsemann, D.; Senker, J.; Ferey, G.; Stock, N. *Inorg. Chem.* **2009**, 48, 3057-3064.
- (30) Nguyen, J. G.; Cohen, S. M. *J. Am. Chem. Soc.* **2010**, 132, 4560-4561.

Chapter 6. The Use of Postsynthetic Modification on Chemically Robust MOFs

6.1 Introduction

As described in the previous chapters as well as many other studies, it has been shown that complex functionality can be introduced into porous MOFs through a postsynthetic modification (PSM) approach.¹ As highlighted in Chapters 4 and 5, access to novel functionalities through PSM and their subsequent exploitation in potential applications of MOF are still limited by the inherent chemical stability of the parent framework. Because of this limitation, utilization of PSM on more chemically robust systems are of interest.² While numerous MOFs exist, only a handful are chemically robust. Moreover, realization of functionalized analogues has been difficult.

Cr-MIL-101 (MIL = Material Institut Lavoisier) is composed of terephthalate ligands and trimeric Cr^{3+} octahedral chemically inert metal clusters (Figure 6-1).³ It is a chemically robust MOF system that is easily amenable to protic and aqueous environments. Until recently, attempts to construct functionalized analogues of this system through solvothermal synthesis failed. For instance, 2-amino-1,4-benzene dicarboxylate (NH_2 -BDC) could not be incorporated into the framework under the standard MOF synthesis of Cr-MIL-101. Due to the harsh standard reaction conditions (i.e. HF, 150 °C) the NH_2 -BDC linker is destroyed during synthesis. The amino analogue, Cr-MIL-101- NH_2 , was realized by the reduction of nitro groups of Cr-MIL-101- NO_2 with SnCl_2 through a PSM approach (Figure 6-1).⁴ However, producing Cr-MIL-101- NH_2 is tedious as it requires up to seven days for synthesis and activation. In addition, its paramagnetic Cr^{3+} metal centers often make characterization through ^1H NMR difficult.

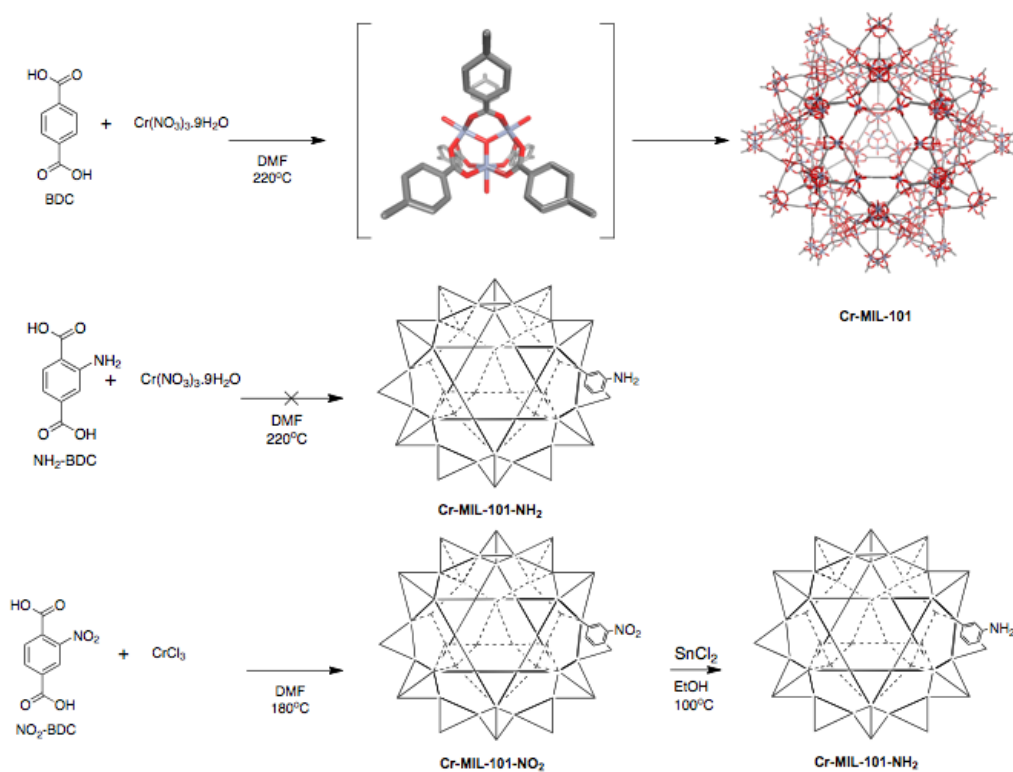


Figure 6-1. A representation of Cr-MIL-101 (top) and synthesis of Cr-MIL-101-NH₂ through the reduction of Cr-MIL-101-NH₂ and functionalization through PSM (bottom).

UiO-66 (UiO =University of Oslo) is composed of Zr_6 -octahedra [$\text{Zr}_6\text{O}_4(\text{OH})_4$] bridged by twelve terephthalate ligands (Figure 6-2). Owing to the highly oxophilic nature of Zr^{4+} of the SBUs, makes these materials very tolerant of polar solvents and elevated pressures.⁵ In addition, larger analogues could be synthesized through the use of extended linkers such as biphenyl- or terphenyl- dicarboxylic acids (Figure 6-2).

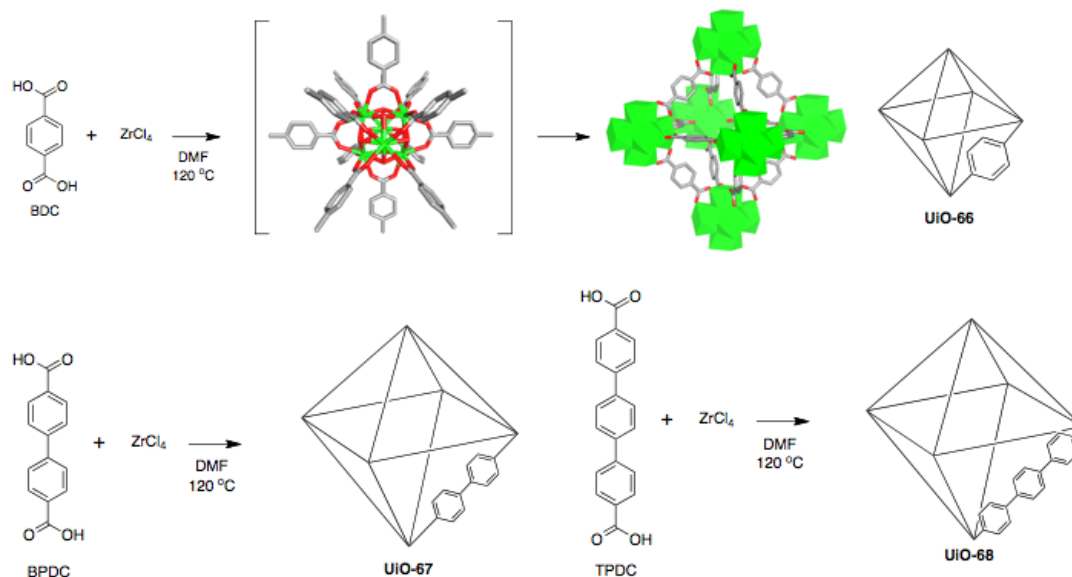


Figure 6-2. Synthesis and schematic representation of UiO-66 with its Zr_6O_6 cuboctahedron SBU (green) and synthesis of extended analogues UiO-67 and UiO-68 (bottom).

Recently, the first example of PSM on UiO-66 was demonstrated when $Cr(CO)_3$ was successfully grafted to the arene moieties of UiO-66 through thermal decomposition (Figure 6-3).⁶ Subsequent photolysis of the $Cr(CO)_3$ modified material with UV light in an N_2 atmosphere led to photoinduced substitution of one of the CO ligands with an N_2 molecule. However, prolonged to UV light ($>30\text{ min}$) led to decomposition of the arene- $Cr(CO)_3$ species.

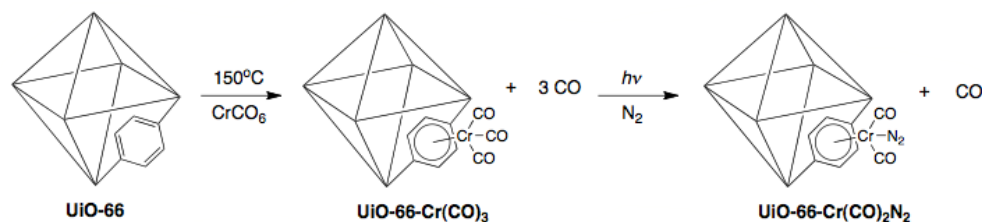
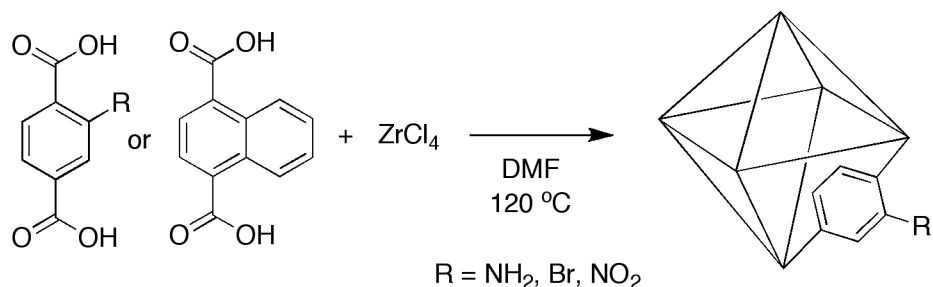


Figure 6-3. Synthesis of UiO-66-Cr(CO)₃ and UiO-66-Cr(CO)₂(N₂) through PSM.

In this chapter, efforts to expand the use of PSM to chemically robust materials such as the UiO family of frameworks will be discussed. The synthesis of NH_2 , -Br , -NO_2 , and naphthalene-substituted UiO-66 analogues along with the modification of an amine and bromide functionalized UiO-66 analogues are described. Furthermore, the synthesis of expanded analogues of UiO-66 with naphthalene and -NH_2 , -NO_2 , -OH functionalized linkers are presented.

6.2 Results and Discussion

The incorporation of a variety of organic functional groups into the UiO-66 framework was first attempted through a prefunctionalization approach (Scheme 6-1). The synthesis of -NH_2 , -Br , -NO_2 , and naphthalene functionalized UiO-66 analogues were performed using a slightly modified procedure from that reported by Lillerud et al.⁵ To obtain these materials, equal molar amounts of ZrCl_4 and BDC precursors (0.35 mmol) were combined and reacted solvothermally in 4 mL of DMF at $150\text{ }^\circ\text{C}$ for 24 hours in a Teflon lined stainless steel autoclave. Under these conditions all of the functionalized terephthalic acid precursors led to materials possessing powder X-ray diffraction (PXRD) patterns that were remarkably consistent with that reported for the UiO-66 topology (Figure 6-4).^{5,7}



Scheme 6-1. Synthesis of isorecticular UiO-66 functionalized analogues UiO-66- NH_2 , UiO-66-Br, UiO-66- NO_2 ($\text{R}=\text{NH}_2$, Br, or NO_2), and UiO-66-1,4-Naph. The UiO-66 framework is represented as an octahedron.

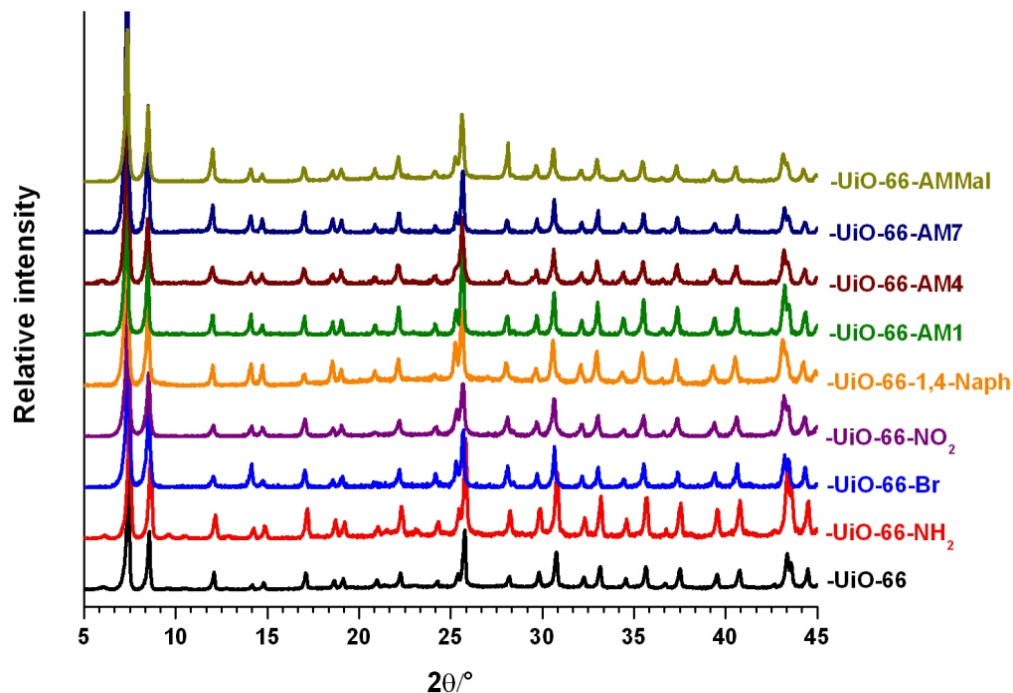


Figure 6-4. PXRD patterns of UiO-66 derivatives.

The thermal stability of the UiO-66 analogues varied depending on the functional group appended to the BDC ligand. While the bromide and naphthalene analogues UiO-66-Br and UiO-66-1,4-Naph show thermal stability comparable to the parent UiO-66 material ($T_d = 550$ °C), the amino- and nitro- functionalized analogues UiO-66-NH₂ and UiO-66-NO₂ showed significant weight losses (25% to 30%) at ~400 °C, presumably due to ligand decomposition (Figure 6-5). Overall, the UiO-66 framework is found to be a robust motif that is highly amenable to isorecticular functionalization.

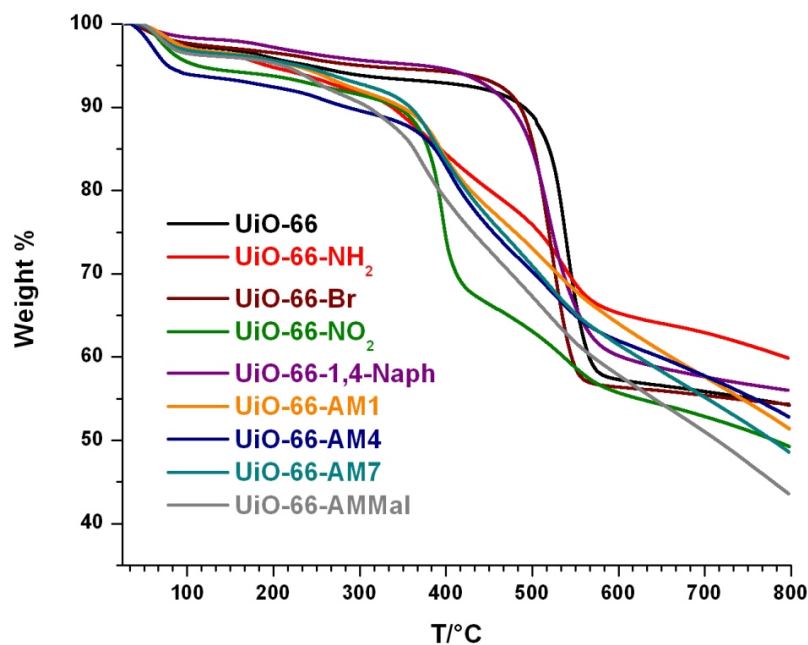
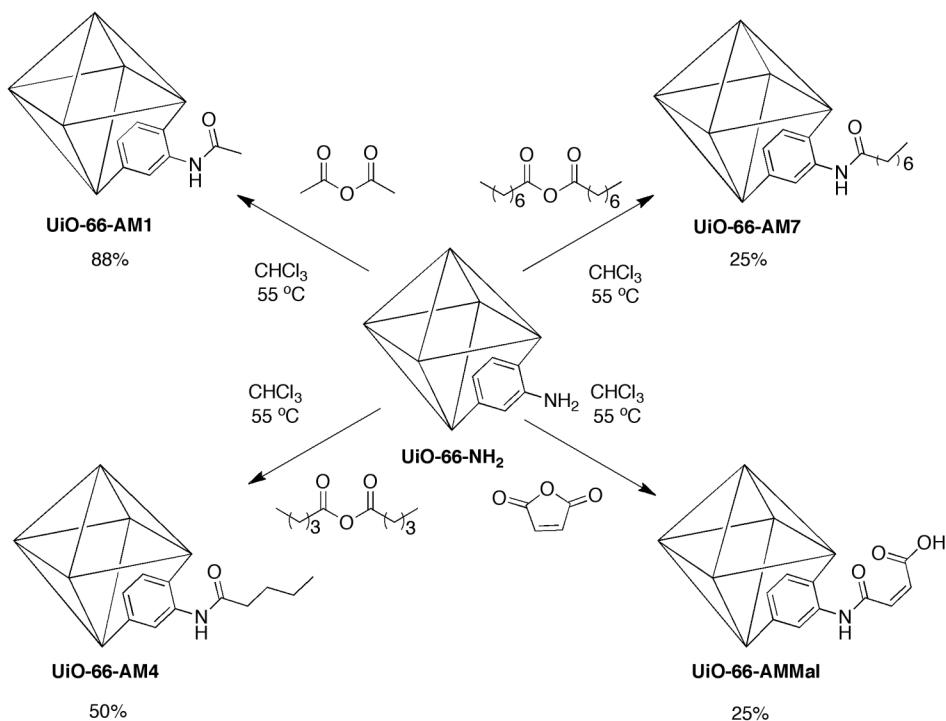


Figure 6-5. Thermogravimetric analysis of UiO-66 (black), UiO-66-NH₂ (red), UiO-66-Br (brown), UiO-66-NO₂ (green), UiO-66-1,4-Naph (purple), UiO-66-AM1 (orange), UiO-66-AM4 (blue), UiO-66-AM7 (cyan), and UiO-66-AMMal (gray).

PSM of UiO-66-NH₂ was explored using a series of alkyl anhydrides to produce amide modified frameworks designated UiO-66-AM (Scheme 6-2). In a typical reaction UiO-66-NH₂ (~60 mg, 0.2 mmol-NH₂) was suspended in 2 mL of CHCl₃, treated with one equivalent of anhydride, and heated at 55 °C for 24 h, followed by extensive rinsing with MeOH to extract by-products from the porous solids.



Scheme 6-2. Postsynthetic modification of UiO-66-NH₂ with various anhydrides.

As described in our earlier studies, modification was confirmed by nuclear magnetic resonance (NMR) spectroscopy.^{2,8} Samples of PSM treated UiO-66-NH₂ materials were digested with HF and *d*⁶-DMSO and analyzed by ¹H NMR spectroscopy. Digestion of unmodified UiO-66-NH₂ displayed predominantly resonances associated with 2-amino-1,4-benzenedicarboxylic acid, but some minor impurities were also observed in the aromatic region. These impurities appear to be associated with the NH₂-BDC ligand, as they were not observed upon digestion of UiO-66, UiO-66-Br, UiO-66-NO₂, or UiO-66-Naph (Figure 6-6). Nonetheless, the ¹H NMR spectra of modified samples showed a distinct downfield shift of the aromatic proton resonances associated with the BDC ligand (Figure 6-7).

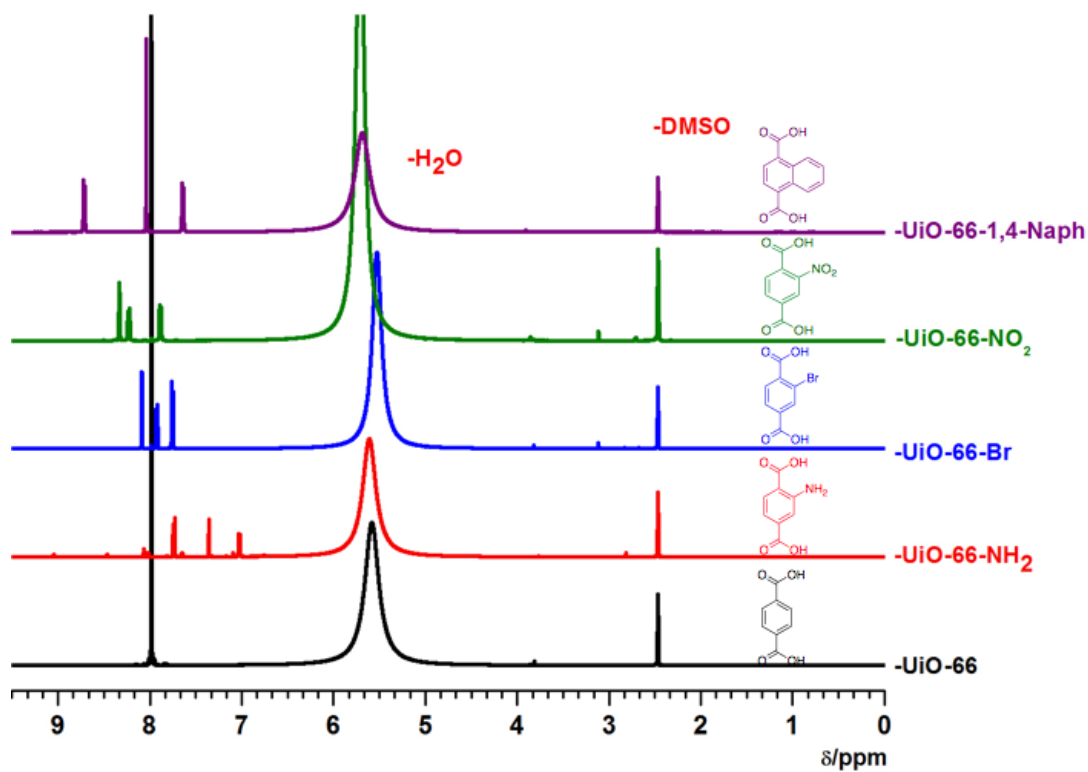


Figure 6-6. $^1\text{H NMR}$ Spectra of digested UiO-66 and UiO-66 functionalized samples.

The percent conversion of the amine groups in the framework to amides was determined by comparing the relative integrated areas of the aromatic resonances (corresponding to the C-3 position of the BDC ring) between the modified and unmodified BDC ligands. The results are summarized in Table 6-1.

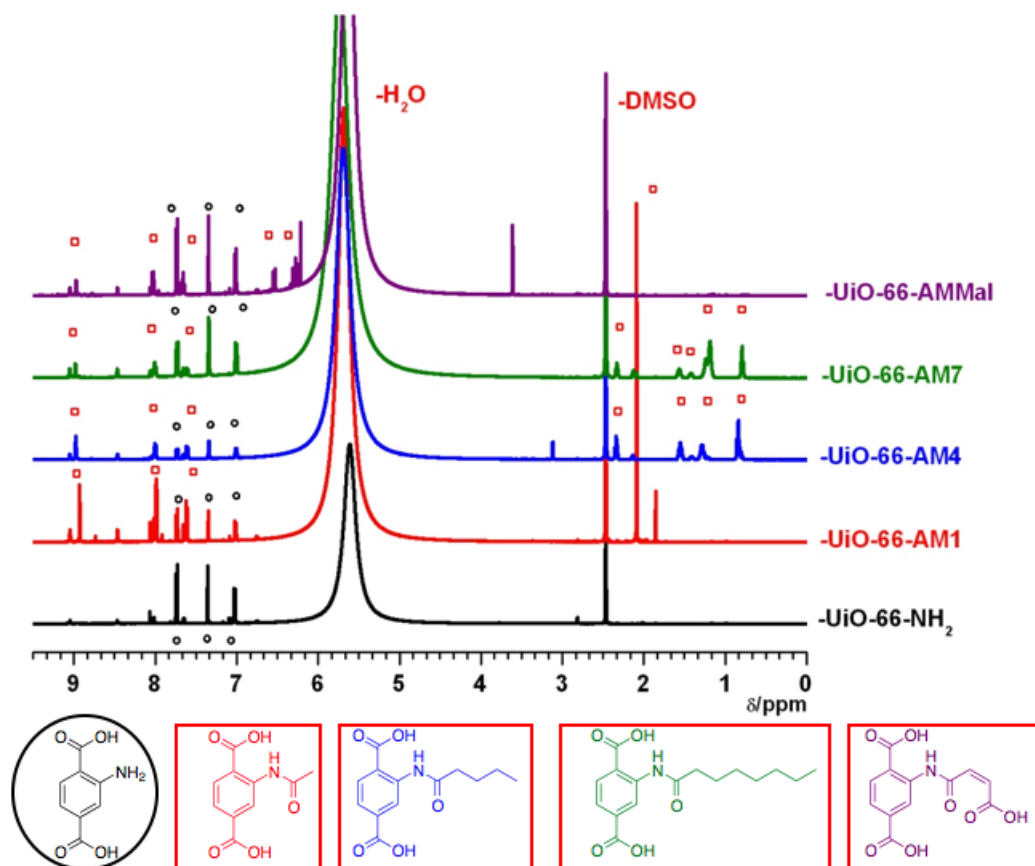


Figure 6-7. ^1H NMR spectra of digested UiO-66 modified samples. Black circles indicate unmodified NH_2 -BDC and red squares are from modified BDC ligands.

Table 6-1. Conversion of UiO-66- NH_2 to UiO-66-AM derivatives using different anhydrides.

UiO-66-	Anhydride	% Conversion	STD ^a
AM1	Acetic	88	± 6
AM4	Valeric	49	± 7
AM7	Octanoic	25	± 6
AMMal	Maleic	25	± 5

^a Percent conversion values are averaged from at least three independent experiments.

As previously observed for other MOF systems, conversion to the amide products decreased with increasing size (chain length) of the anhydride with yields of 88%, 49%, and 25% for acetic (-AM1), valeric (-AM4), and octanoic anhydride (-

AM7), respectively. Additionally, reaction with the maleic anhydride produced UiO-66-AMMal with 25% conversion. The latter modification introduces a free carboxylate group into the framework, which could not be readily obtained by direct solvothermal synthesis and has been shown to generate acidic materials with catalytic properties.^{9,10}

Additional evidence for modification was obtained via infrared spectroscopy (ATR-FTIR) on UiO-66-AM1, UiO-66-AM4, UiO-66-AM7, and UiO-66-AMMal, which displayed a weak, but reproducible stretching frequency around 1700 cm^{-1} associated with the carbonyl moieties of the amide functionality (Figure 6-8). Consistent with the UiO-66-NH₂ precursor framework, the amide-functionalized frameworks UiO-66-AM1, UiO-66-AM4, UiO-66-AM7, and UiO-66-AMMal show somewhat decreased thermal stabilities relative to UiO-66 (Figure 6-5).

The affect of functionalization on the porosity of the UiO-66 systems were investigated by measuring the Brunauer-Emmett-Teller (BET) surface areas with N₂ adsorption at 77 K. The results are summarized in Table 6-2. As shown by the surface measurements, the amino moieties in UiO-66-NH₂ do not perturb the porosity of the UiO-66 system; however, increasingly larger functional groups lead to diminished porosities (e.g. -Br, -NO₂, -Naph). Similarly, longer aliphatic chains introduced through PSM progressively reduced the inherent porosity of UiO-66-AM compounds.

Table 6-2. BET surface areas of UiO-66 functionalized systems (m^2g^{-1}).

	BET Surface Area ^a	Langmuir Surface Area ^a
UiO-66	1110 ± 86	1311 ± 102
UiO-66-NH ₂	1112 ± 77	1313 ± 89
UiO-66-Br	851 ± 117	1004 ± 137
UiO-66-NO ₂	756 ± 34	893 ± 41
UiO-66-1,4-Naph	615 ± 71	732 ± 84
UiO-66-AM1	818 ± 11	965 ± 13
UiO-66-AM4	717 ± 3	847 ± 4
UiO-66-AM7	646 ± 29	762 ± 33
UiO-66-AMMal	814 ± 85	962 ± 100
UiO-66-CN	661 ± 53	784 ± 45

^a The results are the average from two independent experiments.

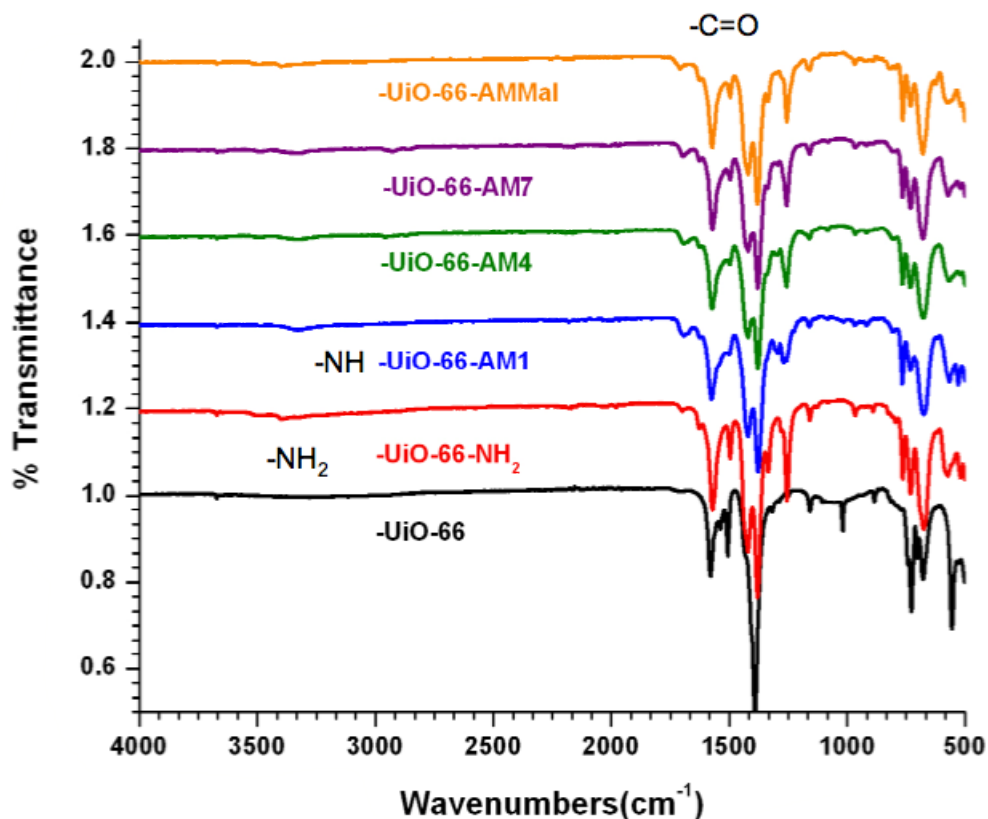
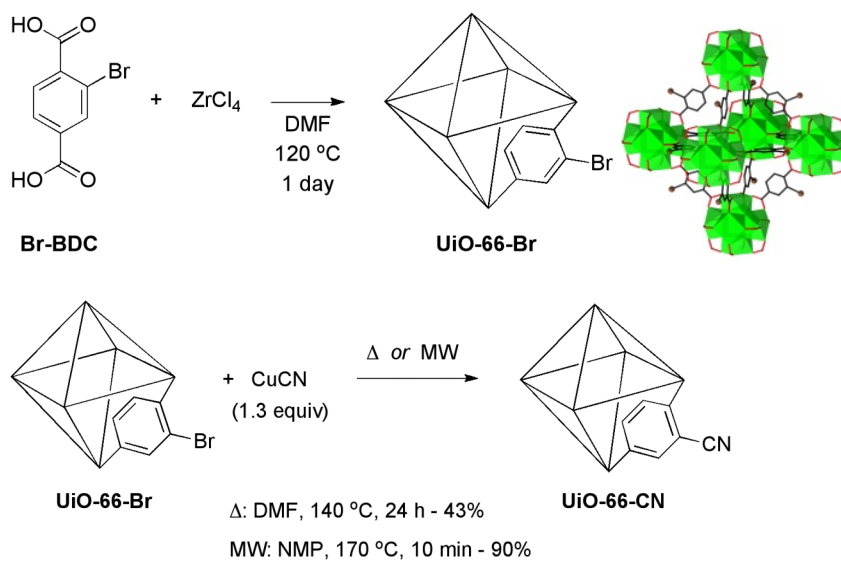


Figure 6-8. FT-IR spectra of modified UiO-66-NH₂ samples.

Despite significant advances, the majority of PSM reactions have been confined to MOFs bearing only a few different functional group ‘handles’ including amines, aldehydes, alkynes, and hydroxyls.^{2,4,8,11-21} The ability to use aryl halides as handles for PSM chemistry has become an important goal in the MOF community. Aryl halides can undergo a wide variety of chemical transformations such as the Rosenmund-von Braun reaction²² and Sandmeyer²³ reaction for the preparation of aryl nitriles. The nitrile group is an important precursor for various other functional groups, such as carboxylic acids, aliphatic amines, and heterocyclic compounds.²⁴ Indeed, an aryl bromide containing MOF, termed IRMOF-2 was synthesized in 2002.²⁵ However, many aryl halide reactions require solvents or reagents (e.g. base)

that are incompatible with traditional Zn^{2+} -carboxylate based MOFs. In attempt to realize aryl halide PSM reactions, the chemically robust UiO-66 system was utilized. UiO-66-Br was subject to cyanation with CuCN (1.3 equiv) in a DMF suspension for 24 h at 140 °C (Scheme 6-3).²⁶ After removal of excess copper by washing with DMF, an aqueous KCN solution, and methanol, the bromo groups of UiO-66-Br were found to be 43% converted to nitrile groups. The percent conversion from bromo to nitrile was determined by ^1H NMR upon digestion of the MOF in HF in CD_3OD .²⁷ In the ^1H NMR spectra, the 2-cyano-1,4-benzenedicarboxylate (CN-BDC) resonances generated from the UiO-66-CN product (Figure 6-9) are shifted downfield relative to the Br-BDC starting material.



Scheme 6-3. Synthesis of UiO-66-Br (top) and PSM cyanation to UiO-66-CN (bottom). A representation of the UiO-66 framework is shown (top right) with the Zr_6O_6 cuboctahedron SBUs highlighted in green.

Encouraged by these preliminary results, we sought to improve the cyanation reaction conditions. The high chemical and thermal stability of UiO-66-Br led us to attempt microwave-assisted cyanation (Figure 6-5). UiO-66-Br was suspended in *N*-methyl-2-pyrrolidone (NMP) and subjected to microwave irradiation (170 °C, 10 min) producing UiO-66-CN in 90% yield as determined by ^1H NMR analysis (Figure 6-9). ESI-MS and FT-IR also confirmed conversion to the modified CN-BDC ligand (Figures 6-10, 6-11). To the best of our knowledge this is the first time microwave irradiation has been utilized in the PSM of a MOF. Importantly, microwave irradiation resulted in a much faster and higher yielding PSM reaction when compared to standard thermal conditions.

Complete characterization on UiO-66-CN confirmed that it is a stable, microporous material. Powder X-ray diffraction (PXRD) shows that the crystallinity

of UiO-66-CN is retained (Figure 6-12). Scanning electron microscopy (SEM) images showed that the crystallites were identical in appearance before and after the PSM reaction (Figure 6-13). UiO-66-CN gave a BET surface area of $\sim 661 \text{ m}^2\text{g}^{-1}$ which is comparable to that of the parent UiO-66-Br ($\sim 851 \text{ m}^2\text{g}^{-1}$),²⁷ indicating that the material remains microporous even after the microwave modification procedure.

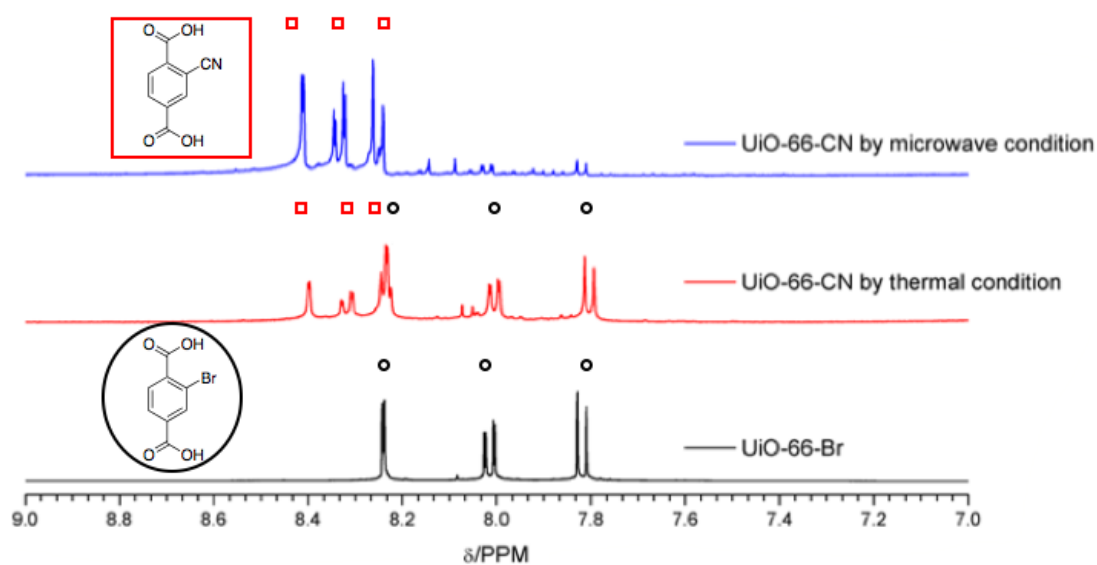


Figure 6-9. ¹H NMR spectra of UiO-66-CN produced by thermal and microwave procedures (spectra obtained by digestion with HF in CD₃OD). Open black circles indicate Br-BDC and open red squares indicate CN-BDC. A spectrum of unmodified UiO-66-Br is shown for reference.

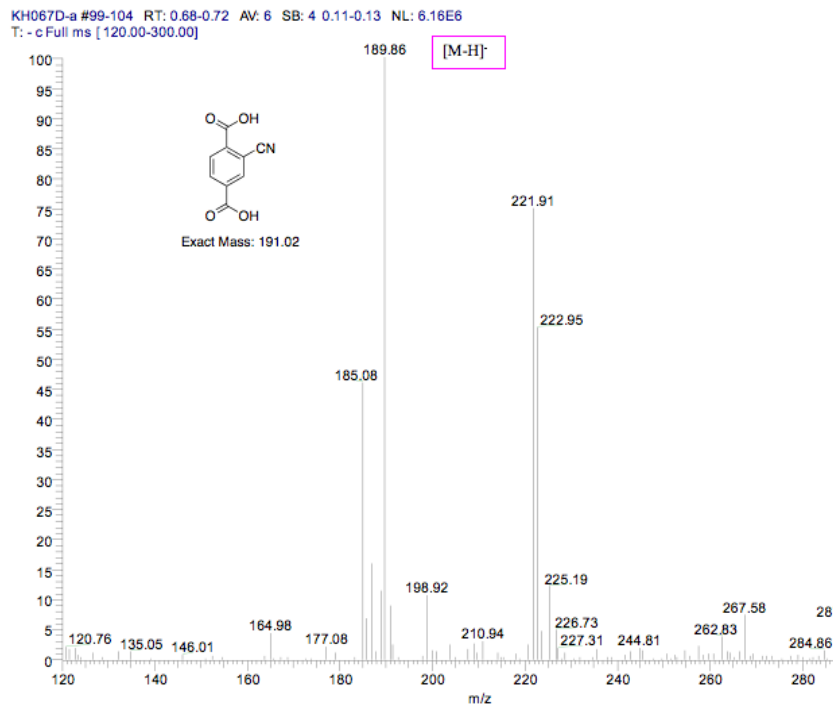


Figure 6-10. ESI-MS(-) of digested UiO-66-CN showing the molecular ion peak associated with the cyano functionalized ligand.

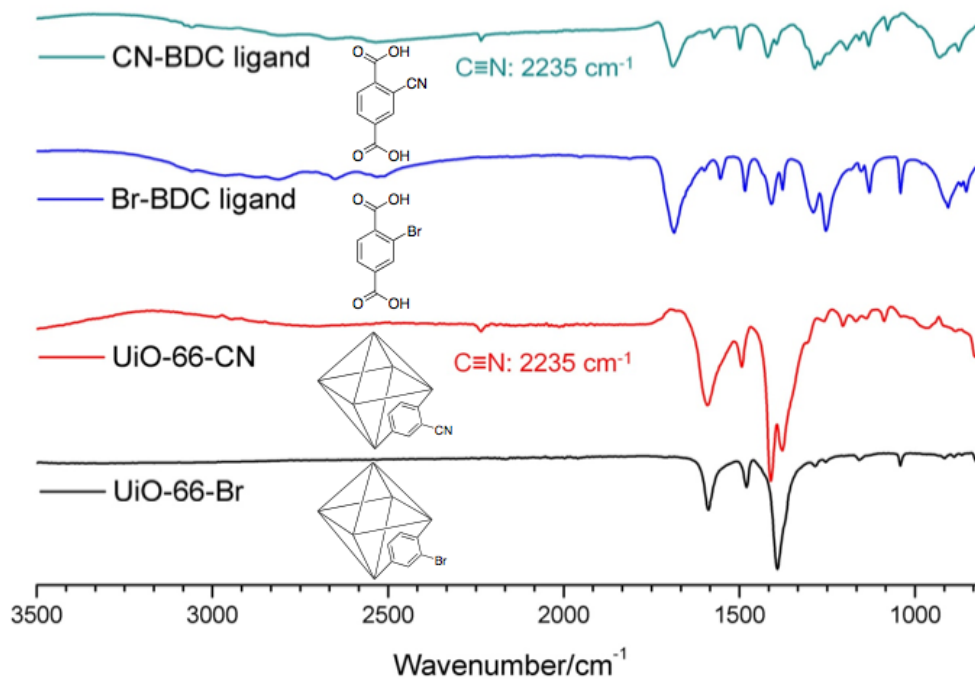


Figure 6-11. Infrared spectrum (FT-IR) of CN-BDC (cyan), Br-BDC (blue), UiO-66-Br (black), and UiO-66-CN (red).

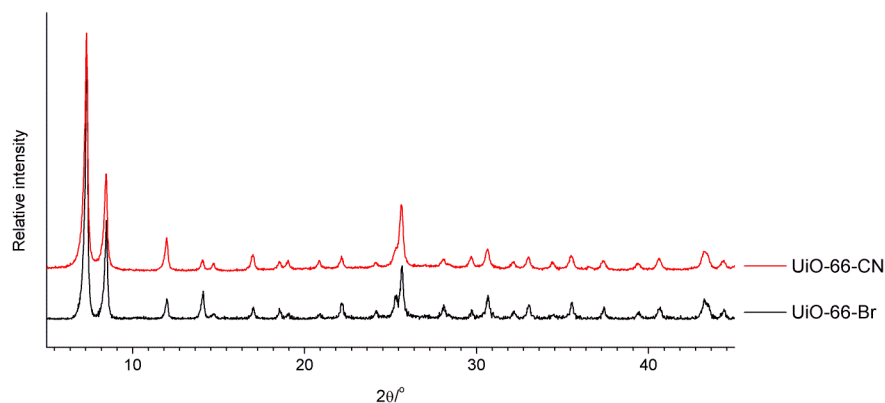


Figure 6-12. PXRD patterns of UiO-66-Br and UiO-66-CN. The UiO-66-CN sample was produced through PSM under microwave irradiation reaction conditions.

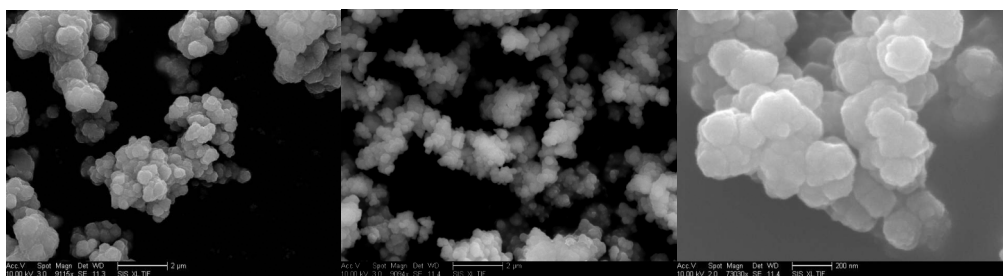
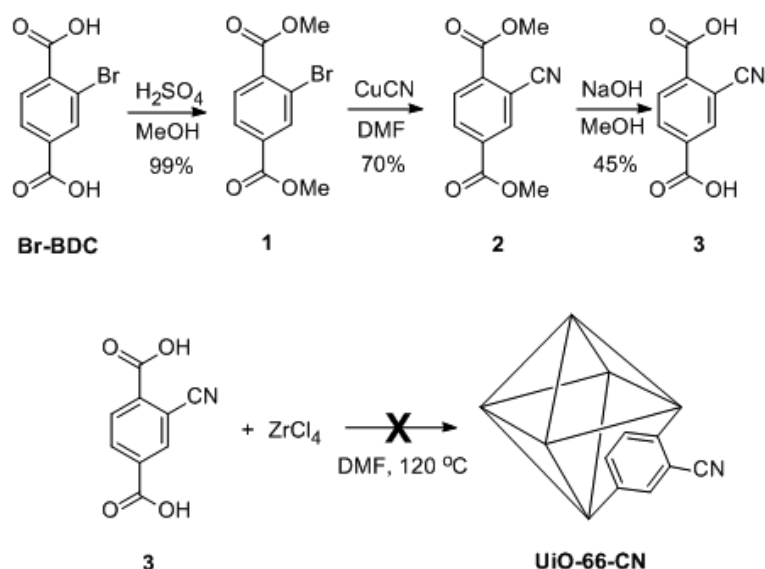


Figure 6-13. Scanning electron microscopy images (SEM) of UiO-66-Br (left) and UiO-66-CN (center and right) produced by microwave-assisted PSM, two different magnifications).

Several studies on the microwave-assisted synthesis of MOFs have been described.^{28,29} In light of these reports, we attempted the microwave synthesis of UiO-66-Br and UiO-66-CN from $ZrCl_4$ with Br-BDC or CN-BDC, respectively. The CN-BDC ligand was prepared starting from Br-BDC in three steps (Scheme 6-4). Utilizing the same microwave heating conditions used in the PSM cyanation (in either DMF or NMP), neither UiO-66-Br nor UiO-66-CN was produced. These important control reactions demonstrate that the microwave-assisted PSM cyanation is operating

heterogeneously on UiO-66-Br and not on soluble species that are assembling in situ to form the MOF. These experiments strongly suggest that the microwave PSM reaction conditions used here are truly a heterogeneous transformation of the UiO-66-Br framework, not involving a series of dissolution, modification, and reformation steps.

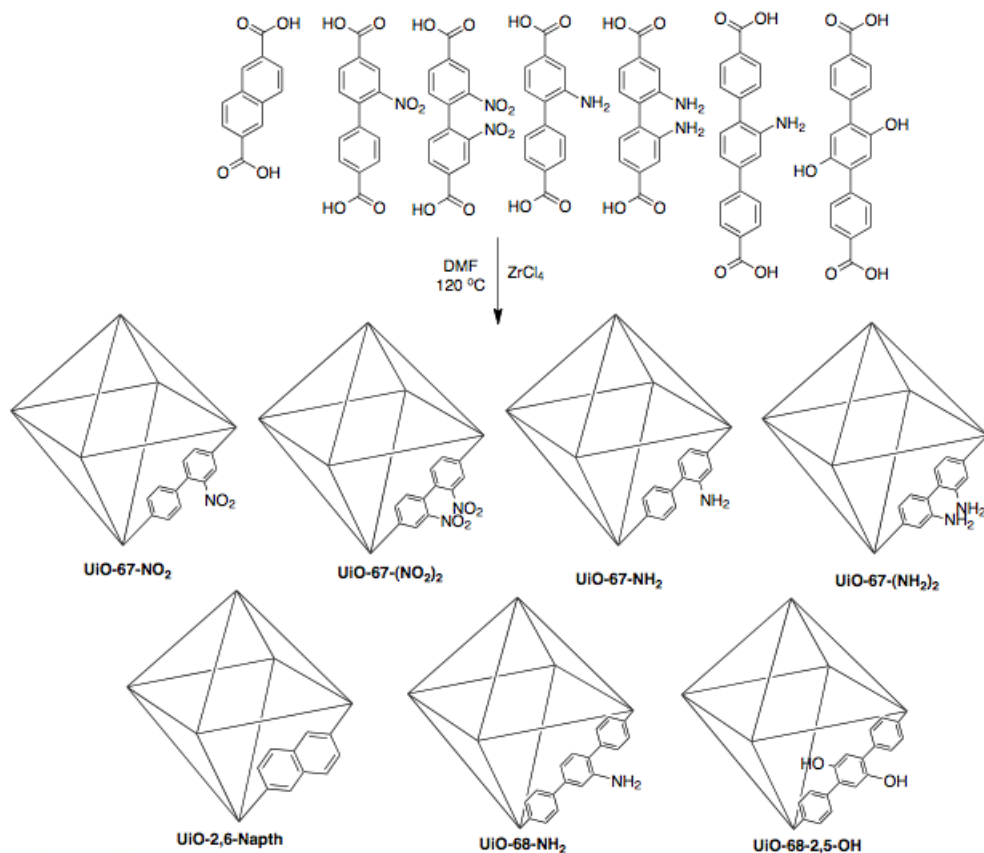


Scheme 6-4. Synthesis of CN-BDC (**3**) and the failed direct solvothermal synthesis of UiO-66-CN.

Fundamentally, introduction of labile and reactive functional groups on an organic ligand can complicate the solvothermal synthesis of MOFs. Use of CN-BDC with ZrCl_4 in DMF under standard UiO-66 synthesis solvothermal condition (120 °C, 24 h) failed to produce UiO-66-CN (Scheme 6-4). The ability of nitrile groups to bind metal ions, as well as their susceptibility to hydrolysis under forcing conditions, prompted us to explore whether UiO-66-CN could be prepared directly from CN-BDC under alternative solvothermal conditions.

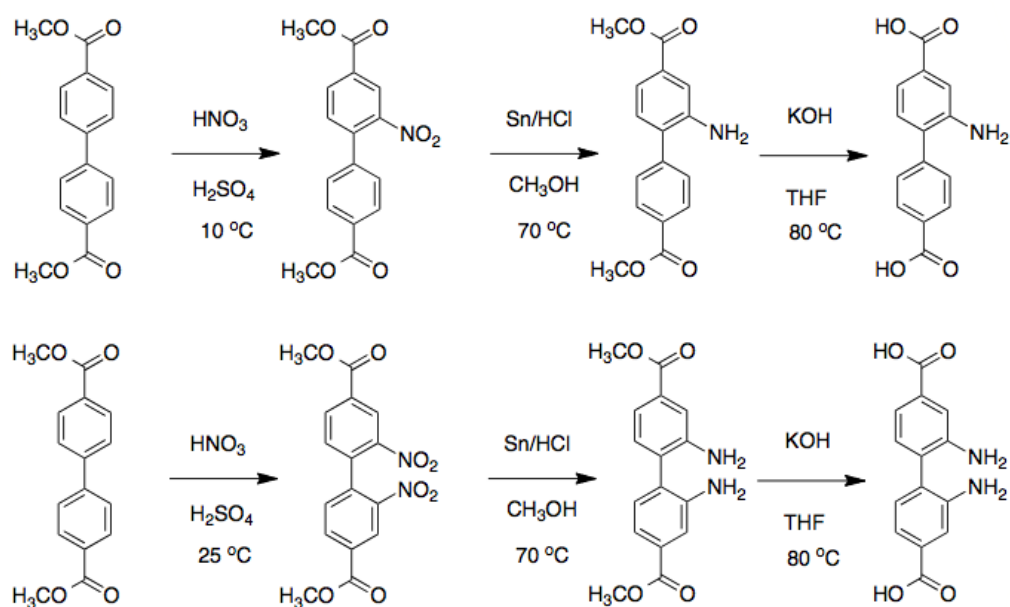
After testing several conditions, UiO-66-CN was produced under lower temperature conditions (85 °C) than the standard UiO-66 synthesis condition. This illustrates the utility of PSM on MOF. Even in a MOF system highly tolerant of ligand derivatization, some functional groups will have different reactivity or interfere with MOF formation. Subsequently, more time and effort is required to obtain synthetic conditions compatible with new functional groups and facilitate direct MOF formation. Direct MOF synthesis of UiO-66-CN with a 31% yield needs a total of 4 steps that takes 98 h without drying steps. However, UiO-66-CN with a 90% yield can be obtained through PSM with only 2 steps including UiO-66-Br synthesis requiring 24 h 10 min.

Chemically robust MOFs such as UiO-66 facilitate the use of alternative PSM chemical reactions which may provide greater access to novel functional groups that can be incorporated into MOFs. However, new PSM reactions may be inhibited by the small triangular windows ($\sim 6 \text{ \AA}$ in diameter) within the UiO-66 framework.⁵ Similar to the IRMOF series, the UiO framework is amenable to the use of longer organic linkers which facilitates formation of isoreticular extended frameworks. A variety of functionalized biphenyl and terphenyl ligands were used to prepare expanded UiO materials (Scheme 6-5).



Scheme 6-5. UiO-67 and UiO-68 functionalized materials.

The mono or double nitro and amino biphenyl ligands were synthesized through nitration and subsequent reduction of dimethyl [1,1'-biphenyl]-4,4'-dicarboxylate (Scheme 6-6). With the exception of UiO-68-NH₂, all UiOs could be readily and repetitively synthesized through standard solvothermal synthesis. Repeated attempts to synthesize UiO-68-NH₂ with 2'-amino-[1,1':4',1''-terphenyl]-4,4''-dicarboxylic acid produced broad amorphous PXRD patterns. Unlike the 1,4-Naphthalene-dicarboxylic acid, which produces a framework analogous to UiO-66, using 2,6-naphthalene-dicarboxylic acid produces a PXRD pattern that does not match either UiO-66 or UiO-67 but resembles an intermediate of both (Figure 6-14).



Scheme 6-6. Synthesis of biphenyl carboxylate ligands.

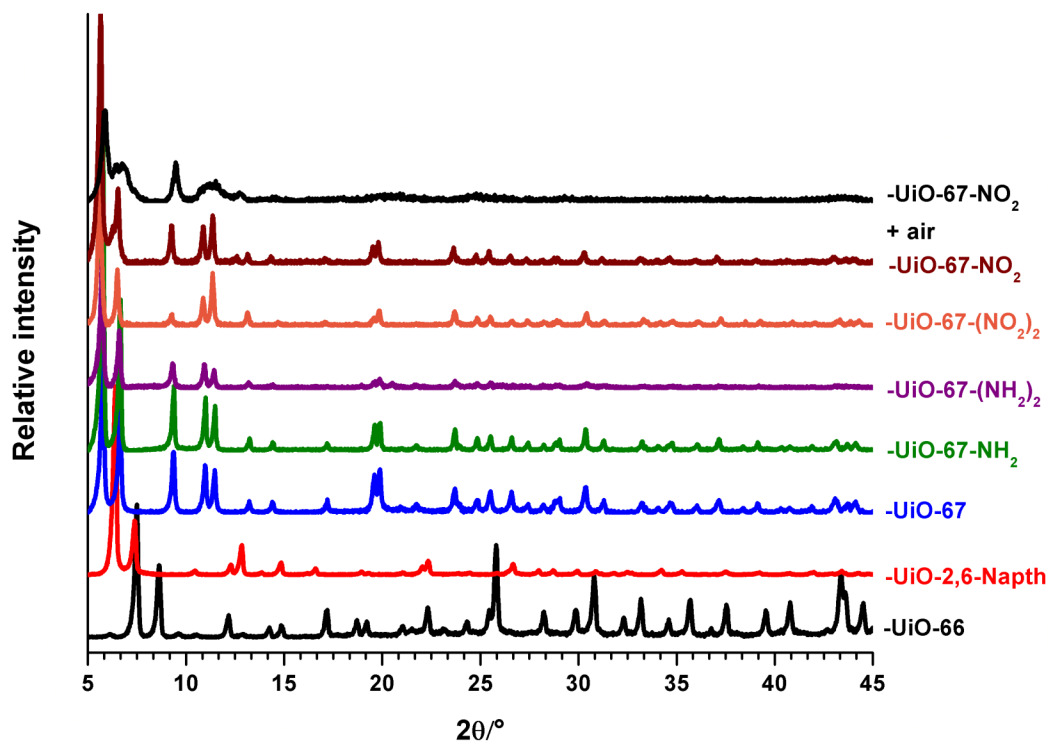


Figure 6-14. PXRD patterns of UiO-66 (black), UiO-2,6-Naphth (red), UiO-67 (blue), UiO-67- NH_2 (green), UiO-67 $(\text{NH}_2)_2$ (purple), UiO-67- $(\text{NO}_2)_2$ (orange), UiO-67- NO_2 (brown), and UiO-67- NO_2 exposed to air (teal).

The measured BET and Langmuir surface areas of UiO-67, UiO-67-NH₂ and UiO-67-(NH₂)₂ are summarized in Table 6-3. While the Langmuir surface area of UiO-67-NH₂ (1834 m²g⁻¹) is reasonably close to that of UiO-67 (1702 m²g⁻¹) it is nowhere near the reported calculated Langmuir surface area of ~3000 m²g⁻¹.⁵ The double amine moieties of UiO-67-(NH₂)₂ could be inhibiting access to the pores which may be responsible for the relatively low surface area (538 m²g⁻¹). Repeated attempts to obtain BET surface area measurements on both UiO-67-NO₂ and UiO-67-(NO₂)₂ gave values less than 5 m²g⁻¹ suggesting these nitro functionalized UiO-67 derivatives are relatively unstable to their amino counterparts.

Indeed, while UiO-67-NO₂ could be synthesized it was found to be unstable after minimal exposure to air as evidenced by PXRD (Figure 6-14). This result prompted investigations of the structural stability of the UiO-67 framework analogues to air. Indeed, all UiO-67 analogues showed similar broad amorphous PXRD patterns after prolonged (> 30 minutes) exposure to air. A recent study explored the use of modulators for the synthesis of UiO derivatives.³⁰ The utilization of benzoic or acetic acids in the synthesis of UiO frameworks were found to both greatly enhance the crystallinity and size of the UiO materials. Moreover, surface areas greater than 3000 m²g⁻¹ were obtained with this new synthetic methodology. Indeed, utilization of acetic acid in MOF synthesis facilitated formation of UiO-68-NH₂ and UiO-68-2,5-(OH)₂ (Figure 6-15). Surprisingly, the modulator synthetic method was found to greatly enhance the structural stability of the UiO-67 and UiO-68 analogues towards exposure to air. For instance, while as synthesized UiO-2,6-Naph, or any other UiO-67

derivative, degraded upon prolonged exposure to air, the UiO materials synthesized with modulators remained crystalline after exposure (Figure 6-16).

Table 6-3. BET surface areas of UiO-67 functionalized systems (m^2g^{-1}).

	BET Surface Area ^a	Langmuir Surface Area ^a
UiO-67	1441 ± 240	1702 ± 283
UiO-67-NH ₂	1571 ± 10	1834 ± 11
UiO-67-(NH ₂) ₂	578 ± 28	685 ± 53

^a The results are the average from two independent experiments

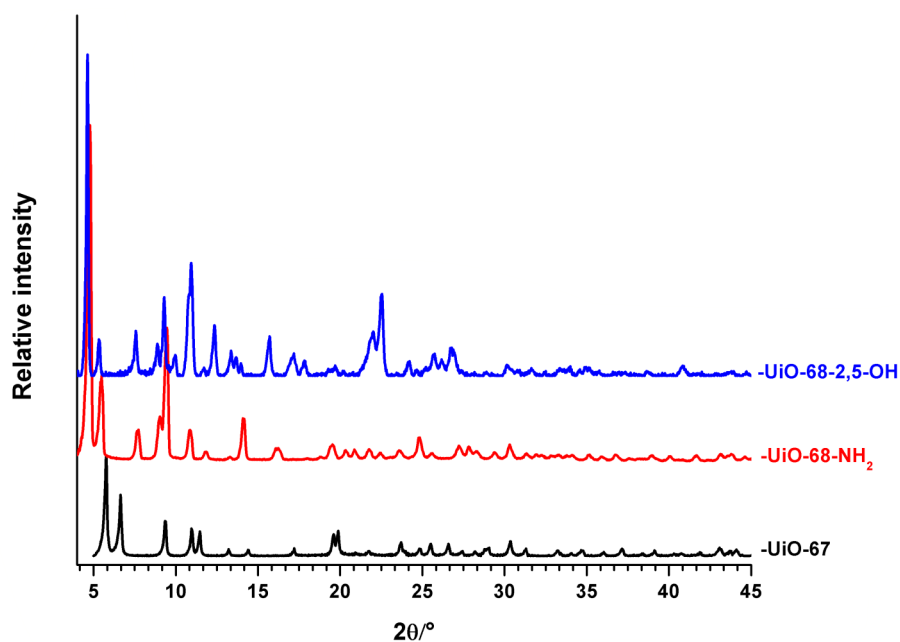


Figure 6-15. PXRD patterns of UiO-68-NH₂ (red) and UiO-68-2,5-OH (blue) synthesized with acetic acid compared with that of UiO-67 (black).

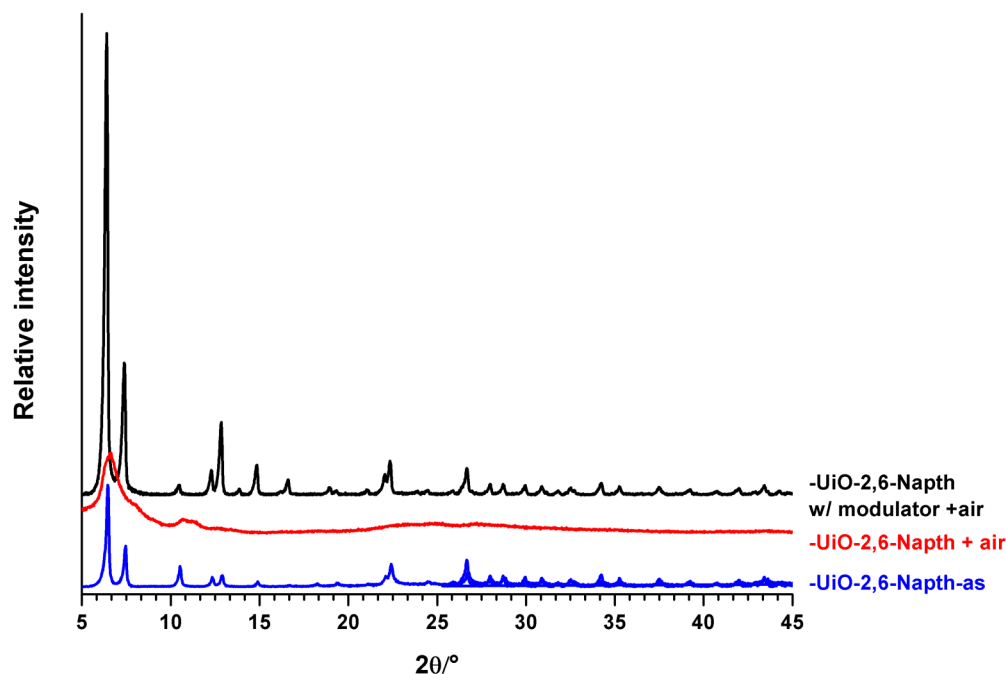


Figure 6-16. PXRD pattern of as synthesized UiO-2,6-Naph (blue), UiO-2,6-Naph exposed to air (red) and UiO-2,6-Naph synthesized with acetic acid exposed to air.

PSM was investigated on UiO-67-NH₂ with acetic anhydride. Digestion of unmodified UiO-66-NH₂ displayed resonances associated with 2-amino-4,4'-biphenyldicarboxylic acid, however, it additionally contained a predominant amount of impurities (Figure 6-17). As previously discussed, UiO-66-NH₂ similarly produces impurities upon digestion but to a smaller extent than UiO-67-NH₂. It appears that digestion with *d*⁶-DMSO and aqueous HF facilitates an unknown modification reaction as the peak at 9.5 ppm is characteristic of amide formation. UiO-67-NH₂ was treated with one equivalent of acetic anhydride (0.2 mmol) at 55 °C for 24 h. However, due to the ¹H NMR spectra being complex, the degree of modification could not be adequately determined.

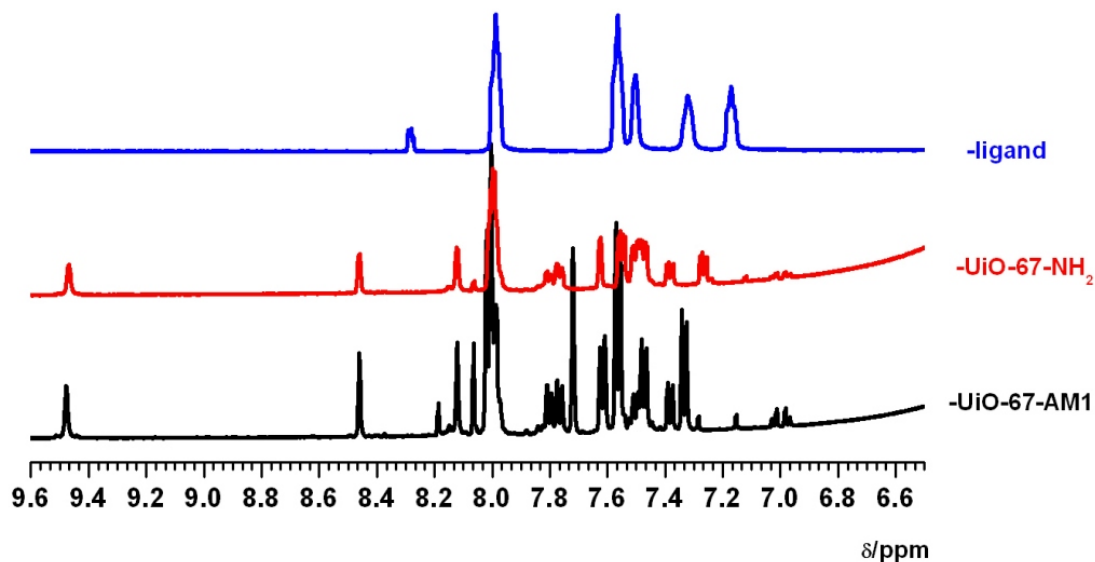


Figure 6-17. ^1H NMR of 2-amino-[1,1'-biphenyl]-4,4'-dicarboxylic acid (blue), UiO-67-NH₂ (red), and UiO-67-AM1 (black), digested in d^6 -DMSO and aqueous HF.

6.3 Conclusions

In summary, we have synthesized and characterized -NH₂, -Br, -NO₂, and naphthalene functionalized UiO-66 frameworks along with -NH₂, -NO₂, and 2,6-naphthalene functionalized UiO-67 and analogues in an isorecticular manner. In comparison to UiO-66, the thermal stability of the amino and nitro functionalized UiO-66-NH₂ and UiO-66-NO₂ is somewhat decreased. The postsynthetic modification of UiO-66-NH₂ was accomplished with aliphatic and cyclic anhydrides and verified through a combination of ^1H NMR, FT-IR, and ESI-MS analysis. In addition, the first PSM reaction utilizing an aryl halide chemical handle within a MOF was performed. For the first time, microwave irradiation was used to obtain rapid and clean PSM, which performed better than standard thermal conditions. The use of both aryl halides and microwave irradiation opens up new tools and hence new possibilities for tuning the pore environment in MOFs. The chemical stability of the UiO-66

framework and facile incorporation of functionalized, through reticular synthesis or PSM, shows that this class of porous solid can serve as a tunable, microporous scaffold for novel applications in separations, catalysis, and biotechnology.

6.4 Experimental Methods

General. Starting materials and solvents were purchased and used without further purification from commercial suppliers (Sigma-Aldrich, Alfa Aesar, EMD, TCI, Cambridge Isotope Laboratories, Inc., and others). 2'-amino-[1,1':4',1''-terphenyl]-4,4''-dicarboxylic acid and 2',5'-dihydroxy-[1,1':4',1''-terphenyl]-4,4''-dicarboxylic acid were generously donated to the group. Solutions were concentrated by using a rotary evaporator, and generally followed by removal of residual solvents on a vacuum line. Flash column chromatography was performed on silica gel (400-630 mesh). Proton nuclear magnetic resonance spectra (^1H NMR) were recorded Varian FT-NMR spectrometer (400 MHz) or JEOL ECA spectrometer (500 MHz). The following abbreviations were used to describe peak patterns when appropriate: br = broad, s = singlet, d = doublet, t = triplet, q = quartet, and m = multiplet. Coupling constants, J , were reported in Hertz unit (Hz). Microwave reactions were performed in a 10 mL microwave tube using a CEM Discover S microwave reactor.

^1H NMR Digestion and Analysis. Approximately 10 mg of microcrystalline UiO-66 was digested by sonication in 570 μL of d^6 -DMSO and 30 μL of HF. After complete dissolution of the material, the solution was used to collect a ^1H NMR spectrum. Approximately 10 mg of UiO-66-Br or UiO-66-CN materials were dried

under vacuum at 100 °C and digested with sonication in 580 μL of CD_3OD and 20 μL of HF (48% aqueous solution).

ESI-MS Analysis. Electrospray ionization mass spectrometry (ESI-MS) was performed using a ThermoFinnigan LCQ-DECA mass spectrometer and the data were analyzed using the Xcalibur software suite in negative ion mode. UiO-66 samples were digested by sonicating the materials in a mixture of 10 μL of HF and 1.0 mL of CH_3CN or MeOH.

Thermal Gravimetric Analysis. Approximately 10-20 mg of modified BET analyzed UiO-66 samples were used for TGA measurements. Samples were analyzed under a stream of dinitrogen using a TA Instrument Q600 SDT running from room temperature to 800 °C with a scan rate of 5 °C min^{-1} .

PXRD Analysis. PXRD data were collected at ambient temperature on a Bruker Advance D8 diffractometer at 40 kV, 40 mA for $K\alpha$ ($\lambda = 1.5418 \text{ \AA}$) with a scan speed of 3° min^{-1} , a step size of 0.02° in 2θ , and a 2θ range of 5-45°. Approximately 15 mg of microcrystalline UiO-66 samples were dried at 150 °C for at least 2 h before PXRD analysis. The experimental backgrounds were corrected using the Jade 5.0 software package.

FT-IR Analysis. Approximately 5-10 mg of modified UiO-66 was dried at 150 °C for at least 2 h before FT-IR analysis. FT-IR spectra were collected using a Bruker ALPHA-P FT-IR spectrometer with a diamond ATR.

BET Surface Area Analysis. BET surface area (m^2g^{-1}) measurements were collected at 77 K using dinitrogen on an ASAP 2020 using the volumetric technique.

Approximately 40-60 mg of activated UiO-66 samples were evacuated on a vacuum line for 5-18 h. The sample was then transferred to a preweighed sample tube and degassed at 105 °C for approximately 24 h or until the outgas rate was <5 μmHg . The sample tube was re-weighed to obtain a consistent mass for the degassed UiO-66 samples.

Dimethyl 2-bromoterephthalate (1). To an oven-dried round-bottom flask, 2-bromo-1,4-benzenedicarboxylic acid (2.45 g, 10 mmol) was dissolved in 200 mL of methanol and 5 mL of conc. H_2SO_4 was added by dropwise. The mixture was heated to reflux for 48 h. After cooling to room temperature, MeOH was removed by evaporation and then 100 mL of CH_2Cl_2 was added. The solution was washed with 5% NaHCO_3 . After drying with MgSO_4 , the desired compound was obtained after removal of solvent in 99% yield. ^1H NMR (400 MHz, CDCl_3) δ 8.27 (1H, s), 7.96 (1H, d, $J = 8.1$ Hz), 7.78 (1H, d, $J = 8.1$ Hz), 3.93 (3H, s), 3.92 (3H, s); ^{13}C NMR (125 MHz, CDCl_3) δ 166.0, 164.9, 136.0, 135.1, 133.6, 131.0, 128.1, 121.4, 52.8, 52.7. HR-EI-MS m/z calcd. for $\text{C}_{10}\text{H}_9\text{BrO}_4$ $[M]^+$: 271.9679, found $[M]^+$: 271.9680.

Dimethyl 2-cyanoterephthalate (2). To an oven-dried 20 mL dram vial, dimethyl 2-bromoterephthalate (0.246 g, 0.9 mmol) was dissolved in 1 mL of DMF and copper cyanide (98 mg, 1.1 mmol) was added. The mixture was heated to 140 °C in an oil bath for 30 min. After cooling to room temperature, 2 mL of cold water was added, and the mixture was stirred at room temperature for 1 h. The solids were filtered and transfer to new vials with 2 mL of water. Potassium cyanide (175 mg, 2.7 mmol) was added, and the solution was heated to 50 °C in an oil bath for 1 h. After cooling to room temperature, the solid was filtered and washed twice with water. The

solid was dissolved in 5 mL of CHCl_3 and dried with MgSO_4 . The desired compound was obtained after removal of solvent in 70% yield. ^1H NMR (400 MHz, CD_3OD) δ 8.43 (1H, s), 8.33 (1H, d, $J = 8.2$ Hz), 8.24 (1H, d, $J = 8.2$ Hz), 4.00 (3H, s), 3.97 (3H, s); ^{13}C NMR (125 MHz, CHCl_3) δ 164.3, 163.8, 135.7, 135.6, 134.1, 133.3, 131.4, 113.3 ($\text{C}\equiv\text{N}$), 53.2, 53.0. HR-ESI-FT-MS m/z calcd. for $\text{C}_{11}\text{H}_{10}\text{NO}_4$ $[M+H]^+$: 220.0604, found $[M+H]^+$: 220.0603.

2-Cyano-1,4-benzenedicarboxylic acid (3). To an oven-dried round bottom flask, dimethyl 2-cyanoterephthalate (88 mg, 0.4 mmol) was dissolved in 3 mL of MeOH and 1.1 mL of 1.0 M NaOH aqueous solution was added by dropwise. The mixture was stirred at room temperature for 24 h. Once conversion was complete (by TLC), the MeOH was removed by evaporation and the mixture was diluted with 3 mL of water and 3 mL of CHCl_3 . The mixture was acidified with ca. 2 mL of 1.0 M HCl aqueous solution. The precipitate was collected by filtration, and washed with water and hexane. The desired compound was obtained by air drying in 45% yield. ^1H NMR (400 MHz, CD_3OD) δ 8.41 (1H, s), 8.33 (1H, d, $J = 8.2$ Hz), 8.25 (1H, d, $J = 8.2$ Hz). HR-MS m/z calcd. for $\text{C}_9\text{H}_5\text{NO}_4$ $[M+H]^+$: 192.0219, found $[M+H]^+$: 192.0290.

UiO-66-CN. UiO-66-Br (ca. 70 mg, 0.2 mmol equiv. in bromide) and copper cyanide (23 mg, 0.26 mmol) were suspended in 2 mL of NMP in a microwave tube. The mixture was heated in a microwave reactor at 170 °C for 10 min without stirring (Maximum power = 200 W). After cooling down to room temperature, the suspension was transferred and rinsed with 10 mL of DMF to a vial. After centrifugation, 10 mL of 0.01 M KCN was added to remove remaining copper and the solids were isolated by centrifugation again. Then, the solids were washed three times with 10 mL of

MeOH then emersed with 10 mL of MeOH to soak overnight. The solids were then rinsed with 10 mL of MeOH and left to soak for 3 days with fresh MeOH added every 24 h. After 3 days of soaking, the solids were stored in the air after centrifugation and dried at 120 °C in a oven. The solid was stored in air with solid state. Yield: 90% (based on three independent samples).

Dimethyl-2-nitro-4,4'-biphenyldicarboxylate. Dimethyl-4,4'-biphenyldicarboxylate (5g, 18.5 mmol) was dissolved with 50 mL of concentrated H₂SO₄ and placed in a dry ice/p-dioxane cold bath ~10 °C. A mixture of 68% or 15M HNO₃ (18.5 mmol, 1.23 mL) in 1 mL of concentrated H₂SO₄ was slowly added drop-wise over 30 minutes. The solution was allowed to stir at ~10 °C for 1.5 h. The solution was then added to ~200 g of ice. The precipitate was then filtered and washed with H₂O (50 mL). The crude product was then recrystallized with hot isopropyl alcohol (~300 mL). Yield, 2.8, 49%. ¹H-NMR (*d*⁶-DMSO): δ = 3.85 (s, 3H), 3.9 (s, 3H), 7.5 (d, 2H), 7.7 (d, 1H), 8.0 (d, 2H), 8.27 (d, 1H), 8.7 (s, 1H).

2-nitro-4,4'-biphenyldicarboxylic acid. Dimethyl-2-nitro-4,4'-biphenyldicarboxylate (0.7g, 2.2 mmol) was dissolved with 20 mL of THF. Aqueous 1 M KOH (20mL) was added and the flask was refluxed (80 °C) under nitrogen for ~18 h. The THF was removed by rotary evaporation and the aqueous solvent was acidified with 12M HCl (~6 mL). The white precipitate was filtered on a glass frit funnel and washed with H₂O (20 mL x 3) and methanol (10 mL x 3) and dried under vacuum. The crude product was then recrystallized with hot isopropyl alcohol (~300 mL). Yield, 0.64g, 84%. ¹H-NMR (*d*⁶-DMSO): δ = 7.5 (d, 2H), 7.7 (d, 1H), 7.98 (d, 2H), 8.23 (d, 1H), 8.4 (s, 1H).

Dimethyl-2-amino-4,4'-biphenyldicarboxylate. Dimethyl-2-nitro-4,4'-biphenyldicarboxylate (2 g, 6.3 mmol) was dissolved with 80 mL of methanol. Tin powder (4.5 g, 38 mmol) was added to the flask. Then ~112 mL of 1M aq. HCl was added. The solution was heated at 70 °C for 2 hours. The clear yellow solution was poured onto ~200 g of ice and basified with 1 M NaOH (~10 mL). The crude product was filtered and taken up with hot ethyl acetate and additionally filtered on a glass frit funnel and celite. The solvent was removed by rotary evaporation. The yellow crude powder was recrystallized with hot ethyl acetate (~200 mL). Yield, 0.77 g, 43%. ¹H-NMR (*d*⁶-DMSO): δ = 3.8 (s, 3H), 3.85 (s, 3H), 5.21 (s, 2H), 7.11 (d, 1H), 7.17 (d, 1H), 7.4 (s, 1H), 7.56 (d, 2H), 8.0 (d, 2H).

2-amino-4,4'-biphenyldicarboxylic acid. Dimethyl-2-amino-4,4'-biphenyldicarboxylate (0.7g, 2.2 mmol) was dissolved with 20 mL of THF. Aqueous 1 M KOH (20mL) was added and the flask was refluxed (80 °C) under nitrogen for ~18 h. The THF was removed by rotary evaporation and the aqueous solvent was acidified with 12M HCl (~6 mL). The white precipitate was filtered on a glass frit funnel and washed with H₂O (20 mL x 3) and methanol (10 mL x 3) and dried under vacuum. The crude product was then recrystallized with hot isopropyl alcohol (~300 mL). Yield, 0.64g, ~100%. ¹H-NMR (*d*⁶-DMSO): δ = 7.17 (d, 1H), 7.32 (d, 1H), 7.5 (s, 1H), 7.56 (d, 2H), 7.98 (d, 2H).

Dimethyl-2,2'-dinitro-4,4'-biphenyldicarboxylate. Dimethyl-4,4'-biphenyldicarboxylate (5g, 18.5 mmol) was dissolved with 50 mL of concentrated H₂SO₄ and placed in a ice/water bath. A mixture of 68% or 15M HNO₃ (45 mmol, 3 mL) in 4 mL of concentrated H₂SO₄ was slowly added drop-wise over 30 minutes.

The solution was allowed to stir at 25 °C for 1.5 h. The solution was then added to ~200 g of ice. The precipitate was then filtered and washed with H₂O (50 mL). The crude product was then recrystallized with hot isopropyl alcohol (~300 mL). Yield, 5.83 g, ~100%. ¹H-NMR (*d*⁶-DMSO): δ = 3.9 (s, 3H), 7.67 (d, 1H), 8.33 (d, 1H), 8.65 (s, 1H).

Dimethyl-2,2'-diamino-4,4'-biphenyldicarboxylate. Dimethyl-2,2'-dinitro-4,4'-biphenyldicarboxylate (1 g, 2.8 mmol) was dissolved with 40 mL of methanol. Tin powder (2.25 g, 19 mmol) was added to the flask. Then ~56 mL of 1M aq. HCl was added. The solution was heated at 70 °C for 2 h. The clear yellow solution was poured onto ~200 g of ice and basified with 1 M NaOH (~10 mL). The crude product was filtered and taken up with hot ethyl acetate and additionally filtered on a glass frit funnel and celite. The solvent was removed by rotary evaporation. The yellow crude powder was recrystallized with hot ethanol (~200 mL). Yield, 0.84 g, ~100%. ¹H-NMR (*d*⁶-DMSO): δ = 3.8 (s, 3H), 4.96 (s, 2H), 7.0 (d, 1H), 7.2 (d, 1H), 7.4 (s, 1H).

2,2'-diamino-4,4'-biphenyldicarboxylic acid. Dimethyl-2,2'-diamino-4,4'-biphenyldicarboxylate (0.87g, 2.2 mmol) was dissolved with 40 mL of THF. Aqueous 1 M KOH (40mL) was added and the flask was refluxed (80 °C) under nitrogen for ~18 h. The THF was removed by rotary evaporation and the aqueous solvent was acidified with 12M HCl (~10 mL). The yellow precipitate was filtered on a glass frit funnel and washed with H₂O (20 mL x 3) and methanol (10 mL x 3) and dried under vacuum. The crude product was then recrystallized with hot isopropyl alcohol (~300 mL). Yield, 0.63g, 78%. ¹H-NMR (*d*⁶-DMSO): δ = 7.25 (d, 1H), 7.48 (d, 1H), 7.67 (d, 1H).

UiO-67. 4,4'-biphenyldicarboxylic acid (0.35 mmol, 85 mg), ZrCl₄ (0.35 mmol, 82 mg) and 4 mL of DMF were added to a small Teflon-line Parr autoclave and heated at 120 °C for 24 h. After cooling, the material was isolated by centrifugation, heated at 100 °C for 30 minutes then washed with CH₂Cl₂ (10 mL x 3) for 3 days. The material was then activated by heating at 60 °C for ~4 h under vacuum.

UiO-67-NO₂. 2-nitro-4,4'-biphenyldicarboxylic acid (0.35 mmol, 101 mg), ZrCl₄ (0.35 mmol, 82 mg) and 4 mL of DMF were added to a small Teflon-line Parr autoclave and heated at 120 °C for 24 h. After cooling, the material was isolated by centrifugation, heated at 100 °C for 30 minutes then washed with CH₂Cl₂ (10 mL x 3) for 3 days. The material was then activated by heating at 60 °C for ~4 h under vacuum.

UiO-67-(NO₂)₂. 2,2'-dinitro-4,4'-biphenyldicarboxylic acid (0.35 mmol, 116 mg), ZrCl₄ (0.35 mmol, 82 mg) and 4 mL of DMF were added to a small Teflon-line Parr autoclave and heated at 120 °C for 24 h. After cooling, the material was isolated by centrifugation, heated at 100 °C for 30 minutes then washed with CH₂Cl₂ (10 mL x 3) for 3 days. The material was then activated by heating at 60 °C for ~4 h under vacuum.

UiO-67-NH₂. 2-amino-4,4'-biphenyldicarboxylic acid (0.35 mmol, 90 mg), ZrCl₄ (0.35 mmol, 82 mg) and 4 mL of DMF were added to a small Teflon-line Parr autoclave and heated at 120 °C for 24 h. After cooling, the material was isolated by centrifugation, heated at 100 °C for 30 minutes then washed with CH₂Cl₂ (10 mL x 3) for 3 days. The material was then activated by heating at 60 °C for ~4 h under vacuum.

UiO-67-(NH₂)₂. 2,2'-diamino-4,4'-biphenyldicarboxylic acid (0.35 mmol, 95 mg), ZrCl₄ (0.35 mmol, 82 mg) and 4 mL of DMF were added to a small Teflon-line Parr autoclave and heated at 120 °C for 24 h. After cooling, the material was isolated by centrifugation, heated at 100 °C for 30 minutes then washed with CH₂Cl₂ (10 mL x 3) for 3 days. The material was then activated by heating at 60 °C for ~4 h under vacuum.

6.5 Acknowledgements

Text, schemes, and figures in this chapter, in part, are reprints of the materials published in the following papers: Garibay, S. J., Cohen, S. M. "Isorecticular synthesis and modification of frameworks with the UiO-66 topology" *Chem. Commun.* **2010**, *46*, 7200-7702 and Kim, M, Garibay, S. J., Cohen, S. M. "Microwave-Assisted Cyanation of an Aryl Bromide Directly on a Metal-Organic Framework" *Inorg. Chem.* **2011**, *50*, 729-731. The dissertation author was the primary researcher and author for the data presented. The co-authors listed in these publications also participated in the research.

6.6 References

- (1) Wang, Z.; Cohen, S. M. *Chem. Soc. Rev.* **2009**, *38*, 1315-1329.
- (2) Volkringer, C.; Cohen, S. M. *Angew. Chem. Int. Ed.* **2010**, *49*, 4644-4648.
- (3) Ferey, G.; Mellot-Draznieks, C.; Serre, C.; Millange, F.; Dutour, J.; Surble, S.; Margiolaki, I. *Science* **2005**, *309*, 2040-2042.
- (4) Bernt, S.; Guillerm, V.; Serre, C.; Stock, N. *Chem. Commun.* **2011**, *47*, 2838-2840.
- (5) Cavka, J. H.; Jakobsen, S.; Olsbye, U.; Guillou, N.; Lamberti, C.; Bordiga, S.; Lillerud, K. P. *J. Am. Chem. Soc.* **2008**, *130*, 13850-13851.
- (6) Chavan, S.; Vitillo, J. G.; Uddin, M. J.; Bonino, F.; Lamberti, C.; Groppo, E.; Lillerud, K. P.; Bordiga, S. *Chem. Mater.* **2010**, *22*, 4602-4611.
- (7) Guillerm, V.; Gross, S.; Serre, C.; Devic, T.; Bauer, M.; Ferey, G. *Chem. Commun.* **2010**, *46*, 767-769.
- (8) Wang, Z. Q.; Tanabe, K. K.; Cohen, S. M. *Inorg. Chem.* **2009**, *48*, 296-306.
- (9) Garibay, S. J.; Wang, Z. Q.; Tanabe, K. K.; Cohen, S. M. *Inorg. Chem.* **2009**, *48*, 7341-7349.
- (10) Garibay, S. J.; Wang, Z.; Cohen, S. M. *Inorg. Chem.* **2010**, *49*, 8086-8091.
- (11) Doonan, C. J.; Morris, W.; Furukawa, H.; Yaghi, O. M. *J. Am. Chem. Soc.* **2009**, *131*, 9492-9493.
- (12) Burrows, A. D.; Frost, C. G.; Mahon, M. F.; Richardson, C. *Angew. Chem. Int. Ed.* **2008**, *47*, 8482-8486.
- (13) Goto, Y.; Sato, H.; Shinkai, S.; Sada, K. *J. Am. Chem. Soc.* **2008**, *130*, 14354-14355.

- (14) Gadzikwa, T.; Lu, G.; Stern, C. L.; Wilson, S. R.; Hupp, J. T.; Nguyen, S. T. *Chem. Commun.* **2008**, 5493-5495.
- (15) Dybtsev, D. N.; Chun, H.; Kim, K. *Angew. Chem. Int. Ed.* **2004**, *43*, 5033-5036.
- (16) Savonnet, M.; Bazer-Bachi, D.; Bats, N.; Perez-Pellitero, J.; Jeanneau, E.; Lecocq, V.; Pinel, C.; Farrusseng, D. *J. Am. Chem. Soc.* **2010**, *132*, 4518-4519.
- (17) Savonnet, M.; Kockrick, E.; Camarata, A.; Bazer-Bachi, D.; Bats, N.; Lecocq, V.; Pinel, C.; Farrusseng, D. *New. J. Chem.* **2011**, *35*, 1892-1897.
- (18) Marx, S.; Kleist, W.; Huang, J.; Maciejewski, M.; Baiker, A. *Dalton. Trans.* **2010**, *39*, 3795-3798.
- (19) Taylor-Pashow, K. M.; Della Rocca, J.; Xie, Z.; Tran, S.; Lin, W. *J. Am. Chem. Soc.* **2009**, *131*, 14261-14263.
- (20) Ahnfeldt, T.; Gunzelmann, D.; Loiseau, T.; Hirsemann, D.; Senker, J.; Ferey, G.; Stock, N. *Inorg. Chem.* **2009**, *48*, 3057-3064.
- (21) Gadzikwa, T.; Farha, O. K.; Mulfort, K. L.; Hupp, J. T.; Nguyen, S. T. *Chem. Commun.* **2009**, 3720-3722.
- (22) Lindley, J. *Tetrahedron* **1984**, *40*, 1433-1456.
- (23) Galli, C. *Chem. Rev.* **1988**, *88*, 765-792.
- (24) Larock, R. C. *Comprehensive Organic transformations; A Guide to Funtional Group Preparations*; VCH: New York, 1989.
- (25) Eddaoudi, M.; Kim, J.; Rosi, N.; Vodak, D.; Wachter, J.; O'Keeffe, M.; Yaghi, O. M. *Science* **2002**, *295*, 469-472.
- (26) Powers, J. J.; Favor, D. A.; Rankin, T.; Sharma, R.; Pandit, C.; Jeganathan, A.; Maiti, S. N. *Tetrahedron Lett.* **2009**, *50*, 1267-1269.

- (27) Garibay, S. J.; Cohen, S. M. *Chem. Commun.* **2010**, 46, 7700-7702.
- (28) Ni, Z.; Masel, R. I. *J. Am. Chem. Soc.* **2006**, 128, 12394-12395.
- (29) Taylor, K. M. L.; Rieter, W. J.; Lin, W. B. *J. Am. Chem. Soc.* **2008**, 130, 14358-14359.
- (30) Schaate, A.; Roy, P.; Godt, A.; Lippke, J.; Waltz, F.; Wiebcke, M.; Behrens, P. *Chem. Eur. J.* **2011**, 17, 6643-6651.